BEILSTEIN JOURNAL OF ORGANIC CHEMISTRY

Novel macrocycles: from synthesis to supramolecular function

Edited by Pablo Ballester, Konrad Tiefenbacher,Carmine Gaeta, Carmen Talotta,Margherita De Rosa and Paolo Della Sala

Imprint

Beilstein Journal of Organic Chemistry
www.bjoc.org
ISSN 1860-5397
Email: journals-support@beilstein-institut.de

The *Beilstein Journal of Organic Chemistry* is published by the Beilstein-Institut zur Förderung der Chemischen Wissenschaften.

Beilstein-Institut zur Förderung der Chemischen Wissenschaften
Trakehner Straße 7–9
60487 Frankfurt am Main
Germany
www.beilstein-institut.de

BEILSTEIN JOURNAL OF ORGANIC CHEMISTRY

Acyclic cucurbit[*n*]uril bearing alkyl sulfate ionic groups

Christian Akakpo, Peter Y. Zavalij and Lyle Isaacs*

Full Research Paper

Open Access

Address:
Department of Chemistry and Biochemistry, University of Maryland, College Park, Maryland 20742, United States

Email:
Lyle Isaacs* - LIsaacs@umd.edu

* Corresponding author

Keywords:
cucurbituril; host–guest chemistry; isothermal titration calorimetry; molecular container; X-ray crystallography

Beilstein J. Org. Chem. **2025,** *21,* 717–726.
https://doi.org/10.3762/bjoc.21.55

Received: 09 January 2025
Accepted: 28 March 2025
Published: 03 April 2025

This article is part of the thematic issue "Novel macrocycles: from synthesis to supramolecular function".

Guest Editor: C. Gaeta

Abstract

We report the synthesis and characterization of a new acyclic cucurbit[*n*]uril (CB[*n*]) host **C1** that features four alkyl sulfate ionic groups. The X-ray crystal structure of the **C1·Me$_6$CHDA** complex is reported. Host **C1** is significantly less soluble in water (4 mM) compared to the analogous acyclic CB[*n*] host **M1** which features sulfonate ionic groups (346 mM). Host **C1** does not undergo significant self-association according to the results of ^{1}H NMR dilution experiments. The molecular recognition behavior of the hosts **C1** and **M1** toward a panel of seven ammonium ions was explored by ^{1}H NMR spectroscopy and isothermal titration calorimetry (ITC). We find that **C1** generally binds slightly more tightly than **M1** toward a specific guest. **C1** binds more tightly to quaternary ammonium guests compared to the corresponding primary ammonium ions.

Introduction

Molecular recognition interactions are key elements of life processes including self- versus non-self-recognition, biosynthesis, molecular and ion transport, and replication. Beginning with the pioneering works of Pedersen, Lehn, and Cram, supramolecular chemists have studied the fundamental aspects of non-covalent interactions in organic solvents and water [1-4]. Building on this fundamental knowledge, supramolecular chemists created a variety of functional systems including supramolecular polymers, sensing ensembles, molecular machines, supramolecular separation phases, and drug delivery systems [5-9]. A primary subfield of supramolecular chemistry involves the synthesis of macrocyclic hosts and studies of their molecular recognition properties. The most widely studied macrocyclic host systems include those created entirely by covalent bonds (crown ethers, cyclodextrins, calixarenes, cyclophanes, pillararenes, cucurbit[*n*]urils (CB[*n*])), and those prepared by metal ligands and H-bonding self-assembly processes [1,2,10-20]. Macrocycles have played key roles in important real-world products including the household deodorizer Febreeze^{TM}, glucose monitors, and as solubilizing excipients [21-26]. Within these families of macrocyclic hosts, CB[*n*] molecular containers have proven particularly versatile because they form high affinity

CB[*n*]–guest complexes in aqueous solution that are responsive to various stimuli (e.g., photochemical, electrochemical, chemical) [27-30]. For this reason, macrocyclic CB[*n*] have been used as key elements of separations processes [31,32], sensing systems [33,34], in pharmaceutical applications [35-38], in bioimaging systems [39,40], and even in household deodorizing products [41].

An important subclass of CB[*n*] hosts are acyclic CB[*n*]-type receptors which have been extensively studied by our lab and others over the past decade [42-52]. Figure 1 shows the chemical structure of the prototypical acyclic CB[*n*]-type known as **M1** [53,54]. **M1** features a central glycoluril tetramer, two aromatic *o*-xylylene walls, and four sulfonates as solubilizing ionic groups. In accord with these structural features, **M1** binds a variety of hydrophobic and cationic guest molecules by the hydrophobic effect, π–π interactions, and electrostatic (ion–dipole and ion–ion) interactions. Although acyclic CB[*n*] are not macrocycles, they are preorganized into a C-shaped geometry by virtue of their polycyclic chemical structure and display binding affinities approaching those of macrocyclic CB[*n*]. **M1** and analogues display outstanding biocompatibility and have been used for a number of in vivo biomedical applications including as a solubilizing excipient for anticancer agents and as an in vivo sequestrant to reverse the biological activity of neuromuscular blocking agents, anesthetics, and drugs of abuse (e.g., methamphetamine and fentanyl) [54-60].

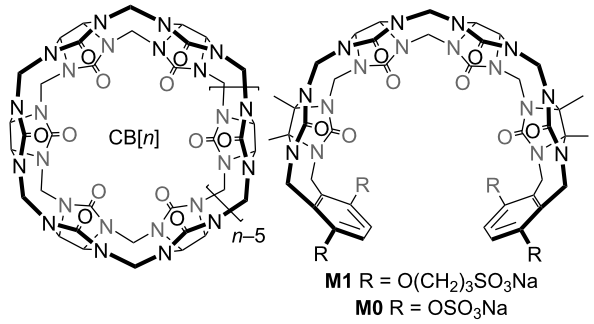

Figure 1: Chemical structures of CB[n] and selected acyclic CB[*n*]-type molecular containers **M1** and **M0**.

As a result of their modular synthesis, acyclic CB[*n*] can be easily modified synthetically [42-47,61]. Acyclic CB[*n*]-type receptors featuring different length glycoluril oligomers (monomer–pentamer) and different aromatic walls (e.g., naphthalene, anthracene, triptycene) have been studied [42,62-67]. Previously, we have studied the influence of the length of the $O(CH_2)_nSO_3Na$ sidearm (n = 0, 2, 3, 4) and found that the **M0** host – where the hydrophobic linker $(CH_2)_n$ was completely removed – displayed higher binding affinity than **M1** which we attributed to the location of the ionic group closer to the ureidyl C=O portals [68,69]. However, a close examination of the structures of **M0** and **M1** show that the ionic group for **M1** is a sulfonate and for **M0** is a sulfate. Accordingly, **M1** and **M0** differ in two ways: a) different $(CH_2)_n$ linker length and b) different ionic group (sulfonate versus sulfate). In this paper, we present the synthesis and molecular recognition properties of a new acyclic CB[*n*]-type receptor **C1** which allows us to disentangle these two effects.

Results and Discussion

This results and discussion section is organized as follows: First, we present the design, synthesis, and spectroscopic characterization of **C1** along with determination of its inherent aqueous solubility and self-association properties. Next, we present the X-ray crystal structure of **C1** as its **C1**·**Me$_6$CHDA** complex. Subsequently, we describe a qualitative investigation of **C1**·guest and **M1**·guest complexation by ^{1}H NMR spectroscopy and quantitative investigation by isothermal titration calorimetry (ITC). Finally, we discuss the trends in binding affinity observed for **C1**·guest and **M1**·guest complexation.

Design, synthesis and characterization of **C1**

In order to disentangle the effects of the ionic group (sulfonate versus sulfate) while maintaining the distance of the ionic group from the ureidyl C=O portal we designed acyclic CB[*n*]-type receptor **C1** (Scheme 1). The only structural difference between **M1** and **C1** is the swapping of one CH_2 group for one O atom in each alkyl chain which effectively changes the sulfonate group to a sulfate group. The synthetic route to **C1** starts with the double electrophilic aromatic substitution reaction of methylene-bridged glycoluril tetramer (**TetBCE**) with **W1** in TFA/Ac_2O 1:1 which adds the sidewalls and transforms the OH groups into OAc groups to give **TetW1$_{OAc}$** in 71% yield as described previously [70]. Saponification of **TetW1$_{OAc}$** with LiOH at 50 °C followed by acidification with 0.1 M HCl gives **TetW1** in 69% yield [70]. Finally, the sulfation of **TetW1** occurs upon treatment with py·SO_3 (20 equiv) in dry pyridine to yield **C1** as a white solid in 68% yield. In accord with the depicted C_{2v}-symmetric geometry (Scheme 1), the ^{1}H NMR spectrum of **C1** displays one aromatic resonance (H_a), two methyl resonances $(CH_3)_j$ and $(CH_3)_k$, two equatorial methine doublets (H_l and H_m), along with three doublets for the diastereotopic methylene bridges around 5.5 ppm (H_d, H_f, H_h) in the expected 2:2:1 ratio (Figure 2a). The 4.0–4.5 ppm region is crowded which precludes precise assignments of the expected resonances for H_e, H_g, H_i, H_b, and H_c. Similarly, the ^{13}C NMR spectrum recorded for **C1** (Figure 2b) shows 15 of the 16 resonances expected based on time averaged C_{2v}-symmetry in solution. For example, we observe two resonances for the C=O groups, three resonances for the aromatic C-atoms, two methyl

resonances, three resonances for the bridging CH_2 groups, and five of the six resonances for the sidearm (b and c) and equatorial glycoluril C-atoms. The negative-ion electrospray ionization mass spectrum shows an ion at m/z = 751.13 which corresponds to $[\mathbf{C1} - 2Na]^{2-}$.

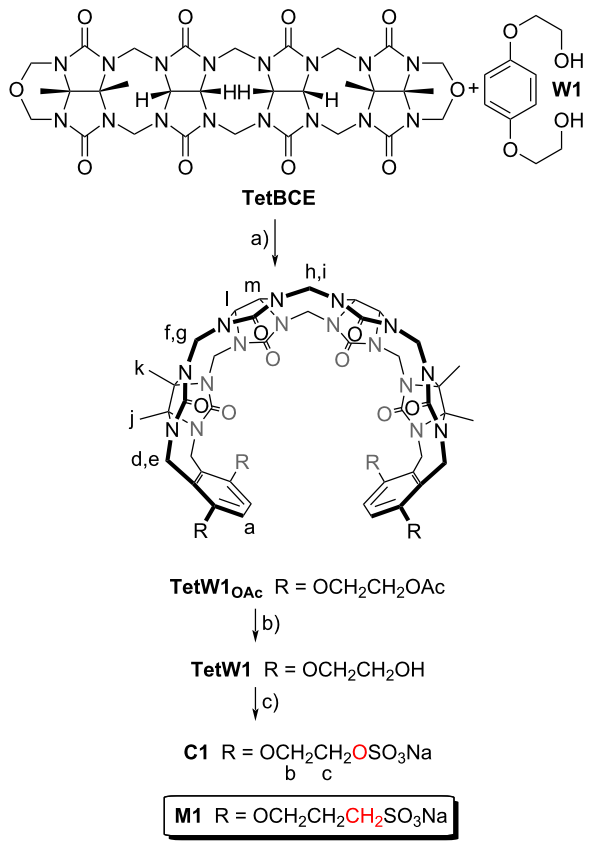

Scheme 1: Synthesis of **C1**. Conditions: a) TFA/Ac_2O, 70 °C, 3.5 h, 71%; b) LiOH, 50 °C, 69%; c) dry pyridine, pyridine sulfur trioxide complex (20 equiv), 90 °C, 18 h, 68%.

Inherent aqueous solubility of C1

After having firmly established the structure of **C1** we decided to determine its inherent aqueous solubility. For this purpose, we added an excess of solid **C1** to D_2O and stirred the solution at room temperature overnight. Afterwards, the mixture was centrifuged (4400 rpm, 10 min) to pellet excess insoluble **C1**. An aliquot of the supernatant and a solution of dimethyl malonic acid as a non-binding internal standard of known concentration were transferred to an NMR tube followed by collection of a ^{1}H NMR spectrum using a delay time between pulses of 20 seconds to ensure accurate integration. The inherent aqueous solubility of **C1** was determined to be 3.97 mM by comparison of the integrals for H_a of **C1** with that of the CH_3-resonance for dimethyl malonic acid (Figure S5 in Supporting Information File 1).

Qualitative study of C1·guest recognition properties by ^{1}H NMR spectroscopy

Next, we decided to perform a qualitative investigation of the host–guest properties of **C1** by ^{1}H NMR spectroscopy. Figure 3 shows the chemical structures of a panel of guests that were studied and the complexation-induced changes in chemical shift (Δδ) for **C1**·guest. As the central hydrophobic binding domain of the guests we selected alkylene, *p*-xylylene, cyclohexane, and adamantane moieties that are known to bind well to (acyclic) CB[*n*] receptors [71-73]. The cross-sectional area of this hydrophobic moiety increases as follows: **PDA** ≈ **HDA** < **PXDA** < **CHDA** < **AdA**. Given that (acyclic) CB[*n*] often bind to ammonium ion guests (e.g., NH_3^+ form) weaker than they do to the corresponding methonium ion guests (e.g., NMe_3^+ form) we elected to study both forms to elucidate related preferences for the sulfated **C1** host relative to the sulfonated **M1** host [69,71,74]. Figure 4 shows a ^{1}H NMR stack plot created for uncomplexed **C1** (Figure 4d), uncomplexed **Me_6PXDA** (Figure 4d), and 1:1 and 1:2 mixtures of **C1** and **Me_6PXDA**. Several spectroscopic features are noteworthy. First, the Ar–H

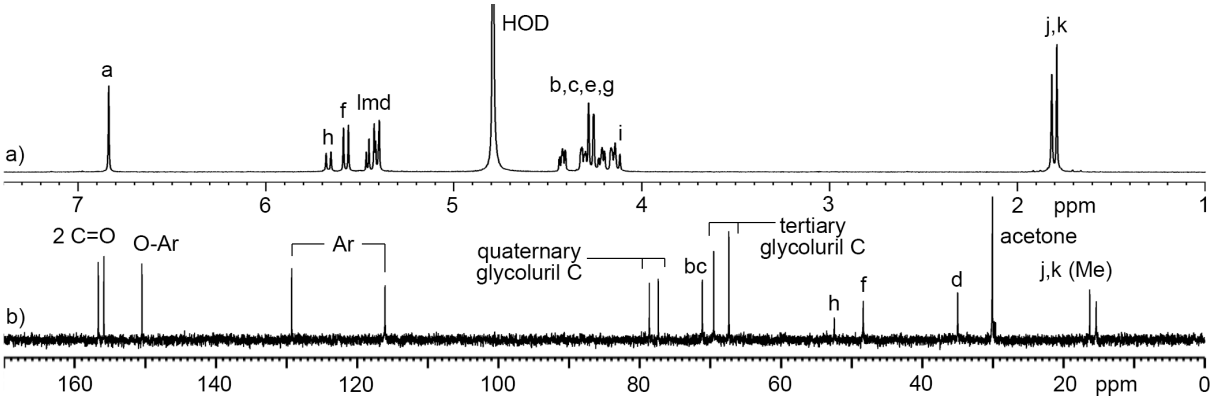

Figure 2: a) ^{1}H NMR spectrum (600, D_2O, rt) and b) ^{13}C NMR spectrum recorded (150 MHz, D_2O, rt) for **C1**.

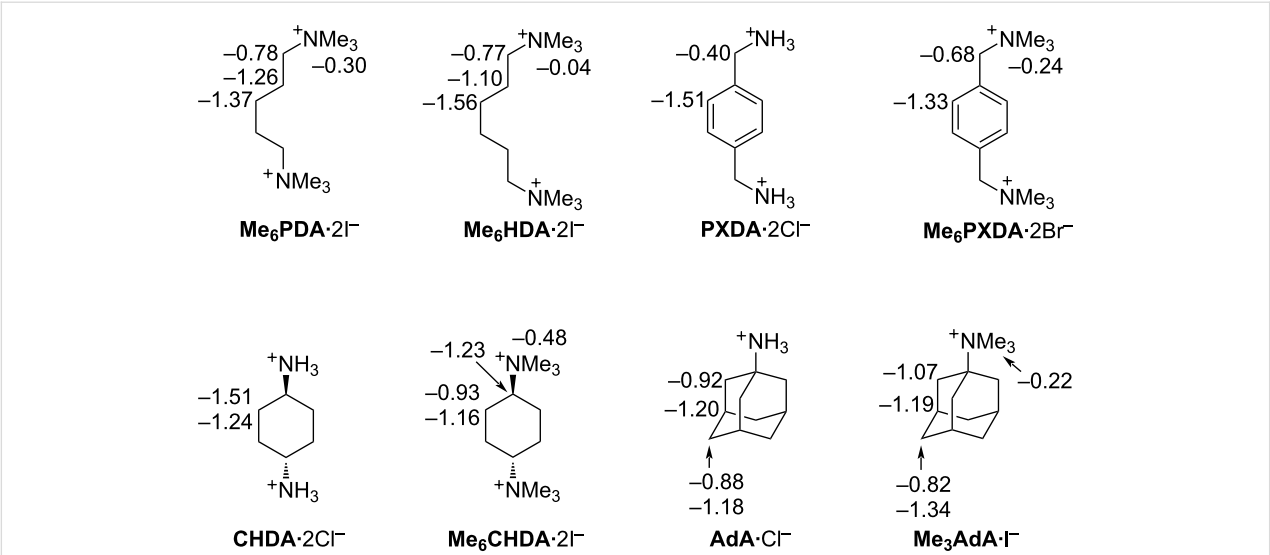

Figure 3: Chemical structures of guests used in this study along with the complexation induced changes in chemical shift (Δδ) upon formation of the **C1**·guest complexes. Negative Δδ values represent upfield shifts upon complexation.

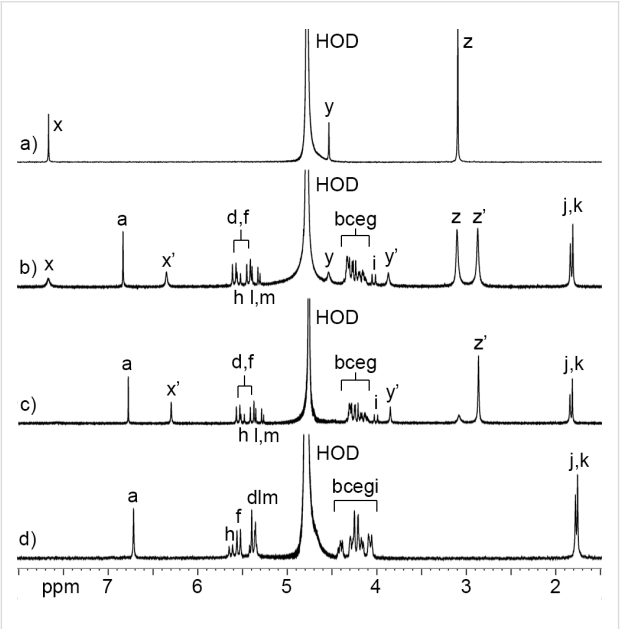

Figure 4: ^{1}H NMR spectra recorded (400 MHz, D_2O, rt) for: a) **Me$_6$PXDA** (0.5 mM), b) a mixture of **C1** (0.5 mM) and **Me$_6$PXDA** (1.0 mM), c) a mixture of **C1** (0.5 mM) and **Me$_6$PXDA** (0.5 mM), and d) **C1** (0.5 mM).

resonance for **Me$_6$PXDA** undergoes a large upfield shift (Δδ = −1.33) upon formation of **C1**·**Me$_6$PXDA** (Figure 4c) whereas the CH_2 (Δδ = −0.68) and NMe_3 (Δδ = −0.24) groups undergo smaller upfield shifts. This observation strongly suggests that the Ar–H protons are located nearer the center of the magnetically shielding cavity of **C1** which is defined by the aromatic sidewalls and the ureidyl π-systems. The small changes in chemical shift for the methonium group suggests it is located near the ureidyl C=O portals and not inside the magnetically shielding cavity. Related complexation-induced changes in chemical shift are observed for the other **C1**·guest complexes (Figure 3 and Supporting Information File 1) which confirms that the hydrophobic central region of the guest binds inside the hydrophobic cavity of **C1** whereas the hydrophilic ammonium and methonium groups reside at the electrostatically negative ureidyl C=O portals. Second, at a 1:2 **C1**/**Me$_6$PXDA** ratio (Figure 4b), we observe separate resonances for free **Me$_6$PXDA** and complexed **C1**·**Me$_6$PXDA** which means that the rate of guest exchange is slow on the chemical shift timescale. Slow kinetics of guest exchange is commonly observed for tight host·guest complexes. In contrast, the kinetics of guest exchange are in the intermediate exchange regime on the chemical shift timescale for the complexes of **C1** with **CHDA**, **Me$_6$CHDA**, **AdA**, **Me$_3$AdA** (Supporting Information File 1, Figures S10–S13) which is typical of weaker complexes. Third, we observe changes in the chemical shift for the H_a resonance of **C1** upon formation of the **C1**·guest complexes. In uncomplexed **C1** the tips of the aromatic rings are pointing toward each other which places H_a in the magnetically shielding region of the opposing sidewall. Upon formation of the **C1**·guest complexes, the tips of the aromatic sidewall change their orientation to accommodate the hydrophobic region of the guest which changes the orientation of H_a with respect to the magnetically shielding region [54,63,64].

X-ray crystal structure of **C1**

We were fortunate to obtain single crystals of the **C1**·**Me$_6$CHDA** complex and solved the crystal structure by X-ray diffraction (CCDC 2411723). Figure 5 shows a cross-

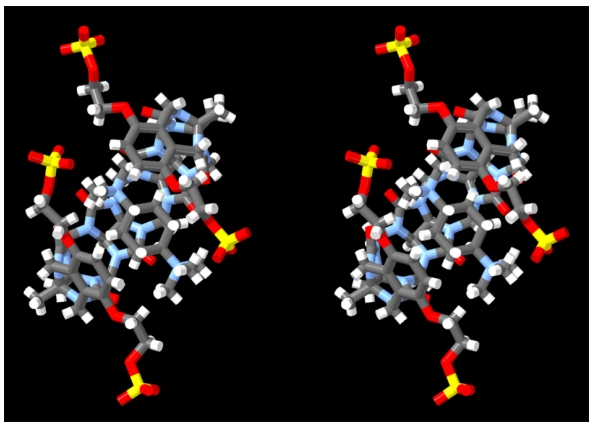

Figure 5: Cross-eyed stereoview of the **C1·Me$_6$CHDA** complex in the crystal. Color code: C, gray; H, white; N, blue; O, red; S, yellow.

eyed stereoview of one **C1·Me$_6$CHDA** complex in the crystal. Several features of this structure are noteworthy. First, the crystal structure confirms the molecular structure of **C1** and its overall C-shaped geometry. Second, within the **C1·Me$_6$CHDA** complex, the aromatic sidewalls are splayed away from the equator of **C1** resulting in a helical geometry [63,65]. Both senses of helical chirality are present in the crystal; values in parenthesis given below refer to the complex with opposite helical chirality. The guest **Me$_6$CHDA** possesses a mirror plane and is therefore achiral. In solution, host **C1** is flexible and the two senses of helicity – and other conformations – undergo rapid equilibrium rendering the **C1** and the **C1·Me$_6$CHDA** complex achiral. The centroids of the aromatic sidewall are 0.9698 Å (1.1193 Å) above and 1.3090 Å (1.4832 Å) below the mean plane of the glycoluril methine and glycoluril quaternary C-atoms. Third, the **Me$_6$CHDA** guest is not symmetrically oriented with respect to the ureidyl carbonyl portals of **C1**. Specifically, one of the methonium N-atoms is located inside the cavity of **C1** at 1.4476 Å (0.6162 Å) below the mean plane of the ureidyl carbonyl O-atoms whereas the other methonium N-atom is located 1.7980 Å (0.9686 Å) outside the cavity.

Figure 6 shows the packing of four molecules of the **C1·Me$_6$CHDA** complex in a single unit cell along with four molecules of **Me$_6$CHDA** located outside the cavity of **C1** to ensure overall charge neutrality. It is well known that CB[*n*]·guest complexation is driven by ion–dipole interactions at the ureidyl C=O portals [75]. Previously, we found that the $Me_3N^+\cdots O{=}C$ distances in the ultratight CB[7]·diamantane$(NMe_3)_2$ complex averaged 4.38(7) Å [74]. For comparison, a histogram of $Me_3N^+\cdots O{=}C$ distances drawn from 89 CCDC structures that contain an acetylcholine-type unit ($Me_3NCH_2CH_2O(C{=}O)R$) range from 3.5 Å to 5 Å with a maximum probability of 4.4 Å [74]. Figure 6 shows $Me_3N^+\cdots O{=}C$ contacts that are less than 4.40 Å. The large number of contacts that are significantly shorter than 4.40 Å establishes that $Me_3N^+\cdots O{=}C$ cation–dipole interactions play an important role driving the inclusion of **Me$_6$CHDA** inside of **C1** to form the **C1·Me$_6$CHDA** complex. Of course, the inclusion of the hydrophobic cyclohexyl moiety inside the cavity of **C1** provides a hydrophobic driving force for complexation in water. Given that **C1** is a tetraanion and that **Me$_6$CHDA** is a dication, an additional molecule of **Me$_6$CHDA** is present per molecule of **C1** to ensure overall charge neutrality in the crystal. Among the four molecules of **Me$_6$CHDA** outside the cavity of **C1** in the molecular cell (Figure 6, only two external **Me$_6$CHDA** are shown for clarity), only one $Me_3N^+\cdots O{=}C$ contact (4.548 Å) with a distance < 5.5 Å is observed. Given the anionic nature of

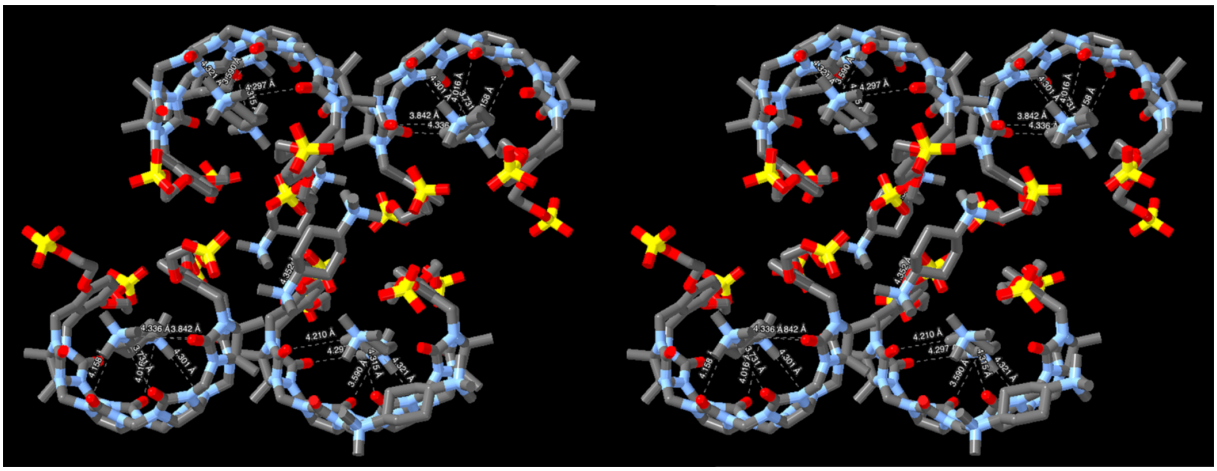

Figure 6: Cross-eyed stereoview of the crystal packing observed in the molecular cell of **C1·Me$_6$CHDA**. H-atoms are omitted for clarity. N···O distances less than 4.40 Å are indicated with dashed lines. Color code: C, gray; N, blue; O, red; S, yellow.

the sulfate substituents, one might expect to observe $Me_3N^+\cdots{}^-O_3SO$ interactions in the crystal. Somewhat surprisingly, only a single short $Me_3N^+\cdots{}^-O_3SO$ contact (4.352 Å) is observed with distance < 4.4 Å. There are, however, numerous longer $Me_3N^+\cdots{}^-O_3SO$ contacts with distances in the 4.4–5.4 Å range which suggests they play a supporting role during crystallization.

Measurement of the self-association of **C1**

Before proceeding to investigate the molecular recognition properties of **C1** by ITC, we wanted to determine whether **C1** undergoes self-association in phosphate-buffered saline (PBS) which might impinge on guest binding and complicate the determination of **C1**·guest binding constants. For this purpose, we performed dilution experiments monitored by ^{1}H NMR spectroscopy. We prepared a series of NMR samples of **C1** in D_2O (from 4 mM to 125 μM) and monitored the chemical shift of H_a (Supporting Information File 1, Figure S14). Over this dilution range, the resonance for H_a remains a sharp singlet at 6.94 ppm. Accordingly, we conclude that **C1** remains monomeric at the low concentration (100 μM) typically employed for isothermal titration calorimetry measurements.

Use of isothermal titration calorimetry to measure the thermodynamic parameters of complexation

Acyclic CB[*n*]-type receptors are known to bind tightly ($K_a > 10^6$ M^{-1}) to hydrophobic diammonium ions [42,65,71]. Accordingly, we elected to use isothermal titration calorimetry (ITC) to measure the binding between **C1** or **M1** with the panel of guests. A single ITC run is capable of delivering both the binding constant (K_a, M^{-1}) and the enthalpy of complexation (ΔH, kcal mol^{-1}). Direct ITC titrations are most appropriate for host·guest complexes with $K_a \leq 10^7$ M^{-1} where Wiseman c-values from 5–500 can be achieved by changing the concentration of host in the ITC cell [76-78]. Figure 7a presents the thermogram recorded when a solution of **C1** (100 μM) in phosphate-buffered saline (PBS) in the ITC cell was titrated with a solution of **CHDA** (1 mM) from the ITC injection syringe. The DP versus time data in Figure 6a was integrated and then plotted as ΔH versus molar ratio in Figure 7b. The ΔH versus molar ratio data was then fitted to the single-set-of-sites binding model in the PEAQ ITC data analysis software which delivered $K_a = (6.49 \pm 0.10) \times 10^5$ M^{-1} and $\Delta H = -7.82 \pm 0.02$ kcal mol^{-1} for the **C1**·**CHDA** complex (Table 1). All ITC experiments were performed in triplicate and the reported values represent the mean ± standard deviation. For stronger complexes, where the Wiseman c-value cannot be adjusted into the ideal range by reducing the host concentration in the ITC cell due to the insufficient heat evolved, competitive ITC titrations must be used. In competitive ITC titrations a solution of the host and an excess of a weak binding competitive guest in the ITC cell is titrated with a solution of the tighter binding guest from the ITC injection syringe [78]. The analysis of competitive titrations requires that the K_a and ΔH values for the host·competitor complexes have been previously determined and used as known inputs to the competitive binding model in the PEAQ data analysis software. To maximize the

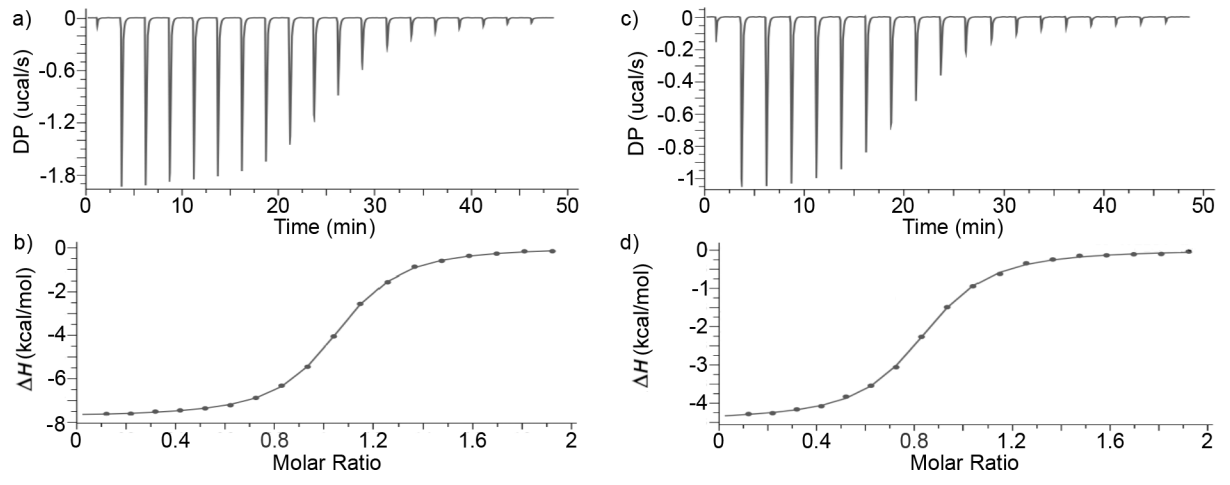

Figure 7: a) Representative plot of DP (μcal s^{-1}) versus time from the titration of **C1** (0.1 mM) in the ITC cell with a solution of **CHDA** (1.0 mM) from the ITC syringe. b) Plot of ΔH versus the **C1**:**CHDA** molar ratio. The solid line represents the best fit of the data to the single-set-of-sites binding model implemented in the PEAQ ITC data analysis software. The measurements were performed in triplicate and yielded $K_a = (6.49 \pm 0.10) \times 10^5$ M^{-1} and $\Delta H = -7.82 \pm 0.02$ kcal mol^{-1}. c) Representative plot of DP versus time from the competitive titration of **C1** (0.1 mM) and **CHDA** (0.8 mM) in the cell with a solution of **Me$_6$PXDA** (1.0 mM) from the syringe. d) Plot of ΔH versus the **C1**:**Me$_6$PXDA** molar ratio. The solid line represents the best fit of the data to the competitive binding model implemented in the PEAQ ITC data analysis software. The measurements were performed in triplicate and yielded $K_a = (2.47 \pm 0.06) \times 10^8$ M^{-1} and $\Delta H = -12.43 \pm 0.02$ kcal mol^{-1}.

Table 1: Thermodynamic parameters (K_a (M^{-1}), $\Delta H°$ (kcal/mol) determined for the **C1**·guest, **M1**·guest and **M0**·guest complexes by ITC. Conditions: 298.0 K, phosphate-buffered saline, pH 7.4.

Guest	**C1**		**M1**	
	K_a	$\Delta H°$	K_a (M^{-1})	$\Delta H°$
Me_6PDA	(3.40 ± 0.09) × 10^{7d}	−13.47 ± 0.03	(1.31 ± 0.05) × 10^{6a}	−5.98 ± 0.03
Me_6HDA	(6.54 ± 0.59) × 10^{7b}	−10.13 ± 0.02	(2.95 ± 0.12) × 10^{6a}	−5.27 ± 0.02
PXDA	(1.44 ± 0.03) × 10^{8c}	−10.07 ± 0.01	(3.42 ± 0.05) × 10^{7c}	−5.67 ± 0.01
Me_6PXDA	(2.47 ± 0.06) × 10^{8b}	−12.43 ± 0.02	(7.52 ± 0.18) × 10^{7b}	−8.64 ± 0.02
CHDA	(6.49 ± 0.10) × 10^{5a}	−7.82 ± 0.02	(2.79 ± 0.07) × 10^{5a}	−4.38 ± 0.02
Me_6CHDA	(1.75 ± 0.06) × 10^{6a}	−7.83 ± 0.03	(1.20 ± 0.04) × 10^{6a}	−7.44 ± 0.03
AdA	(2.41 ± 0.04) × 10^{6a}	−7.54 ± 0.03	(1.99 ± 0.06) × 10^{6a}	−4.11 ± 0.03
Me_3AdA	(2.31 ± 0.07) × 10^{6a}	−11.00 ± 0.04	(2.09 ± 0.07) × 10^{6a}	−7.42 ± 0.02

[a]Measured by direct ITC titration of host (100 μM) in the cell with guest (1 mM) in the syringe. [b]Measured by ITC competition assay using **CHDA** (0.8 mM) as competitor included in the cell. [c]Measured by ITC competition assay using **CHDA** (0.5 mM) as competitor included in the cell. [d]Measured by ITC competition assay using **CHDA** (0.1 mM) as competitor included in the cell.

heat evolved in the competitive ITC titrations, the host·competitor and host·tight guest complexes should have very different ΔH values. Figure 7c shows the competitive ITC titration of a mixture of **C1** (0.1 mM) and **CHDA** (0.8 mM) in the ITC cell with a solution of **Me_6PXDA** (1.0 mM) from the syringe. The DP versus time plot was integrated and a plot of ΔH versus molar ratio was created (Figure 7d) and fitted to the competitive binding model in the PEAQ ITC data analysis software to determine K_a = (2.47 ± 0.06) × 10^8 M^{-1} and ΔH = −12.43 ± 0.02 kcal mol^{-1} for the **C1**·**Me_6PXDA** complex. The K_a and ΔH values for the remaining **C1**·guest and **M1**·guest complexes were determined by analogous direct or competitive ITC titrations (Table 1 and Supporting Information File 1).

Comparison of the thermodynamic parameters for **C1**·guest and **M1**·guest complexation

Overall, **C1** is the more potent host with K_a values ranging from 2.41 × 10^5 (**AdA**) to 2.49 × 10^8 M^{-1} (**Me_6PXDA**) relative to **M1** whose K_a values range from 1.99 × 10^5 (**AdA**) to 7.52 × 10^7 M^{-1} (**Me_6PXDA**). Similarly, the enthalpic contributions to binding are more favorable for **C1** with ΔH values ranging from −7.54 (**AdA**) to −13.47 kcal mol^{-1} (**Me_6PDA**) than for **M1** with ΔH values ranging from −4.11 (**AdA**) to −8.64 kcal mol^{-1} (**Me_6PXDA**). The more favorable enthalpic contributions to binding is likely due to stronger electrostatic interactions between the guest and the sulfate ionic groups. For both **C1** and **M1**, the **Me_6HDA** and **Me_6PXDA** are the strongest binding guests whereas the cyclohexane and adamantane-based guests with a larger cross-sectional area bind 10–100-fold more weakly. The ratio of the binding constants of a common guest to **C1** versus **M1** is as follows: **Me_6PDA** (26.0), **Me_6HDA** (22.2), **PXDA** (4.2), **Me_6PXDA** (3.3), **CHDA** (2.3), **Me_6CHDA** (1.3), **AdA** (1.2), **Me_3AdA** (1.1). The **C1** host is both a tighter and more selective host for the narrower guests than **M1**. We can also tease out the effect of chain length by a comparison of **Me_6PDA** with **Me_6HDA**. We find that the longer and more hydrophobic **Me_6HDA** guest binds 1.92-fold stronger to **C1**; similarly, **Me_6HDA** binds 2.25-fold stronger to **M1**. These differences are likely due to the increased hydrophobicity of the additional CH_2 group. Finally, we can compare the binding of the primary ammonium versus the corresponding quaternary ammonium ion guest toward **C1** and separately **M1**. We find that **C1** binds the quaternary ammoniums somewhat stronger: **Me_6PXDA** vs **PXDA** (1.72-fold), **Me_6CHDA** vs **CHDA** (2.42-fold), **Me_3AdA** vs **AdA** (4.59-fold). A similar trend holds for **M1**: **Me_6PXDA** vs **PXDA** (2.20-fold), **Me_6CHDA** vs **CHDA** (4.30-fold), **Me_3AdA** vs **AdA** (10.50-fold).

Conclusion

In summary, we have designed, synthesized, and characterized a new acyclic CB[*n*]-type receptor **C1** that bears sulfate ionic groups and compared its properties with **M1** which features sulfonate ionic groups. We find that **C1** is much less soluble (4 mM) than **M1** (346 mM) in water. Host **C1** does not undergo self-association in PBS buffer according to ^{1}H NMR dilution experiments. Analysis of complexation-induced changes in chemical shifts establish that the hydrophobic regions of the guests bind within the anisotropic shielding cavity of **C1** whereas the ionic groups reside closer to the ureidyl carbonyl portals of **C1**. Direct and competitive ITC titrations were used to measure the thermodynamic parameters of binding for **C1**·guest and **M1**·guest complexes in PBS solution. Overall, we find that **C1** – with its sulfate ionic groups – binds tighter than **M1** toward each member of the guest panel with largest differences observed for the narrowest **Me_6PDA** (26-fold) and **Me_6HDA** (22.2-fold) guests. Similarly, we find that **C1** binds the quater-

nary ammonium stronger than the corresponding primary ammonium ion guest by 1.72 to 9.59-fold. In conclusion, we find that **C1** displays somewhat enhanced molecular recognition properties than **M1** but possesses less desirable aqueous solubility properties.

Experimental

General experimental details

All chemicals were purchased from commercial suppliers and were used without further purification. Guest molecules were available from previous studies [65,71]. Compounds **TetW1$_{OAc}$** and **TetW1** were prepared according to the literature procedures with slight modifications [70]. NMR spectra were recorded using commercial spectrometers operating at 600 or 400 MHz for ^{1}H and 150 or 100 MHz for ^{13}C. Melting points were measured on a Meltemp apparatus in open capillary tubes and are uncorrected. IR spectra were measured on a Thermo Nicolet NEXUS 670 FT/IR spectrometer by attenuated total reflectance (ATR) and are reported in cm^{-1}. Mass spectrometry was performed using a JEOL AccuTOF electrospray instrument. ITC data was collected on a Malvern Microcal PEAQ-ITC instrument with a cell volume of 200 µL and an injection syringe with a capacity of 40 µL. For ITC experiments, the host and guest solutions were prepared in a 20 mM phosphate-buffered water (pH 7.4). The sample cell was filled (200 µL) with the host solution and the guest solution was titrated (first injection = 0.4 µL, subsequent 18 injections = 2 µL) into the cell. All ITC experiments were analyzed using the MicroCal PEAQ-ITC data analysis software.

Compound **C1**

A mixture of **TetW1** (0.430 g, 0.376 mmol) and pyridine sulfur trioxide (1.1838 g, 7.437 mmol) was dissolved in dry pyridine (57 mL). The resulting mixture was heated at 90 °C under N_2 for 18 h and then cooled to rt. The precipitate was collected by first decanting some of the solvent and then the remaining mixture was transferred to a 50 mL centrifuge tube and centrifuged (7200 rpm, 5 min). The supernatant was carefully poured off. Next, the crude solid was dissolved in 1 M NaOH (25 mL) which results in a yellow and then red solution. Afterwards, EtOH (144 mL) was added which gave a white precipitate that was collected by centrifugation (7200 rpm, 10 min). The crude solid was analyzed by ^{1}H NMR which showed residual pyridine. The crude solid was subsequently dissolved in water (150 mL) and re-precipitated by the addition of EtOH (144 mL) followed by centrifugation (7200 rpm, 5 min) to obtain a white solid. The solid was dried overnight under high vacuum to yield **C1** as a white solid (0.3444 g, 68% yield). Mp > 300 °C; IR (ATR, cm^{-1}): 3456 (w), 1720 (m), 1472 (m), 1378 (w), 1226 (m), 1101 (s), 1023 (m), 972 (w), 790 (w); ^{1}H NMR (400 MHz, D_2O) 6.71 (s, 4H), 5.67 (d, J = 15.4 Hz, 2H), 5.57 (d, J = 15.8 Hz, 4H), 5.46 (d, J = 8.9 Hz, 2H), 5.42 (d, J = 8.9 Hz, 2H), 5.41 (d, J = 16.3 Hz, 4H), 4.45–4.40 (m, 4H), 4.35–4.30 (m, 4H), 4.27 (d, J = 15.8 Hz, 2 × 4H), 4.25–4.18 (m, 4H), 4.18–4.13 (m, 4H), 4.12 (d, J = 15.4 Hz, 2H), 1.78 (s, 6H), 1.75 (s, 6H); ^{13}C NMR (100 MHz, D_2O/acetone-d_6 6:1 (v:v)) 156.7, 155.9, 150.5, 129.3, 116.1, 78.6, 77.4, 71.2, 69.5, 67.4, 52.5, 48.4, 35.0, 16.3, 15.4 ppm; ESIMS (m/z): 751.13 ([M − 2Na]$^{2-}$), calcd for $[C_{50}H_{56}N_{16}Na_2S_4O_{28}]^{2-}$, 751.1064.

Supporting Information

The X-ray crystal structure of **C1** is deposited with the Cambridge Crystallographic Data Centre (CCDC 2411723).

Supporting Information File 1

Synthesis and characterization of compounds, solubility determination, ^{1}H NMR dilution experiments, ^{1}H NMR and ITC binding studies.
[https://www.beilstein-journals.org/bjoc/content/supplementary/1860-5397-21-55-S1.pdf]

Funding

We thank the National Science Foundation (CHE-1807486) for past financial support. We thank the National Institute of General Medical Sciences of the National Institutes of Health (R35GM153362) for current financial support of this project.

Conflict of Interest

L.I. is co-founder and holds equity in Reversal Therapeutics (National Harbor, Maryland). L.I. holds equity in Clear Scientific (Cambridge, Massachusetts). The other authors declare no competing financial interests.

Author Contributions

Christian Akakpo: investigation; writing – original draft. Peter Y. Zavalij: investigation. Lyle Isaacs: conceptualization; funding acquisition; project administration; resources; supervision; visualization; writing – original draft; writing – review & editing.

ORCID® iDs

Christian Akakpo - https://orcid.org/0000-0002-3870-974X
Peter Y. Zavalij - https://orcid.org/0000-0001-5762-3469
Lyle Isaacs - https://orcid.org/0000-0002-4079-332X

Data Availability Statement

Data generated and analyzed during this study is openly available in Digital Repository at the University of Maryland (UMD DRUM) at https://doi.org/10.13016/4gal-sini.

References

1. Pedersen, C. J. *Angew. Chem., Int. Ed. Engl.* **1988,** *27,* 1021–1027. doi:10.1002/anie.198810211
2. Cram, D. J. *Angew. Chem., Int. Ed. Engl.* **1988,** *27,* 1009–1020. doi:10.1002/anie.198810093
3. Lehn, J.-M. *Angew. Chem., Int. Ed. Engl.* **1988,** *27,* 89–112. doi:10.1002/anie.198800891
4. Anslyn, E. V. *J. Org. Chem.* **2007,** *72,* 687–699. doi:10.1021/jo0617971
5. Kolesnichenko, I. V.; Anslyn, E. V. *Chem. Soc. Rev.* **2017,** *46,* 2385–2390. doi:10.1039/c7cs00078b
6. Aida, T.; Meijer, E. W.; Stupp, S. I. *Science* **2012,** *335,* 813–817. doi:10.1126/science.1205962
7. Stoddart, J. F. *Angew. Chem., Int. Ed.* **2017,** *56,* 11094–11125. doi:10.1002/anie.201703216
8. Borsley, S.; Leigh, D. A.; Roberts, B. M. W. *Angew. Chem., Int. Ed.* **2024,** *63,* e202400495. doi:10.1002/anie.202400495
9. Feringa, B. L. *Angew. Chem., Int. Ed.* **2017,** *56,* 11060–11078. doi:10.1002/anie.201702979
10. Rekharsky, M. V.; Inoue, Y. *Chem. Rev.* **1998,** *98,* 1875–1918. doi:10.1021/cr970015o
11. Gutsche, C. D. *Acc. Chem. Res.* **1983,** *16,* 161–170. doi:10.1021/ar00089a003
12. Dale, E. J.; Vermeulen, N. A.; Juríček, M.; Barnes, J. C.; Young, R. M.; Wasielewski, M. R.; Stoddart, J. F. *Acc. Chem. Res.* **2016,** *49,* 262–273. doi:10.1021/acs.accounts.5b00495
13. Jordan, J. H.; Gibb, B. C. *Chem. Soc. Rev.* **2015,** *44,* 547–585. doi:10.1039/c4cs00191e
14. Diederich, F. *Angew. Chem., Int. Ed. Engl.* **1988,** *27,* 362–386. doi:10.1002/anie.198803621
15. Rebek, J., Jr. *Acc. Chem. Res.* **2009,** *42,* 1660–1668. doi:10.1021/ar9001203
16. Ogoshi, T.; Yamagishi, T.-a.; Nakamoto, Y. *Chem. Rev.* **2016,** *116,* 7937–8002. doi:10.1021/acs.chemrev.5b00765
17. Xue, M.; Yang, Y.; Chi, X.; Zhang, Z.; Huang, F. *Acc. Chem. Res.* **2012,** *45,* 1294–1308. doi:10.1021/ar2003418
18. Wu, J.-R.; Yang, Y.-W. *Chem. Commun.* **2019,** *55,* 1533–1543. doi:10.1039/c8cc09374a
19. Harris, K.; Fujita, D.; Fujita, M. *Chem. Commun.* **2013,** *49,* 6703–6712. doi:10.1039/c3cc43191f
20. Zarra, S.; Wood, D. M.; Roberts, D. A.; Nitschke, J. R. *Chem. Soc. Rev.* **2015,** *44,* 419–432. doi:10.1039/c4cs00165f
21. Febreze.com “Ingredients”. https://www.febreze.com/en-us/ingredients-safety/our-ingredients (accessed March 27, 2025).
22. Meadows, M. K.; Anslyn, E. V. Three Tales of Supramolecular Analytical Chemistry. In *Macrocyclic and Supramolecular Chemistry: How Izatt–Christensen Award Winners Shaped the Field;* Izatt, R. M., Ed.; John Wiley & Sons: Chichester, UK, 2016; pp 92–126. doi:10.1002/9781119053859.ch5
23. Rajewski, R. A.; Stella, V. J. *J. Pharm. Sci.* **1996,** *85,* 1142–1169. doi:10.1021/js960075u
24. Stella, V. J.; Rajewski, R. A. *Pharm. Res.* **1997,** *14,* 556–567. doi:10.1023/a:1012136608249
25. Davis, A. P. *Chem. Soc. Rev.* **2020,** *49,* 2531–2545. doi:10.1039/c9cs00391f
26. Tromans, R. A.; Samanta, S. K.; Chapman, A. M.; Davis, A. P. *Chem. Sci.* **2020,** *11,* 3223–3227. doi:10.1039/c9sc05406e
27. Isaacs, L. *Acc. Chem. Res.* **2014,** *47,* 2052–2062. doi:10.1021/ar500075g
28. Sindelar, V.; Silvi, S.; Kaifer, A. E. *Chem. Commun.* **2006,** 2185–2187. doi:10.1039/b601959e
29. Ko, Y. H.; Kim, E.; Hwang, I.; Kim, K. *Chem. Commun.* **2007,** 1305–1315. doi:10.1039/b615103e
30. del Barrio, J.; Ryan, S. T. J.; Jambrina, P. G.; Rosta, E.; Scherman, O. A. *J. Am. Chem. Soc.* **2016,** *138,* 5745–5748. doi:10.1021/jacs.5b11642
31. Zhang, G.; Emwas, A.-H.; Shahul Hameed, U. F.; Arold, S. T.; Yang, P.; Chen, A.; Xiang, J.-F.; Khashab, N. M. *Chem* **2020,** *6,* 1082–1096. doi:10.1016/j.chempr.2020.03.003
32. Zhang, G.; Lin, W.; Huang, F.; Sessler, J.; Khashab, N. M. *J. Am. Chem. Soc.* **2023,** *145,* 19143–19163. doi:10.1021/jacs.3c06175
33. Ghale, G.; Nau, W. M. *Acc. Chem. Res.* **2014,** *47,* 2150–2159. doi:10.1021/ar500116d
34. Sinn, S.; Biedermann, F. *Isr. J. Chem.* **2018,** *58,* 357–412. doi:10.1002/ijch.201700118
35. Sun, C.; Zhang, H.; Li, S.; Zhang, X.; Cheng, Q.; Ding, Y.; Wang, L.-H.; Wang, R. *ACS Appl. Mater. Interfaces* **2018,** *10,* 25090–25098. doi:10.1021/acsami.8b06598
36. Zou, L.; Braegelman, A. S.; Webber, M. J. *ACS Cent. Sci.* **2019,** *5,* 1035–1043. doi:10.1021/acscentsci.9b00195
37. Walker, S.; Oun, R.; McInnes, F. J.; Wheate, N. J. *Isr. J. Chem.* **2011,** *51,* 616–624. doi:10.1002/ijch.201100033
38. Gu, A.; Wheate, N. J. *J. Inclusion Phenom. Macrocyclic Chem.* **2021,** *100,* 55–69. doi:10.1007/s10847-021-01055-9
39. Sasmal, R.; Das Saha, N.; Pahwa, M.; Rao, S.; Joshi, D.; Inamdar, M. S.; Sheeba, V.; Agasti, S. S. *Anal. Chem. (Washington, DC, U. S.)* **2018,** *90,* 11305–11314. doi:10.1021/acs.analchem.8b01851
40. Sasmal, R.; Som, A.; Kumari, P.; Nair, R. V.; Show, S.; Barge, N. S.; Pahwa, M.; Das Saha, N.; Rao, S.; Vasu, S.; Agarwal, R.; Agasti, S. S. *ACS Cent. Sci.* **2024,** *10,* 1945–1959. doi:10.1021/acscentsci.4c01080
41. Aqdot Limited Home Page, “Odour & VOC Elimination Technology”. https://aqdot.com/our-technology/ (accessed March 27, 2025).
42. Ganapati, S.; Isaacs, L. *Isr. J. Chem.* **2018,** *58,* 250–263. doi:10.1002/ijch.201700098
43. Bauer, D.; Andrae, B.; Gaß, P.; Trenz, D.; Becker, S.; Kubik, S. *Org. Chem. Front.* **2019,** *6,* 1555–1560. doi:10.1039/c9qo00156e
44. Jiang, S.; Lan, S.; Mao, D.; Yang, X.; Shi, K.; Ma, D. *Chem. Commun.* **2018,** *54,* 9486–9489. doi:10.1039/c8cc05552a
45. Wu, Y.; Yang, J.; Zhuang, S.-Y.; Yu, S.-B.; Zong, Y.; Liu, Y.-Y.; Wu, G.; Qi, Q.-Y.; Wang, H.; Tian, J.; Zhou, W.; Ma, D.; Zhang, D.-W.; Li, Z.-T. *J. Med. Chem.* **2024,** *67,* 2176–2187. doi:10.1021/acs.jmedchem.3c02110
46. Zhang, S.; Zhou, C.; Gao, C.; Yang, J.; Liao, X.; Yang, B. *J. Mol. Liq.* **2023,** *390,* 122942. doi:10.1016/j.molliq.2023.122942
47. Zhu, P.; Kong, L.; Zhang, Y.; Liu, Q.; Liao, X.; Song, Y.; Yang, B. *J. Mol. Liq.* **2023,** *372,* 121198. doi:10.1016/j.molliq.2023.121198
48. Peng, W.-C.; Lei, Z.; Lin, Q.-H.; Wu, Y.; Yang, J.-Y.; Wang, H.; Zhou, W.; Zhang, D.-W.; Li, Z.-T.; Ma, D. *ChemPlusChem* **2023,** *88,* e202300465. doi:10.1002/cplu.202300465
49. Feng, K.; Liu, Y.-Y.; Zong, Y.; Lei, Z.; Wu, Y.; Yang, J.; Lin, F.; Qi, Q.-Y.; Li, Q.; Zhuang, S.-Y.; Zhang, J.; Tian, J.; Zhou, W.; Ma, D.; Zhang, D.-W.; Li, Z.-T.; Yu, S.-B. *J. Med. Chem.* **2024,** *67,* 17905–17918. doi:10.1021/acs.jmedchem.4c01960
50. Huo, M.; Song, S.-Q.; Dai, X.-Y.; Li, F.-F.; Hu, Y.-Y.; Liu, Y. *Chem. Sci.* **2024,** *15,* 5163–5173. doi:10.1039/d4sc00160e
51. Stancl, M.; Hodan, M.; Sindelar, V. *Org. Lett.* **2009,** *11,* 4184–4187. doi:10.1021/ol9017886

52. Gilberg, L.; Zhang, B.; Zavalij, P. Y.; Sindelar, V.; Isaacs, L. *Org. Biomol. Chem.* **2015,** *13,* 4041–4050. doi:10.1039/c5ob00184f
53. Ma, D.; Hettiarachchi, G.; Nguyen, D.; Zhang, B.; Wittenberg, J. B.; Zavalij, P. Y.; Briken, V.; Isaacs, L. *Nat. Chem.* **2012,** *4,* 503–510. doi:10.1038/nchem.1326
54. Ma, D.; Zhang, B.; Hoffmann, U.; Sundrup, M. G.; Eikermann, M.; Isaacs, L. *Angew. Chem., Int. Ed.* **2012,** *51,* 11358–11362. doi:10.1002/anie.201206031
55. Hoffmann, U.; Grosse-Sundrup, M.; Eikermann-Haerter, K.; Zaremba, S.; Ayata, C.; Zhang, B.; Ma, D.; Isaacs, L.; Eikermann, M. *Anesthesiology* **2013,** *119,* 317–325. doi:10.1097/aln.0b013e3182910213
56. Haerter, F.; Simons, J. C. P.; Foerster, U.; Moreno Duarte, I.; Diaz-Gil, D.; Ganapati, S.; Eikermann-Haerter, K.; Ayata, C.; Zhang, B.; Blobner, M.; Isaacs, L.; Eikermann, M. *Anesthesiology* **2015,** *123,* 1337–1349. doi:10.1097/aln.0000000000000868
57. Diaz-Gil, D.; Haerter, F.; Falcinelli, S.; Ganapati, S.; Hettiarachchi, G. K.; Simons, J. C. P.; Zhang, B.; Grabitz, S. D.; Moreno Duarte, I.; Cotten, J. F.; Eikermann-Haerter, K.; Deng, H.; Chamberlin, N. L.; Isaacs, L.; Briken, V.; Eikermann, M. *Anesthesiology* **2016,** *125,* 333–345. doi:10.1097/aln.0000000000001199
58. Ganapati, S.; Grabitz, S. D.; Murkli, S.; Scheffenbichler, F.; Rudolph, M. I.; Zavalij, P. Y.; Eikermann, M.; Isaacs, L. *ChemBioChem* **2017,** *18,* 1583–1588. doi:10.1002/cbic.201700289
59. Thevathasan, T.; Grabitz, S. D.; Santer, P.; Rostin, P.; Akeju, O.; Boghosian, J. D.; Gill, M.; Isaacs, L.; Cotten, J. F.; Eikermann, M. *Br. J. Anaesth.* **2020,** *125,* e140–e147. doi:10.1016/j.bja.2020.02.019
60. Brockett, A. T.; Deng, C.; Shuster, M.; Perera, S.; DiMaggio, D.; Cheng, M.; Murkli, S.; Briken, V.; Roesch, M. R.; Isaacs, L. *Chem. – Eur. J.* **2021,** *27,* 17476–17486. doi:10.1002/chem.202102919
61. Mao, D.; Liang, Y.; Liu, Y.; Zhou, X.; Ma, J.; Jiang, B.; Liu, J.; Ma, D. *Angew. Chem., Int. Ed.* **2017,** *56,* 12614–12618. doi:10.1002/anie.201707164
62. Liu, W.; Lu, X.; Meng, Z.; Isaacs, L. *Org. Biomol. Chem.* **2018,** *16,* 6499–6506. doi:10.1039/c8ob01575a
63. Lu, X.; Samanta, S. K.; Zavalij, P. Y.; Isaacs, L. *Angew. Chem., Int. Ed.* **2018,** *57,* 8073–8078. doi:10.1002/anie.201803132
64. Zhang, B.; Isaacs, L. *J. Med. Chem.* **2014,** *57,* 9554–9563. doi:10.1021/jm501276u
65. Murkli, S.; Klemm, J.; King, D.; Zavalij, P. Y.; Isaacs, L. *Chem. – Eur. J.* **2020,** *26,* 15249–15258. doi:10.1002/chem.202002874
66. DiMaggio, D.; Brockett, A. T.; Shuster, M.; Murkli, S.; Zhai, C.; King, D.; O'Dowd, B.; Cheng, M.; Brady, K.; Briken, V.; Roesch, M. R.; Isaacs, L. *ChemMedChem* **2022,** *17,* e202200046. doi:10.1002/cmdc.202200046
67. Brady, K. G.; Gilberg, L.; Sigwalt, D.; Bistany-Riebman, J.; Murkli, S.; Klemm, J.; Kulhánek, P.; Šindelář, V.; Isaacs, L. *Supramol. Chem.* **2020,** *32,* 479–494. doi:10.1080/10610278.2020.1795173
68. Sigwalt, D.; Moncelet, D.; Falcinelli, S.; Mandadapu, V.; Zavalij, P. Y.; Day, A.; Briken, V.; Isaacs, L. *ChemMedChem* **2016,** *11,* 980–989. doi:10.1002/cmdc.201600090
69. Lu, X.; Zebaze Ndendjio, S. A.; Zavalij, P. Y.; Isaacs, L. *Org. Lett.* **2020,** *22,* 4833–4837. doi:10.1021/acs.orglett.0c01637
70. Zhang, B.; Zavalij, P. Y.; Isaacs, L. *Org. Biomol. Chem.* **2014,** *12,* 2413–2422. doi:10.1039/c3ob42603c
71. Xue, W.; Zavalij, P. Y.; Isaacs, L. *Org. Biomol. Chem.* **2019,** *17,* 5561–5569. doi:10.1039/c9ob00906j
72. Barrow, S. J.; Kasera, S.; Rowland, M. J.; del Barrio, J.; Scherman, O. A. *Chem. Rev.* **2015,** *115,* 12320–12406. doi:10.1021/acs.chemrev.5b00341
73. Masson, E.; Ling, X.; Joseph, R.; Kyeremeh-Mensah, L.; Lu, X. *RSC Adv.* **2012,** *2,* 1213–1247. doi:10.1039/c1ra00768h
74. Cao, L.; Šekutor, M.; Zavalij, P. Y.; Mlinarić-Majerski, K.; Glaser, R.; Isaacs, L. *Angew. Chem., Int. Ed.* **2014,** *53,* 988–993. doi:10.1002/anie.201309635
75. Mock, W. L.; Shih, N.-Y. *J. Org. Chem.* **1986,** *51,* 4440–4446. doi:10.1021/jo00373a018
76. Wiseman, T.; Williston, S.; Brandts, J. F.; Lin, L.-N. *Anal. Biochem.* **1989,** *179,* 131–137. doi:10.1016/0003-2697(89)90213-3
77. Broecker, J.; Vargas, C.; Keller, S. *Anal. Biochem.* **2011,** *418,* 307–309. doi:10.1016/j.ab.2011.07.027
78. Velazquez-Campoy, A.; Freire, E. *Nat. Protoc.* **2006,** *1,* 186–191. doi:10.1038/nprot.2006.28

License and Terms

BEILSTEIN JOURNAL OF ORGANIC CHEMISTRY

Dicarboxylate recognition based on ultracycle hosts through cooperative hydrogen bonding and anion–π interactions

Wen-Hui Mi[‡1,2], Teng-Yu Huang[‡1], Xu-Dong Wang[1], Yu-Fei Ao[1,2], Qi-Qiang Wang[*1,2] and De-Xian Wang[*1,2]

Letter

Open Access

Address:
[1]Beijing National Laboratory for Molecular Sciences, CAS Key Laboratory of Molecular Recognition and Function, Institute of Chemistry, Chinese Academy of Sciences, Beijing 100190, China and [2]University of Chinese Academy of Sciences, Beijing 100049, China

Email:
Qi-Qiang Wang[*] - qiqiangw@iccas.ac.cn; De-Xian Wang[*] - dxwang@iccas.ac.cn

* Corresponding author ‡ Equal contributors

Keywords:
anion–π interactions; anion recognition; hydrogen bonding; dicarboxylates; ultracycles

Beilstein J. Org. Chem. **2025,** *21,* 884–889.
https://doi.org/10.3762/bjoc.21.72

Received: 03 March 2025
Accepted: 24 April 2025
Published: 06 May 2025

This article is part of the thematic issue "Novel macrocycles: from synthesis to supramolecular function".

Guest Editor: C. Gaeta

Abstract

The efficient binding of dicarboxylates represents an important yet challenging issue in supramolecular chemistry. In this study, we designed functional ultracycles as hosts to accommodate large organic dicarboxylate anions. These ultracycles were synthesized via a one-pot strategy starting from macrocyclic precursors. Host–dicarboxylate binding was investigated using ^{1}H NMR titrations, revealing that **B4aH** exhibits strong binding affinities toward a series of dicarboxylates, with association constants reaching up to 6896 M^{-1}. The selectivity for heptanedioate (**C7**$^{2-}$) was attributed to cooperative hydrogen bonding, anion–π interactions, and a size-matching effect, as supported by DFT optimizations.

Introduction

Macrocycles containing more than 50 atoms in the macrocyclic skeleton are denoted as ultracycles [1]. These very large macrocycles are prevalent in nature and exhibit unique functions. For instance, the archaeal lipid GDGT-0 enables archaea to thrive in extreme environments [2]; cycloamyloses enhance the stability of drug metabolism [3,4]; cyclic peptides play critical roles in plant or bacterial defenses and as well as animal hormone signaling [5,6]; cyclic proteins exhibit diverse therapeutic functions [7]; and cyclic nucleotides are essential for molecular cloning and hold potential for disease treatment [8]. In contrast, synthetic ultracycles remain relatively unexplored due to the significant synthetic challenges [9-19]. Among these, very large macrocycles constructed from smaller macrocyclic building units are particularly underexplored. Such macrocycle-containing ultracycles are anticipated to exhibit high association efficiency and selectivity for large guests, driven by cooperative effects of their convergent macrocyclic elements.

Dicarboxylates are crucial species in biological system and chemistry [20]. Examples such as malonate, succinate, and

glutarate play key roles in cellular metabolism; they regulate the activity of numerous enzyme receptors, and serve as intermediates in the synthesis of more complex biomolecules [21]. However, excessive consumption or production, as well as insufficient clearance of dicarboxylates, can lead to various health problems [22]. Additionally, dicarboxylates like tartrate, adipate or citrate are widely used as food additives [23,24]. Furthermore, functional materials based on dicarboxylates are expected to play a significant role in future technologies [25]. Therefore, the recognition and detection of dicarboxylates are of great importance. Despite the development of a number of receptors for dicarboxylates [21,26,27], their recognition remains a challenging task due to their strong hydrophilicity (−400 kJ/mol) [28,29], dispersed negative charges at both ends, complex shapes, and flexible conformations. Moreover, the similar carbon skeletons of many dicarboxylates make selective recognition particularly difficult. To address these challenges, we envisioned that ultracycles composed of macrocycles with anion-binding capabilities could serve as suitable hosts for efficient and selective dicarboxylate recognition. In this study, we report the design of ultracycles constructed from functional tetraoxacalix[2]arene[2]triazine submacrocycles. These submacrocycles feature hydroxy groups as hydrogen-bonding (HB) donors on the lower rim, which, in combination with electron-deficient triazines, create cooperative HB and anion–π binding sites to enhance anion binding [30]. The recognition capabilities of these ultracycles toward a range of dicarboxylates were successfully demonstrated.

Results and Discussion

Synthesis and structure

The ultracycles **B4aH**, **B5aH**, and **B6aH** were synthesized following the previously reported procedure [29,31]. A one-pot reaction of submacrocycle **1a** and 2-(benzyloxy)benzene-1,3-diol (**2a**) in the presence of 8.0 equivalents of CsF yielded the ultracycle precursor compounds. Three reorganized products **B4a**, **B5a**, and **B6a** with different ring sizes were isolated. As previously observed, the structural reorganization likely involves the cleavage and re-formation of the dynamic $C_{triazine}$–OAr bonds, and the presence of an excess of base could facilitate the formation of the thermodynamic-favored reorganized products [29,31]. The benzyl groups were subsequently removed under Pd/C and H_2 conditions to afford the target ultracyclic hosts. The synthesized ultracycles were fully characterized by spectrometric and elemental analysis (Scheme 1 and Schemes S1–S3 in Supporting Information File 1).

Single crystals of **B4aH** were obtained by slow vapor diffusion of ethyl ether into an acetonitrile/chloroform 1:1 (v/v) solution of the compound at 4 °C, enabling structural analysis of the ultracycle. As illustrated in Figure 1, the backbone of **B4aH** adopts a Z-like shape with a flexible conformation. The two oxacalix[2]arene[2]triazine subcavities are positioned along the short axis in a staggered face-to-face arrangement, while the glycol chains are oriented along the long axis in the opposite orientations. In packing mode, the submacrocycle units form close contacts through intermolecular hydrogen bonding, C–H···π, and lone pair–π interactions, resulting in a 1D linear assembly.

Anion recognition

With the functional ultracycles in hand, we investigated the binding between the [2 + 2] ultracycle **B4aH**, which contains two electron-deficient cavities, and a series of dicarboxylate anions (**C2**$^{2-}$–**C8**$^{2-}$ as tetrabutylammonium salts) by ^{1}H NMR titration experiments (Figure 2). Taking **C6**$^{2-}$ as an example, when it was added dropwise to a solution of **B4aH**, the aromatic proton H^a exhibited continuous upfield shifts, while H^b initially shifted upfield and then downfield upon the addition of 1.5 equiv of **C6**$^{2-}$ (Figure 2b and Figure S8 in Supporting Information File 1). These chemical shift changes indicate the interaction between the carboxylate heads and the submacrocycles. Additionally, the protons H^d and H^e on the glycol chain showed initial downfield shifts followed by upfield shifts. These discontinuous chemical shift movements suggest the host–dicarboxylate interactions and the simultaneous conformational changes in the host upon guest inclusion. Similar chemical shift changes of **B4aH** were observed for other dicarboxylates, indicating a consistent binding mode across the series (Figure 2b and c and Figures S4–S10 in Supporting Information File 1).

The titration curves (H^a) were analyzed using the Bindfit program [32-34] to determine the binding constants of **B4aH** with guests. A 1:1 binding stoichiometry best fit the titration curves for **C5**$^{2-}$–**C8**$^{2-}$, with binding constants following the order of **C7**$^{2-}$ > **C8**$^{2-}$ ≈ **C6**$^{2-}$ > **C5**$^{2-}$, suggesting a dependence on the length of the dicarboxylates (Figure 2c and d). We proposed that the dicarboxylates interact with each subcavity of **B4aH** through their terminal anionic groups, utilizing cooperative hydrogen bonding and anion–π interactions. The optimal size matching between dicarboxylate and the host cavity, as seen with **C7**$^{2-}$, enhances the synergistic effect between the two subcavities, resulting in a higher binding strength. Dicarboxylates longer or shorter than **C7**$^{2-}$ (e.g., **C8**$^{2-}$, **C6**$^{2-}$, or **C5**$^{2-}$) exhibit weaker binding due to their less-matched host–guest sizes. For the shorter dicarboxylates (**C2**$^{2-}$–**C4**$^{2-}$), the binding behavior is more complex. For instance, the [**B4aH**·**C2**$^{2-}$] complex fits a 1:2 binding model, with two-step binding constants of K_{11} = 259 M^{-1} and K_{12} = 251 M^{-1}, implying that **B4aH** can accommodate two **C2**$^{2-}$ anions as a dimer within its cavity [29]. Malonate (**C3**$^{2-}$) and succinate (**C4**$^{2-}$) exhibited irregular titra-

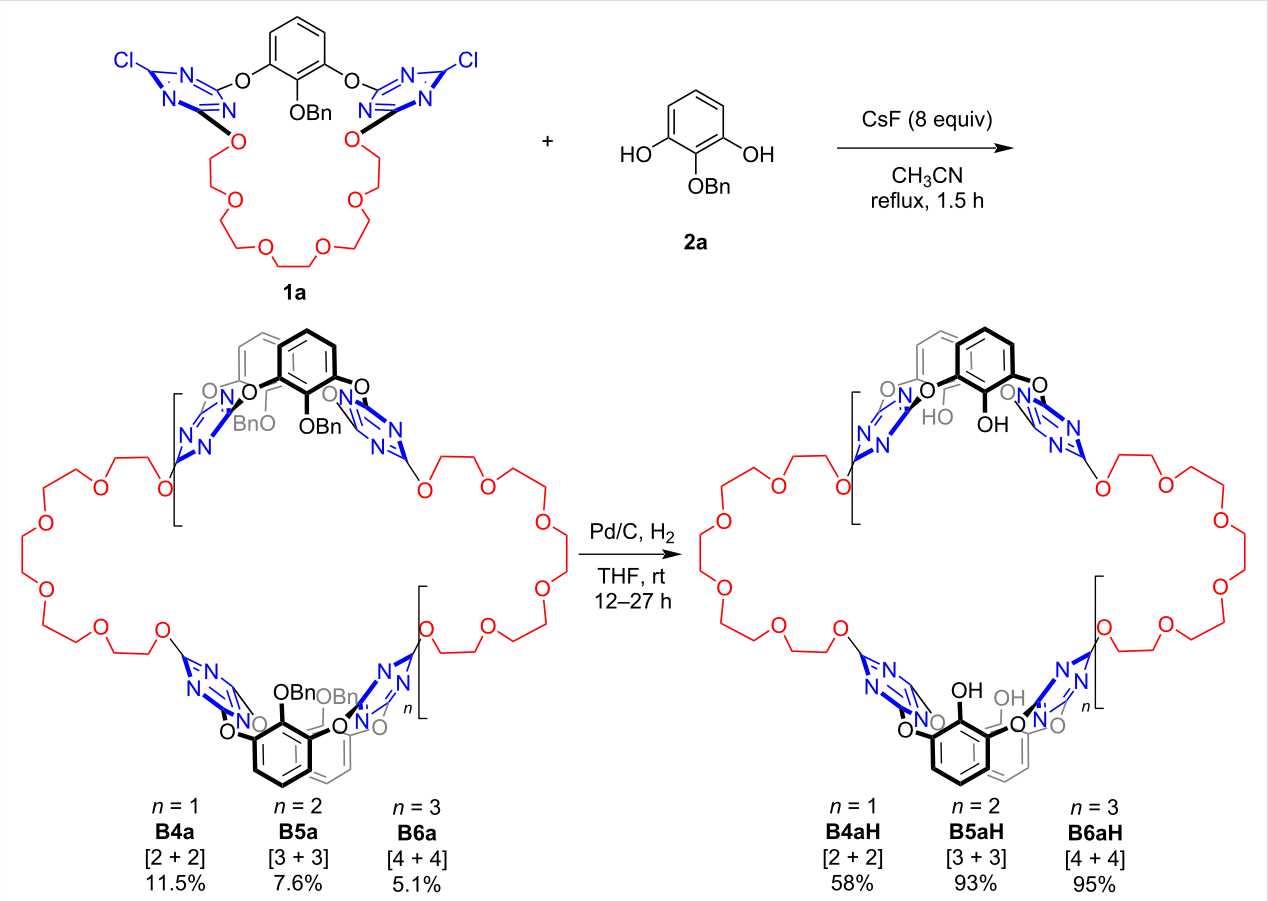

Scheme 1: Synthesis of ultracycles.

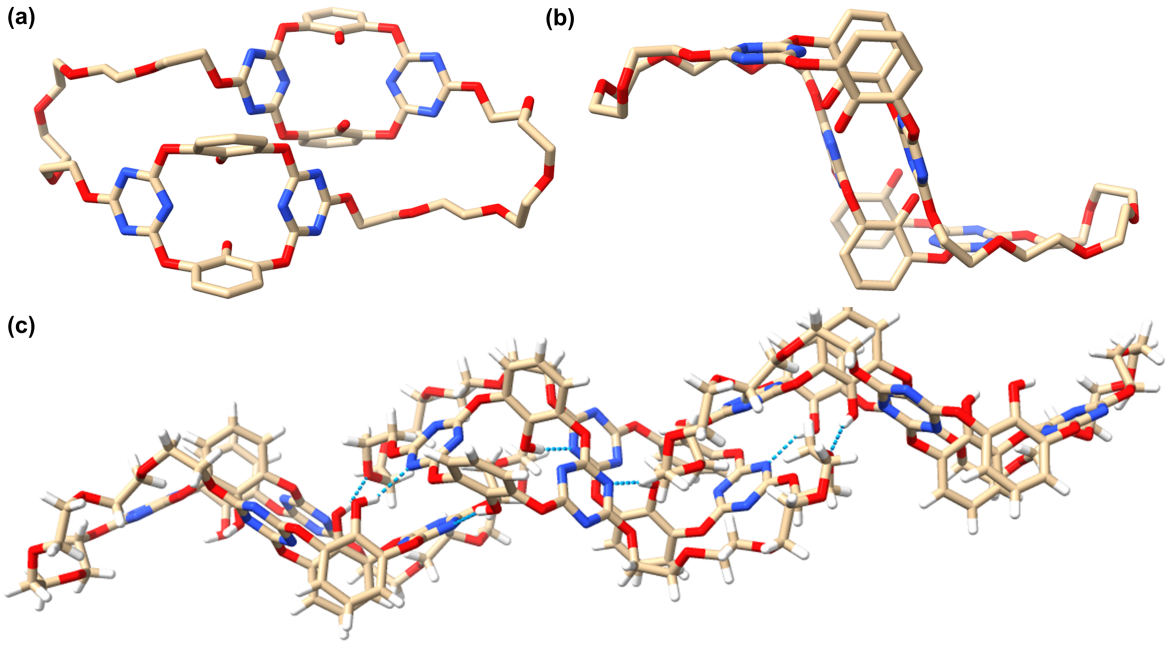

Figure 1: (a, b) Crystal structure of **B4aH** (hydrogen atoms are omitted for clarity), and (c) the stacking structure of the crystal of **B4aH** (the blue dotted lines represent hydrogen bonds).

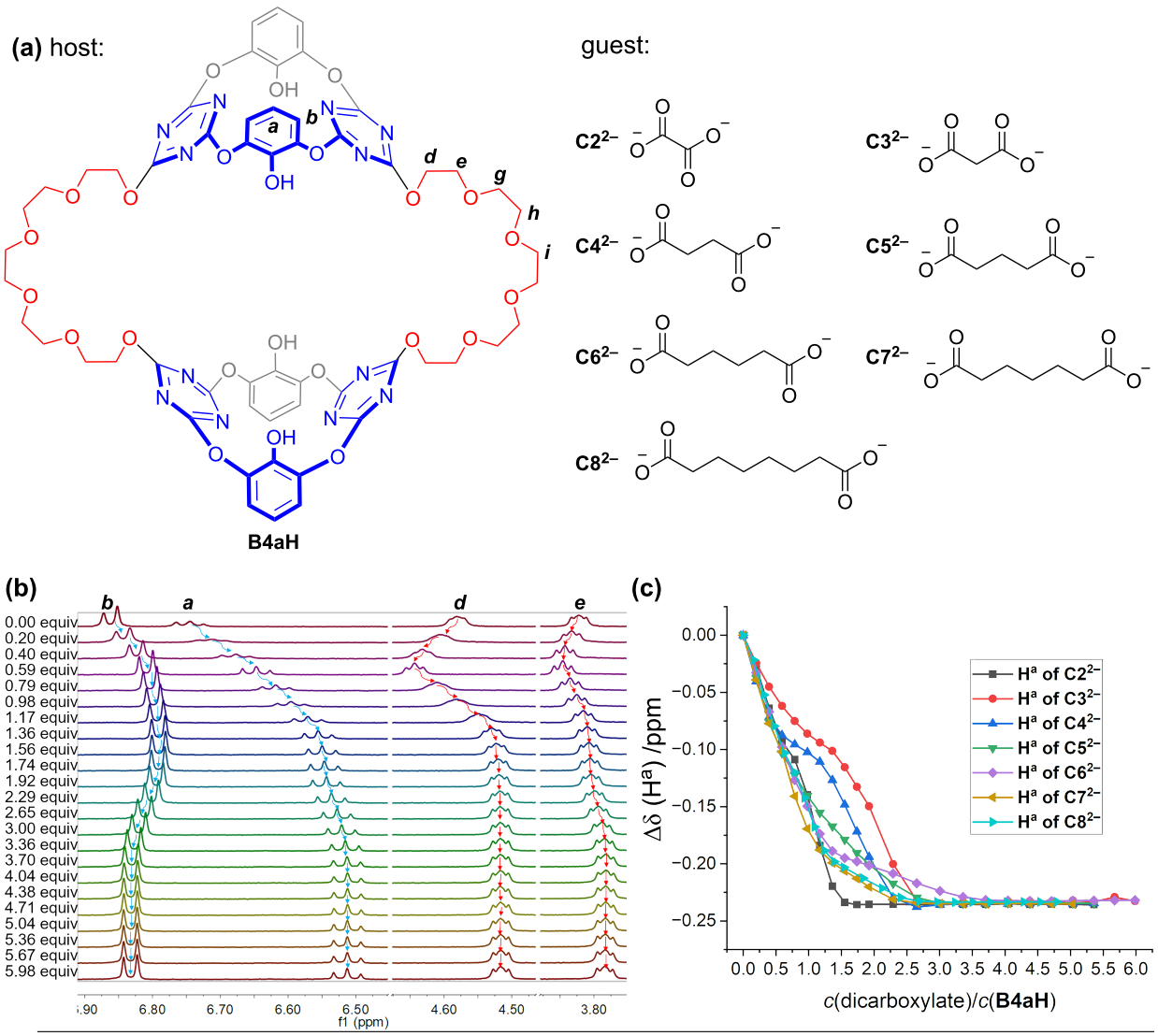

(d)

Guest	$C2^{2-}$	[a]$C3^{2-}$	[a]$C4^{2-}$	$C5^{2-}$	$C6^{2-}$	$C7^{2-}$	$C8^{2-}$
K_{11} (M^{-1})	259	–	–	2853	4455	6896	4423
K_{12} (M^{-1})	251						

[a] no reliable constants were obtained

Figure 2: (a) The structures of host and guests, (b) ^{1}H NMR spectra (298 K, 400 MHz, CD_3CN) of **B4aH** upon titration with $\mathbf{C6^{2-}}$ (*c*(**B4aH**) = 1 mM), (c) chemical shift changes of H^a versus titration equivalents *c*(dicarboxylate)/*c*(**B4aH**), and (d) association constants of host and guests.

tion curves (Figure 2c), and no reliable binding constants could be obtained using either 1:1 or 1:2 binding models. This is likely due to their intermediate size of chain lengths, which are neither long enough for 1:1 binding nor capable of squeezing a dimer for 1:2 complexation. Notably, the unsubstituted ultracycle **B4** [31] without the pendant OH groups on the lower rim, which relies on solely anion–π interactions, showed weak binding affinity for $\mathbf{C6^{2-}}$ (Figure S11 in Supporting Information File 1). This underscores the importance of cooperative hydrogen bonding and anion–π interactions for the efficient dicarboxylate binding.

To visualize the proposed synergistic hydrogen bonding and anion–π interactions between the host and guest, we carried out geometry optimizations using M06-2X at the 6-31G(d) level of theory, taking the [$\mathbf{B4aH{\cdot}C7^{2-}}$] complex as a representative example [35,36]. The optimized structure, shown in Figure 3, reveals a 1:1 complex in which the dicarboxylate $\mathbf{C7^{2-}}$ is

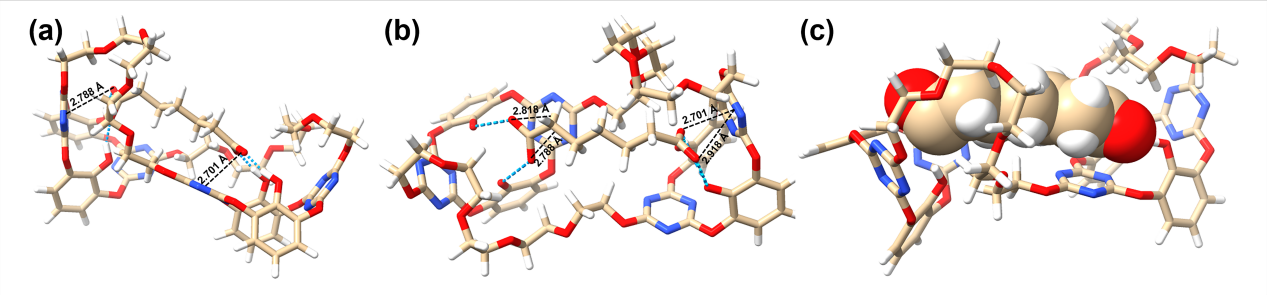

Figure 3: (a–c) DFT-optimized structure of the **B4aH-C7**$^{2-}$ complex. The blue dotted lines represent hydrogen bonds and the black dotted lines represent anion–π interactions.

included within the cavity of **B4aH**. The two subcavities interact synergistically with the included dicarboxylate; the two terminal carboxylate groups are respectively positioned within electron-deficient cavities of the submacrocycles, forming hydrogen bonds (2.49–2.59 Å) with the two hydroxy groups and engaging in anion–π interactions (2.70–2.92 Å) with the triazine rings (Figure 3). Additionally, the glycol arms of the macrocycle may further stabilize the anion binding through van der Waals interactions with the alkyl chains of the dianions. Driven by these multiple noncovalent interactions, the host undergoes conformational adjustments: the distance between the two submacrocycles increases, and the glycol chains adopt extended conformations compared to the structure shown in Figure 1. These results suggest that the experimentally observed strong binding capability and selectivity of **B4aH** for **C7**$^{2-}$ likely arise from cooperative noncovalent interactions and a size-matching effect.

Conclusion

In conclusion, we synthesized a series of hydroxy-substituted ultracycles of varying sizes on the lower-rim using a one-pot cyclization strategy. ^{1}H NMR titration experiments indicate that the introduction of lower-rim hydroxy substituents effectively enhances the dicarboxylate binding through cooperative hydrogen bonding and anion–π interactions. The selective recognition of long and flexible dicarboxylates holds exciting promise for the use of dicarboxylate sensors in medicine and industry.

Supporting Information

Supporting Information File 1

Experimental details and characterization data (including ^{1}H NMR, ^{13}C NMR, IR, and HRMS of precursor compounds and ultracycles, X-ray data for **B4aH**, theoretical calculations, and NMR titration data).
[https://www.beilstein-journals.org/bjoc/content/supplementary/1860-5397-21-72-S1.pdf]

Funding

Financial support from the National Natural Science Foundation of China (Nos. 22171271, 22371285) and Beijing National Laboratory for Molecular Sciences (BNLMS-CXXM-202002) is gratefully acknowledged.

ORCID® iDs

Yu-Fei Ao - https://orcid.org/0000-0002-9415-2181
Qi-Qiang Wang - https://orcid.org/0000-0001-5988-1293
De-Xian Wang - https://orcid.org/0000-0002-9059-5022

Data Availability Statement

All data that supports the findings of this study is available in the published article and/or the supporting information of this article.

References

1. Prautzsch, V.; Ibach, S. *J. Inclusion Phenom. Macrocyclic Chem.* **1999,** *33,* 427–458. doi:10.1023/a:1017193104870
2. Gräther, O.; Arigoni, D. *J. Chem. Soc., Chem. Commun.* **1995,** 405–406. doi:10.1039/c39950000405
3. Fujii, K.; Minagawa, H.; Terada, Y.; Takaha, T.; Kuriki, T.; Shimada, J.; Kaneko, H. *Appl. Environ. Microbiol.* **2005,** *71,* 5823–5827. doi:10.1128/aem.71.10.5823-5827.2005
4. Srisimarat, W.; Powviriyakul, A.; Kaulpiboon, J.; Krusong, K.; Zimmermann, W.; Pongsawasdi, P. *J. Inclusion Phenom. Macrocyclic Chem.* **2011,** *70,* 369–375. doi:10.1007/s10847-010-9890-5
5. Thorstholm, L.; Craik, D. J. *Drug Discovery Today: Technol.* **2012,** *9,* e13–e21. doi:10.1016/j.ddtec.2011.07.005
6. Empting, M. An Introduction to Cyclic Peptides. In *Cyclic Peptides: From Bioorganic Synthesis to Applications;* Koehnke, J.; Naismith, J.; van der Donk, W. A., Eds.; The Royal Society of Chemistry: Cambridge, UK, 2017; pp 1–14. doi:10.1039/9781788010153
7. Conlan, B. F.; Gillon, A. D.; Craik, D. J.; Anderson, M. A. *Pept. Sci.* **2010,** *94,* 573–583. doi:10.1002/bip.21422
8. Li, J.; Mohammed-Elsabagh, M.; Paczkowski, F.; Li, Y. *ChemBioChem* **2020,** *21,* 1547–1566. doi:10.1002/cbic.202000003
9. Ma, C.; Lo, A.; Abdolmaleki, A.; MacLachlan, M. J. *Org. Lett.* **2004,** *6,* 3841–3844. doi:10.1021/ol0483549
10. Kawano, S.-i.; Ishida, Y.; Tanaka, K. *J. Am. Chem. Soc.* **2015,** *137,* 2295–2302. doi:10.1021/ja510585u

11. Gregoliński, J.; Ślepokura, K.; Paćkowski, T.; Panek, J.; Stefanowicz, P.; Lisowski, J. *J. Org. Chem.* **2016,** *81,* 5285–5294. doi:10.1021/acs.joc.6b00531
12. Zhang, Z.-Y.; Li, C. *Acc. Chem. Res.* **2022,** *55,* 916–929. doi:10.1021/acs.accounts.2c00043
13. Moore, J. S.; Zhang, J. *Angew. Chem., Int. Ed. Engl.* **1992,** *31,* 922–924. doi:10.1002/anie.199209221
14. Höger, S.; Enkelmann, V. *Angew. Chem., Int. Ed. Engl.* **1995,** *34,* 2917–2919. doi:10.1002/anie.199527131
15. Itoh, Y.; Chen, S.; Hirahara, R.; Konda, T.; Aoki, T.; Ueda, T.; Shimada, I.; Cannon, J. J.; Shao, C.; Shiomi, J.; Tabata, K. V.; Noji, H.; Sato, K.; Aida, T. *Science* **2022,** *376,* 738–743. doi:10.1126/science.abd0966
16. Zhang, Y.; Wada, T.; Sasabe, H. *Chem. Commun.* **1996,** 621–622. doi:10.1039/cc9960000621
17. Vögtle, F.; Puff, H.; Friedrichs, E.; Müller, W. M. *Angew. Chem., Int. Ed. Engl.* **1982,** *21,* 431. doi:10.1002/anie.198204311
18. Lhoták, P.; Kawaguchi, M.; Ikeda, A.; Shinkai, S. *Tetrahedron* **1996,** *52,* 12399–12408. doi:10.1016/0040-4020(96)00738-7
19. Hoffmann, M.; Kärnbratt, J.; Chang, M.-H.; Herz, L. M.; Albinsson, B.; Anderson, H. L. *Angew. Chem., Int. Ed.* **2008,** *47,* 4993–4996. doi:10.1002/anie.200801188
20. Butler, S. M.; Jolliffe, K. A. *Org. Biomol. Chem.* **2020,** *18,* 8236–8254. doi:10.1039/d0ob01761b
21. Curiel, D.; Más-Montoya, M.; Sánchez, G. *Coord. Chem. Rev.* **2015,** *284,* 19–66. doi:10.1016/j.ccr.2014.09.010
22. Hoppe, B. *Nat. Rev. Nephrol.* **2012,** *8,* 467–475. doi:10.1038/nrneph.2012.113
23. Koo, O. M. Y., Ed. *Pharmaceutical Excipients: Properties, Functionality, and Applications in Research and Industry;* John Wiley & Sons: Hoboken, NJ, USA, 2016. doi:10.1002/9781118992432
24. Hou, M.-L.; Lu, C.-M.; Lin, C.-H.; Lin, L.-C.; Tsai, T.-H. *Molecules* **2016,** *21,* 367. doi:10.3390/molecules21030367
25. Dang, S.; Zhu, Q.-L.; Xu, Q. *Nat. Rev. Mater.* **2018,** *3,* 17075. doi:10.1038/natrevmats.2017.75
26. Wang, Q.-Q.; Day, V. W.; Bowman-James, K. *Chem. Sci.* **2011,** *2,* 1735–1738. doi:10.1039/c1sc00292a
27. Fitzmaurice, R. J.; Kyne, G. M.; Douheret, D.; Kilburn, J. D. *J. Chem. Soc., Perkin Trans. 1* **2002,** 841–864. doi:10.1039/b009041g
28. Marcus, Y. *J. Chem. Soc., Faraday Trans.* **1991,** *87,* 2995–2999. doi:10.1039/ft9918702995
29. Mi, W.-H.; Huang, T.-Y.; Ao, Y.-F.; Wang, X.-D.; Wang, Q.-Q.; Wang, D.-X. *Chin. Chem. Lett.* **2024,** *35,* 109077. doi:10.1016/j.cclet.2023.109077
30. Wang, X.-D.; Li, S.; Ao, Y.-F.; Wang, Q.-Q.; Huang, Z.-T.; Wang, D.-X. *Org. Biomol. Chem.* **2016,** *14,* 330–334. doi:10.1039/c5ob02291f
31. Luo, J.; Ao, Y.-F.; Wang, Q.-Q.; Wang, D.-X. *Angew. Chem., Int. Ed.* **2018,** *57,* 15827–15831. doi:10.1002/anie.201810836
32. *Bindfit,* v0.5; Supramolecular.org, http://supramolecular.org.
33. Thordarson, P. *Chem. Soc. Rev.* **2011,** *40,* 1305–1323. doi:10.1039/c0cs00062k
34. Hibbert, D. B.; Thordarson, P. *Chem. Commun.* **2016,** *52,* 12792–12805. doi:10.1039/c6cc03888c
35. Petersson, G. A.; Bennett, A.; Tensfeldt, T. G.; Al-Laham, M. A.; Shirley, W. A.; Mantzaris, J. *J. Chem. Phys.* **1988,** *89,* 2193–2218. doi:10.1063/1.455064
36. Zhao, Y.; Truhlar, D. G. *Theor. Chem. Acc.* **2008,** *120,* 215–241. doi:10.1007/s00214-007-0310-x

License and Terms

BEILSTEIN JOURNAL OF ORGANIC CHEMISTRY

Selective monoformylation of naphthalene-fused propellanes for methylene-alternating copolymers

Kenichi Kato*[1], Tatsuki Hiroi[1], Seina Okada[1], Shunsuke Ohtani[1] and Tomoki Ogoshi*[1,2]

Full Research Paper

Open Access

Address:
[1]Department of Synthetic Chemistry and Biological Chemistry, Graduate School of Engineering, Kyoto University, Katsura, Nishikyo-ku, Kyoto, 615-8510, Japan and [2]WPI Nano Life Science Institute, Kanazawa University, Kakuma-machi, Kanazawa, 920-1192, Japan

Email:
Kenichi Kato* - katok@sbchem.kyoto-u.ac.jp; Tomoki Ogoshi* - ogoshi@sbchem.kyoto-u.ac.jp

* Corresponding author

Keywords:
alternating copolymer; building block; formylation; gas adsorption; propellane

Beilstein J. Org. Chem. **2025,** *21,* 1183–1191.
https://doi.org/10.3762/bjoc.21.95

Received: 15 April 2025
Accepted: 05 June 2025
Published: 18 June 2025

This article is part of the thematic issue "Novel macrocycles: from synthesis to supramolecular function".

Guest Editor: C. Gaeta

Abstract

Development of three-dimensional (3D) building blocks is a key to change tight molecular assemblies of rigid π-conjugated planes into organic functional materials endowed with molecular-size cavities. To increase the diversity of available 3D building blocks, we herein report electrophilic formylation of naphthalene-fused [3.3.3]- and [4.3.3]propellanes as the first selective single-point functionalization by virtue of through-space electronic communications between the naphthalene units. The propellane skeletons have well-defined 3D structures and moderate flexibility at the same time. Therefore, the monoformyl products are good precursors for soft materials which show molecular-size cavities and require desymmetrized building blocks. As a proof of concept, methylene-alternating copolymers were prepared by reduction to corresponding alcohols followed by acid-mediated condensation. The linear copolymers show good solubility and carbon dioxide adsorption.

Introduction

Combination of sp^2- and sp^3-hybridized atoms in core π-skeletons [1-3] is a key to go beyond common organic functional materials composed of rigid π-conjugated planes and flexible peripheral substituents. Because larger π-conjugated planes mostly display low solubility and dense packing due to the π–π stacking and CH–π interactions, surrounding alkyl and other flexible moieties are widely adopted to improve the solubility and modulate the molecular assemblies [4-9]. By contrast, the presence of sp^3-hybridized atoms in core π-skeletons can lead to three-dimensional (3D) structures with appropriate rigidity, thereby giving macrocyclic arenes [10,11], molecule-based cages and frameworks [12-19], polymers of intrinsic microporosity [20-24], and so forth. Characteristically, they possess molecular-size cavities, which contribute to intricate molecular recognition [25], confined spaces for reactions [26], and small-molecule storage and transport [27-29]. Further progress in such

unique organic materials largely depends on the exploitation of 3D π-building blocks. However, the variety of building blocks are limited to a few families such as tetraphenylmethane and triptycene [30-39].

Widespread use of 3D π-skeletons requires not only efficient construction of the skeletons but also functionalization with precise control of substitution numbers and positions. Along this line, fully π-fused [4.4.4]- and [3.3.3]propellanes [40-43] were able to be brominated and nitrated at six positions while retaining molecular symmetry (Figure 1) [44-46]. One functional group was selectively introduced to each naphthalene ring of fully π-fused [4.3.3]- and [3.3.3]propellane, **[4.3.3]** and **[3.3.3]**, respectively [47-55]. In this work, we report the introduction of a single functional group to a whole skeleton of **[4.3.3]** and **[3.3.3]**, using formylation [55,56]. The reaction is

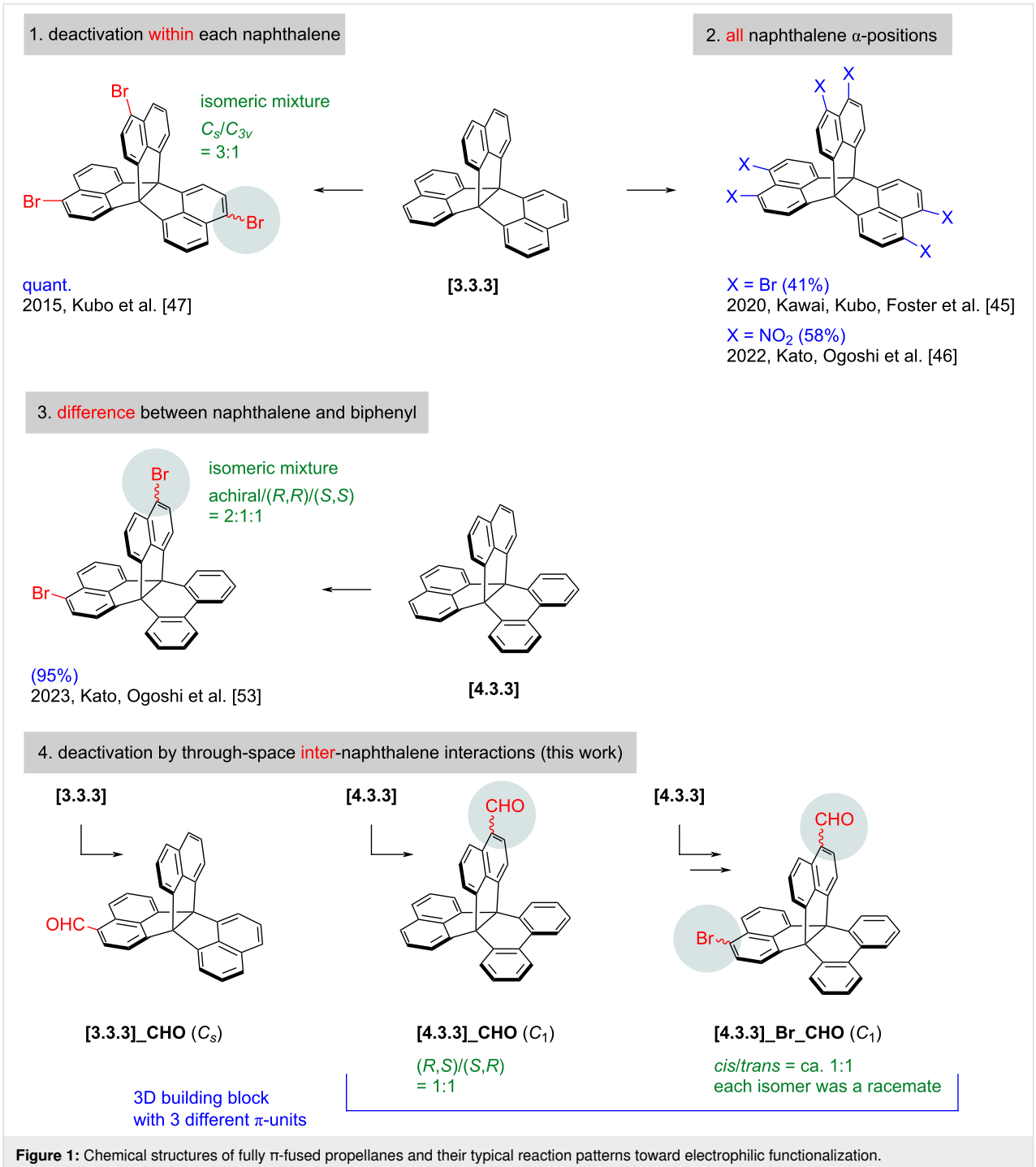

Figure 1: Chemical structures of fully π-fused propellanes and their typical reaction patterns toward electrophilic functionalization.

electrophilic, and the substrates are effectively deactivated toward further reactions upon introduction of an electron-withdrawing formyl group because of through-space electronic interactions between the naphthalene units. The monoformyl products are reduced to corresponding alcohols, which are then reacted under Friedel–Crafts conditions. Amorphous methylene-alternating copolymers are obtained without particular macrocyclic oligomers. Due to the 3D components, the linear copolymers display good solubility in $CHCl_3$ and THF and adsorption properties for CO_2 gas.

Results and Discussion

Selective monoformylation

Initially, we tried introducing formyl groups into a fully π-fused [4.3.3]propellane via organometal species, which had been effective for functional π-extended systems [57-60]. This scheme also enables control of the number of formyl groups by starting materials and reagents. Brominated [4.3.3]propellane was reacted with *n*-BuLi or iPrMgCl·LiCl to generate an organometal species, which was quenched with *N*,*N*-dimethylformamide (DMF) as an electrophile (Table S201 in Supporting Information File 1). Despite several trials, the reactions led to complicated mixtures owing to decomposition and debromination or predominant recovery of the starting material, respectively.

Then, we turned our attention to electrophilic formylation. Vilsmeier–Haack [61] and Duff [62] reactions led to recovery of starting material or a complicated mixture probably owing to the modestly electron-rich and sterically demanding naphthalene α-positions (Table S202, entries 1–3, Supporting Information File 1). By contrast, a combination of dichloromethyl methyl ether and $TiCl_4$ (Rieche reaction) [55,56,63-66] yielded the monoformyl product **[4.3.3]_CHO**, in a selective manner (Table 1, entry 1). To suppress decomposition in the overnight reaction at room temperature, the reaction time was reduced to 1.5 h, which afforded **[4.3.3]_CHO** in an isolated yield of 80% (Table 1, entry 2). The same protocol was successfully applicable to pristine π-fused [3.3.3]propellane **[3.3.3]**, giving **[3.3.3]_CHO** selectively in 67% yield (Table 1, entry 3).

In electrophilic aromatic substitutions, multifold reactions are possible, and the number of substitution is sometimes difficult to control by tuning reaction temperature and time. Indeed, bromination of **[3.3.3]** and **[4.3.3]** was reported as three/six- and two-fold reactions, respectively [45,47,53]. If the amount of bromine was limited, the resulting nearly random mixtures of brominated compounds would be practically impossible to separate by chromatography on silica gel because of their low polarity and poor solubility in *n*-hexane. On the other hand, nitration of **[3.3.3]** gave solely the six-fold nitrated product due to low solubility of the starting material [46]. The current reaction is the first practical method for the selective monofunctionalization of **[3.3.3]** and **[4.3.3]**, to the best of our knowledge. It is also noteworthy that this reaction further desymmetrized the [4.3.3]propellane skeleton of **[4.3.3]** into a 3D building block bearing three different fused π-units.

Diformylation and computed electronic structures

In the formylation of **[3.3.3]**, diformylated product **[3.3.3]_2CHO** was obtained in 5.1% yield. In expectation of successful multifold formylation, the equivalents of dichloromethyl methyl ether and $TiCl_4$ were doubled (Table 1, entry 4). The yield of **[3.3.3]_2CHO** modestly increased to 25% with a slight decrease in the yield of **[3.3.3]_CHO** (61%). Although further increase of the equivalents and prolonged reaction time may potentially provide better results for **[3.3.3]_2CHO**, we gave up such attempts because of the competing decomposition in these strongly acidic conditions. In the case of **[4.3.3]**, diformylation gave only 1.8% of **[4.3.3]_2CHO** after 1.5 h (Table 1, entry 5), which was consistent with the absence of **[4.3.3]_2CHO** in monoformylation. Due to the low reactivity, the reaction time was elongated to 18 h (Table 1, entry 6). The yield of **[4.3.3]_2CHO** was improved to 9.9%, whereas the yield of **[4.3.3]_CHO** decreased to 33% owing to competing decomposition. As a substrate, a mixture obtained by monobromination of **[4.3.3]** could be used, giving difunctional building block **[4.3.3]_Br_CHO** in 39% yield (Table 1, entry 7). The reaction was highly successful because the bromination gave nearly random 1:2:1 mixtures of **[4.3.3]**, **[4.3.3]_Br** and **[4.3.3]_2Br**.

To gain insight into the different reactivity between **[3.3.3]** and **[4.3.3]**, theoretical calculations were performed at the ωB97X-D/6-31G(d,p) level of theory (Figures S901–S903 in Supporting Information File 1). Although distribution of the highest occupied molecular orbitals (HOMOs) was similarly delocalized to multiple naphthalene units, the energy for **[3.3.3]** (−7.23 eV) was higher than that of **[4.3.3]** (−7.32 eV). Upon formylation, the HOMO energies of **[3.3.3]** and **[4.3.3]** were stabilized to −7.44 eV and −7.55 eV by 0.21 eV and 0.23 eV, respectively. These values correlated well with the observed reactivities and selectivity.

Attempted macrocyclization leading to linear polymers

Formyl groups have diverse reactivities and enable facile condensation, dynamic covalent chemistry, and so on. In this work, we tried the synthesis of cyclic oligomers composed of naphthalene-fused propellanes simply by reduction into the correspond-

Table 1: Formylation of naphthalene-fused propellanes.

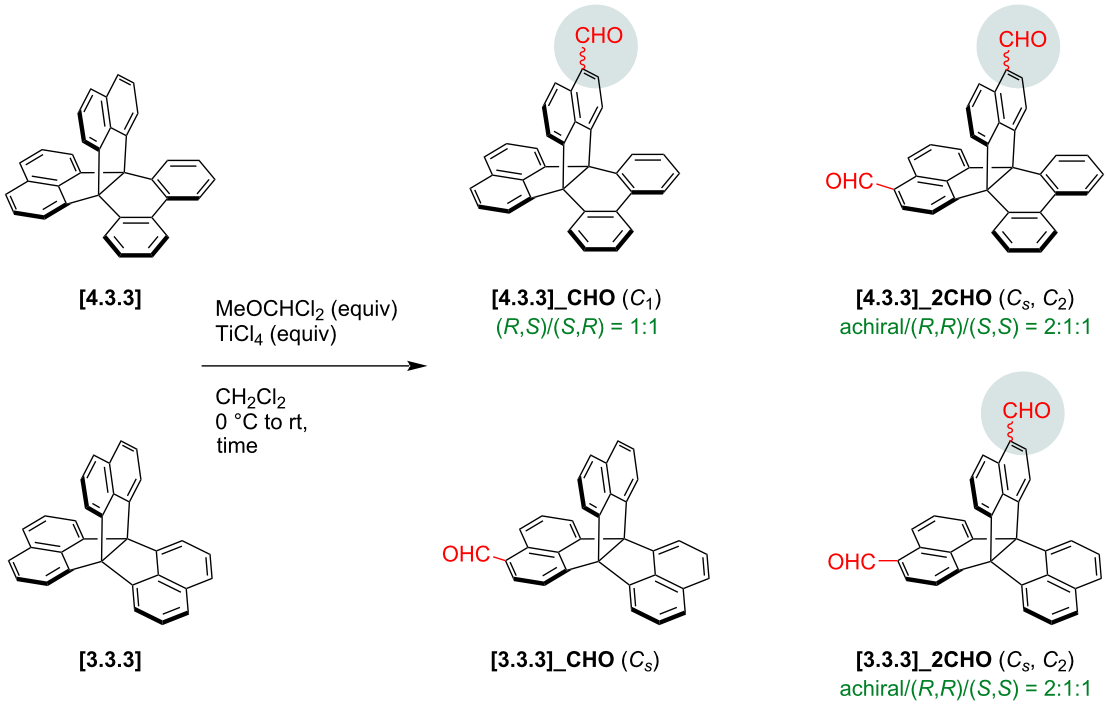

entry	substrate	equiv	time	results
1	**[4.3.3]**	1.25	29 h	**[4.3.3]_CHO** (48%)
2	**[4.3.3]**	1.2	1.5 h	**[4.3.3]_CHO** (80%), **[4.3.3]** (18%)
3	**[3.3.3]**	1.2	1.5 h	**[3.3.3]_CHO** (67%), **[3.3.3]** (12%), **[3.3.3]_2CHO** (5.1%)
4	**[3.3.3]**	2.4	1.5 h	**[3.3.3]_2CHO** (25%), **[3.3.3]_CHO** (61%)
5	**[4.3.3]**	2.4	1.5 h	**[4.3.3]_2CHO** (1.8%), **[4.3.3]_CHO** (56%)
6	**[4.3.3]**	2.4	18 h	**[4.3.3]_2CHO** (9.9%), **[4.3.3]_CHO** (33%)
7[a]	**[4.3.3]_Br**	1.2	18 h	**[4.3.3]_Br_CHO** (39% in 2 steps from **[4.3.3]**)

[a]Substrate was a 1:2:1 mixture of **[4.3.3]**, **[4.3.3]_Br**, and **[4.3.3]_2Br**, obtained by bromination of **[4.3.3]** with 1.03 equiv of Br_2 (Figure S201 in Supporting Information File 1) [53].

ing alcohols followed by acid-mediated Friedel–Crafts-type reactions (Figure 2a and Figure S201 in Supporting Information File 1) [67,68]. Reduction by $NaBH_4$ proceeded well for both monoaldehydes **[4.3.3]_CHO** and **[3.3.3]_CHO** resulting in over 90% yield. Alcohol products, **[4.3.3]_CH_2OH** and **[3.3.3]_CH_2OH**, were then tested in acidic conditions using anhydrous $FeCl_3$ as a Lewis acid. After the reactions, the alcohol proton signals at 1.54–1.58 ppm disappeared in the ^{1}H NMR spectra, and aliphatic carbon ones at 63.1–63.2 ppm were largely up-field-shifted to ca. 34 ppm in the ^{13}C NMR spectra due to conversion into methylene groups (Figure 2b and Figures S315 and S316 in Supporting Information File 1). However, all ^{1}H NMR signals were broad, and gel permeation chromatography (GPC) charts indicated broad patterns due to multiple products with varying molecular weights. These results implied that formation of well-defined cyclic oligomers was quite limited.

To increase the well-defined species, **[4.3.3]_CH_2OH** was separated into two enantiopure fractions (Supporting Information File 1, Figure S505), one of which was used for the acid-mediated reaction. Despite the stereocontrolled substrate, the resonances in the ^{1}H NMR spectrum of the product remained broad. Therefore, we concluded that these systems were difficult to give specific macrocyclic oligomers but instead provided linear polymers composed of fully π-fused propellanes.

After the reactions, each product was separated into oligomer and linear polymer by preparative GPC using $CHCl_3$ as eluent. According to analytical GPC in THF (Figures S501–504 in Supporting Information File 1), oligomer fractions were mainly composed of tetramer for **[3.3.3]_oligo** and dimer and trimer for **[4.3.3]_oligo**. Fractions of linear polymers indicated peak top molecular weights at around octamer for **[3.3.3]_linear** and

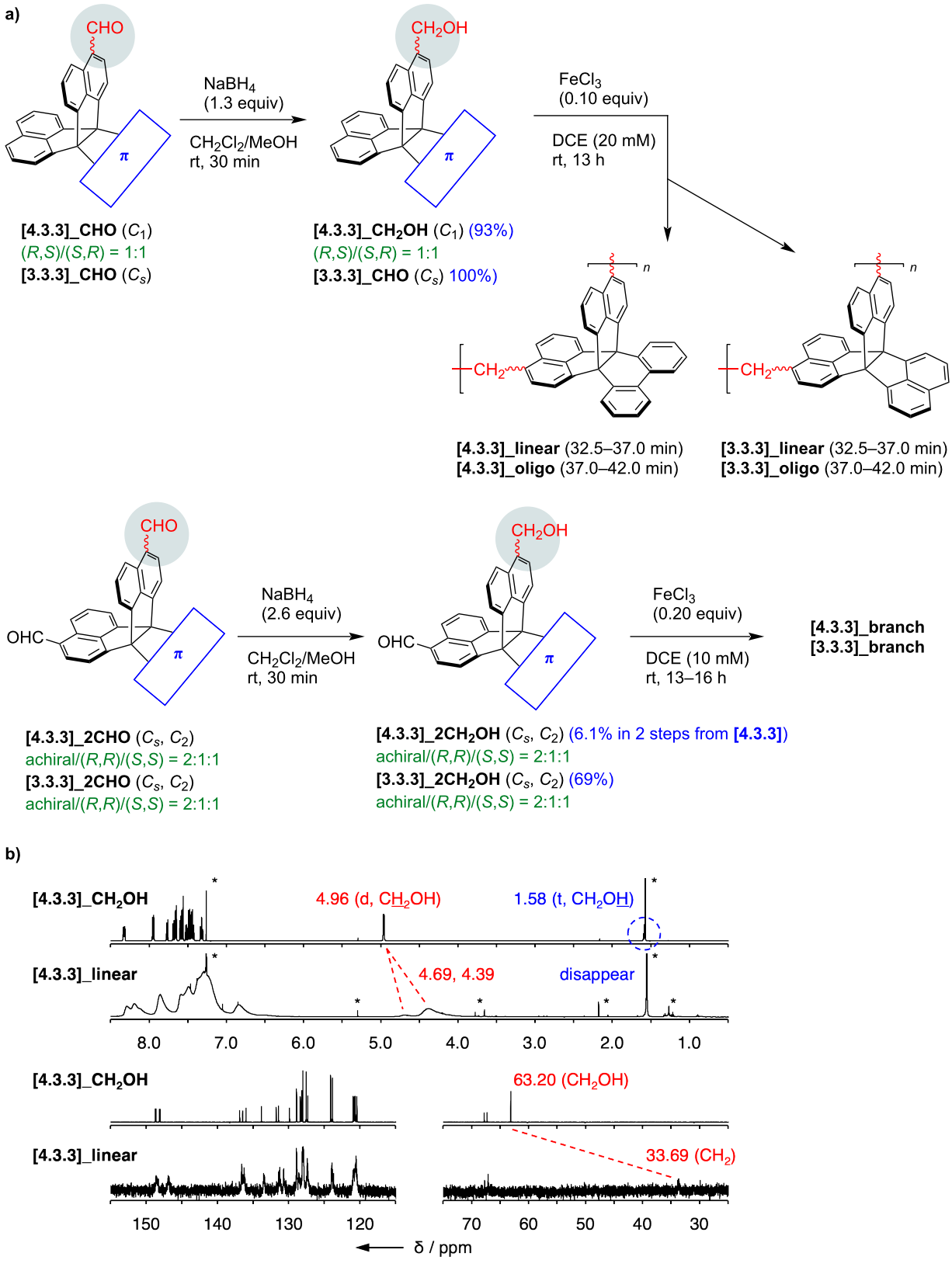

Figure 2: a) Synthesis of methylene-alternating copolymers of fully π-fused propellanes. DCE, 1,2-dichloroethane. b) ^{1}H NMR (500 MHz, top) and ^{13}C (126 MHz, bottom) NMR spectra of **[4.3.3]_CH$_2$OH** and **[4.3.3]_linear** in $CDCl_3$ at room temperature.

Table 2: Properties of methylene-alternating copolymers.[a]

	M_n	M_w	M_w/M_n	T_{90} [°C]	CY [wt %]	V (CO_2) [$cm^3\ g^{-1}$]	S_{BET} [$m^2\ g^{-1}$]
[3.3.3]_oligo	–	–	–	532	76	22	–
[3.3.3]_linear	3.29×10^3	3.79×10^3	1.15	528	68	24	–
[3.3.3]_branch	–	–	–	415	64	18	61
[4.3.3]_oligo	–	–	–	468	47	15	–
[4.3.3]_linear	2.69×10^3	3.16×10^3	1.17	491	46	15	–
[4.3.3]_branch	–	–	–	543	75	29	323

[a]M_n, number-average molar mass; M_w, mass-average molar mass; T_{90}, temperature at which weight loss reaches 10%; CY, carbonization yield; V (CO_2), CO_2 uptake (STP) at 90 kPa; S_{BET}, BET surface area.

pentamer and hexamer for **[4.3.3]_linear** (see also Table 2). In analogy with monoaldehydes, dialdehydes were reduced to dialcohols, **[3.3.3]_2CH$_2$OH** and **[4.3.3]_2CH$_2$OH**, and polymerized in acidic conditions (Figure 2a). Insoluble solids, **[3.3.3]_branch** and **[4.3.3]_branch**, were obtained due to formation of bonding networks and washed repeatedly with CH_2Cl_2, H_2O, and acetone.

Characterization of methylene-alternating copolymers

The thermal stability of the oligomers and polymers were evaluated with thermogravimetric analysis (TGA) (Figure S703 in Supporting Information File 1). Temperatures at which weight loss reached 10% (T_{90}) were 468–491 °C and carbonization yields at 900 °C (CY) were ca. 46 wt % for **[4.3.3]_oligo** and **[4.3.3]_linear**. T_{90} and CY of **[4.3.3]_branch** showed higher values of 543 °C and 75 wt % probably owing to the network structure. By contrast, soluble **[3.3.3]_oligo** and **[3.3.3]_linear** had relatively high T_{90} of 528–532 °C and CY of 68–76 wt %. The high values were ascribed to two unsubstituted naphthalene rings in precursor **[3.3.3]_CH$_2$OH**, which caused facile branching in the reaction or heating process. T_{90} and CY of **[3.3.3]_branch** (415 °C and 64 wt %) were lower than those of **[3.3.3]_linear** because of two-step decay profile (Figure S703a in Supporting Information File 1).

All the samples showed broad powder X-ray diffraction (PXRD) patterns with unclear peaks at around 2θ = 11° and 20° (Supporting Information File 1, Figure S601) and continuous curves in differential scanning calorimetry (DSC) between −70 and 300 °C (Figures S701 and S702, Supporting Information File 1). The results indicated that the polymers were amorphous while giving relatively high thermal stability toward phase transition and decomposition.

Then, gas adsorption properties [46,69-72] were evaluated after the samples were activated in vacuo at 120 °C (Figure 3 and Figures S801 and S802 in Supporting Information File 1). Their chemical structures did not necessarily contain branched or ladder-type connections, but all of them displayed CO_2 adsorption properties at 298 K probably due to the 3D components. The uptake values at standard temperature and pressure (STP) were 15–29 $cm^3 \cdot g^{-1}$ at 90 kPa. In this series, a sample with higher T_{90} and CY values tended to exhibit a higher adsorption capacity for CO_2. By contrast, the linear oligomers and polymers did not adsorb N_2 gas at 77 K. The adsorption isotherms of branched polymers did not have major IUPAC type-I contributions either, indicating the absence of micropores suitable for N_2 adsorption. The curve for **[3.3.3]_branch** looked like type-II, and that of **[4.3.3]_branch** showed multistep uptake. In the desorption step, both samples retained most of the adsorbed N_2 molecules even at 30 kPa. These observations and slow equilibrium in the adsorption processes suggested that presence of

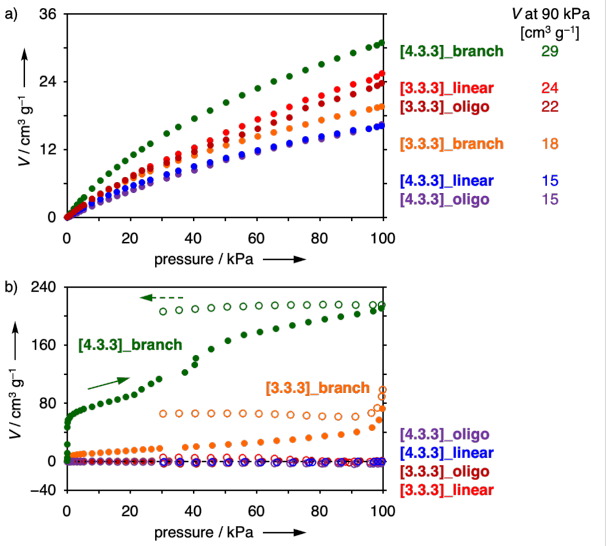

Figure 3: Gas adsorption (filled circles) and desorption (open circles) isotherms of **[3.3.3]_oligo** (dark red), **[3.3.3]_linear** (red), **[3.3.3]_branch** (orange), **[4.3.3]_oligo** (purple), **[4.3.3]_linear** (blue), and **[4.3.3]_branch** (green). a) CO_2 at 298 K and b) N_2 at 77 K.

narrow connections between molecular-size cavities disturbed smooth N_2 adsorption and desorption. Molecular design for uniform microporosity and efficient polymerization is a next challenge.

Conclusion

In this work, we developed formylation on a naphthalene ring in [3.3.3]- and [4.3.3]-type fully π-fused propellanes. High selectivity was achieved for monoformylation on a naphthalene ring. It was reported that bromination proceeded in three- or six-fold manners for a [3.3.3]propellane [45,47-52], and in two-fold one for a [4.3.3]propellane [53,54]. Nitration of the [3.3.3]propellane also yielded an exclusive six-fold product [46]. The current formylation is valuable as the first reliable method for monofunctionalization of naphthalene-fused propellanes without giving inseparable mixtures with multi-functionalized products. Due to the wide reactivities of the formyl group, the monoformyl propellanes would promote new research domains on non-branched linear polymers, macrocyclic compounds, and molecular assemblies that incorporate propellanes as key 3D components. As a proof of concept, the formylated products were reduced to the corresponding alcohols and polymerized in acidic conditions. Although the degrees of polymerization were not high, the methylene-alternating copolymers displayed gas adsorption properties. Further studies are underway towards novel functional materials containing fully π-fused propellanes as flexible 3D building blocks.

Supporting Information

Supporting information includes general information, synthetic procedures and compound data, NMR and MS spectra, HPLC charts, and results of PXRD, DSC, TGA, gas adsorption, and theoretical calculations.

Supporting Information File 1

Experimental.
[https://www.beilstein-journals.org/bjoc/content/supplementary/1860-5397-21-95-S1.pdf]

Acknowledgements

The authors acknowledge Dr. Takeshi Yamamoto and Prof. Dr. Michinori Suginome of Kyoto University for PXRD measurement.

Funding

This work was supported by JSPS KAKENHI Grant Numbers JP21K14611 (Early-Career Scientists, K.K.), JP23H04027 (Transformative Research Areas (A), K.K.), JP25K18019 (Early-Career Scientists, K.K.), and JP22H00334 and JP25H00896 (Scientific Research (A), T.O.), and MEXT World Premier International Research Center Initiative (WPI), Japan. K.K. acknowledge Tokuyama Science Foundation and Yazaki Memorial Foundation for Science and Technology.

Author Contributions

Kenichi Kato: conceptualization; funding acquisition; investigation; methodology; visualization; writing – original draft; writing – review & editing. Tatsuki Hiroi: investigation; writing – review & editing. Seina Okada: investigation; writing – review & editing. Shunsuke Ohtani: writing – review & editing. Tomoki Ogoshi: funding acquisition; project administration; supervision; writing – review & editing.

ORCID® iDs

Kenichi Kato - https://orcid.org/0000-0001-5348-5521

Data Availability Statement

The data that supports the findings of this study is available in the supporting information of this article. Further data generated and analyzed during this study is available from the corresponding author upon reasonable request.

Preprint

A non-peer-reviewed version of this article has been previously published as a preprint: https://doi.org/10.3762/bxiv.2025.23.v1

References

1. Seiki, N.; Shoji, Y.; Kajitani, T.; Ishiwari, F.; Kosaka, A.; Hikima, T.; Takata, M.; Someya, T.; Fukushima, T. *Science* **2015,** *348,* 1122–1126. doi:10.1126/science.aab1391
2. Ma, T.; Kapustin, E. A.; Yin, S. X.; Liang, L.; Zhou, Z.; Niu, J.; Li, L.-H.; Wang, Y.; Su, J.; Li, J.; Wang, X.; Wang, W. D.; Wang, W.; Sun, J.; Yaghi, O. M. *Science* **2018,** *361,* 48–52. doi:10.1126/science.aat7679
3. Koner, K.; Karak, S.; Kandambeth, S.; Karak, S.; Thomas, N.; Leanza, L.; Perego, C.; Pesce, L.; Capelli, R.; Moun, M.; Bhakar, M.; Ajithkumar, T. G.; Pavan, G. M.; Banerjee, R. *Nat. Chem.* **2022,** *14,* 507–514. doi:10.1038/s41557-022-00908-1
4. Rehahn, M.; Schlüter, A.-D.; Wegner, G.; Feast, W. J. *Polymer* **1989,** *30,* 1054–1059. doi:10.1016/0032-3861(89)90078-5
5. Rehahn, M.; Schlüter, A.-D.; Wegner, G.; Feast, W. J. *Polymer* **1989,** *30,* 1060–1062. doi:10.1016/0032-3861(89)90079-7
6. Remmers, M.; Müller, B.; Martin, K.; Räder, H.-J.; Köhler, W. *Macromolecules* **1999,** *32,* 1073–1079. doi:10.1021/ma981260s
7. Tsuda, A.; Osuka, A. *Science* **2001,** *293,* 79–82. doi:10.1126/science.1059552
8. Aratani, N.; Takagi, A.; Yanagawa, Y.; Matsumoto, T.; Kawai, T.; Yoon, Z. S.; Kim, D.; Osuka, A. *Chem. – Eur. J.* **2005,** *11,* 3389–3404. doi:10.1002/chem.200401306
9. Rieger, R.; Müllen, K. *J. Phys. Org. Chem.* **2010,** *23,* 315–325. doi:10.1002/poc.1644
10. Liu, Z.; Nalluri, S. K. M.; Stoddart, J. F. *Chem. Soc. Rev.* **2017,** *46,* 2459–2478. doi:10.1039/c7cs00185a
11. Han, X.-N.; Han, Y.; Chen, C.-F. *Chem. Soc. Rev.* **2023,** *52,* 3265–3298. doi:10.1039/d3cs00002h

12. Little, M. A.; Cooper, A. I. *Adv. Funct. Mater.* **2020,** *30,* 1909842. doi:10.1002/adfm.201909842
13. Zhang, G.; Hua, B.; Dey, A.; Ghosh, M.; Moosa, B. A.; Khashab, N. M. *Acc. Chem. Res.* **2021,** *54,* 155–168. doi:10.1021/acs.accounts.0c00582
14. El-Kaderi, H. M.; Hunt, J. R.; Mendoza-Cortes, J. L.; Côte, A. P.; Taylor, R. E.; O'Keeffe, M.; Yaghi, O. M. *Science* **2007,** *316,* 268–272. doi:10.1126/science.1139915
15. Geng, K.; He, T.; Liu, R.; Dalapati, S.; Tan, K. T.; Li, Z.; Tao, S.; Gong, Y.; Jiang, Q.; Jiang, D. *Chem. Rev.* **2020,** *120,* 8814–8933. doi:10.1021/acs.chemrev.9b00550
16. Tian, Y.; Zhu, G. *Chem. Rev.* **2020,** *120,* 8934–8986. doi:10.1021/acs.chemrev.9b00687
17. Hisaki, I.; Xin, C.; Takahashi, K.; Nakamura, T. *Angew. Chem., Int. Ed.* **2019,** *58,* 11160–11170. doi:10.1002/anie.201902147
18. Li, Z.-T.; Yu, S.-B.; Liu, Y.; Tian, J.; Zhang, D.-W. *Acc. Chem. Res.* **2022,** *55,* 2316–2325. doi:10.1021/acs.accounts.2c00335
19. Ami, T.; Oka, K.; Tsuchiya, K.; Tohnai, N. *Angew. Chem., Int. Ed.* **2022,** *61,* e202202597. doi:10.1002/anie.202202597
20. Budd, P. M.; Ghanem, B. S.; Makhseed, S.; McKeown, N. B.; Msayib, K. J.; Tattershall, C. E. *Chem. Commun.* **2004,** 230–231. doi:10.1039/b311764b
21. Budd, P. M.; Elabas, E. S.; Ghanem, B. S.; Makhseed, S.; McKeown, N. B.; Msayib, K. J.; Tattershall, C. E.; Wang, D. *Adv. Mater. (Weinheim, Ger.)* **2004,** *16,* 456–459. doi:10.1002/adma.200306053
22. Budd, P. M.; McKeown, N. B.; Fritsch, D. *J. Mater. Chem.* **2005,** *15,* 1977–1986. doi:10.1039/b417402j
23. Carta, M.; Malpass-Evans, R.; Croad, M.; Rogan, Y.; Jansen, J. C.; Bernardo, P.; Bazzarelli, F.; McKeown, N. B. *Science* **2013,** *339,* 303–307. doi:10.1126/science.1228032
24. Ghanem, B. S.; Swaidan, R.; Litwiller, E.; Pinnau, I. *Adv. Mater. (Weinheim, Ger.)* **2014,** *26,* 3688–3692. doi:10.1002/adma.201306229
25. Guo, C.; Sedgwick, A. C.; Hirao, T.; Sessler, J. L. *Coord. Chem. Rev.* **2021,** *427,* 213560. doi:10.1016/j.ccr.2020.213560
26. Grommet, A. B.; Feller, M.; Klajn, R. *Nat. Nanotechnol.* **2020,** *15,* 256–271. doi:10.1038/s41565-020-0652-2
27. Zou, L.; Sun, Y.; Che, S.; Yang, X.; Wang, X.; Bosch, M.; Wang, Q.; Li, H.; Smith, M.; Yuan, S.; Perry, Z.; Zhou, H.-C. *Adv. Mater. (Weinheim, Ger.)* **2017,** *29,* 1700229. doi:10.1002/adma.201700229
28. Huang, T.; Alyami, M.; Kashab, N. M.; Nunes, S. P. *J. Mater. Chem. A* **2021,** *9,* 18102–18128. doi:10.1039/d1ta02982g
29. Zhang, R.; Daglar, H.; Tang, C.; Li, P.; Feng, L.; Han, H.; Wu, G.; Limketkai, B. N.; Wu, Y.; Yang, S.; Chen, A. X.-Y.; Stern, C. L.; Malliakas, C. D.; Snurr, R. Q.; Stoddart, J. F. *Nat. Chem.* **2024,** *16,* 1982–1988. doi:10.1038/s41557-024-01622-w
30. Bezzu, C. G.; Carta, M.; Tonkins, A.; Jansen, J. C.; Bernardo, P.; Bazzarelli, F.; McKeown, N. B. *Adv. Mater. (Weinheim, Ger.)* **2012,** *24,* 5930–5933. doi:10.1002/adma.201202393
31. Zhu, K.; Kamochi, K.; Kodama, T.; Tobisu, M.; Amaya, T. *Chem. Sci.* **2020,** *11,* 9604–9610. doi:10.1039/d0sc02452j
32. Park, J.; Kim, J.; Yun, H.-S.; Paik, M. J.; Noh, E.; Mun, H. J.; Kim, M. G.; Shin, T. J.; Seok, S. I. *Nature* **2023,** *616,* 724–730. doi:10.1038/s41586-023-05825-y
33. Chen, Y.; Xu, J.; Gao, P. *Org. Chem. Front.* **2024,** *11,* 508–539. doi:10.1039/d3qo01735d
34. Okubo, K.; Oka, K.; Tsuchiya, K.; Tomimoto, A.; Tohnai, N. *Angew. Chem., Int. Ed.* **2024,** *63,* e202400475. doi:10.1002/anie.202400475
35. Swager, T. M. *Acc. Chem. Res.* **2008,** *41,* 1181–1189. doi:10.1021/ar800107v
36. Chong, J. H.; MacLachlan, M. J. *Chem. Soc. Rev.* **2009,** *38,* 3301–3315. doi:10.1039/b900754g
37. Zhao, L.; Li, Z.; Wirth, T. *Chem. Lett.* **2010,** *39,* 658–667. doi:10.1246/cl.2010.658
38. Chen, C.-F.; Han, Y. *Acc. Chem. Res.* **2018,** *51,* 2093–2106. doi:10.1021/acs.accounts.8b00268
39. Ueberricke, L.; Mastalerz, M. *Chem. Rec.* **2021,** *21,* 558–573. doi:10.1002/tcr.202000161
40. Wittig, G.; Schoch, W. *Justus Liebigs Ann. Chem.* **1971,** *749,* 38–48. doi:10.1002/jlac.19717490106
41. Dyker, G.; Körning, J.; Jones, P. G.; Bubenitschek, P. *Angew. Chem., Int. Ed. Engl.* **1993,** *32,* 1733–1735. doi:10.1002/anie.199317331
42. Dyker, G.; Körning, J.; Bubenitschek, P.; Jones, P. G. *Liebigs Ann./Recl.* **1997,** 203–209. doi:10.1002/jlac.199719970129
43. Hackfort, T.; Kuck, D. *Eur. J. Org. Chem.* **1999,** 2867–2878. doi:10.1002/(sici)1099-0690(199911)1999:11<2867::aid-ejoc2867>3.0.co;2-b
44. Debroy, P.; Lindeman, S. V.; Rathore, R. *Org. Lett.* **2007,** *9,* 4091–4094. doi:10.1021/ol7015466
45. Kawai, S.; Krejčí, O.; Nishiuchi, T.; Sahara, K.; Kodama, T.; Pawlak, R.; Meyer, E.; Kubo, T.; Foster, A. S. *Sci. Adv.* **2020,** *6,* eaay8913. doi:10.1126/sciadv.aay8913
46. Kato, K.; Seto, N.; Chida, K.; Yoshii, T.; Mizuno, M.; Nishihara, H.; Ohtani, S.; Ogoshi, T. *Bull. Chem. Soc. Jpn.* **2022,** *95,* 1296–1302. doi:10.1246/bcsj.20220180
47. Kubo, T.; Miyazaki, S.; Kodama, T.; Aoba, M.; Hirao, Y.; Kurata, H. *Chem. Commun.* **2015,** *51,* 3801–3803. doi:10.1039/c4cc09883h
48. Kodama, T.; Hirao, Y.; Nishiuchi, T.; Kubo, T. *ChemPlusChem* **2017,** *82,* 1006–1009. doi:10.1002/cplu.201700045
49. Kodama, T.; Miyazaki, S.; Kubo, T. *ChemPlusChem* **2019,** *84,* 599–602. doi:10.1002/cplu.201800614
50. Lv, L.; Roberts, J.; Xiao, C.; Jia, Z.; Jiang, W.; Zhang, G.; Risko, C.; Zhang, L. *Chem. Sci.* **2019,** *10,* 4951–4958. doi:10.1039/c9sc00849g
51. Lv, L.; Sun, W.; Jia, Z.; Zhang, G.; Wang, F.; Tan, Z.; Zhang, L. *Mater. Chem. Front.* **2020,** *4,* 3539–3545. doi:10.1039/c9qm00668k
52. Kato, K.; Uchida, Y.; Kaneda, T.; Tachibana, T.; Ohtani, S.; Ogoshi, T. *Chem. – Asian J.* **2024,** *19,* e202400080. doi:10.1002/asia.202400080
53. Kato, K.; Tanaka, S.; Seto, N.; Wada, K.; Gon, M.; Fa, S.; Ohtani, S.; Tanaka, K.; Ogoshi, T. *Chem. Commun.* **2023,** *59,* 7080–7083. doi:10.1039/d3cc01809a
54. Kato, K.; Tanaka, K.; Okada, S.; Kaneda, T.; Ohtani, S.; Ogoshi, T. *Chem. – Eur. J.* **2024,** *30,* e202402828. doi:10.1002/chem.202402828
55. Kodama, T.; Aoba, M.; Hirao, Y.; Rivero, S. M.; Casado, J.; Kubo, T. *Angew. Chem., Int. Ed.* **2022,** *61,* e202200688. doi:10.1002/anie.202200688
56. Kodama, T.; Hirao, Y.; Kubo, T. *Precis. Chem.* **2023,** *1,* 183–191. doi:10.1021/prechem.3c00024
57. Fujimoto, K.; Yorimitsu, H.; Osuka, A. *Eur. J. Org. Chem.* **2014,** 4327–4334. doi:10.1002/ejoc.201402391
58. Niko, Y.; Sasaki, S.; Narushima, K.; Sharma, D. K.; Vacha, M.; Konishi, G.-i. *J. Org. Chem.* **2015,** *80,* 10794–10805. doi:10.1021/acs.joc.5b01987
59. Kato, K.; Kim, W.; Kim, D.; Yorimitsu, H.; Osuka, A. *Chem. – Eur. J.* **2016,** *22,* 7041–7045. doi:10.1002/chem.201600473

60. Kato, K.; Furukawa, K.; Osuka, A. *Angew. Chem., Int. Ed.* **2018,** *57,* 9491–9494. doi:10.1002/anie.201804644
61. Vilsmeier, A.; Haack, A. *Ber. Dtsch. Chem. Ges. B* **1927,** *60,* 119–122. doi:10.1002/cber.19270600118
62. Duff, J. C.; Bills, E. J. *J. Chem. Soc.* **1932,** 1987–1988. doi:10.1039/jr9320001987
63. Rieche, A.; Gross, H.; Höft, E. *Chem. Ber.* **1960,** *93,* 88–94. doi:10.1002/cber.19600930115
64. Yamato, T.; Miyazawa, A.; Tashiro, M. *J. Chem. Soc., Perkin Trans. 1* **1993,** 3127–3137. doi:10.1039/p19930003127
65. Unikela, K. S.; Merner, B. L.; Ghasemabadi, P. G.; Warford, C. C.; Qiu, C. S.; Dawe, L. N.; Zhao, Y.; Bodwell, G. J. *Eur. J. Org. Chem.* **2019,** 4546–4560. doi:10.1002/ejoc.201900707
66. Kato, K.; Ohtani, S.; Gon, M.; Tanaka, K.; Ogoshi, T. *Chem. Sci.* **2022,** *13,* 13147–13152. doi:10.1039/d2sc04168e
67. Zhang, G.-W.; Li, P.-F.; Meng, Z.; Wang, H.-X.; Han, Y.; Chen, C.-F. *Angew. Chem., Int. Ed.* **2016,** *55,* 5304–5308. doi:10.1002/anie.201600911
68. Wang, J.-Q.; Li, J.; Zhang, G.-W.; Chen, C.-F. *J. Org. Chem.* **2018,** *83,* 11532–11540. doi:10.1021/acs.joc.8b01437
69. Taylor, R. G. D.; Bezzu, C. G.; Carta, M.; Msayib, K. J.; Walker, J.; Short, R.; Kariuki, B. M.; McKeown, N. B. *Chem. – Eur. J.* **2016,** *22,* 2466–2472. doi:10.1002/chem.201504212
70. Kato, K.; Hiroi, T.; Seto, N.; Ohtani, S.; Ogoshi, T. *Chem. Lett.* **2022,** *51,* 975–977. doi:10.1246/cl.220320
71. Chen, Y.; Zhao, Y.; Zhao, Y.; Chen, X.; Liu, X.; Li, L.; Cao, D.; Wang, S.; Zhang, L. *Angew. Chem., Int. Ed.* **2024,** *63,* e202401706. doi:10.1002/anie.202401706
72. Kato, K.; Okada, S.; Mizuno, M.; Seto, N.; Iwano, R.; Ohtani, S.; Ogoshi, T. *ChemRxiv* **2025**. doi:10.26434/chemrxiv-2025-pkb6x

License and Terms

BEILSTEIN JOURNAL OF ORGANIC CHEMISTRY

3,3'-Linked BINOL macrocycles: optimized synthesis of crown ethers featuring one or two BINOL units

Somayyeh Kheirjou[1], Jan Riebe[1], Maike Thiele[1], Christoph Wölper[2] and Jochen Niemeyer*[1]

Full Research Paper

Open Access

Address:
[1]Faculty of Chemistry (Organic Chemistry) and Center for Nanointegration Duisburg-Essen (CENIDE), University of Duisburg-Essen, 45141 Essen, Germany and [2]Faculty of Chemistry (Inorganic Chemistry), University of Duisburg-Essen, 45141 Essen, Germany

Email:
Jochen Niemeyer* - jochen.niemeyer@uni-due.de

* Corresponding author

Keywords:
BINOL; chirality; crown ethers; macrocycles; supramolecular chemistry

Beilstein J. Org. Chem. **2025,** *21,* 1719–1729.
https://doi.org/10.3762/bjoc.21.134

Received: 15 May 2025
Accepted: 31 July 2025
Published: 28 August 2025

This article is part of the thematic issue "Novel macrocycles: from synthesis to supramolecular function".

Guest Editor: C. Gaeta

Abstract

Chiral macrocycles hold significant importance in various scientific fields due to their unique structural and chemical properties. By controlling their size, shape, and substituents, chiral macrocycles offer a platform for designing and synthesizing highly efficient catalysts, chemosensors, and functional materials. We have recently made strides in developing macrocyclic organocatalysts; however, their synthesis remains challenging. In this work, we aimed to discover a straightforward method for producing a diverse range of chiral macrocycles, thereby enabling further exploration in the field of interlocked and macrocyclic organocatalysts. We successfully established optimized synthetic routes for the synthesis of chiral macrocycles containing one or two stereogenic units, featuring varying ring sizes and substituents (21 examples in total).

Introduction

Crown ethers are at the heart of supramolecular chemistry [1]. Ever since their discovery in 1960, a vast number of different crown ethers has been synthesized and their interactions with guest molecules have been studied. The pioneering works in this area by Cram, Lehn and Pedersen marked the beginning of modern supramolecular chemistry and were honoured with the Nobel Prize in Chemistry in 1987 [2-4]. Soon, it was realized that chiral crown ethers are highly promising host molecules for enantioselective molecular recognition. Different chiral backbones were used for the construction of such chiral crown ethers, especially chiral 1,2-diols such as tartaric acid [5-8], propane-1,2-diol [9-13], cyclohexane-1,2-diol [14], carbohydrates [15], 1,1'-binapthyl-2,2'-diol (BINOL) [16-23] and more [24]. Especially BINOL-based crown ethers proved to be highly useful and were applied for stereoselective molecular recognition [25-27], for catalysis [25,28-31], as stationary

phases for chromatography [32-34], but also as building blocks for incorporation into larger frameworks, such as interlocked molecules [25,35].

In most BINOL-based crown ethers, the macrocycle is attached to the BINOL unit via the oxygens in the 2,2'-positions. This structural motif has been used to construct crown ethers featuring either one or two BINOL units (see Figure 1a) [16-23].

In a related approach, a single BINOL can be equipped with two crown ethers by attaching these via the 2,3 and 2',3'-positions, respectively (see Figure 1b) [36,37]. Less frequently, the 7,7'-positions (see Figure 1c) [38-40] or the 3,3'-positions (see Figure 1d) [41-43] have been used for attaching the crown ether macrocycle, although this strategy has the advantage that the 2,2'-hydroxy groups remain intact and can be used for further binding or functionalization. Our group recently became interested in synthesizing BINOL derivatives featuring macrocyclic

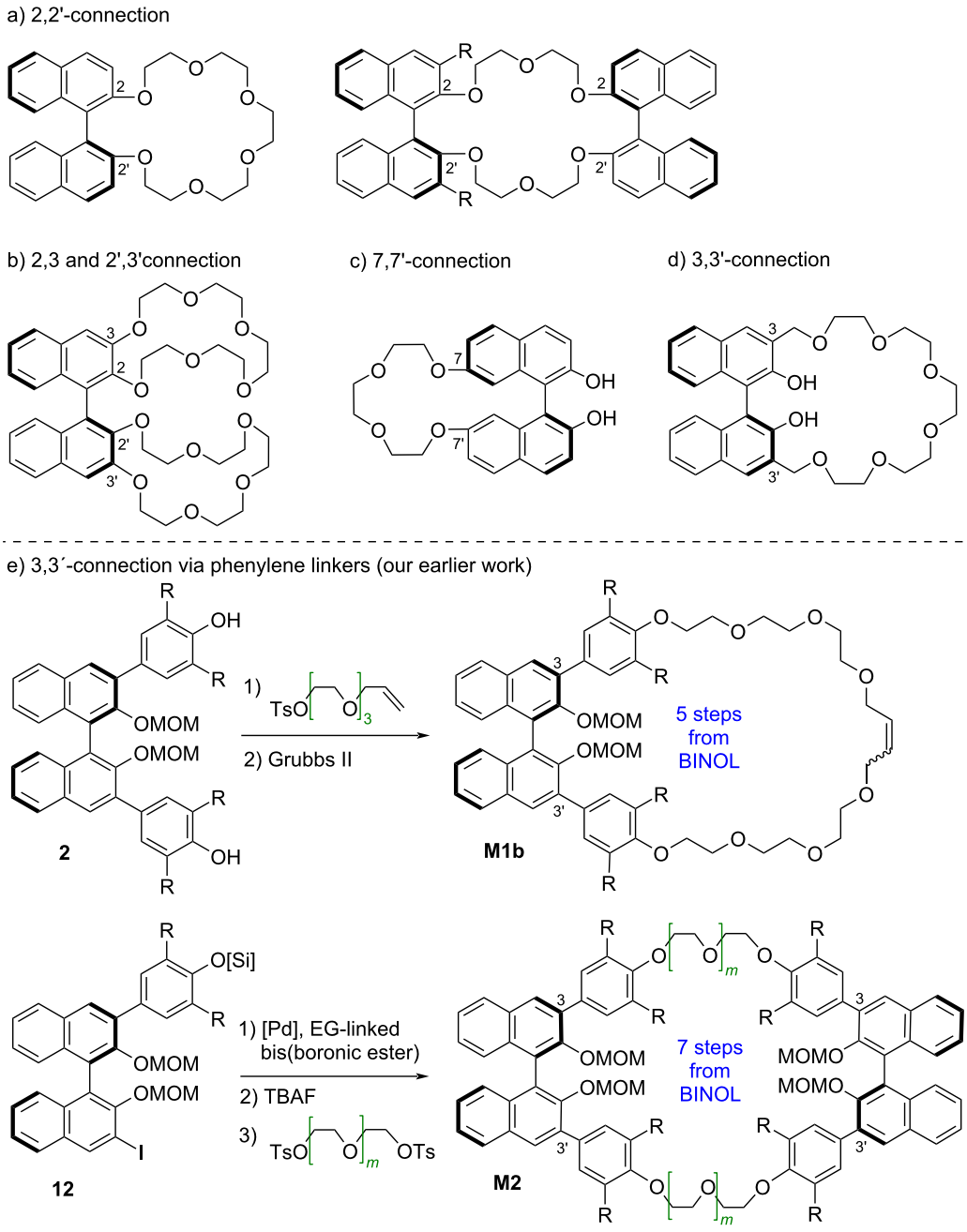

Figure 1: a–d) Selected structures of previously reported BINOL-based crown ether macrocycles; e) previous synthetic routes towards 3,3'-substituted BINOL crown ethers from our group.

crown ethers that are attached at the 3,3'-positions via additional phenylene spacers (see Figure 1e) [35,44,45]. Macrocycles **M1b** with a single BINOL unit were generated from the corresponding diol **2** by attachment of allylated linkers, followed by ring-closing metathesis [46-50]. For the synthesis of macrocycles **M2** with two BINOL units, we relied on the monoiodide **12**, which was first reacted in a two-fold Suzuki coupling to install the first linker, followed by silyl deprotection and introduction of the second linker via nucleophilic substitution [51]. Both procedures require multiple steps towards the desired macrocycles. The route towards the bis-BINOL macrocycles additionally requires the synthesis of the unsymmetric monoiodide **12**. In our previous work, the route starting from **12** had been designed to give access to macrocyclic and singly linked bis-BINOL derivatives from a single precursor, but this is unnecessary if only macrocyclic bis-BINOL derivatives are desired.

For this reason, we sought to find optimized syntheses for such BINOL-based macrocycles (see Figure 2).

After investigating different synthetic routes (vide infra), we found that Williamson-type ether syntheses were the best-yielding approach towards the desired macrocycles. This route was then applied for the synthesis of macrocycles featuring one or two BINOL units, featuring differently substituted phenylene linkers and featuring ethylene glycol linkers of different lengths.

Results and Discussion

Unless otherwise stated, all BINOL derivatives were used as the (*S*)-enantiomers and the stereochemistry will not be mentioned further.

Synthesis of macrocycles featuring one BINOL unit

We first investigated the synthesis of crown ether-type macrocycles **M1** which feature a single BINOL unit. Our previous synthetic approaches (see Figure 1e) toward BINOL macrocycles had successfully used either Williamson-type reactions or Suzuki couplings for the synthesis of intermediates. Thus, we chose to compare the use of two-fold Suzuki coupling or two-fold Williamson reaction for the synthesis of macrocycles **M1**.

For the approach via Suzuki coupling, we employed the previously reported BINOL-diiodide **1** [52], which was reacted with bisboronic acids (see Figure 3a).

Here we chose bisboronic esters **7**$_{5/6/7/8}$ which feature dimethylphenyl groups that are linked via penta/hexa/hepta/octaethylene glycol chains (throughout this publication, the suffix denotes

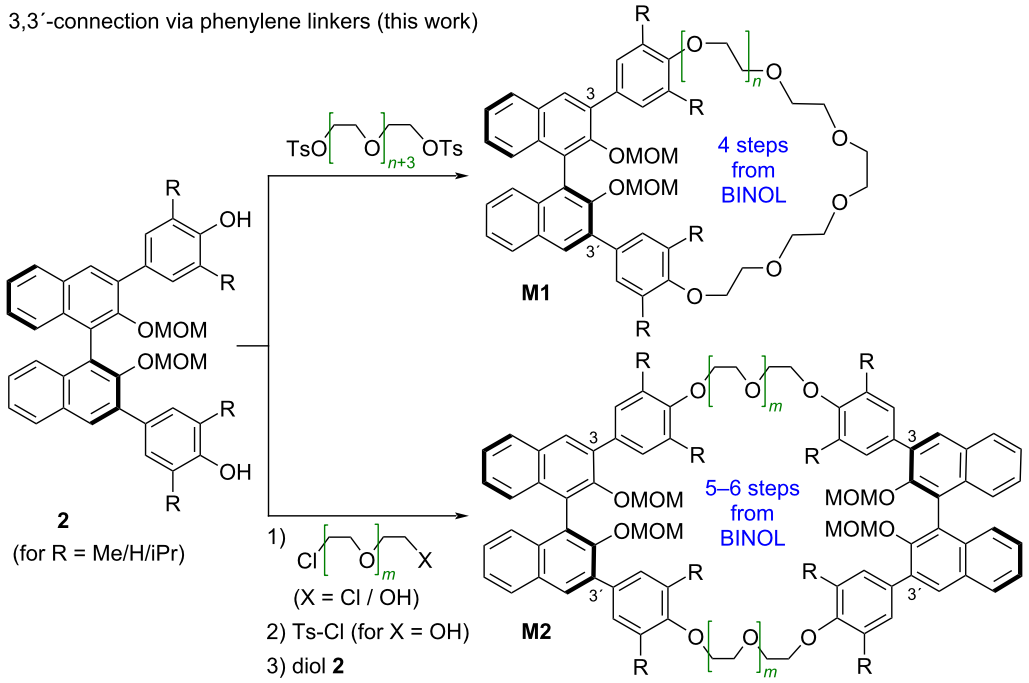

Figure 2: Optimized synthetic routes towards 3,3'-substituted BINOL crown ethers (this work).

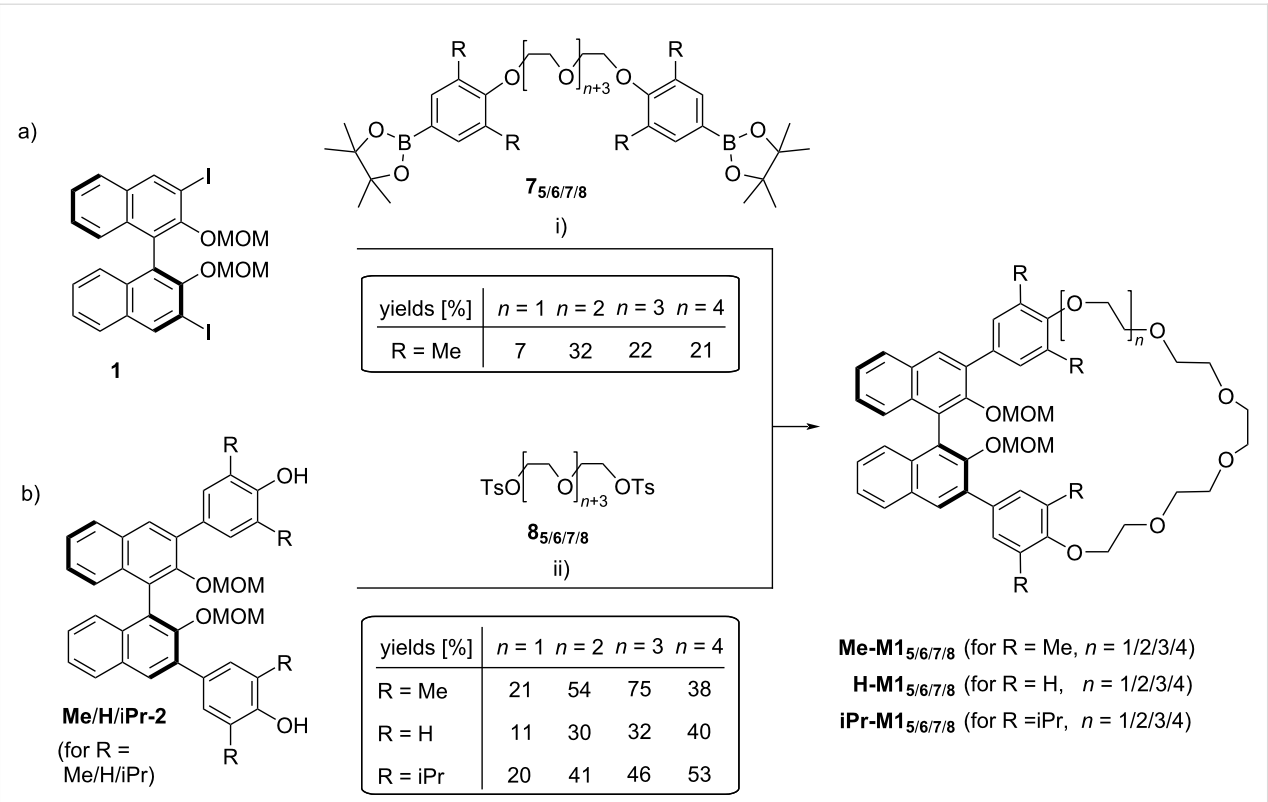

Figure 3: Synthetic routes towards macrocycles featuring one BINOL unit. a) Two-fold Suzuki coupling and b) two-fold Williamson synthesis. Reagents and conditions: i) bis(boronic ester) $\mathbf{7}_{5/6/7/8}$ (1.0. equiv), $Pd_2(dba)_3$ (0.1 equiv), P(*o*-Tol)$_3$ (0.2 equiv), *n*-$Bu_4N^+OH^-$ (3.2. equiv), toluene/H_2O 5:1, 90 °C; ii) ethylene glycol bistosylates $\mathbf{8}_{5/6/7/8}$ (1.0 equiv), Cs_2CO_3 (2.0 equiv), CH_3CN, 80 °C.

the number of ethylene glycol units in a single linker, for the structures of $\mathbf{7}_{5/6/7/8}$, see Figure 3a). The reactivity of $\mathbf{7}_{6}$ had previously been established in the reaction with the unsymmetric monoiodide **12** (see Figure 1e), which proceeded in 59% yield [51]. However, under the same coupling conditions ($Pd_2(dba)_3$, P(*o*-Tol)$_3$, *n*-$Bu_4N^+OH^-$, toluene/H_2O, 90 °C), the reaction of diiodide **1** with bisboronic acids $\mathbf{7}_{5/6/7/8}$ gave only low yields of the desired macrocycles **Me-M1** (7/32/22/21% for $\mathbf{Me\text{-}M1}_{5/6/7/8}$). Thus, the macrocyclization via two-fold Suzuki coupling was not suitable in our hands.

Therefore, we turned our attention towards the two-fold Williamson reaction (see Figure 3b). First, we employed the tetramethyl-substituted diol **Me-2**, which gives access to the same macrocyles $\mathbf{Me\text{-}M1}_{5/6/7/8}$ which we could only generate in low yields via two-fold Suzuki coupling (vide supra). To this end, **Me-2** was reacted with the bistosylated ethylene glycols $\mathbf{8}_{5/6/7/8}$ in the presence of Cs_2CO_3 as a base (CH_3CN, 80 °C). To our delight, we could isolate the macrocyles $\mathbf{Me\text{-}M1}_{5/6/7/8}$ in significantly higher yields of 21/54/75/38%. Cesium carbonate was chosen as the base, because in initial experiments, we obtained consistently higher yields and fewer side-products in comparison to other bases (such as NEt_3 or K_2CO_3), as reported in the literature for related macrocyclizations [53-55].

We then investigated the impact of different substituents on the phenylene linkers on the macrocycle formation. In comparison to the Me-derivative **Me-2**, both the unsubstituted diol **H-2** and the isopropyl derivative **iPr-2** gave generally lower yields for the smaller macrocycles (11/30/32% for $\mathbf{H\text{-}M1}_{5/6/7}$, 20/41/46% for $\mathbf{iPr\text{-}M1}_{5/6/7}$), while the yields for the largest macrocycles $\mathbf{H/iPr\text{-}M1}_{8}$ were slightly increased (40% for $\mathbf{H\text{-}M1}_{8}$, 53% for $\mathbf{iPr\text{-}M1}_{8}$). As a general trend, we observed that the pentaethylene glycol linker seems to be too short to result in efficient macrocyclization (both in Suzuki and Williamson reactions), while the longer linkers give moderate to good yields of the desired macrocycles. In the Williamson approach, we find increasing yields in the series $\mathbf{H\text{-}M1}_{5/6/7/8}$ and $\mathbf{iPr\text{-}M1}_{5/6/7/8}$, with the best yield obtained for the longest octaethylene glycol linkers in $\mathbf{H/iPr\text{-}M1}_{8}$. To our surprise, the Me-series not only gives generally better yields, but also shows the maximum yield for the shorter heptaethylene glycol macrocycle $\mathbf{Me\text{-}M1}_{7}$. The synthesis of the octaethyleneglycol derivative $\mathbf{Me\text{-}M1}_{8}$ was repeated several times but gave reproducibly lower yields than the shorter version $\mathbf{Me\text{-}M1}_{7}$.

All macrocycles were fully characterized by standard analytical methods (see Supporting Information File 1). The structure of **Me-M1$_6$** was additionally verified by single-crystal X-ray analysis (the enantiomeric compound (*R*)-**Me-M1$_6$** resulting from a separate synthesis was crystallized, see Figure 4). Due to the macrocyclic structure, the two ethylene glycol units directly attached to each dimethylphenyl linker adapt a *gauche*-conformation (∠O3–C21–C22–O4 = 66.9(3)°, ∠O4–C23–C24–O5 = −77.3(2)°), and only the central ethylene glycol can be found in a *trans*-conformation (∠O5–C25–C26–O6 = −173.0(5)°). Probably induced by the linker, the commonly preferred perpendicular orientation of the naphthyl-units in the BINOL core is slightly distorted (∠C2–C1–C1'–C2' = −79.2(3)°).

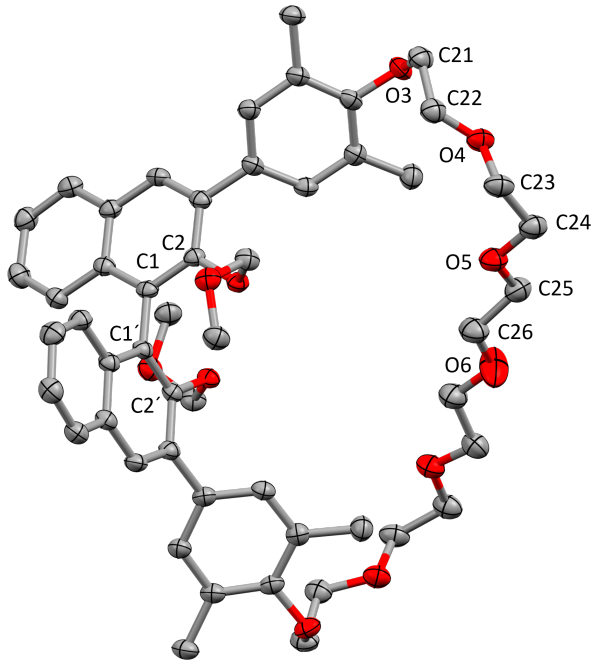

Figure 4: Molecular structure of macrocycle (*R*)-**Me-M1$_6$** in the solid state (hydrogen atoms are omitted for clarity and thermal ellipsoids are set at the 60% probability level). The ethylene glycol chain is partially disordered, only one component is shown.

In summary, we could obtain the desired macrocycles **M1** containing a single BINOL unit in satisfying yields (11–75% from diols **Me**/**H**/**iPr-2**). The previously published route based on ring-closing metathesis gave macrocycle **M1b** (see Figure 1e), which is a 38-membered macrocycle, in 38% yield. Our novel route gives access to 30/33/36/39-membered rings (**M1$_{5/6/7/8}$**), thus complementing the previous approach. Although yields are not consistently better than with the previous route, the novel route has three key advantages: Firstly, the two-step synthesis of the allyl tosyl ethylene glycol (see Figure 1e) can be avoided and the bistosylated ethylene glycol **8** (available in one step) can be used instead. Secondly, the ring-closing metathesis was substituted for an operationally simple Williamson reaction. This results in macrocycles with regular ethylene glycol linkers and removes the internal double bond, which was previously generated as an *E*/*Z*-mixture from the ring-closing metathesis. Thirdly, this route also give access to the smaller macrocylces **M1$_{5/6}$**, while similar ring sizes were difficult to obtain by ring-closing metathesis in our hands [56].

Synthesis of macrocycles featuring two BINOL units

For the synthesis of macrocycles featuring two BINOL units, our first goal was the introduction of two hexaethylene glycol chains between the two BINOL units. These derivatives had proven to be highly efficient organocatalysts in our earlier work, based on the large conformational freedom that is given by the long, flexible linkers [51].

To achieve a convergent synthesis, we first designed the hexaethylene glycol linker **9$_6$**, which features a tosylate leaving group at one end and a phenylboronic ester at the other end (see Figure 5).

This would allow a two-step synthesis of the desired macrocycles by performing a sequence of two-fold Suzuki coupling, followed by two-fold Williamson synthesis or vice versa. However, attempts to realize the first step of either sequence, i.e., reaction of the precursor **9$_6$** with either the BINOL diiodide **1** (in a two-fold Suzuki coupling) or with the BINOL-derived diol **Me-2** (in a two-fold Williamson reaction) gave no meaningful yields of the desired intermediates **Me-3$_6$** or **Me-4$_6$**, respectively.

For this reason, we resorted to an alternative synthesis of the BINOL-based bistosylates **Me**/**H**/**iPr-3$_6$**. For the long hexaethylene glycol linker, a direct reaction of the diols **Me**/**H**/**iPr-2** with a hexaethylene glycol bistosylate did not seem feasible, since this would lead to the mono-BINOL macrocycles **Me**/**H**/**iPr-M1$_6$** even in the presence of a large excess of bistosylate. Thus, we first reacted diols **Me**/**H**/**iPr-2** with chloroalcohol **10$_6$** in the presence of Cs_2CO_3 (CH_3CN, 80 °C), which gave the desired bisglycolated products **Me**/**H**/**iPr-5** (Supporting Information File 1). Subsequent reaction with tosyl chloride in the presence of triethylamine and DMAP (CH_2Cl_2, 25 °C) gave the desired BINOL bistosylates **Me**/**H**/**iPr-3$_6$** in good yields (69/61/72% over two steps, see Figure 6). However, only if temperature and reaction times in this step were carefully controlled, the reaction proceeded cleanly. Deviations from the optimized conditions (see Supporting Information File 1 for details) resulted in greatly diminished yields due to the formation of various by-products.

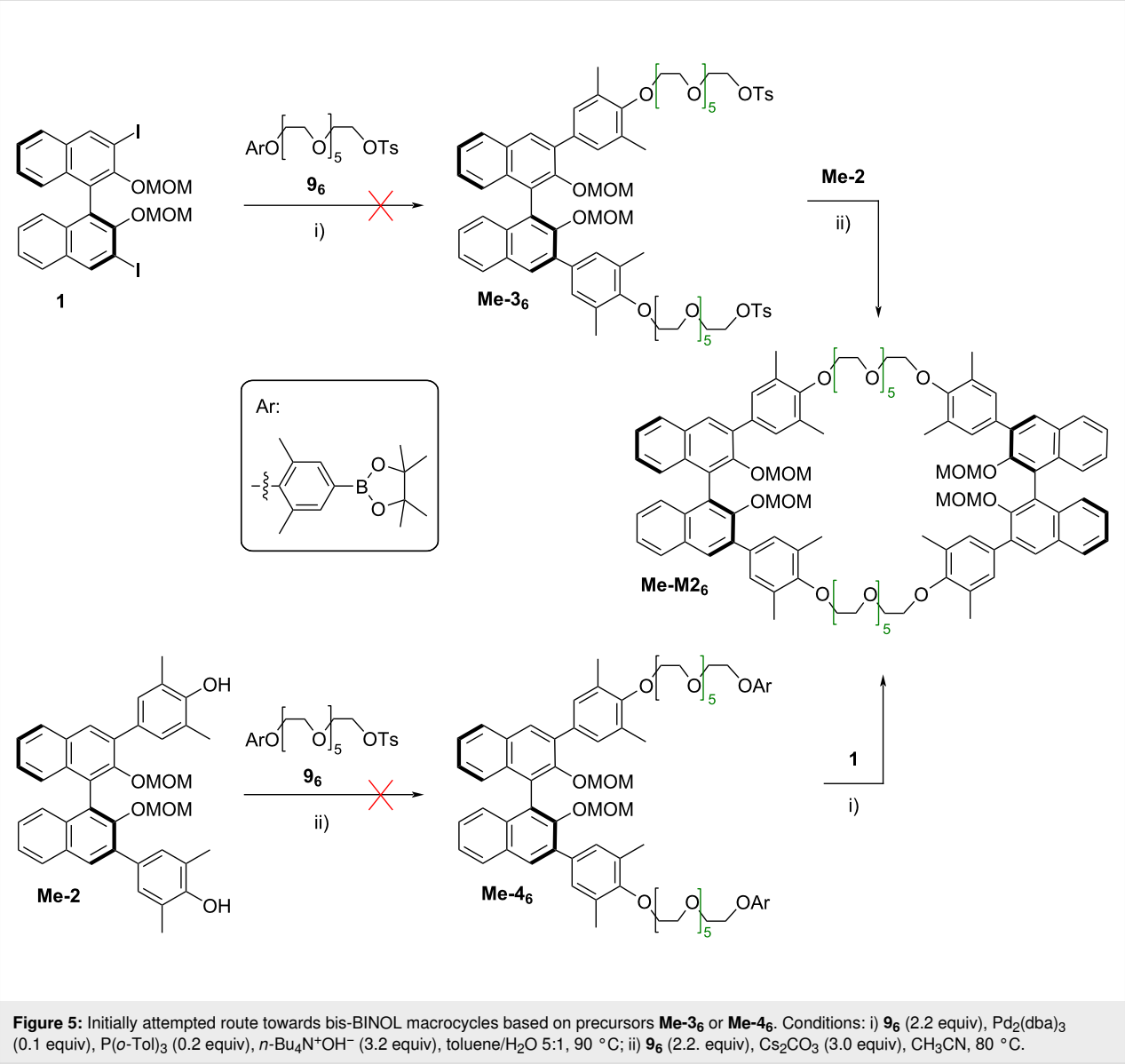

Figure 5: Initially attempted route towards bis-BINOL macrocycles based on precursors **Me-3$_6$** or **Me-4$_6$**. Conditions: i) **9$_6$** (2.2 equiv), $Pd_2(dba)_3$ (0.1 equiv), P(*o*-Tol)$_3$ (0.2 equiv), *n*-$Bu_4N^+OH^-$ (3.2 equiv), toluene/H_2O 5:1, 90 °C; ii) **9$_6$** (2.2. equiv), Cs_2CO_3 (3.0 equiv), CH_3CN, 80 °C.

Starting from the bistosylates **Me/H/iPr-3$_6$**, reaction with the diols **Me/H/iPr-2** in the presence of Cs_2CO_3 as base (CH_3CN, 80 °C) proceeded cleanly to give the desired hexaethylene glycol-linked bis-BINOL macrocycles that feature a 66-membered ring structure. Here, we successfully generated the C_2-symmetric macrocycles **Me/H/iPr-M2$_6$** (obtained in 62/67/54% yield) and the unsymmetrically substituted, C_1-symmetric derivative **HiPr-M2$_6$** (56% yield from **iPr-3$_6$** and **H-2**). Thus, the overall yields for the large macrocycles **Me/H/iPr/HiPr-M2$_6$** range from 15 to 17% (6 steps from BINOL, 35–42% over 3 steps from diols **Me/H/iPr-2**). This is an improvement in comparison to the yield obtained with the previous method, based on sequential introduction of both hexaethylene glycol linkers (see Figure 1b), which gave 11% yield for compound **Me-M2$_6$** over 7 steps from BINOL.

As a second synthetic aim, we wanted to realize the synthesis of smaller bis-BINOL macrocycles that feature two diethylene glycol linkers, thus yielding 42-membered macrocylces. In this case, it was possible to directly react diols **Me/H/iPr-2** with the corresponding dichloride **11$_2$** (Cs_2CO_3, CH_3CN, 80 °C, see Figure 7), since this is too short to result in a mono-BINOL macrocycle.

The corresponding BINOL-based dichlorides **Me/H/iPr-6$_2$** could be obtained in good yields (59/78/76%) and further reacted with the diols **Me/H/iPr-2** in the presence of Cs_2CO_3 (CH_3CN, 80 °C). This cyclization yielded the symmetrically tetrasubstitued macrocycles **Me/H/iPr-M2$_2$** in good yields of 59/78/77%. Again, we applied this protocol for the synthesis of the unsymmetric derivative **HiPr-M2$_2$**, this time in two dia-

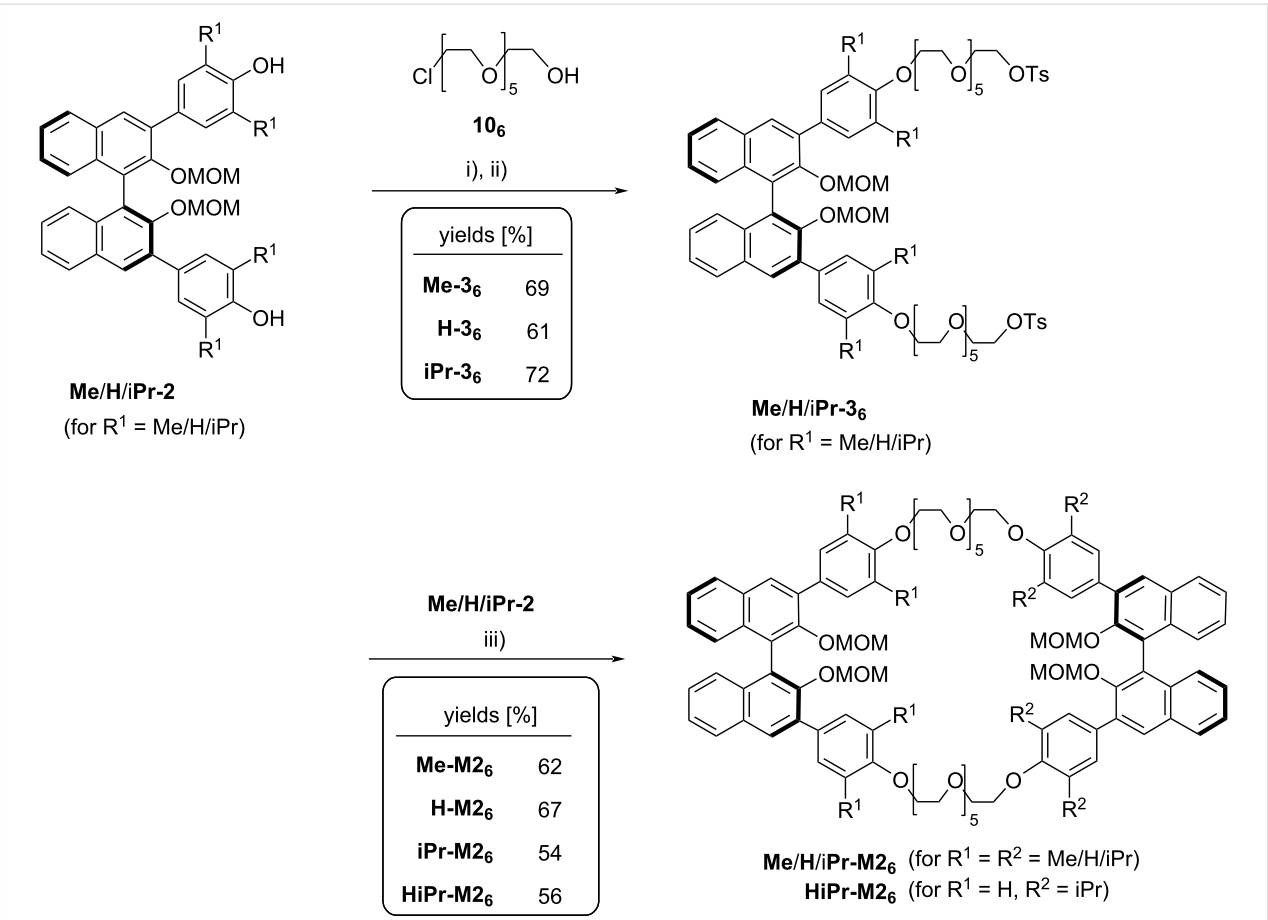

Figure 6: Synthetic route towards macrocycles featuring two BINOL units linked via hexaethylene glycol spacers. Conditions: i) chloroalcohol **10_6** (2.2 equiv), Cs_2CO_3 (2.2 equiv), CH_3CN, 80 °C; ii) tosyl chloride (2.5 equiv), triethylamine (4.0 equiv), DMAP (0.4 equiv), CH_2Cl_2, 25 °C (69/61/72% yield over two steps for **Me**/**H**/**iPr-3_6**); iii) **Me**/**H**/**iPr-2** (1.0 equiv), Cs_2CO_3 (3.2 equiv), CH_3CN, 80 °C (62/67/54/56% yield for **Me**/**H**/**iPr**/**HiPr-$M2_6$**).

stereomeric forms. In the unsymmetric case, the introduction of two BINOL units with opposite configuration does not furnish a *meso*-compound, so that we reacted either (*S*)- or (*R*)-**H-2** with the dichloride (*S*)-**iPr-6_2** to give the diastereomeric macrocycles (*S*,S)-**HiPr-$M2_2$** and (*R*,*S*)-**HiPr-$M2_2$** in 73/49% yield, respectively.

The ^{1}H NMR spectra of the C_2-symmetric derivatives (*S*,*S*)-**H**/**iPr-$M2_2$** (see Figure 8a/b) differ most significantly in the splitting of the signals corresponding to the MOM-methylene protons near 4.3 ppm (H-21), which are clearly split into two doublets for (*S*,*S*)-**H-$M2_2$**, but resemble more of a second order signal with a very small coupling constant in (*S*,*S*)-**iPr-$M2_2$**. As expected, the two BINOL units in the symmetric macrocycles only give one set of signals, e.g., one singlet for H-4 and one doublet for H-6. When comparing these to the C_1-symmetric compound (*S*,*S*)-**HiPr-$M2_2$** (see Figure 8a–c), separate signals for the 4- and 6-positions of each BINOL unit can be observed (i.e., H-4/H-27 and H-6/H-29). In contrast, the signals of the MOM-methylene protons appear closer to the shift observed for (*S*,*S*)-**H-$M2_2$**, however, also two differentiable sets for either BINOL unit can be observed. The MOM-CH_2 signals of the diisopropylphenyl-substituted BINOL unit (i.e., H-21/H-21') show a smaller splitting between the diastereomeric protons than the analogous MOM-CH_2 protons (H-36/H-36') of the phenyl-substituted BINOL unit, in line with the observations for the C_2-symmetric compounds. The two diastereomeric macrocycles (*S*,*S*)- and (*R*,*S*)-**HiPr-$M2_2$** (compare Figure 8c,d) show distinct, but small differences in the ^{1}H chemical shifts. This indicates that despite the short diethylene glycol linkers, the mutual influence of both BINOL units on each other is small in the bis-BINOL macrocycle.

Conclusion

In summary, we have developed novel approaches towards the synthesis of crown ethers that contain one or two BINOL units. The ethylene glycol units were attached to the BINOL backbone via differently substituted phenylene linkers, either featuring two methyl groups, two isopropyl groups, or no additional substituent.

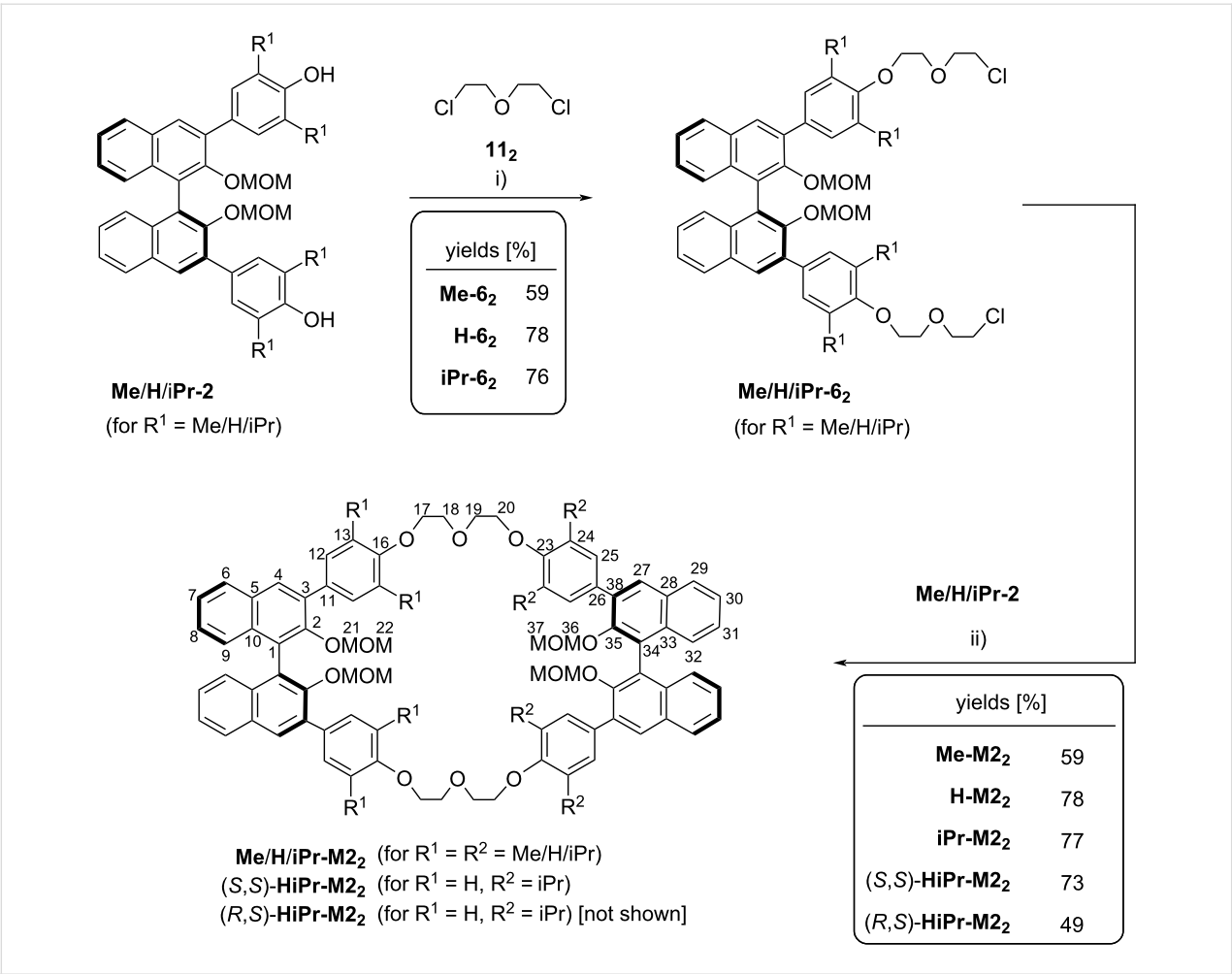

Figure 7: Synthetic route towards macrocycles featuring two BINOL units linked via diethylene glycol spacers. Conditions: i) dichloride **11₂** (2.5 equiv), Cs_2CO_3 (2.5 equiv), CH_3CN, 80 °C (59/78/76% yield for **Me/H/iPr-6₂**; ii) **Me**/(*S*)-**H**/(*R*)-**H/iPr-2** (1.0 equiv), Cs_2CO_3 (3.2 equiv), CH_3CN, 80 °C.

First, we could show that the corresponding diols **Me/H/iPr-2** can be transformed into the corresponding mono-BINOL macrocycles via two-fold Williamson reaction with ethylene glycol bistosylates. Using penta-/hexa-/hepta-/octaethylene glycol bistosylates **8₅/₆/₇/₈**, the corresponding 30/33/36/39-membered macrocycles could be synthesized from all three diols **Me/H/iPr-2**, yielding a library of 12 different mono-BINOL macrocycles. Yields for the macrocyclization step depended strongly on ring size and substitution pattern and ranged from 11–74%.

Second, we could use **Me/H/iPr-2** as starting materials for bis-BINOL macrocycles. Attachment of ethylene glycol chains with suitable leaving groups (tosylate or chloride), followed by macrocyclization with a second equivalent of diols **Me/H/iPr-2** gave access to 4 different hexaethylene glycol-based macrocycles **M2₆** (66-membered rings) and 5 different diethylene glycol-based macrocycles **M2₂** (42-membered rings). Here, the yields for the macrocyclization were consistently high and ranged from 49–78%. In this fashion, we could not only generate the symmetrically tetrasubstituted macrocycles with either hexaethylene glycol linkers (**Me/H/iPr-M2₆**) or diethylene glycol linkers (**Me/H/iPr-M2₂**), but also the unsymmetrically substituted macrocycles **HiPr-M2₆** and **HiPr-M2₂**. Furthermore, the latter compound was generated in both diastereomeric forms, namely (*S*,*S*)- and (*R*,*S*)-**HiPr-M2₂**.

We believe that these systems are highly promising candidates for further application in enantioselective chemosensing or organocatalysis, e.g., after transformation into the corresponding BINOL phosphoric acids. However, at this point, the application of BINOL-based crown ethers with 3,3'-appended ethylene glycol chains remains underdeveloped, partially due to the lack of simple and high-yielding synthetic routes. Thus, we believe that our newly developed optimized synthetic strategy

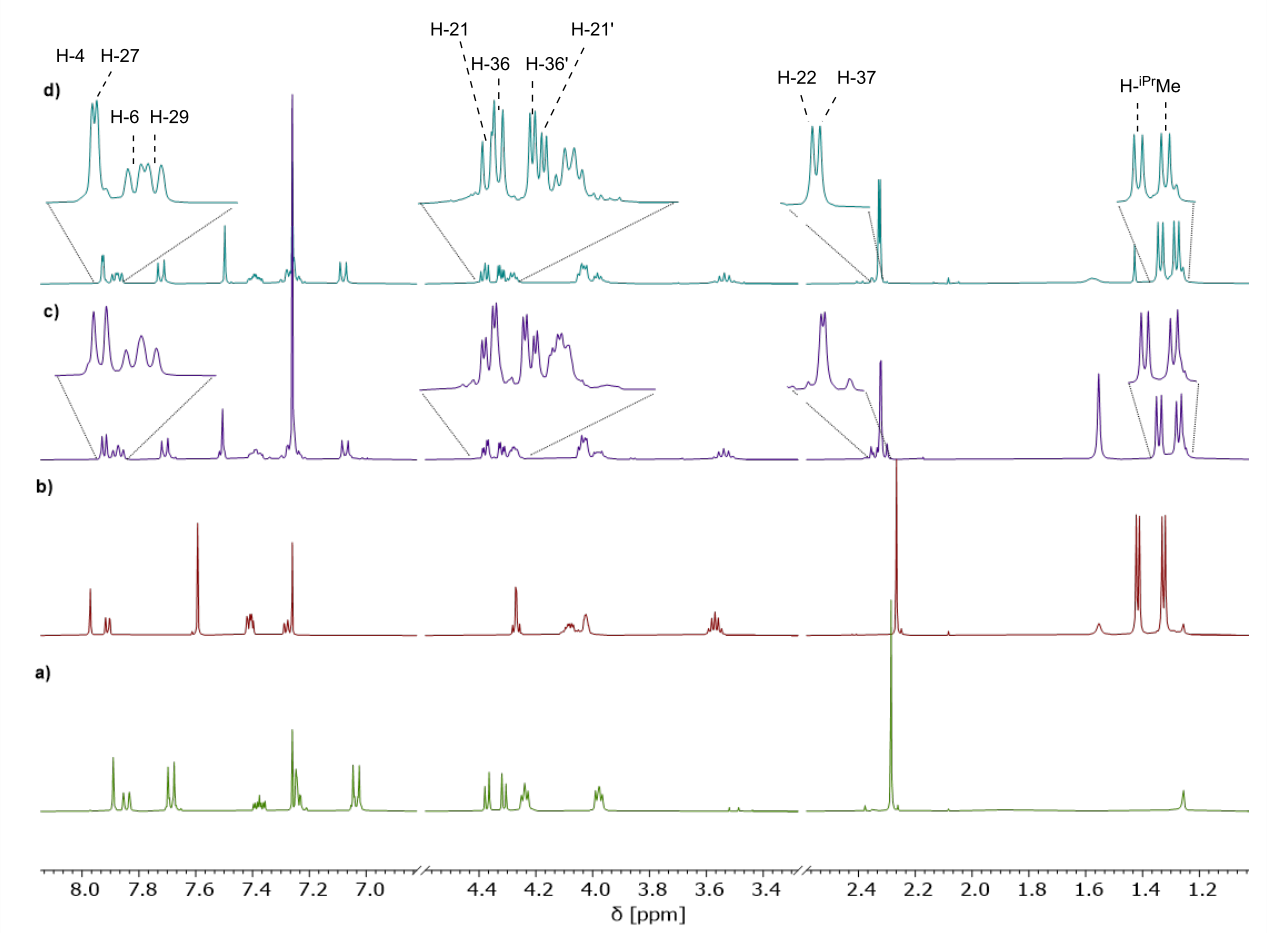

Figure 8: ^{1}H NMR spectra of a) (*S*,*S*)-**H-M2$_2$**, b) (*S*,*S*)-**iPr-M2$_2$**, c) (*S*,*S*)-**HiPr-M2$_2$**, and d) (*R*,*S*)-**HiPr-M2$_2$** (all: 400 MHz, $CDCl_3$, 298 K, for labelling see Figure 7).

will enable further applications of these BINOL-based macrocycles.

Supporting Information

Synthetic procedures and NMR spectra for all new compounds, as well as the crystal structure data for **Me-M1$_6$**. CCDC-2427523 contains the supplementary crystallographic data for this paper. This data can be obtained free of charge from The Cambridge Crystallographic Data Centre via https://www.ccdc.cam.ac.uk/data_request/cif.

Supporting Information File 1

Experimental procedures and characterization data of new compounds.
[https://www.beilstein-journals.org/bjoc/content/supplementary/1860-5397-21-134-S1.pdf]

Supporting Information File 2

Crystallographic Information File (CIF) for the solid-state structure of (*R*)-**Me-M1$_6$**.
[https://www.beilstein-journals.org/bjoc/content/supplementary/1860-5397-21-134-S2.cif]

Funding

J.N. would like to thank the Deutsche Forschungsgemeinschaft DFG (project NI1273/2-2, project NI1273/5-1 and Heisenberg Professorship NI1273/4-1) for funding. S.K. would like to thank the Alexander von Humboldt Foundation for a postdoctoral fellowship.

ORCID® iDs

Jan Riebe - https://orcid.org/0000-0002-5555-5252
Jochen Niemeyer - https://orcid.org/0000-0002-9295-4260

Data Availability Statement

All data that supports the findings of this study is available in the published article and/or the supporting information of this article.

References

1. Steed, J. W.; Atwood, J. L. *Supramolecular Chemistry;* John Wiley & Sons: Chichester, UK, 2009. doi:10.1002/9780470740880
2. Cram, D. J. *Angew. Chem., Int. Ed. Engl.* **1988,** *27,* 1009–1020. doi:10.1002/anie.198810093
3. Lehn, J.-M. *Angew. Chem., Int. Ed. Engl.* **1988,** *27,* 89–112. doi:10.1002/anie.198800891
4. Pedersen, C. J. *Angew. Chem., Int. Ed. Engl.* **1988,** *27,* 1021–1027. doi:10.1002/anie.198810211
5. Behr, J.-P.; Girodeau, J.-M.; Hayward, R. C.; Lehn, J.-M.; Sauvage, J.-P. *Helv. Chim. Acta* **1980,** *63,* 2096–2111. doi:10.1002/hlca.19800630736
6. Behr, J.-P.; Lehn, J.-M.; Vierling, P. *Helv. Chim. Acta* **1982,** *65,* 1853–1867. doi:10.1002/hlca.19820650620
7. Lehn, J.-M.; Sirlin, C. *J. Chem. Soc., Chem. Commun.* **1978,** 949–951. doi:10.1039/c39780000949
8. Lehn, J.-M. *Pure Appl. Chem.* **1979,** *51,* 979–997. doi:10.1351/pac197951050979
9. Jones, B. A.; Bradshaw, J. S.; Izatt, R. M. *J. Heterocycl. Chem.* **1982,** *19,* 551–556. doi:10.1002/jhet.5570190320
10. Izatt, R. M.; Wang, T.; Hathaway, J. K.; Zhang, X. X.; Curtis, J. C.; Bradshaw, J. S.; Zhu, C. Y.; Huszthy, P. *J. Inclusion Phenom. Mol. Recognit. Chem.* **1994,** *17,* 157–175. doi:10.1007/bf00711856
11. Davidson, R. B.; Bradshaw, J. S.; Jones, B. A.; Dalley, N. K.; Christensen, J. J.; Izatt, R. M.; Morin, F. G.; Grant, D. M. *J. Org. Chem.* **1984,** *49,* 353–357. doi:10.1021/jo00176a026
12. Jones, B. A.; Bradshaw, J. S.; Brown, P. R.; Christensen, J. J.; Izatt, R. M. *J. Org. Chem.* **1983,** *48,* 2635–2639. doi:10.1021/jo00164a001
13. Bradshaw, J. S. *J. Inclusion Phenom. Mol. Recognit. Chem.* **1997,** *29,* 221–246. doi:10.1023/a:1007955428644
14. Naemura, K. *Coord. Chem. Rev.* **1996,** *148,* 199–219. doi:10.1016/0010-8545(95)01189-7
15. Bako, P.; Keglevich, G.; Rapi, Z.; Toke, L. *Curr. Org. Chem.* **2012,** *16,* 297–304. doi:10.2174/138527212799499877
16. Cram, D. J.; Helgeson, R. C.; Peacock, S. C.; Kaplan, L. J.; Domeier, L. A.; Moreau, P.; Koga, K.; Mayer, J. M.; Chao, Y. *J. Org. Chem.* **1978,** *43,* 1930–1946. doi:10.1021/jo00404a019
17. Kyba, E. P.; Gokel, G. W.; de Jong, F.; Koga, K.; Sousa, L. R.; Siegel, M. G.; Kaplan, L.; Sogah, G. D. Y.; Cram, D. J. *J. Org. Chem.* **1977,** *42,* 4173–4184. doi:10.1021/jo00862a001
18. Kyba, E. B.; Koga, K.; Sousa, L. R.; Siegel, M. G.; Cram, D. J. *J. Am. Chem. Soc.* **1973,** *95,* 2692–2693. doi:10.1021/ja00789a051
19. Kyba, E. P.; Timko, J. M.; Kaplan, L. J.; de Jong, F.; Gokel, G. W.; Cram, D. J. *J. Am. Chem. Soc.* **1978,** *100,* 4555–4568. doi:10.1021/ja00482a040
20. Newcomb, M.; Toner, J. L.; Helgeson, R. C.; Cram, D. J. *J. Am. Chem. Soc.* **1979,** *101,* 4941–4947. doi:10.1021/ja00511a025
21. Peacock, S. C.; Domeier, L. A.; Gaeta, F. C. A.; Helgeson, R. C.; Timko, J. M.; Cram, D. J. *J. Am. Chem. Soc.* **1978,** *100,* 8190–8202. doi:10.1021/ja00494a029
22. Peacock, S. S.; Walba, D. M.; Gaeta, F. C. A.; Helgeson, R. C.; Cram, D. J. *J. Am. Chem. Soc.* **1980,** *102,* 2043–2052. doi:10.1021/ja00526a046
23. Cram, D. J.; Helgeson, R. C.; Sousa, L. R.; Timko, J. M.; Newcomb, M.; Moreau, P.; de Jong, F.; Gokel, G. W.; Hoffman, D. H.; Domeier, L. A.; Peacock, S. C.; Madan, K.; Kaplan, L. *Pure Appl. Chem.* **1975,** *43,* 327–349. doi:10.1351/pac197543030327
24. Stoddart, J. F. *Top. Stereochem.* **1987,** *17,* 207–288. doi:10.1002/9780470147269.ch3
25. Pu, L. *Chem. Rev.* **1998,** *98,* 2405–2494. doi:10.1021/cr970463w
26. Móczár, I.; Huszthy, P. *Chirality* **2019,** *31,* 97–109. doi:10.1002/chir.23031
27. Yu, S.; Pu, L. *Tetrahedron* **2015,** *71,* 745–772. doi:10.1016/j.tet.2014.11.007
28. Ooi, T.; Maruoka, K. *Angew. Chem., Int. Ed.* **2007,** *46,* 4222–4266. doi:10.1002/anie.200601737
29. Shirakawa, S.; Maruoka, K. *Angew. Chem., Int. Ed.* **2013,** *52,* 4312–4348. doi:10.1002/anie.201206835
30. Zhang, Z.; Shao, Y.; Tang, J.; Jiang, J.; Wang, L.; Li, S. *Green Synth. Catal.* **2021,** *2,* 156–164. doi:10.1016/j.gresc.2021.03.007
31. Schettini, R.; Sicignano, M.; De Riccardis, F.; Izzo, I.; Della Sala, G. *Synthesis* **2018,** *50,* 4777–4795. doi:10.1055/s-0037-1610311
32. Polewski, L.; Springer, A.; Pagel, K.; Schalley, C. A. *Acc. Chem. Res.* **2021,** *54,* 2445–2456. doi:10.1021/acs.accounts.1c00080
33. Hyun, M. H. *J. Chromatogr. A* **2016,** *1467,* 19–32. doi:10.1016/j.chroma.2016.07.049
34. Schalley, C. A. *Mass Spectrom. Rev.* **2001,** *20,* 253–309. doi:10.1002/mas.10009
35. Krajnc, M.; Niemeyer, J. *Beilstein J. Org. Chem.* **2022,** *18,* 508–523. doi:10.3762/bjoc.18.53
36. Goldberg, I. *Acta Crystallogr., Sect. B: Struct. Crystallogr. Cryst. Chem.* **1977,** *33,* 472–479. doi:10.1107/s0567740877003884
37. Tarnowski, T. L.; Cram, D. J. *J. Chem. Soc., Chem. Commun.* **1976,** 661–663. doi:10.1039/c39760000661
38. Liu, Q.-Z.; Xie, N.-S.; Luo, Z.-B.; Cui, X.; Cun, L.-F.; Gong, L.-Z.; Mi, A.-Q.; Jiang, Y.-Z. *J. Org. Chem.* **2003,** *68,* 7921–7924. doi:10.1021/jo034831+
39. Hester, M. R.; Uyeki, M. A.; Diederich, F. *Isr. J. Chem.* **1989,** *29,* 201–212. doi:10.1002/ijch.198900028
40. Diederich, F.; Hester, M. R.; Uyeki, M. A. *Angew. Chem.* **1988,** *100,* 1775–1777. doi:10.1002/ange.19881001217
41. Ito, S.; Koizumi, K.; Fukuda, K.; Kameta, N.; Ikeda, T.; Oba, T.; Hiratani, K. *Tetrahedron Lett.* **2006,** *47,* 8563–8566. doi:10.1016/j.tetlet.2006.09.161
42. Helgeson, R. C.; Tarnowski, T. L.; Cram, D. J. *J. Org. Chem.* **1979,** *44,* 2538–2550. doi:10.1021/jo01328a045
43. Koenig, K. E.; Helgeson, R. C.; Cram, D. J. *J. Am. Chem. Soc.* **1976,** *98,* 4018–4020. doi:10.1021/ja00429a058
44. Kwamen, C.; Niemeyer, J. *Chem. – Eur. J.* **2021,** *27,* 175–186. doi:10.1002/chem.202002876
45. Kauerhof, D.; Niemeyer, J. *ChemPlusChem* **2020,** *85,* 889–899. doi:10.1002/cplu.202000152
46. Kauerhof, D.; Riebe, J.; Vonnemann, C. J.; Thiele, M.; Jansen, D.; Niemeyer, J. *Chem. Commun.* **2024,** *60,* 2393–2396. doi:10.1039/d3cc05482a
47. Pairault, N.; Zhu, H.; Jansen, D.; Huber, A.; Daniliuc, C. G.; Grimme, S.; Niemeyer, J. *Angew. Chem., Int. Ed.* **2020,** *59,* 5102–5107. doi:10.1002/anie.201913781
48. Jansen, D.; Gramüller, J.; Niemeyer, F.; Schaller, T.; Letzel, M. C.; Grimme, S.; Zhu, H.; Gschwind, R. M.; Niemeyer, J. *Chem. Sci.* **2020,** *11,* 4381–4390. doi:10.1039/d0sc01026j

49. Mitra, R.; Zhu, H.; Grimme, S.; Niemeyer, J. *Angew. Chem., Int. Ed.* **2017,** *56,* 11456–11459. doi:10.1002/anie.201704647
50. Mitra, R.; Thiele, M.; Octa-Smolin, F.; Letzel, M. C.; Niemeyer, J. *Chem. Commun.* **2016,** *52,* 5977–5980. doi:10.1039/c6cc01980c
51. Thiele, M.; Rose, T.; Lökov, M.; Stadtfeld, S.; Tshepelevitsh, S.; Parman, E.; Opara, K.; Wölper, C.; Leito, I.; Grimme, S.; Niemeyer, J. *Chem. – Eur. J.* **2023,** *29,* e202202953. doi:10.1002/chem.202202953
52. Wu, T. R.; Shen, L.; Chong, J. M. *Org. Lett.* **2004,** *6,* 2701–2704. doi:10.1021/ol0490882
53. Lee, J. C.; Yuk, J. Y.; Cho, S. H. *Synth. Commun.* **1995,** *25,* 1367–1370. doi:10.1080/00397919508013838
54. Ostrowicki, A.; Koepp, E.; Vögtle, F. *Top. Curr. Chem.* **1992,** *161,* 37–67. doi:10.1007/3-540-54348-1_7
55. van Keulen, B. J.; Kellogg, R. M.; Piepers, O. *J. Chem. Soc., Chem. Commun.* **1979,** 285–286. doi:10.1039/c39790000285
56. Brodt, N.; Niemeyer, J. *unpublished results.*

License and Terms

BEILSTEIN JOURNAL OF ORGANIC CHEMISTRY

Research progress on calixarene/pillararene-based controlled drug release systems

Liu-Huan Yi, Jian Qin, Si-Ran Lu, Liu-Pan Yang*, Li-Li Wang* and Huan Yao*

Review

Open Access

Address:
School of Pharmaceutical Science, Hengyang Medical School, University of South China, Hengyang 421001, China

Email:
Liu-Pan Yang* - yanglp@usc.edu.cn; Li-Li Wang* - wangll@usc.edu.cn; Huan Yao* - yaoh@usc.edu.cn

* Corresponding author

Keywords:
aromatic macrocycle; controlled-release drug delivery systems; stimulus response; supramolecular chemistry

Beilstein J. Org. Chem. **2025,** *21,* 1757–1785.
https://doi.org/10.3762/bjoc.21.139

Received: 21 March 2025
Accepted: 15 August 2025
Published: 03 September 2025

This article is part of the thematic issue "Novel macrocycles: from synthesis to supramolecular function".

Guest Editor: C. Gaeta

Abstract

Intelligent controlled-release drug delivery systems that are responsive to various external stimuli have garnered significant interest from researchers and have broad applications in the biomedical field. Aromatic macrocycles, including calixarenes and pillararenes, are considered ideal candidates for the construction of supramolecular drug delivery systems because of their simple synthesis, ease of modification, electron-rich and hydrophobic cavities, and highly selective molecular recognition. In recent years, numerous supramolecular drug delivery systems utilizing aromatic macrocycles have been developed. This review article provides an overview of the advancements of controlled drug release systems based on host–guest selective recognition, self-assembly, and nano-valves by the use of of calixarenes and pillararenes from five perspectives: pH, light, enzyme, hypoxia, and multi-stimuli combination responses. Furthermore, the article projects the future clinical application prospects of controlled-release technologies, with the aim of offering a reference for the utilization of aromatic macrocycles in drug-controlled release applications.

Introduction

Drugs are defined by the Food and Drug Administration (FDA) as substances used for diagnosing, relieving, treating, or preventing diseases [1]. Traditional forms of drugs typically have a systemic effect, reaching both healthy and diseased areas, leading to a lack of selectivity, low bioavailability, and limited efficacy [2-4]. Nowadays, there are technologies that can better confine the action of drugs to where they are needed. Drug delivery is a technology that administers drugs to patients, which can specifically increase the concentration of drugs in certain parts of the body, thereby enhancing the therapeutic effect [5]. However, conventional drug delivery systems (such as capsules [6], tablets [7], ointments [8], etc.) have poor bioavailability, with fluctuating plasma drug levels and an inability to achieve sustained release. The emergence of con-

trolled-release drug delivery systems has provided the possibility to improve patients' adaptability to medications [8-10]. By using biomedically compatible materials to carry drugs, these systems can release drugs at a controlled, uniform rate, maintaining stable blood drug concentrations, thereby fully exerting the therapeutic effects of the drugs [11-13]. The technology for modern controlled-release drug delivery systems began with the launch of Spansule sustained-release capsules in 1952. Since then, the development of various drug delivery systems has accelerated significantly over the past few decades. These systems include dissolution-controlled, diffusion-controlled, osmotic-controlled (which encompasses osmotic pressure and swelling control), chemically controlled, nanoparticle systems, and supramolecular controlled-release systems. Among these, supramolecular controlled-release systems have advantages such as dynamic adjustability, stimulus responsiveness, specific recognition and binding, and multi-target synergistic action [14-16]. These characteristics enable precise control of drug release and targeted drug delivery, thereby improving drug stability and bioavailability, and reducing drug toxicity and side effects.

Supramolecular chemistry, with molecular recognition at its core [17], utilizes non-covalent interactions such as electrostatic interactions, hydrogen bonding [18], and hydrophobic effects to provide valuable tools for developing new biomaterials and drug delivery systems [18-22]. This article categorizes supramolecular chemistry-based drug-controlled release systems into the following three mechanisms: (1) Drugs are identified and combined with supramolecular hosts through host–guest interactions [23-28]. By adjusting the conditions surrounding the guest molecules, such as changes in pH, light, and enzyme activity, the binding affinity between the guest and host molecules can be altered, thereby achieving controlled drug release and targeted delivery. (2) Drugs are loaded into self-assembled host–guest systems [29-32]. The chemical structure or properties of the host or guest molecules are altered upon exposure to specific stimuli, such as light, pH changes, or enzymes. This modification induces the disassembly of the host–guest complex, thereby releasing the encapsulated drugs. Fundamentally, this mechanism relies on controlling the assembly and disassembly processes. For example, supramolecular self-assembly technology enhances the targeting of chemotherapeutic drugs to tumor tissues, reducing systemic adverse reactions. (3) Macrocyclic aromatic supramolecular nano-valves have a pseudo-rotaxane structure with host–guest coordination and the kinetic properties of supramolecular interactions [33,34]. Different external stimuli, including pH changes, enzymes, light irradiation, hypoxia, and multi-stimuli responses, can alter the supramolecular structure or binding affinity to activate the opening and closing of the nano-valves. In addition to the three mechanisms that will be detailed in this article, researchers have made progress in the transport of amino acids and molecular peptides across membranes using macrocycles in recent years [35-37]. These works have paved the way for the potential application of remote-controlled membrane transport technology in the field of hydrophilic functional biomolecules, and is expected to be applied to stimulus-responsive controlled drug transport across membranes in the future. Currently, various artificially synthesized macrocyclic hosts have found extensive applications in drug-controlled release systems, for example, classic macrocycles like cyclodextrins [38] and cucurbiturils [39]. In recent years, aromatic macrocycles such as calixarenes (CAs) [40] and pillararenes (PAs) [41] have attracted widespread attention from the industry and scientists due to their simple synthesis which only require a one-step synthesis, convenient modification that can be achieved by introducing functional groups, electron rich and hydrophobic cavities that can effectively recognize electron deficient or neutral guest molecules, and high selectivity in binding with the guest. Their applications are extensive in the domain of drug-controlled release.

This article mainly reviews the supramolecular drug delivery systems constructed from aromatic macrocycles (Figure 1). These systems achieve intelligent control over drug release through reasonable manipulation of stimuli, including external factors such as pH, light, enzymatic activity, hypoxia-triggered, and multi-responsive triggers. This article, based on the mechanisms of host–guest recognition, multifunctional assembly, and supramolecular nano-valves, provides several representative examples of CAs and PAs in the field of drug-controlled release. Finally, the article looks forward to future developments in this research area.

Review

1 Aromatic macrocycles for host–guest drug release systems

Aromatic macrocycles are highly valuable in fields such as chemistry, materials science, and life science due to their rigid, electron-rich and hydrophobic cavities, and ease of modification [42]. Among these, CAs and PAs are representative aromatic macrocycles. They can be made water-soluble and exhibit good biocompatibility through carboxyl or phosphate group modification, showing great potential in biomedical carrier applications. Compared with other artificial macrocycles such as crown ethers [43], cyclodextrins, and cucurbiturils, CAs and PAs have unique advantages. Their synthesis is simple (one-step completion), and they have adjustable conformations and π-electron-rich cavities [44,45], enabling efficient recognition of electron-deficient or neutral guest molecules and high-selec-

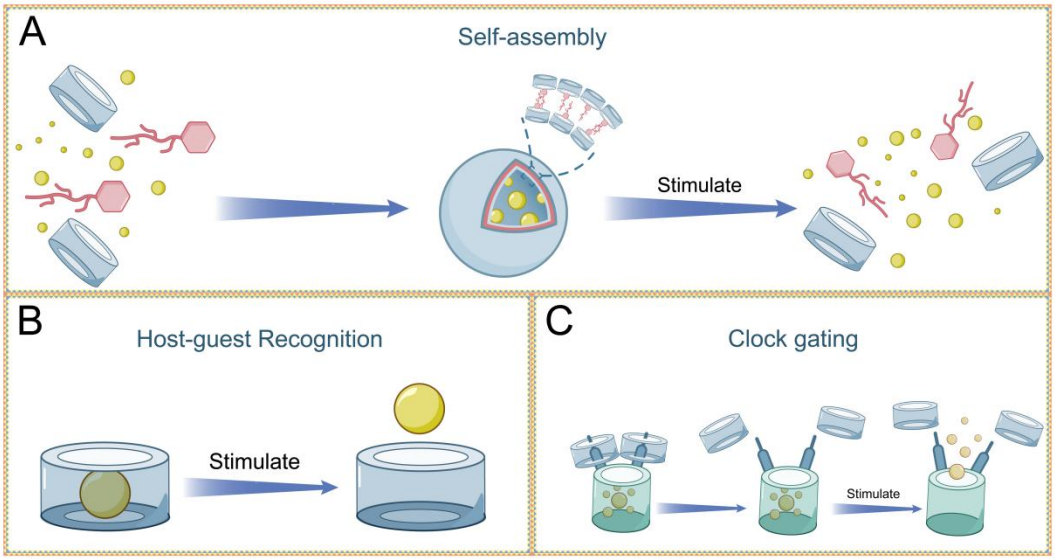

Figure 1: Schematic diagram of drug-controlled release mechanisms based on aromatic macrocycles.

tivity binding in drug-controlled release. Many calix/pillar[*n*]arene hosts are soluble in water, particularly macrocycles that are modified with carboxyl and phosphate groups. Moreover, their amphiphilic modification ability allows easy self-assembly into functional materials like vesicles, micelles and nanoparticles, overcoming the difficulties in modifying cyclodextrin and cucurbituril. These features make CAs and PAs promising candidates for stimulus responsive drug release systems [46]. Their structural diversity and functional designability offer broad prospects for targeted applications. This section will focus on the structural features and applications of CAs and PAs.

1.1 CAs: structure and properties

CAs are the third generation of supramolecular hosts [40], succeeding cyclodextrins and crown ethers. They are macrocycles composed of phenolic units condensed with formaldehyde, connected via methylene bridges. The most common CAs usually consist of 4, 6, or 8 phenolic units (Figure 2) [47-53]. The upper rim of CAs is equipped with hydrophobic alkyl groups, which, together with the benzene rings, form a hydrophobic cavity. In contrast, the lower rim consists of a series of neatly arranged hydrophilic phenolic hydroxy groups that can be selectively modified through chemical reactions [49].

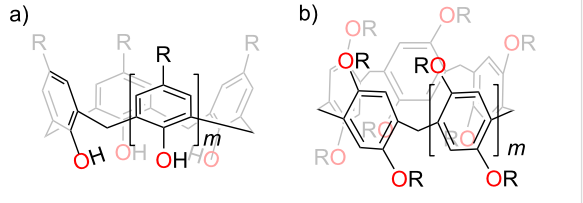

Figure 2: Chemical structure of a) calix[*n*]arene (*m* = 1,3,5), and b) pillar[*n*]arene (*m* = 1,2,3).

CAs feature large hydrophobic cavities whose size can be precisely modulated by varying the number of aromatic rings. This structural tunability enables the cavities of CAs to selectively bind drugs of different sizes through hydrophobic and π–π stacking interactions and undergo targeted modifications to enhance their affinity for various guest molecules, such as choline [54], quaternary ammonium salts [55], drug molecules [56], etc. Although they generally have poor solubility, this can be improved through derivatization. Water-soluble calixarene derivatives can be obtained through functional modifications, including the introduction of sulfonic acid, amine, and carboxylic acid groups [57-59]. These water soluble macrocycle derivatives can be used to increase the solubility of drugs. The modified CAs encapsulate drug molecules within the host through host–guest interactions. The interactions between the drug and the calixarene enhance the solubility of the drug [60]. Further functionalization of these CAs' upper and lower rims with diverse moieties (e.g., amides, imines, sulfur-containing groups, or alkyl chains) significantly expands their multifunctionality and broadens their application scope. Notably, CAs can be readily modified into amphiphilic macrocycles that can self-assemble with guests, and it exhibits superior advantages over crown ethers and cyclodextrins in terms of controllable functionalization [61]. In clinical applications, particularly for anticancer drug conjugation, CAs demonstrate remarkable cancer cell selectivity, minimized off-target effects, enhanced delivery efficiency, and reduced systemic toxicity. Additionally,

their synthetic accessibility, structural adaptability, and responsiveness to external stimuli (pH, light, enzyme, hypoxia) facilitate sustained drug release, side effect mitigation, and therapeutic efficacy, making them increasingly prominent in drug carrier research.

In recent years, the diversity of supramolecular amphiphiles has significantly expanded, bringing revolutionary breakthroughs to drug delivery systems. These structures, which possess both hydrophobic and hydrophilic characteristics, can self-assemble through non-covalent interactions to form well-defined aggregates such as micelles, vesicles, and nanoparticles [62]. Their morphologies mainly depend on molecular structure, concentration, and environmental properties. The cylindrical geometry of vesicles [63] promotes the arrangement of amphiphilic molecules with their hydrophobic tails pointing inward and hydrophilic heads pointing outward, forming a closed bilayer [64]. In contrast, micelles are usually assembled from single-tailed, conical molecules, where the smaller hydrophobic chains and larger head groups form monolayer spherical or rod-like structures [65]. Moreover, nanoparticles can be constructed through the physical or chemical cross-linking of polymers (such as PLGA and PEG), inorganic materials (such as gold and silica), or biomolecules (lipids and proteins), enabling efficient drug loading and controlled release [66-68]. Among them, amphiphilic CAs that incorporate both hydrophilic groups and hydrophobic alkyl chains through dual modifications [69]. These derivatives have emerged as a research hotspot due to their unique combination of water solubility, biocompatibility, and host–guest encapsulation capability [47,52,70]. The aggregation behavior of amphiphilic CAs is closely related to the size of the macrocycle, the length of the alkyl chain, and the nature of the polar head group [71]. Compared with traditional surfactants, amphiphilic CAs have a lower critical micelle concentration and are more likely to self-assemble into various forms of aggregates, such as spherical micelles [72], vesicles, and spherical nanoparticles [73]. Calixarene-based amphiphiles are characterized by their low cytotoxicity and ability to load drugs. The structure of calixarene-drug complexes can respond to external stimuli, causing the self-assembled complex to disassemble, which enables sustained drug release. Based on these characteristics, CAs hold potential for applications in drug delivery systems.

1.2 PAs: structure and properties

Since Ogoshi et al. first introduced pillar[*n*]arenes in 2008, these macrocycles have become essential to the synthetic macrocyclic receptor field [74]. Research on PAs and their derivatives has become a hot topic [75]. PAs can be prepared via the Friedel–Crafts condensation, which involves combining 1,4-dimethoxybenzene with paraformaldehyde in the presence of a Lewis acid. The central axis of these aromatic hydrocarbon molecules possesses *n* fold rotational symmetry [76]. PAs possess highly modifiable ring positions, and many PA derivatives with different functional groups can be obtained through the cyclization reaction of 1,4-dialkoxybenzene monomers or post-synthetic modification reactions [74]. PAs possess a unique internal cavity characterized by an electron-rich and hydrophobic environment, which significantly enhances the density of π-electrons. This structural feature makes pillar[*n*]arenes particularly effective at encapsulating guest molecules that are either electron-deficient or neutral. For example, pillar[5]arene (PA5) has a strong binding affinity for neutral guest molecules in organic solvents, [77] which is not feasible for crown ethers, CAs, and resorcinarenes. In addition, PAs can form supramolecular systems in the following ways: (1) the electron-rich cavity interacts electrostatically with cationic guests, such as methyl viologen derivatives, pyridinium salts, and quaternary ammonium salts [78]. (2) After modification with cationic groups, they can bind with anionic molecules, such as sulfonates [79]. It is worth mentioning that the cavity of PAs can encapsulate photo-responsive guests such as cationic azobenzene derivatives, providing new ideas for the innovation of drug design and therapeutic strategies. Notably, PA derivatives also exhibit specificity in recognizing important molecules in biological processes, such as acetylcholine [80], amino acids [81], doxorubicin (DOX) [82] and antibiotics [83], etc. Among the many derivatives, water-soluble pillar[5]arene (WP5) and pillar[6]arene (WP6) have become representative systems for biomedical applications due to their excellent performance in drug-controlled release [84,85].

Recent research on drug delivery has focused more on amphiphilic PAs, which are mainly constructed through two strategies: one is self-assembly after separately modifying hydrophobic and hydrophilic segments; the other is the formation of host–guest complexes between water-soluble PAs and guest molecules containing hydrophobic chains, followed by self-assembly into bilayer vesicles through host–guest interactions, hydrophobic effects, and π–π stacking interactions [86]. Their amphiphilic nature enables these systems to enter cells efficiently through endocytosis, providing a new drug delivery approach and holding great potential in precision medicine due to their programmable and stimulus-responsive features.

Additionally, PAs can be hybridized with various inorganic materials, such as metal-organic frameworks (MOFs), mesoporous silica nanoparticles (MSNs), metal nanoparticles, and carbon materials [87]. By designing through electrostatic and non-covalent interactions, PAs can be used as "molecular switches" to construct mechanized MOFs with the framework of MOFs, realizing the controlled release of drugs [88]. When integrated

with MSNs, nano valves consist of a mobile macrocyclic host that moves along a linear molecule between two or more binding sites. This movable macrocycle acts as a gate, controlling the movement of cargo into and out of the MSN pores [89]. These materials, with their ideal host–guest recognition characteristics, have provided new ideas for the design and synthesis of nano valve systems. These composite materials not only have the advantages of high specific surface area and large pore volume for drug loading, but also their unique stimulus responsive characteristics break through the limitations of traditional delivery systems: The pH, Zn^{2+}, and competitive agent-responsive characteristics can disrupt the multi-responsive supramolecular nanovalve systems based on PA5, primarily by disrupting the high-affinity host–guest interactions between PA5 and these groups (mainly through phosphonate-quaternary ammonium ion pairing) [90]. Azobenzene guest molecules can achieve dual functions (on and off) as ligands through photo-induced cis-trans isomerization. Using pillar[6]arene as the ion channel, the host–guest complexation realizes a reversible ON-OFF-ON type pseudo-monomeric ligand-gated ion transport switch [91]. The development of these pillararene-based materials has enriched the dynamic regulation methods of supramolecular structures and provided innovative approaches for prodrug design.

2 Stimulus-responsive controlled release in supramolecular systems

Many efforts have been made to prepare stimulus-responsive drug carriers, including some aimed at disease-related stimuli [92]. In the field of supramolecular materials, various stimulus strategies have been introduced to regulate the construction and destruction of aromatic macrocycles and their components. The external triggers include: pH [93], oxidation–reduction states [94], enzymatic actions [95], and light [96]. Specifically, within host–guest frameworks, the capability to meticulously regulate the assembly of complexes and synchronize them with biologically pertinent or biocompatible stimuli holds substantial potential for augmenting the precision of therapeutic interventions [97,98]. In certain scenarios, these stimuli precipitate reversible alterations in the formation of host–guest complexes, while in other cases, they may catalyze irreversible disintegration to avert reversibility. Given the benefits of the chemical stability of most aromatic macrocycles, creating stimulus-responsive complexes usually requires the guest components to undergo stimulus-triggered changes that affect their ability to bind with the host macrocycles. The controllable release of drugs is one of the most important applications of stimulus-responsive supramolecular systems and contributes to targeted therapy. Drugs are loaded into supramolecular nanosystems formed by self-assembled host–guest systems. Under specific stimuli (light, enzymes, hypoxia, pH values, etc.), changes in the host or guest molecules' chemical structure or properties lead to the host–guest system's disassembly, thereby releasing the drugs from the supramolecular systems [99]. Thus, the core principle of controlled release lies in modulating the association and dissociation of host–guest interactions. Aromat-containing macrocycles, such as CAs and PAs, are deemed exceptional hosts for fabricating host–guest nanosystems due to their versatile characteristics and capacity to self-assemble into supramolecular architectures via non-covalent interactions. These host–guest nanosystems play a vital role in controlled release, nanotechnology, materials chemistry, artificial molecular machines, and synthetic ion channels. Numerous host–guest systems have been developed based on their responsiveness to particular external triggers, including pH, enzymes, hypoxia, and light. The following section will review and discuss some of the stimulus responses.

2.1 pH-responsive controlled release

Changes in acidity are a typical stimulus for adjusting host–guest supramolecular nanosystems. It is widely recognized that the acidity levels of various organs, tissues, and cellular compartments differ. For example, the acidity of tumor and inflamed tissues is distinct from that of healthy tissues, offering a potential physiological trigger for pH-responsive drug delivery. Thus, drug release can be regulated by leveraging the variations in acidity between normal and diseased cells [100]. Developing therapeutic materials that react to shifts in pH, particularly the acidification arising from the endocytic pathway of internalized carriers or disease-induced acidification in local tissue microenvironments, is a prevalent approach for fabricating stimulus-sensitive drug carriers. Consequently, the construction of pH-responsive systems based on aromatic macrocycles has been widely promoted, with typical water-soluble carboxylated PAs and CAs frequently employed as host molecules or structural components [100]. This section will examine cases of pH-dependent degradation and drug release mechanisms.

Amphoteric CAs, known for their effective hydrophobic drug-loading capabilities, offer an excellent platform for controlled drug release. Researchers have synthesized amphoteric CAs to introduce pH-responsive properties, allowing each macrocycle to possess positively and negatively charged gates. Amphoteric CA8 were prepared by introducing positively charged groups at the lower rim of sulfonated CA8. The cavity size of the water-soluble CA8 matches with the hydrophobic drug ciprofloxacin (CPF). The efficient encapsulation of CPF (with a loading capacity of 17.8–24.5%) is achieved through the synergistic action of hydrophobic interactions and hydrogen bonding. Under physiological pH conditions (7.0–7.6), the CA8-CPF complex self-assembles into a stable multilayer structure

through electrostatic interactions. When the environmental pH deviates from the neutral range (pH < 6.0 or pH > 8.0), the charge balance is disrupted, leading to the dissociation of the complex and the release of the drug. This pH-sensitive "charge switch" mechanism enables CA8 to precisely control the release behavior of CPF, providing new insights for the development of environmentally responsive antibiotic delivery systems (Figure 3) [101]. This pH-sensitive "charge switch" mechanism enables CA8 to precisely control the release behavior of CPF, providing new insights for the development of environmentally responsive antibiotic delivery systems.

Water-soluble aromatic macrocycles are commonly utilized in drug delivery systems. Vesicles are valuable tools in biology, chemistry, and materials science. Supramolecular pH stimuli-responsiveness has applications at the cellular level and has the potential for controlling drug release in environmental protection. In 2012, Huang and colleagues [78] described the construction of supramolecular vesicles using WP6 and pyridine derivatives (G1) (Figure 4). This supramolecular system achieves controllable assembly and disassembly through pH responsiveness: under acidic conditions (pH 6.0), protonation of the WP6 carboxyl groups leads to vesicle disassembly; whereas in a neutral environment (pH 7.4), deprotonated WP6 can rebind with the guest molecules. The molecular recognition mechanism of this system is based on the synergistic effect of multiple non-covalent interactions, including electrostatic attraction, hydrophobic interactions, and π–π stacking. Researchers have further utilized this feature to achieve reversible transformation of amphiphilic guest molecules between micellar and vesicular states and have successfully applied it to the controlled release of dye molecules. Notably, the system can also effectively neutralize the toxicity of paraquat through host–guest interactions, providing a new approach for the treatment of environmental pollutants. This pH-responsive supramolecular platform shows broad application prospects in targeted drug delivery and environmental remediation.

Later, in 2014, Huang and colleagues synthesized a water-soluble pillar[7]arene (WP7) by adding 14 anionic carboxylic acid groups to both sides [102]. They explored the pH-dependent complexation of WP7 with paraquat derivative G1 in water. The host WP7 and guest G1 form a 1:1 pseudorotaxane, with an association constant of $(2.96 \pm 0.31) \times 10^5$ M^{-1}. Furthermore, they leveraged this new molecular recognition motif to create a supramolecular amphiphilic reagent using WP7 and an amphiphilic paraquat derivative G2. This pH-responsive drug delivery system has considerable potential for future medical applications. Hydrophilic supramolecular polymers that respond to stimuli, especially those formed in aqueous solutions, are poten-

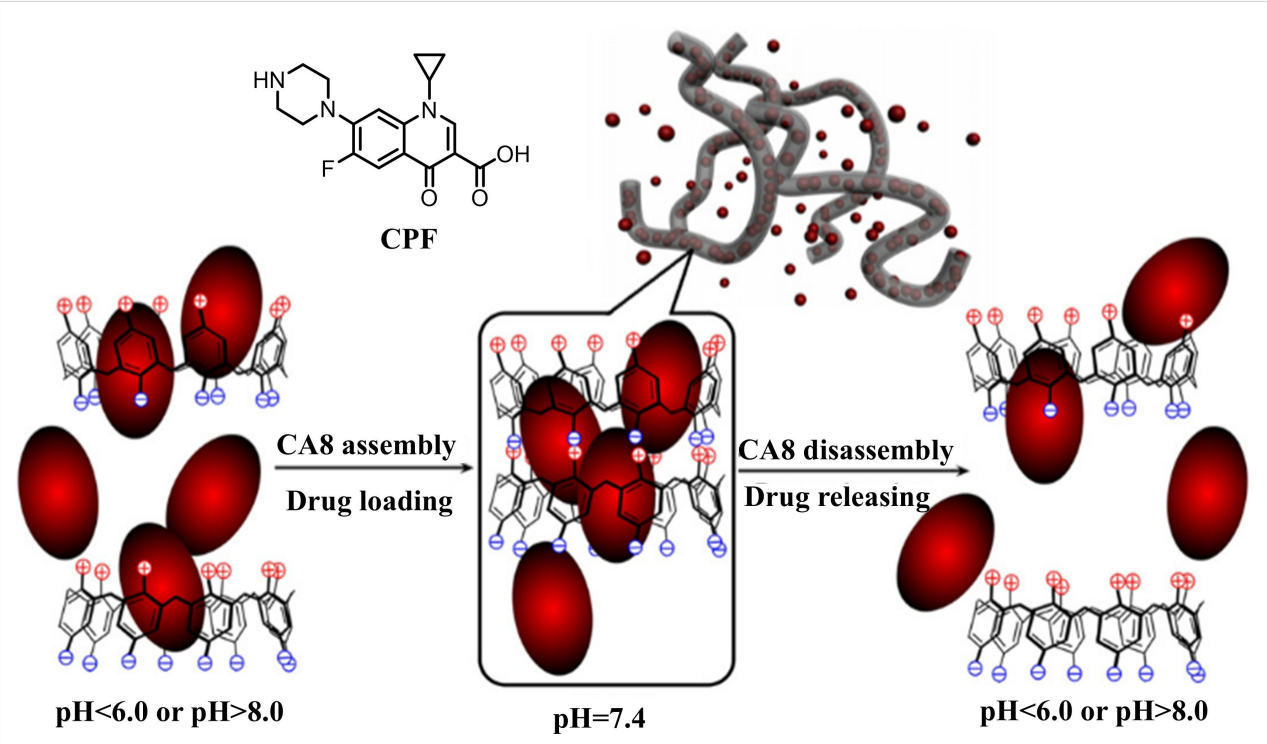

Figure 3: Changes in pH conditions cause the release of drugs from CA8 host–guest complexes [101]. Figure 3 was adapted with permission from [101], *Colloids and Surfaces B: Biointerfaces*, vol. 101, by Y. Xue; Y. Guan; A. Zheng; H. Xiao, "Amphoteric calix[8]arene-based complex for pH-triggered drug delivery", pages 55–60, Copyright (2012), with permission from Elsevier. This content is not subject to CC BY 4.0.

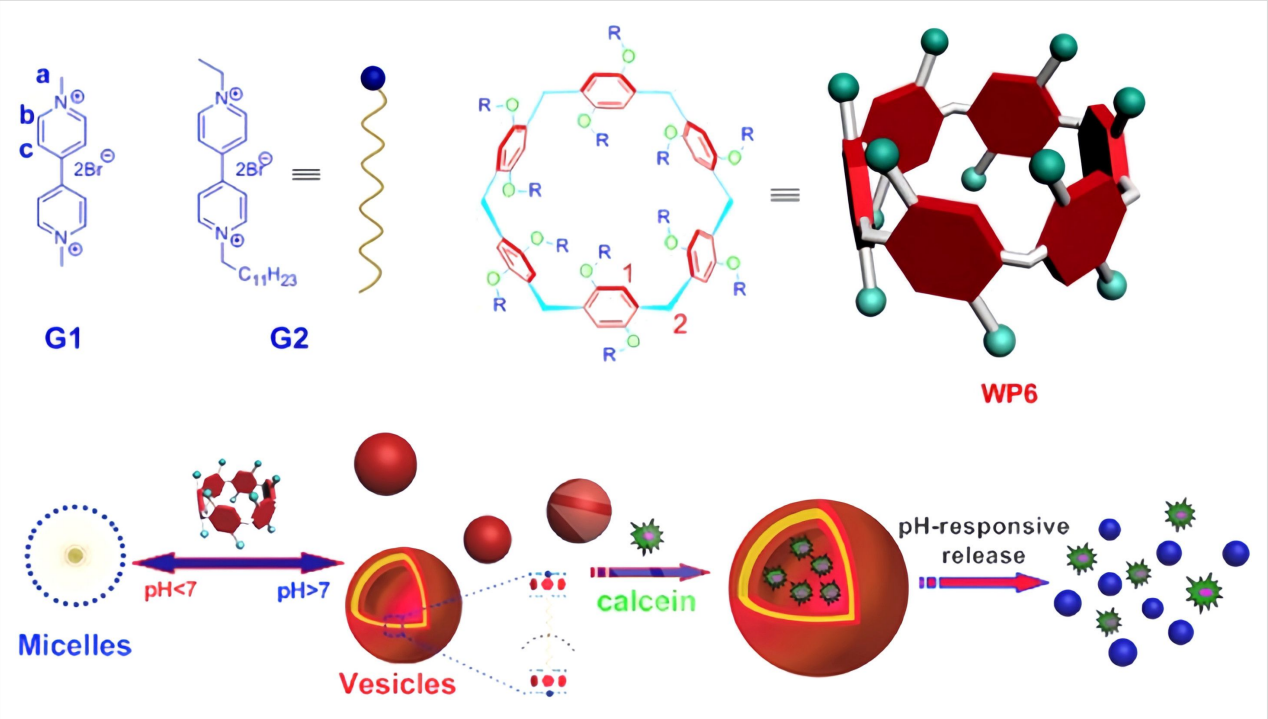

Figure 4: The illustration of the pH-mediated 1:1 complex formation between the host and guest molecules in aqueous solution, along with the pH-triggered release mechanism [78]. Figure 4 was adapted with permission from [78], Copyright 2012 American Chemical Society. This content is not subject to CC BY 4.0.

tial candidates for mimicking biocompatibility or creating important functional materials.

In 2021, Maiti et al. employed small-molecule mannose-modified CA4 to create the core structure CA4-Man3 and produce nano-micelles known as CA4-Man3-NPs (Figure 5) [103]. CA4-Man3-NPs achieve efficient targeted drug delivery through a unique self-assembly mechanism. This system leverages the unique polymeric characteristics of CA4, which reduces the critical aggregation concentration and enhance intermolecular orderliness to form structurally stable nanocarriers [52]. The key design features are: 1) The mannose groups at the upper rim confer specific recognition ability for cancer cell surface receptors; 2) The hydrophobic core formed by the alkyl chains at the lower rim and the hydrogen-bonding network constructed by the thiourea unit can efficiently encapsulate DOX. This structure integrates multiple non-covalent interactions, such as hydrophobic interactions and π–π stacking, endowing the micelles with both structural stability and pH responsiveness. When targeted to the tumor microenvironment (acidic pH), the core of the micelles dissociates to achieve specific release of DOX, significantly improving the delivery efficiency and tumor targeting of hydrophobic drugs.

The release of DOX from PAs also can be regulated by a pH-responsive mechanism. In 2015, Wang and coworkers synthesized a novel supramolecular prodrug nanoparticle exploiting the host–guest interactions between WP6 and DOX-derived prodrugs (Figure 6) [104]. As demonstrated in previous studies, WP6 has shown good biocompatibility and acid-responsive properties in aqueous media [78,105]. Meanwhile, it has been proven that WP6 has a strong binding [106,107] affinity for pyridinium salts in water driven by hydrophobic and electrostatic interactions. DOX-based prodrugs are synthesized by directly conjugating hydrophobic DOX with pyridinium-modified flexible alkyl chains (G3) or short EGn (ethylene glycol) chains (G4) via acid-cleavable hydrazone bonds. The above-mentioned WP6-G3 and WP6-G4 supramolecular complexes, based on their amphiphilic nature, have the ability to form higher-order aggregates in weakly alkaline phosphate-buffered saline (PBS). The resulting supramolecular nanoparticles exhibited stability under physiological conditions. The cumulative release of DOX reached nearly 100% within 30 minutes at a pH of 5.5, which simulates the lysosomal environment at 37 °C. Both CAs and PAs are effective supramolecular platforms for the controlled release of DOX, demonstrating significant potential for various applications.

In 2013, Wang and others reported [93] that WP6 and hydrophobic ferrocene derivatives (FC) self-assembled into supramolecular vesicles loaded with mitoxantrone (MTZ) exhibiting significant pH-responsive behavior in aqueous solutions, excep-

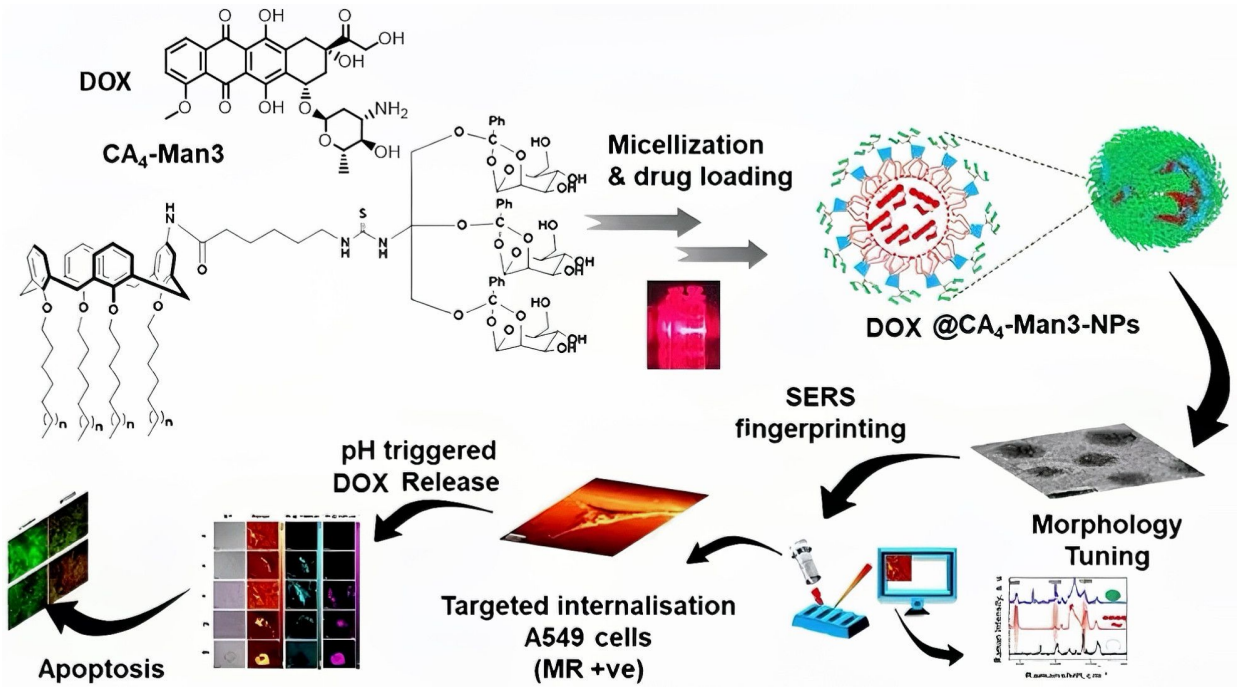

Figure 5: Illustration of the pH-responsive self-assembly of mannose-modified CA4 into micelles and the subsequent release of DOX [103]. Figure 5 was adapted with permission from [103], *Journal of Controlled Release*, vol. 339, by Sreedevi, P.; Nair, J. B.; Joseph, M. M.; Murali, V. P.; Suresh, C. H.; Varma, R. L.; Maiti, K. K, "Dynamic self-assembly of mannosylated-calix [4] arene into micelles for the delivery of hydrophobic drugs", pages 284–296, Copyright (2021), with permission from Elsevier. This content is not subject to CC BY 4.0.

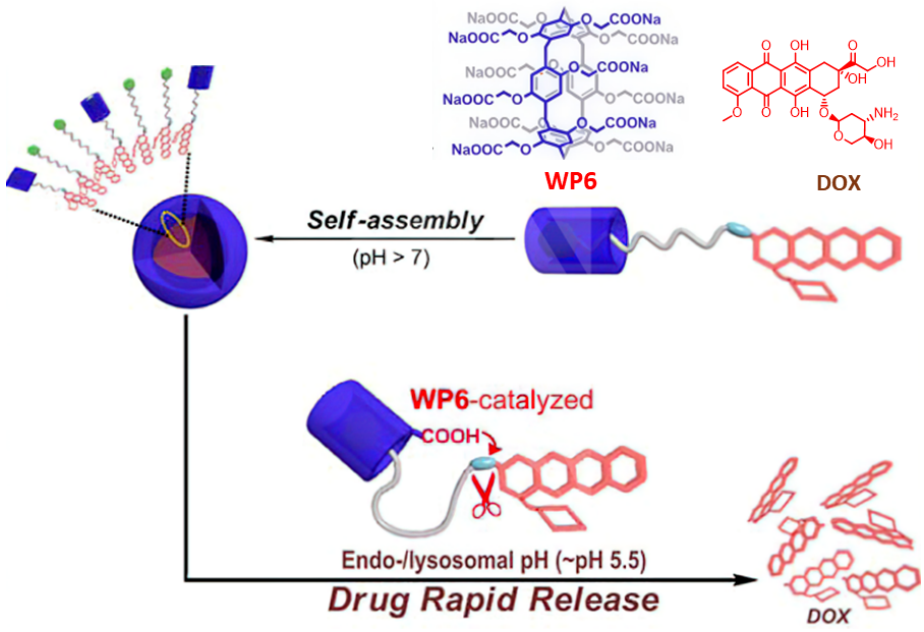

Figure 6: Illustration of the assembly of supramolecular prodrug nanoparticles from WP6 and DOX-derived prodrugs (G3 and G4) for WP6-mediated rapid release of the drug [104]. Figure 6 was adapted with permission from [104], Copyright 2015 American Chemical Society. This content is not subject to CC BY 4.0.

tionally rapid release of MTZ in a low pH environment (Figure 7). The complex exhibits significant amphiphilicity: the carboxylate residues of WP6 confer hydrophilicity, while the alkyl chains of FC contribute hydrophobicity, driving the molecules to self-assemble into supramolecular vesicles in the aqueous phase. The vesicle structure features a bilayer characteristic, with two hydrophilic carboxylate shell layers enveloping a hydrophobic alkyl chain core. The assembly driving force directly relies on the host–guest interaction between WP6 and FC. Further studies have shown that by regulating the deprotonation/protonation state of the WP6 carboxyl groups through pH control, the reversible dissociation and reassembly of the vesicle structure can be achieved, thereby constructing a pH-responsive drug carrier. The novel supramolecular vesicles assembled from WP6 and guest molecules in aqueous environments are promising for controlled release and drug delivery applications. They have established a foundation for pH-responsive controlled release systems based on WP6, encouraging increased research participation within this domain.

Photothermal construction and manipulation of optical materials are crucial in pharmaceutical or biological fields. In 2016, Zhang and colleagues [108] developed a supramolecular nanovesicle with improved photodynamic therapy (PDT) capabilities. This system was based on the host–guest interactions between polyethylene glycol-functionalized pillar[5]arene (PEG-P[5]A) and a pyridinium-capped porphyrin derivative containing a disulfide bond (TPPC6-SS-Py). The supramolecular amphiphile could self-assemble into spherical micelles, demonstrating excellent colloidal stability in aqueous solutions, as evidenced by transmission electron microscopy (TEM) and dynamic light scattering (DLS). The PEG-P[5]A/TPPC6-SS-Py micelles showed rapid release of the porphyrin photosensitizer under reducing conditions. Furthermore, in 2023, Zhang and colleagues [109] constructed a tumor microenvironment (TME)-activated supramolecular nanoplatform (Figure 8) which was consisted of a pillar[5]arene-based amphiphilic polymer (POPD), a phototherapeutic agent (Cy7-CN), an antimalarial drug with respiratory function (atovaquone, ATO), and a chemotherapeutic agent (pyridinium camptothecin, CPT-Py). This platform was designed for imaging-guided phototherapy to alleviate hypoxia. They created a new supramolecular amphiphile that enabled rapid drug release and efficient cellular internalization, potentially providing a robust platform for drug delivery and controlled release systems.

The excellent biocompatibility of both supramolecular vesicles and nano-fragments with the body indicates that aromatic macrocycles have great potential for biomedical applications. These macrocycles are distinguished by their unique structures and superior performance in host–guest interactions. Creating functional and intelligent supramolecular nano-drug carriers for controlled drug delivery is promising. In this context, water-soluble carboxylated arenes are the primary host molecules for most pH-responsive nanosystems. The nanosystem is broken down by the highly acidic environment of tumor cells, which acts as an exogenous or endogenous stimulus to enable the con-

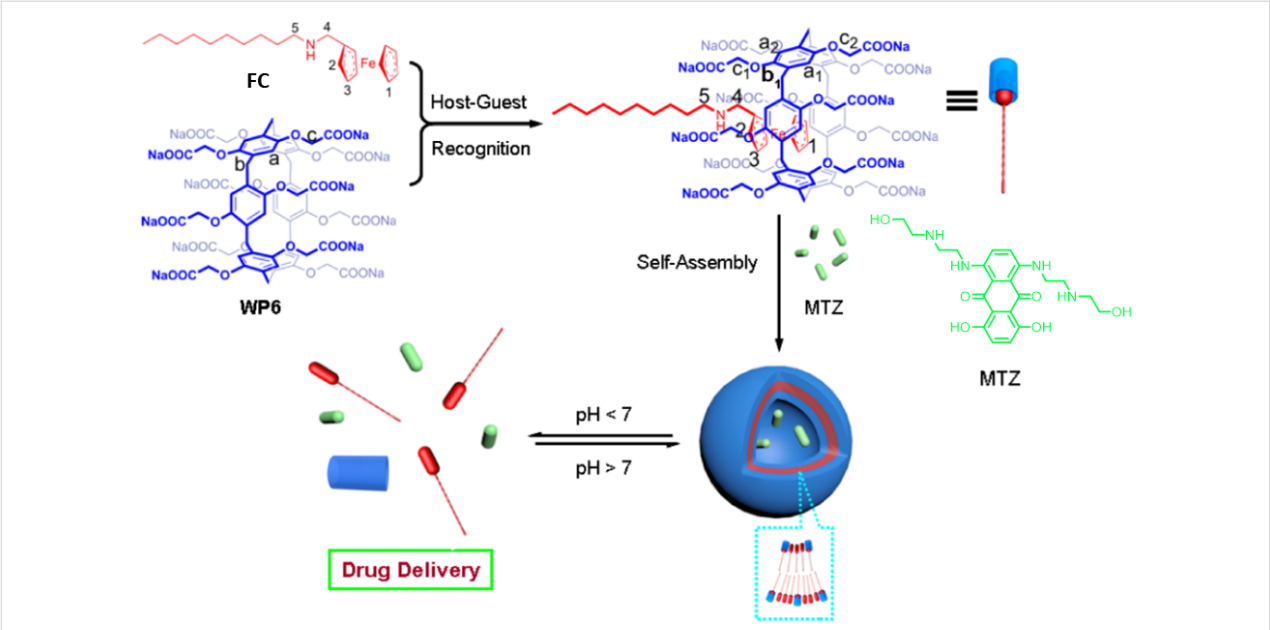

Figure 7: Illustration of the formation of supramolecular vesicles and their pH-dependent drug release [93]. Figure 7 was adapted with permission from [93], Copyright 2013 American Chemical Society. This content is not subject to CC BY 4.0.

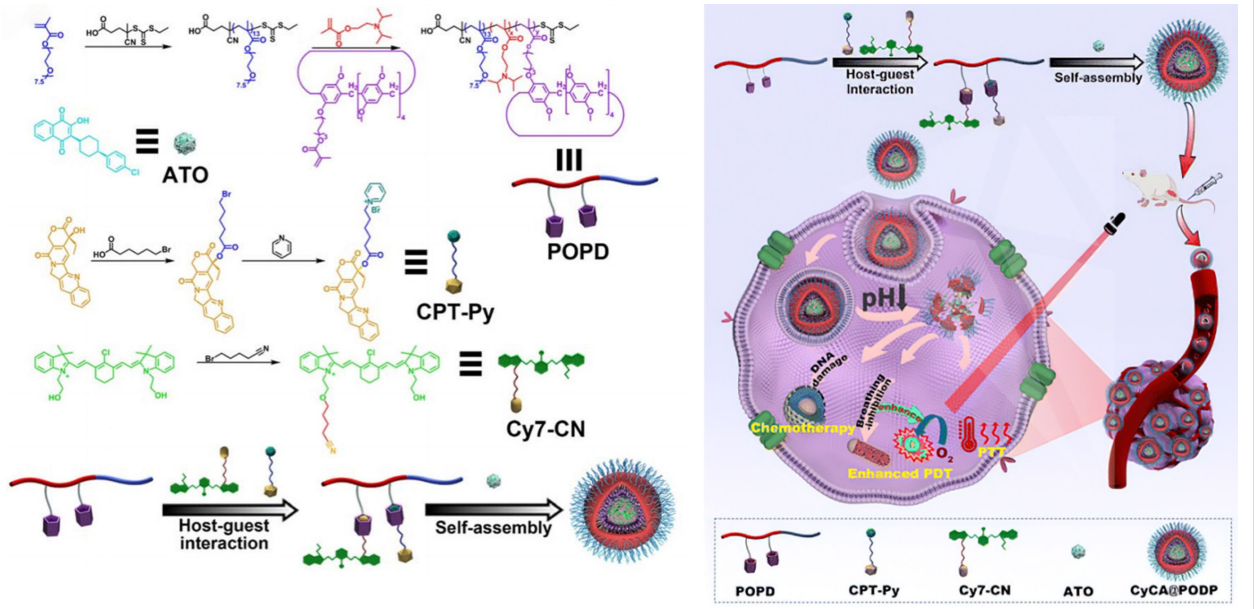

Figure 8: Schematic illustration of the application of the multifunctional nanoplatform CyCA@POPD in combined PDT, photothermal therapy (PTT), and chemotherapy [109]. Figure 8 was reproduced from [109] ("A supramolecular nanoplatform for imaging-guided phototherapies via hypoxia tumour microenvironment remodeling", © 2023 W. J. Zhou et al., published by The Royal Society of Chemistry, distributed under the terms of the Creative Commons Attribution-NonCommercial 3.0 Unported License, https://creativecommons.org/licenses/by-nc/3.0/). This content is not subject to CC BY 4.0.

trolled release of the encapsulated drugs. These nanosystems are highly compatible with the body and comprise biocompatible, water-dispersible, and low-toxicity small molecules.

2.2 Light-responsive controlled release

Light is an ideal external stimulus due to its ease of use, low cost, and safety [110,111]. Its unique advantages include being easily turned on and off, providing high spatial and temporal resolution with precise control over irradiation wavelength and intensity, and facilitating rapid responses in confined spaces [111]. Its tunable parameters, such as wavelength, duration, and intensity, along with these characteristics, have contributed to its extensive application in innovative materials and molecular devices. Ultraviolet light, in particular, is commonly employed as an external trigger for supramolecular systems. Azobenzene can regulate geometry, shape, and interfacial curvature under ultraviolet or visible light irradiation. It undergoes *cis–trans* isomerization, which can trigger alterations in bioactivity or assembly configurations. Methods for creating photo-responsive cages or capsules include fabricating cages and capsules from photoactive building blocks, and developing cages and capsules encapsulating photo-responsive guest molecules [112,113]. Incorporating supramolecular amphiphiles into photo-sensitized systems has propelled the creation of novel multifunctional photo-responsive materials. This section will discuss drug molecule capture and release systems based on two hosts.

The photo-sensitive assembly has drawn considerable interest in degradable materials, drug delivery systems, and tissue engineering. Anthracene (AnPy) derivatives are recognized for their high reactivity when exposed to light and are frequently employed as photo-degradable molecules. Liu described a photo-sensitized system composed of amphiphilic 9-alkoxy-substituted AnPy and *p*-sulfonato calix[4]arenes (SC4A) (Figure 9) [114]. SCnAs have a unique propensity to regulate the aggregation behavior of aromatic or amphiphilic molecules by reducing the critical aggregation concentration, enhancing the compactness of aggregates, and modulating the orderliness within aggregates, which is referred to as calixarene-induced aggregation (CIA) [52]. Taking the SC4A-AnPy system as an example, SC4A encapsulates the pyridine group of AnPy with its electron-rich cavity, neutralizing the electrostatic repulsion of the cationic head group and promoting the close packing of the AnPy rings through hydrophobic interactions and π-π stacking, while its deprotonated phenolic groups maintain water solubility. This assembly approach not only suppresses the fluorescence self-quenching of AnPy in the aggregated state (enhancing the yield of singlet oxygen) [115], but also boosts its photo-sensitivity – under light irradiation, the anthracene in the complex can be efficiently converted to the active drug form, anthraquinone [116]. The CIA strategy effectively improves the solubility, bioavailability, and light-response efficiency of hydrophobic photo-sensitizing drugs, offering new ideas for light-controlled drug delivery systems.

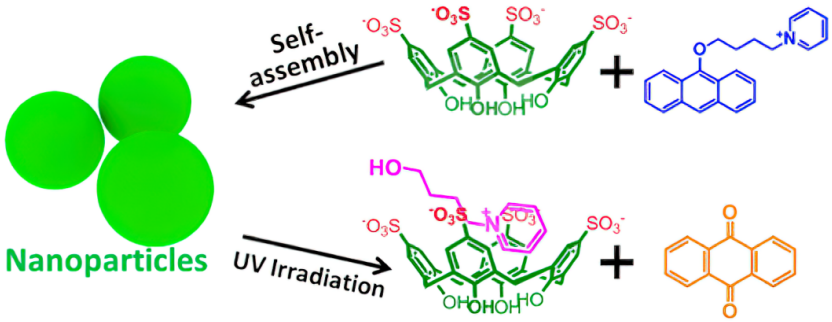

Figure 9: Illustration of the photolysis of an amphiphilic assembly via CA-induced aggregation [114]. Figure 9 was reprinted with permission from [114], Copyright 2015 American Chemical Society. This content is not subject to CC BY 4.0.

In 2018, Sun and colleagues designed and synthesized a chiral CA named chiral azo-calix[4]arene derivative (FC4AD) (Figure 10) [117]. Its interaction with enantiomers of aminoindanol in solution was investigated. It was found that FC4AD has high selective binding and release for (1*R*,2*S*)-1-amino-2-indanol, forming a 1:1 complex. *S*-phenethylamine was used as a chiral ligand, which was modified on the upper rim of calixarene through hydrogen bonding. An azobenzene group

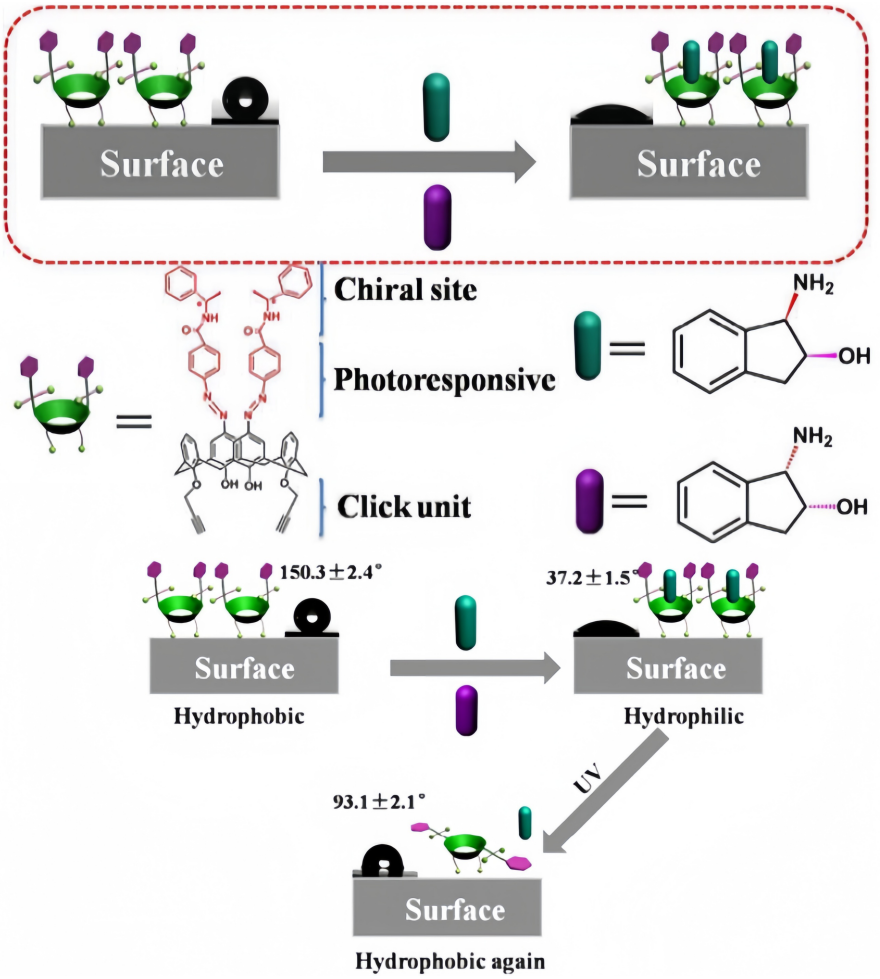

Figure 10: Schematic illustration of drug release controlled by the photo-responsive macroscopic switch based on FC4AD [117]. Figure 10 was used with permission of The Royal Society of Chemistry, from [117] ("A photo-responsive macroscopic switch constructed using a chiral azo-calix[4]arene functionalized silicon surface" by H. Pang et al., *Chem. Commun.*, vol. 54, issue 24, © 2018); permission conveyed through Copyright Clearance Center, Inc. This content is not subject to CC BY 4.0.

was introduced as the photo-regulating part at the upper edge of calixarene. The alkyne at the lower edge of FC4AD was used to form self-assembled monolayers (SAMs) on a silicon surface through Cu-catalyzed click chemistry to construct a photo-responsive macroscopic switch. This switch can achieve photo-controlled chiral reversible recognition of (1*R*,2*S*)-1-amino-2-indanol through changes in contact angle, and it holds promise for applications in chiral drug controlled release and other biotechnological fields. Further research can be conducted on the stability and performance of this switch under different environmental conditions. Its practical application in chiral drug controlled release can be expanded. Exploration of its interactions with other biomolecules can also be carried out to develop more applications in biosensing and biotechnology.

In 2024, Thongnuek and coworkers crafted a PA5-linked gelatin hydrogel incorporating the Azo-SMX drug (referred to as A-hydrogel), aiming to achieve light-regulated uptake and delivery of antibiotics (Figure 11) [118]. Azobenzene, when subjected to particular light wavelengths, displays reversible switching between its *trans* and *cis* forms, a molecular behavior well-documented in light-responsive systems. Initially, Azo-SMX, bearing an azobenzene unit, exists in a trans form and creates a stable complex with the PA5 component within the hydrogel. Upon exposure to 365 nm UV light, Azo-SMX transitions from the *trans* to the *cis* state, prompting its release from the complex. Research on antibacterial efficacy has confirmed that the modified Azo-SMX antibiotic is effective against a range of microorganisms, including both Gram-positive and Gram-negative bacteria.

2.3 Enzyme-responsive controlled release

Elevated enzyme levels often mark the microenvironment of many pathological tissues, as well as intracellular and cellular compartments. These enzymes can serve as effective triggers for drug release in stimulus-responsive systems. Owing to the specificity of enzymatic reactions, enzyme-responsive systems can act as targeted drug-delivery vehicles. Proteases such as esterases and ureases are particularly overexpressed in cancerous tissues. Thus, incorporating specific substrate groups or sequences can enhance drug release. Among the various stimuli used to control responsive assemblies, enzymatic methods offer several benefits, including biocompatibility, high efficiency, specificity, and mild reaction conditions.

Liu and colleagues reported an enzyme-responsive supramolecular ternary polymer (DiCh@a-CD-bisSC4A) (Figure 12) [95]. The supramolecular polymer with suberyl dicholine (DiCh) as the axle, with α-CD as the thread wheel and bisSC4A macrocycles as the iterative end cap units. Due to the hydrolysis of DiCh by cholinesterase, the formed supramolecular polymer assembly can be dispersed through enzymatic reactions. They

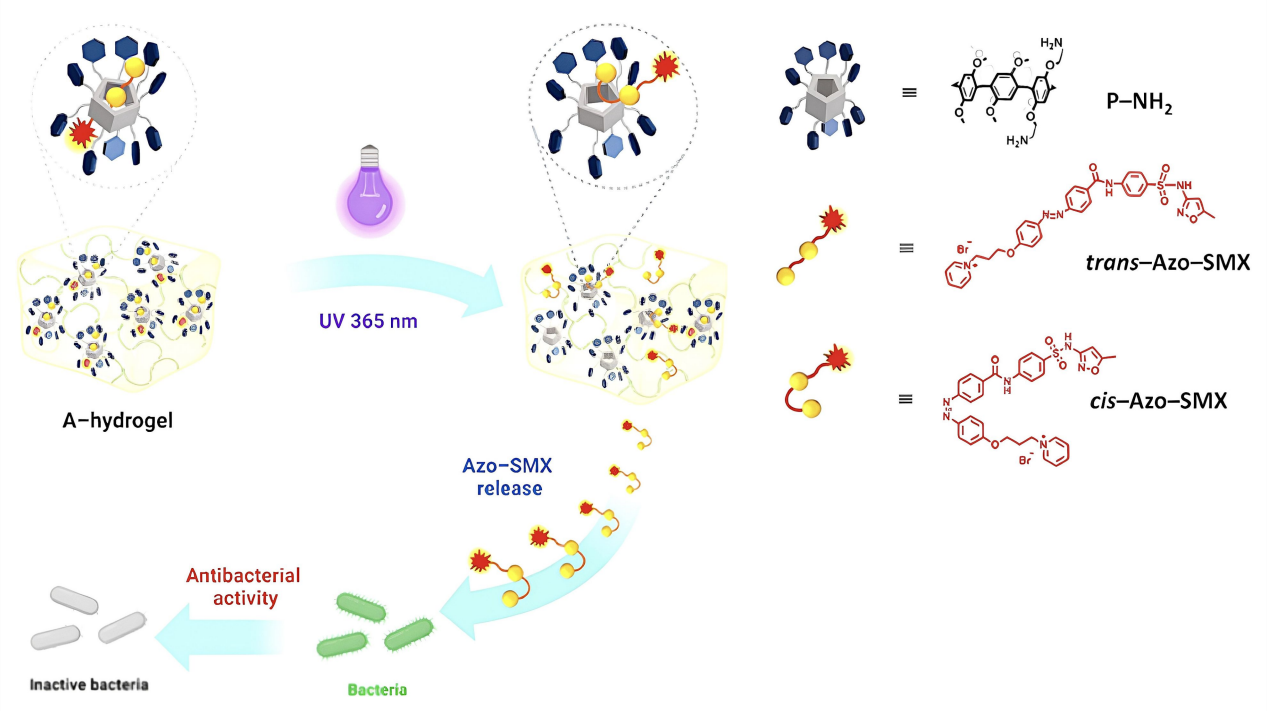

Figure 11: Schematic illustration of the formation process of Azo-SMX and its photoisomerization reaction under 365 nm UV light, transitioning from the trans to the cis form, which triggers its release from the inclusion complex [118]. Figure 11 was adapted with permission from [118], Copyright 2024 American Chemical Society. This content is not subject to CC BY 4.0.

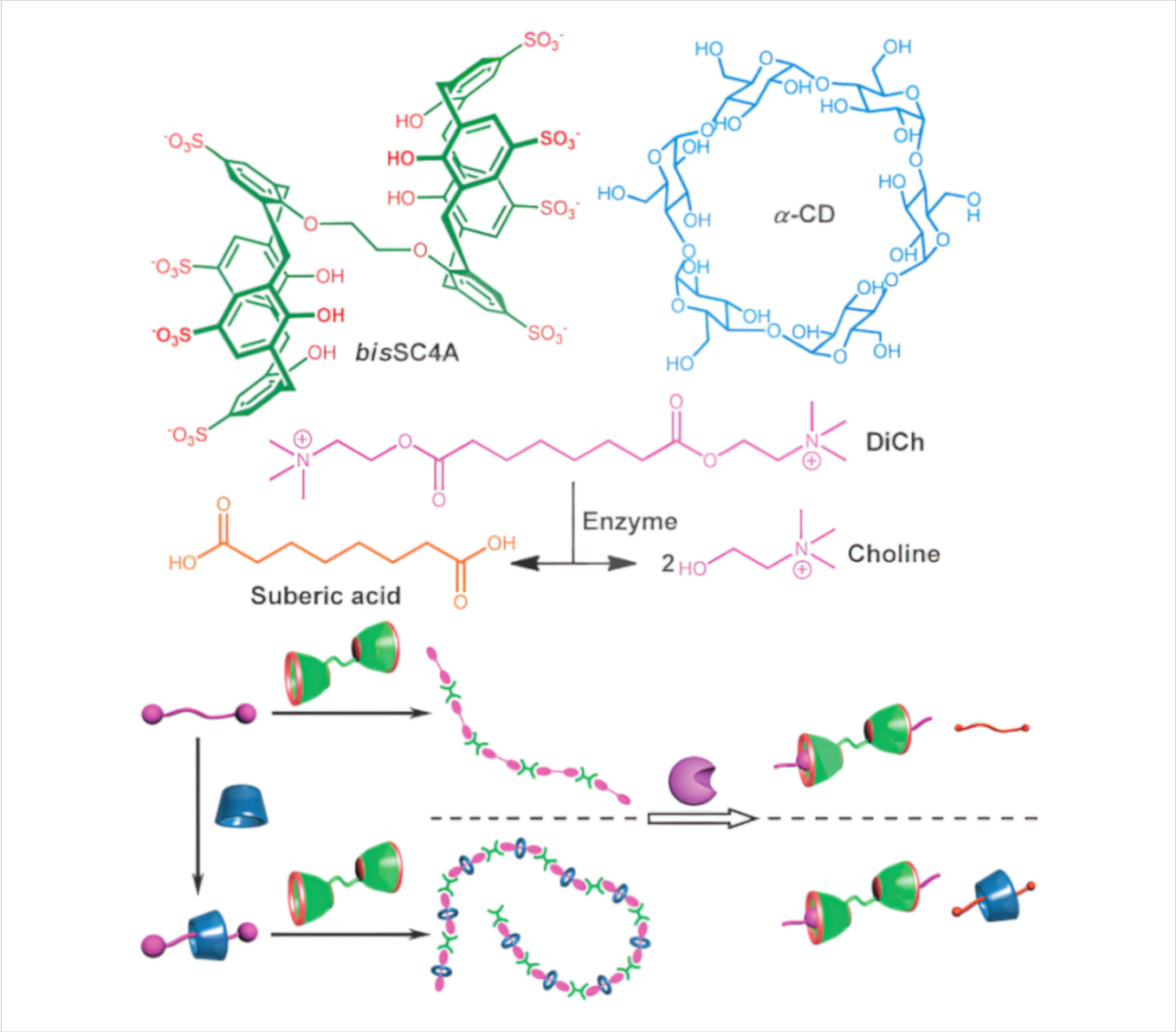

Figure 12: Schematic illustration of the enzyme-responsive behavior of supramolecular polymers [95]. Figure 12 was used with permission of The Royal Society of Chemistry, from [95] ("Enzyme-responsive supramolecular polymers by complexation of bis (*p*-sulfonatocalixarenes) with suberyl dicholine-based pseudorotaxane" by Guo, D.-S. et al., *Chem. Commun.*, vol. 49, © 2013); permission conveyed through Copyright Clearance Center, Inc. This content is not subject to CC BY 4.0.

successfully prepared a novel supramolecular ternary polymer DiCh@a-CD-bisSC4A and binary polymers DiCh@bisSC4A Compared to binary DiCh@bisSC4A, ternary DiCh@a-CD-bisSC4A has not only a larger polymer size but also a better size distribution and topological structure due to the integration of quasi rotaxanes with supramolecular polymers. Introducing α-CD onto DiCh effectively adjusts the flexibility of the spacer group, which in turn enhances supramolecular polymerization. Despite DiCh being captured by both α-CD and bisSC4A, the resultant assembly retains enzyme responsiveness, attributed to the dynamic equilibrium inherent in non-covalent interactions. Building on biocompatibility studies, they also developed an enzyme-responsive supramolecular vesicle for treating Alzheimer's disease. This vesicle is assembled via the host–guest interaction between SC4A and myristoyl choline (Figure 13) [119]. The host–guest complexation between SC4A and myristoylcholine is stabilized by the electrostatic interaction between the negatively charged sulfonate groups and the positively charged quaternary ammonium groups. The interaction between the host and guest reduces the critical aggregation concentration (CAC) to form binary vesicles, with the hydrophobic alkyl chains of myristoylcholine packing together and the inner and outer surfaces composed of the hydrophilic phenolic OH groups of SC4A exposed to the aqueous solution. Subsequently, cholinesterase (acetylcholinesterase (AChE) and butyrylcholinesterase (BChE)) specifically converts myristoylcholine into myristic acid and choline [120]. SC4A binds to the non-amphiphilic choline but not to the amphiphilic myristic

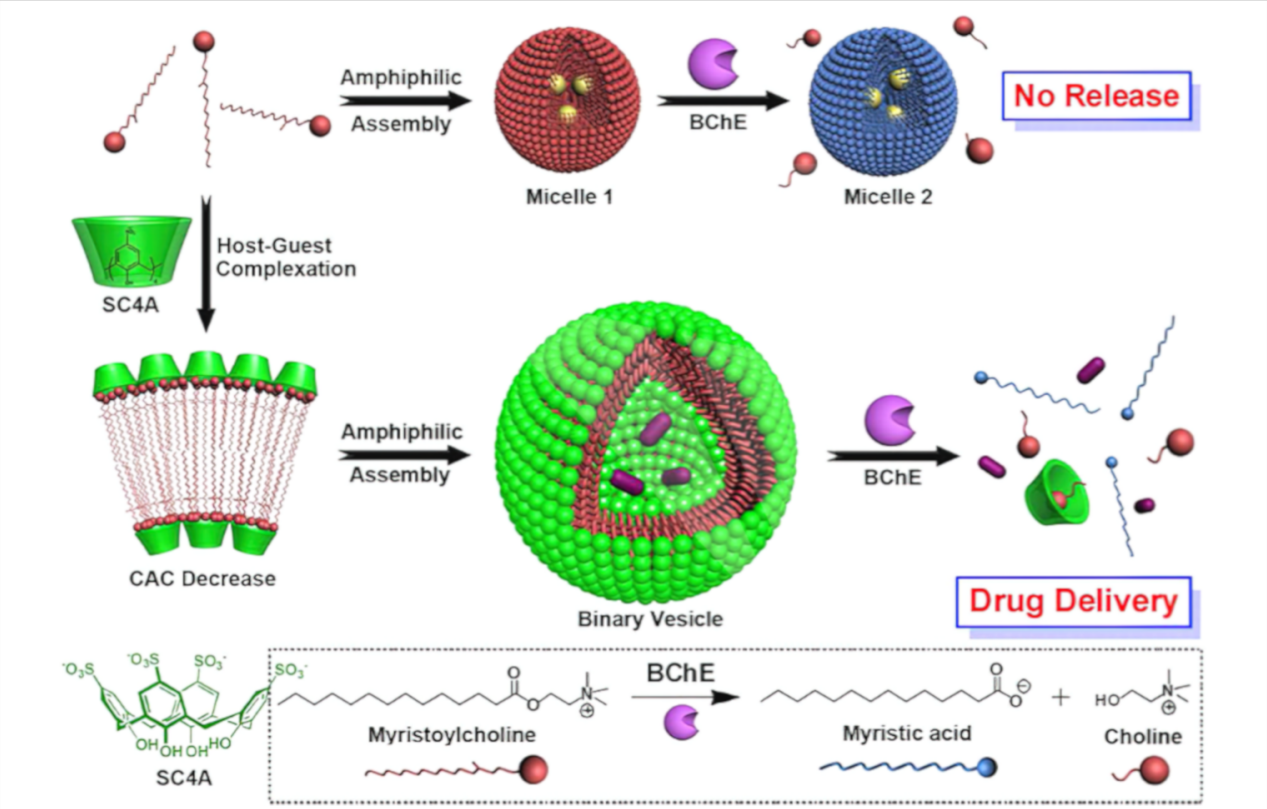

Figure 13: Schematic illustration of the amphiphilic assembly of SC4A and its enzyme-responsive applications [119]. Figure 13 was reprinted with permission from [119], Copyright 2012 American Chemical Society. This content is not subject to CC BY 4.0.

acid, leading to the disassembly of the composite vesicles. Currently, the clinical treatment of Alzheimer's disease is mainly based on cholinesterase inhibitors, such as tacrine. Therefore, this vesicle system may be suitable for the controlled release of Alzheimer's disease drugs.

Extensive research has been conducted on MSN carriers fitted with supramolecular nano valves. Yang and co-workers [121] designed an enzyme-responsive supramolecular nanovalve composed of MSNs and choline sulfonatocalixarene[2]pseudorotaxane. Two different choline derivatives with distinct structures and lengths (Figure 14) were grafted onto the pores of MSNs via ester or urea linkages, serving as enzyme-cleavable sites. Negatively charged SC4A macrocycles were introduced to envelop the choline stems on the surface of MSN-NPs through host–guest interactions, forming pseudorotaxanes as the mobile/cleavable components of the nanovalves. It was experimentally demonstrated that esterase could selectively activate the ester-linked nanovalve (MSN-C1), while urease could selectively activate the urea-linked nanovalve (MSN-C2). This innovative enzyme-activated method provides inherent biocompatibility, mild reaction conditions, high efficiency, and specificity for the degradation of supramolecular polymers.

2.4 Hypoxia-responsive controlled release

In the last few years, notable strides have been achieved in boosting the targeting accuracy and clinical utility of drug release mechanisms. Tumor cells are characterized by unique attributes, such as acidity, hypoxia, and altered metabolism, which set them apart from healthy cells. These distinct features underscore the importance of focusing on the tumor microenvironment to develop supramolecular systems that are highly specific and capable of responding to multiple stimuli. These advanced systems aim to target and penetrate tumor cells effectively, mitigate drug resistance caused by tumor cell uptake, and ultimately enhance clinical efficacy.

Guo and associates developed hypoxia-responsive molecular carriers, namely carboxylated or sulfonated azo-calix[4/5]arenes [122,123]. These CAs, utilizing their azo groups that are easily reduced in low-oxygen settings, provide the potential for tumor-targeted drug release while reducing side effects. The azo-calix[4/5]arenes have demonstrated strong binding capabilities with a range of chemotherapeutic drugs, which underscores their potential as supramolecular drug carriers. They have verified the efficacy of this hypoxia-targeted therapy through both in vitro and in vivo experiments, and the carrier has made significant progress in the field of hypoxia-targeted drug delivery.

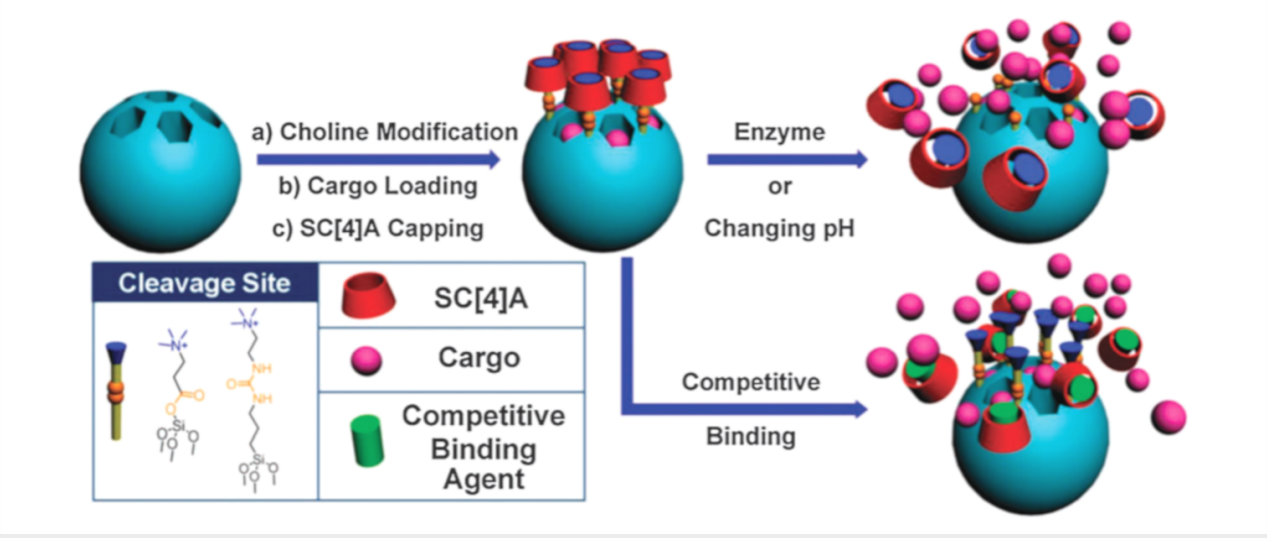

Figure 14: Stimuli-responsive nanovalves based on MSNs and choline-SC4A[2]pseudorotaxanes, MSN-C1 with ester-linked stalks and MSN-C2 with urea-linked stalks [121]. Figure 14 was used with permission of The Royal Society of Chemistry, from [121] ("Enzyme-responsive supramolecular nanovalves crafted by mesoporous silica nanoparticles and choline-sulfonatocalix [4] arene [2] pseudorotaxanes for controlled cargo release" by Sun, Y.-L. et al., *Chem. Commun.*, vol. 49, issue 79, © 2013); permission conveyed through Copyright Clearance Center, Inc. This content is not subject to CC BY 4.0.

This section highlights several recent studies on stimulus-responsive drug release within hypoxic tumor environments.

Among anti-cancer drugs, BE-43547A2 (BE) exhibits high cytotoxicity against hypoxic pancreatic cancer cells, which is in line with the current hypoxic tumor environment, making it a promising candidate for hypoxia-targeted therapies. The Guo group modified calixarene to obtain sulfonated azocalix[5]arene (SAC5A), and then combined the BE prodrug (NMP-BE) with the SAC5A to create a supramolecular complex, NMP-BE@SAC5A, that is responsive to dual hypoxia signals (Figure 15) [123]. The azo group in SAC5A endows it with hypoxia responsiveness, allowing it to enhance the accumulation of NMP-BE in tumors under hypoxic conditions in

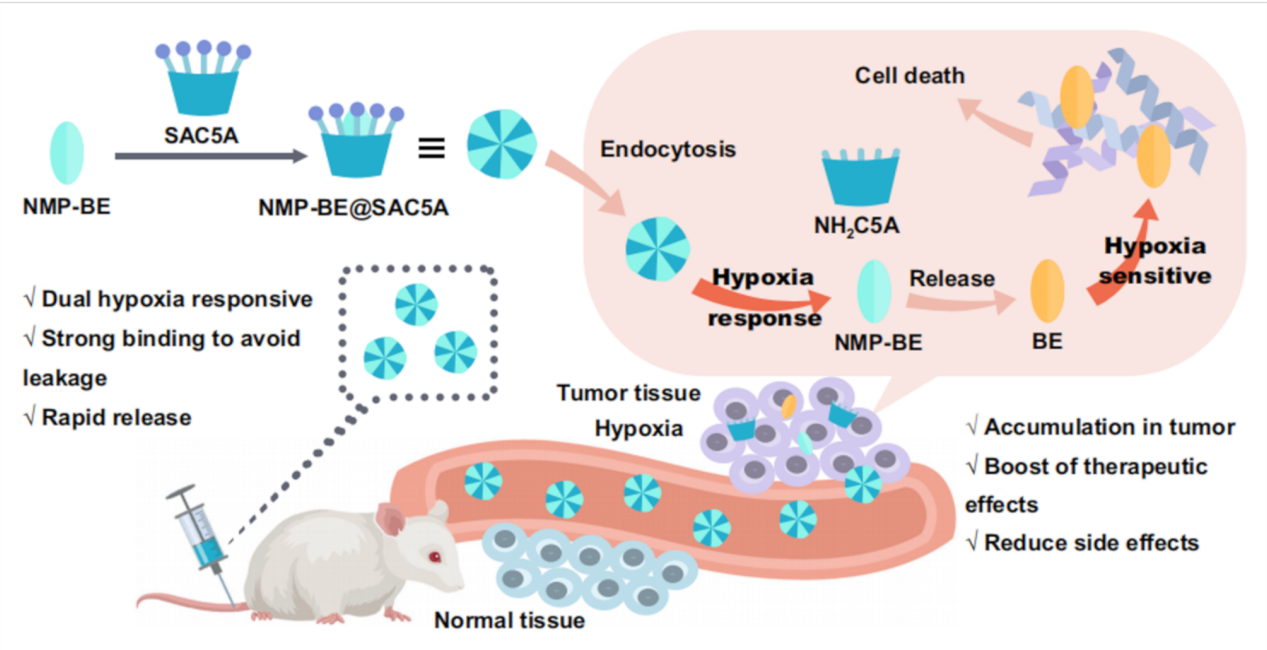

Figure 15: A schematic diagram showing the construction of a supramolecular system by host–guest interaction between SAC5A and the NMP-BE prodrug under hypoxic conditions [123]. Figure 15 was reproduced from [123] (© 2023 J.-S. Guo et al., published by Springer Nature, distributed under the terms of the Creative Commons Attribution 4.0 International License, https://creativecommons.org/licenses/by/4.0).

cancer cells. Upon intracellular release in cancer cells, NMP-BE releases the hypoxia-sensitive toxin BE, achieving the dual hypoxia-responsive therapeutic goal through host–guest interactions. Due to the specific cellular uptake and discharge process, NMP-BE@SAC5A effectively suppresses the proliferation of pancreatic cancer in a mouse model with human tumor cells at minimal concentrations, while avoiding adverse effects throughout the body. In the future, it could be attempted to combine it with more anti-tumor drugs and apply it in clinical settings.

In addition to the aforementioned SAC5A that can respond to stimuli under hypoxic conditions, they also synthesized Biotin-SAC4A by modifying SAC4A with biotin. (Figure 16) [124]. Monocarboxylated azocalixarene and aminated biotin were synthesized. Subsequently, using a coupling agent, the carboxyl group of the azocalixarene was modified through amidation to obtain biotin-modified SAC4A. The formation of amide bonds and azo linkages deepened the cavity and enhanced the interaction strength with drugs. The biotin on the upper rim endows biotin-SAC4A with the ability to actively target tumor cells based on the interaction between biotin and biotin receptors, thereby improving antitumor efficacy. DOX@biotin-SAC4A exhibited high cytotoxicity against cancer cells but low toxicity to normal cells. They further combined Biotin-SAC4A with DOX and injected it into mice. The experimental results showed that Biotin-SAC4A could firmly bind DOX and promote its release under hypoxic conditions.

In 2024, Guo and colleagues developed a SAC4A grafted self-assembled peptide hydrogel for hypoxia-responsive controlled drug release in anti-inflammatory treatment of ischemic stroke (Figure 17) [125]. Following PBS induction, the peptide hydrogel was tailored to exhibit a rheological modulus and shear-thinning behavior similar to that of brain tissue. The hydrogel's hypoxia-responsive properties were validated through three different systems: sodium dithionite (SDT), rat liver microsomes, and the oxygen-glucose deprivation (OGD) model. Under hypoxic conditions, the hydrogel achieved

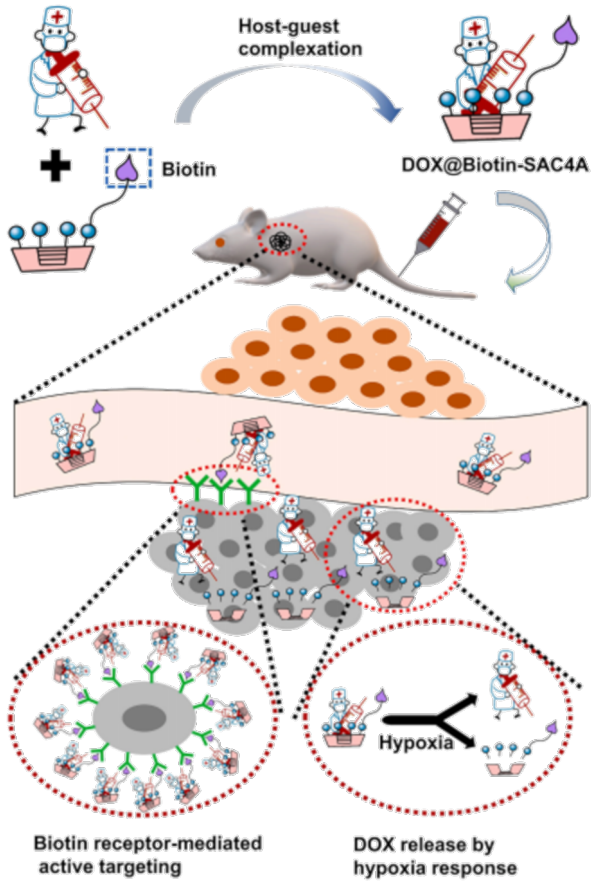

Figure 16: A schematic diagram showing the formation of the host–guest complex DOX@Biotin-SAC4A by biotin modification of SAC4 and the release of DOX under hypoxic conditions in mice [124]. Figure 16 was reprinted from [124], *Journal of Controlled Release*, vol. 368, by Chen, M.-M.; Tang, X.; Li, J.-J.; Chen, F.-Y.; Jiang, Z.-T.; Fu, R.; Li, H.-B.; Hu, X.-Y.; Geng, W.-C.; Guo, D.-S., "Active targeting tumor therapy using host–guest drug delivery system based on biotin functionalized azocalix [4] arene", pages 691–702, Copyright (2024), with permission from Elsevier. This content is not subject to CC BY 4.0.

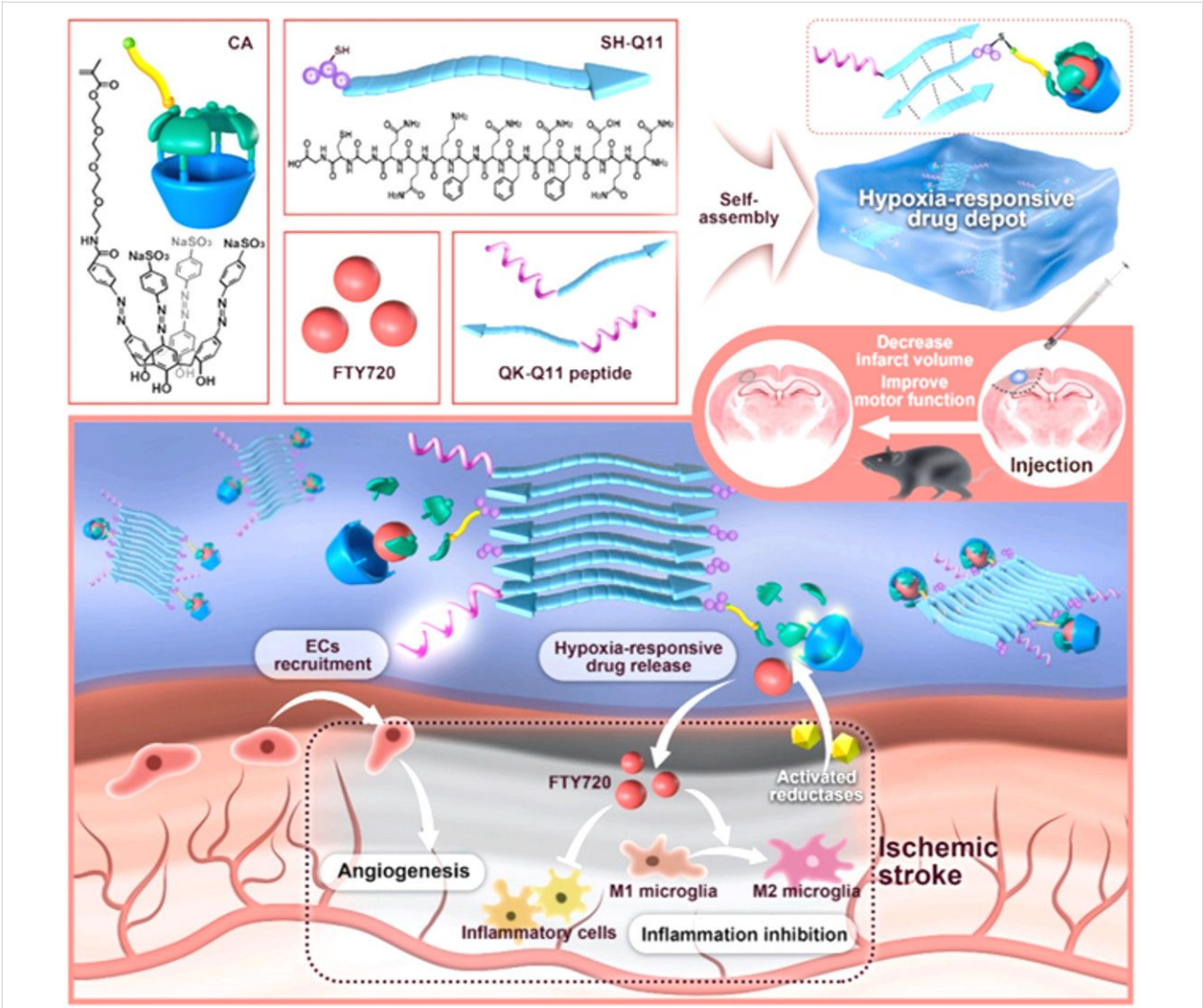

Figure 17: A schematic diagram showing the self-assembly of CA4 into a hypoxia-responsive peptide hydrogel, which achieves targeted release of CY5-DM or FTY720 in vitro [125]. Figure 17 was reprinted from [125], *Nano Today*, vol. 54, by Zheng, W.; Yao, S.-Y.; Hu, H.; Chen, X.; Qian, Z.; Liu, W.; Zhu, Y.; Mao, Z.; Guo, D.-S.; Gao, C., "Hypoxia-responsive calixarene-grafted self-assembled peptide hydrogel for inflammation suppression in ischemic stroke", article no. 102064, Copyright (2023), with permission from Elsevier. This content is not subject to CC BY 4.0.

targeted release of cyanine 5-dimethyl (CY5-DM) or fingolimod (FTY720) in vitro. Upon local administration, the hypoxia-responsive self-assembling peptide hydrogel resulted in improved motor function and reduced inflammation in vivo.

Recently, Geng and colleagues created additional binding sites by modifying the upper rim of CA4 with glucose and enhanced the overall solubility and biocompatibility of the azo-calixarene structure, designing it as a drug carrier (Figure 18) [126]. This carrier binds to the ferroptosis inhibitor liproxstatin-1 (Lip) and releases it selectively in hypoxic environments. This mechanism aims to counteract the side effects associated with intravenous thrombolysis using recombinant tissue-type plasminogen activator (rtPA) for treating ischemic stroke. The interaction between GluAC4A and Lip results in a significant improvement in Lip's solubility. The glucose modification on the upper rim of GluAC4A serves multiple functions: it expands the calixarene cavity, creates additional binding sites, and enhances the overall solubility and biocompatibility of the azo-calixarene structure. The azo moiety in GluAC4A imparts hypoxia responsiveness, enabling the targeted release of Lip specifically at ischemic sites. GluAC4A effectively promotes drug accumulation in the brain. Moreover, the Lip@GluAC4A complex significantly reduces iron deposition, blood-brain barrier leakage, and neurological deficits that are commonly observed with rtPA treatment.

2.5 Multi-responsive controlled release

The previous sections discussed the controlled drug release of single-stimulus-responsive systems, adopting a relatively simple

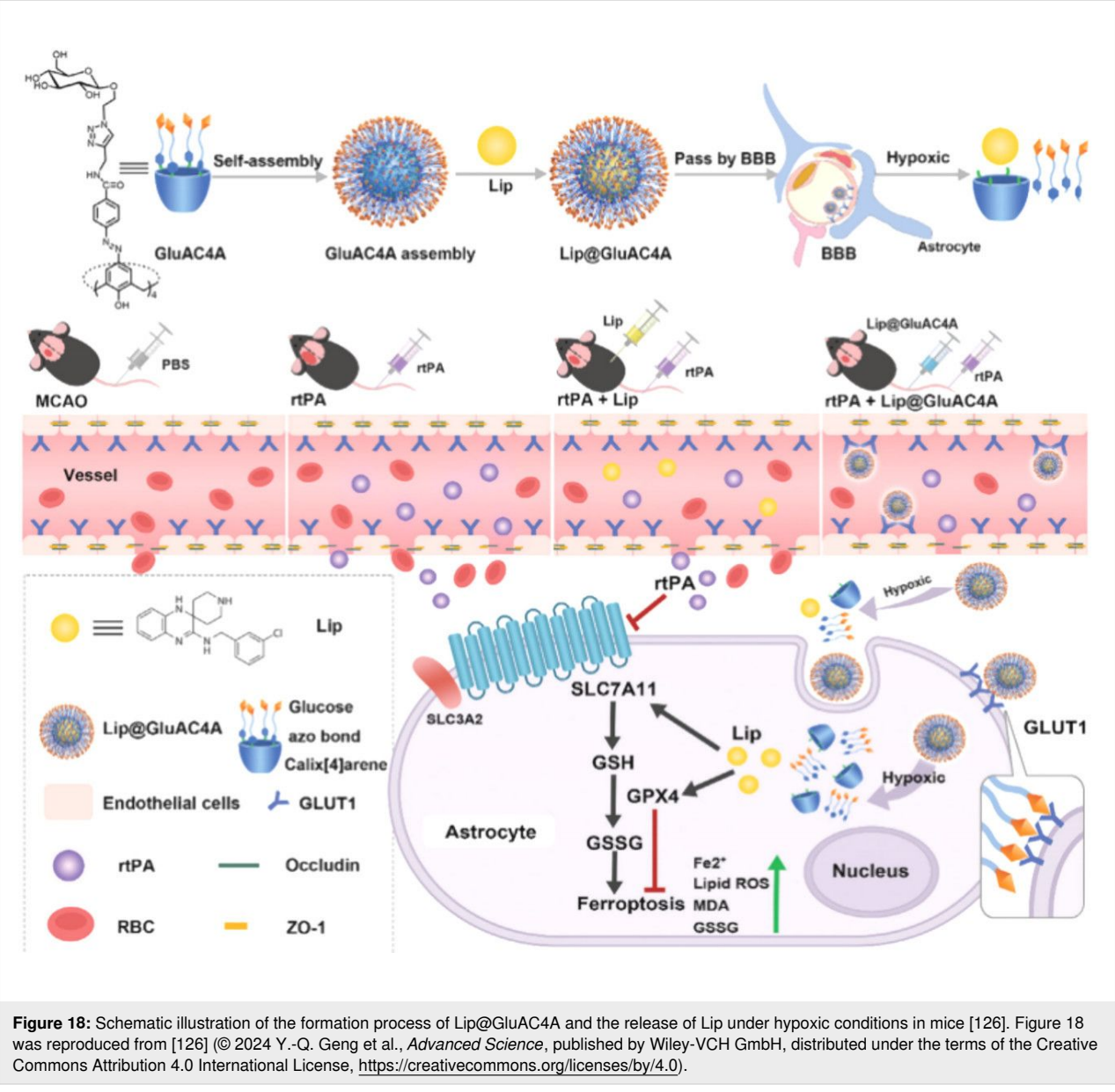

Figure 18: Schematic illustration of the formation process of Lip@GluAC4A and the release of Lip under hypoxic conditions in mice [126]. Figure 18 was reproduced from [126] (© 2024 Y.-Q. Geng et al., *Advanced Science*, published by Wiley-VCH GmbH, distributed under the terms of the Creative Commons Attribution 4.0 International License, https://creativecommons.org/licenses/by/4.0).

perspective of a single stimulus-response. Multistimuli responsiveness also holds potential applications in terms of responsiveness and efficient drug release. One of the major challenges faced by researchers in this field has long been the difficulty of incorporating two or more functional groups simultaneously when constructing multi-stimuli-responsive systems. Supramolecular materials can also be designed to be responsive to multiple stimuli. In addition to those mentioned above, multistimulus responses have a broad application prospect in controlling drug release. For example, supramolecular peptide assemblies that naturally respond to pH or ion strength can be designed to include light-responsive elements or feature-specific enzyme substrates, thus utilizing two separate stimulus-response pathways.

In 2011, Liu and colleagues [127] created a multi-stimulus-responsive supramolecular bis-vesicle through the complexation of water-soluble calixarene (C4AS) with 1-dodecyl-1'-methyl-4,4'-bipyridinium (MVC12). The term "bis-vesicle" refers to a structure with two fused or nested vesicular domains, typically featuring shared membrane interfaces or segregated internal spaces. They subsequently loaded the anticancer drug DOX into the vesicle. The formation mechanism benefits from the rigid conical structure of C4AS, which significantly reduces the critical aggregation concentration of MVC12 by 1000 times. This bis-vesicle structure possesses the following intelligent responsive characteristics: (1) temperature sensitivity originating from the enthalpy-driven nature of the host–guest interaction; (2) redox responsiveness due to the reversible electron

transfer of MVC12; (3) competitive complexation making the system sensitive to cyclodextrins. Experiments have confirmed that this carrier can efficiently encapsulate DOX and trigger drug release through multiple stimuli, demonstrating good potential for anticancer therapy in vitro. This intelligent delivery system, integrating temperature, redox, and molecular recognition responses, provides important ideas for the development of new cancer treatment strategies.

In 2021, Han et al. explored the interactions WP5 and aniline tetramer (TANI) as host and guest molecules (Figure 19) [128]. The WP5⊃TANI complex is capable of self-assembling into supramolecular vesicles. WP5 has a large hydrophobic cavity that can accommodate TANI, and the interaction between WP5 and TANI leads to the formation of an amphiphilic complex. The amphiphilicity of the WP5-TANI complex, the π–π stacking interactions between the two components, and the high hydrophobicity of TANI promote the host–guest interactions between WP5 and TANI, leading to the further formation of supramolecular vesicles by the WP5⊃TANI complex. These vesicles are non-toxic to normal cells but exhibit toxicity towards cancer cells. The WP5⊃TANI supramolecular vesicles can effectively encapsulate the anticancer drug DOX. Both the acidic microenvironment at the tumor site and photothermal effects can induce the release of DOX. DOX delivered by these vesicles, in combination with NIR light irradiation, can significantly suppress tumor growth.

Wang and colleagues [107] designed a supramolecular binary vesicle system based on WP6 and SAINT molecules (G5), which exhibits multiple stimulus-responsive characteristics to pH, Ca^{2+} and temperature (Figure 20). WP6 and G5, as amphiphilic molecules containing pyridine groups and alkyl chains, form supramolecular amphiphiles through host–guest interactions, with the assembly process driven by both hydrophobic and electrostatic interactions. The vesicles can efficiently encapsulate drug molecules such as calcein and DOX, and trigger their release under acidic conditions or Ca^{2+} stimulation. The fusion process of WP6⊃G5 vesicles can be divided into three stages: First, Ca^{2+} binds to the carboxyl groups on the outer surface of the WP6⊃G5 vesicles. Second, the binding of Ca^{2+} to WP6 further induces vesicle aggregation. Third, vesicle

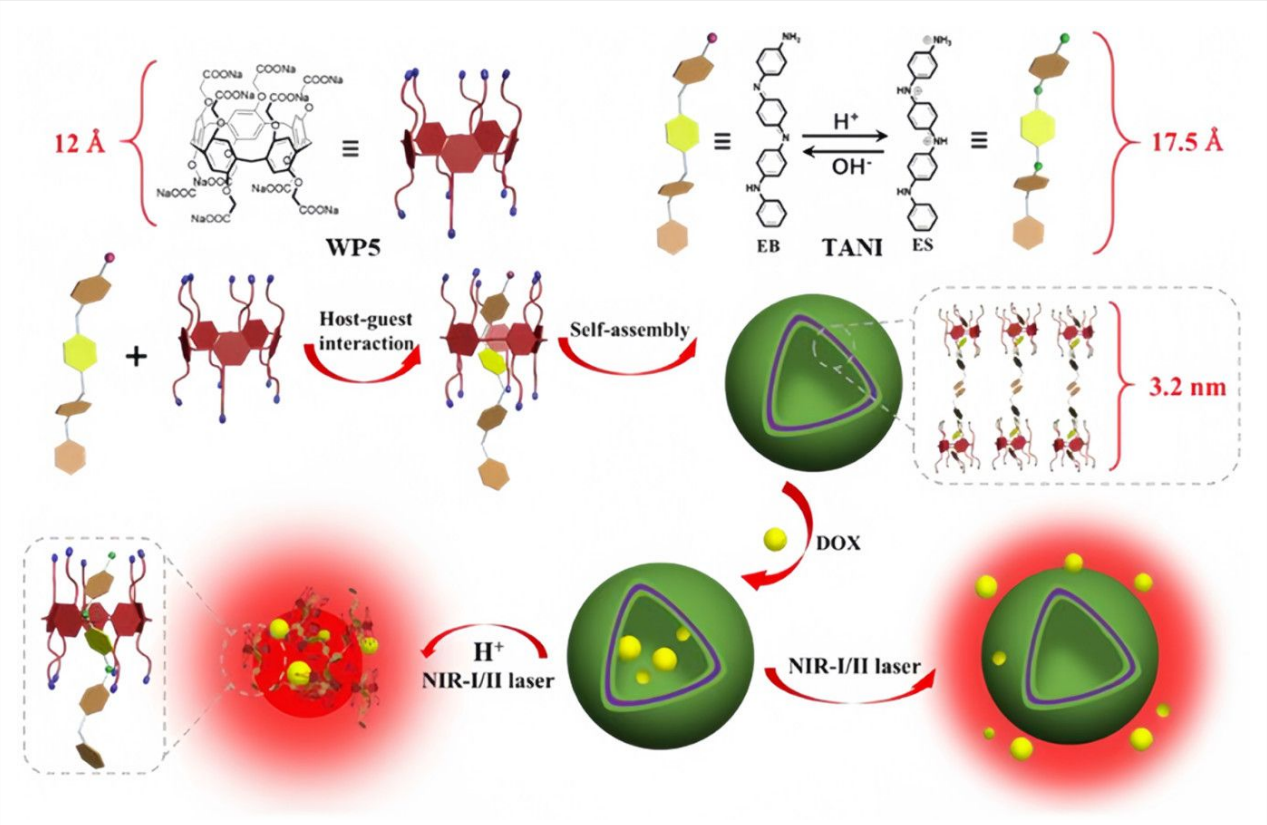

Figure 19: Schematic illustration of the construction of a supramolecular vesicle based on the host–guest complexation between WP5 and TANI, and the release of DOX under acidic conditions or NIR irradiation [128]. Figure 19 was reprinted from [128], *Chemical Engineering Journal*, vol. 403, by Chen, X.; Wang, Z.; Sun, X.; Han, Y.; Huang, Y.; Xi, J.; Bian, X.; Han, J.; Guo, R., "Photothermal supramolecular vesicles coassembled from pillar [5] arene and aniline tetramer for tumor eradication in NIR-I and NIR-II biowindows", Copyright (2020), with permission from Elsevier. This content is not subject to CC BY 4.0.

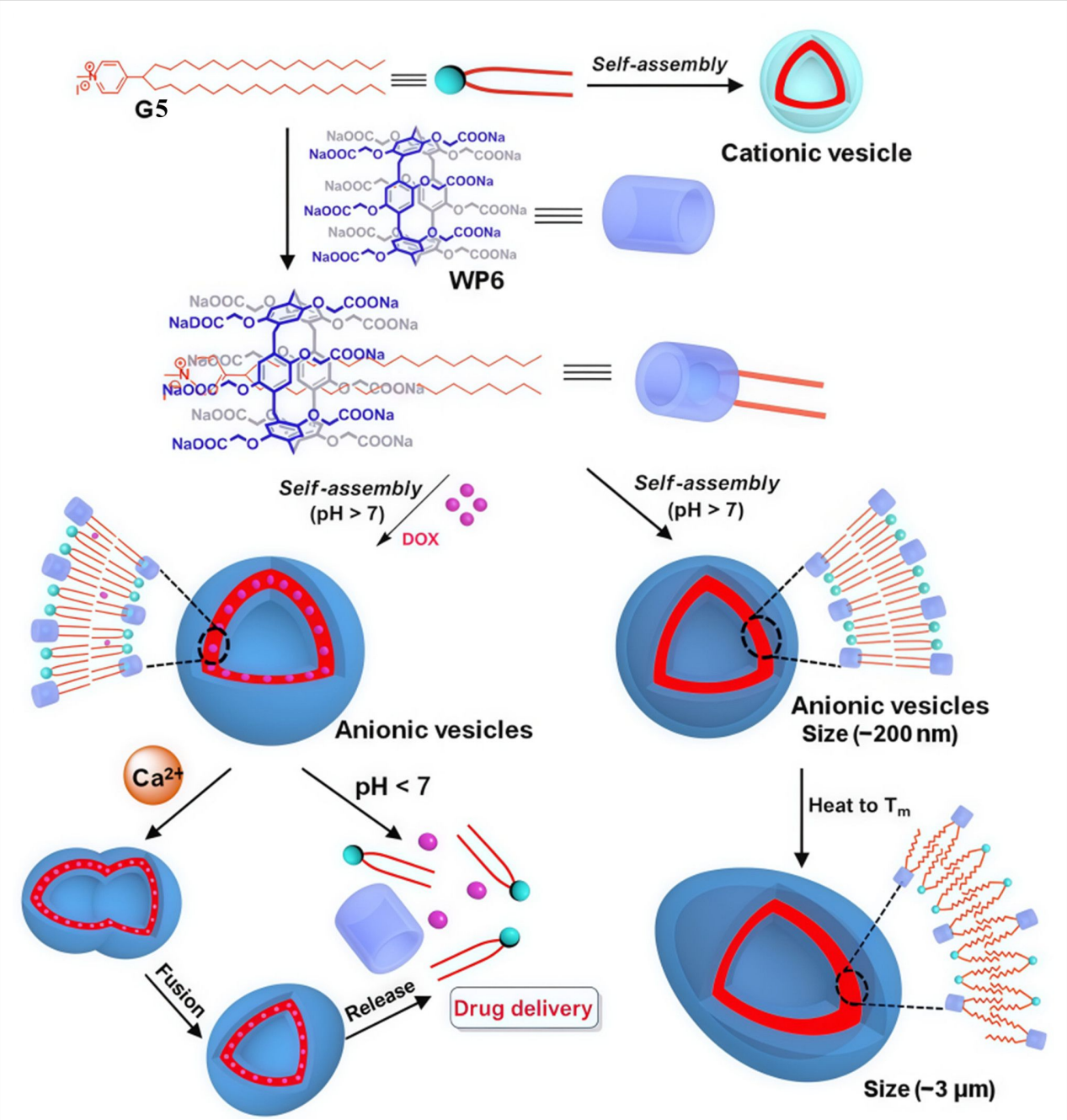

Figure 20: Schematic illustration of WP6 self-assembly at pH > 7, and the stimulus-responsive drug release behavior under varying conditions of Ca^{2+} concentration, pH, and temperature [107]. Figure 4 was adapted with permission from [107], Copyright 2014 American Chemical Society. This content is not subject to CC BY 4.0.

fusion occurs. Moreover, temperature regulation can achieve reversible changes in vesicle size; heating forms stable vesicles with an increased internal cavity and a size of approximately 3 micrometers, providing a potential carrier for bioimaging applications. This intelligent vesicle system, which combines drug-controlled release and tunable structural properties, holds significant value in the fields of targeted drug delivery and biomedical applications.

Subsequently, Wang and colleagues [129] in 2017 employed WP5 and pyridinium boronic acid derivatives (G6) to encapsulate insulin and achieve controlled release under physiological conditions (Figure 21). The host–guest binding affinity, which occurs in a 1:1 ratio, is primarily driven by synergistic electrostatic and hydrophobic interactions. The WP5⊃G6 supramolecular vesicles exhibit unique dual responsiveness to glucose and pH, originating from the specific binding of the pyridine-

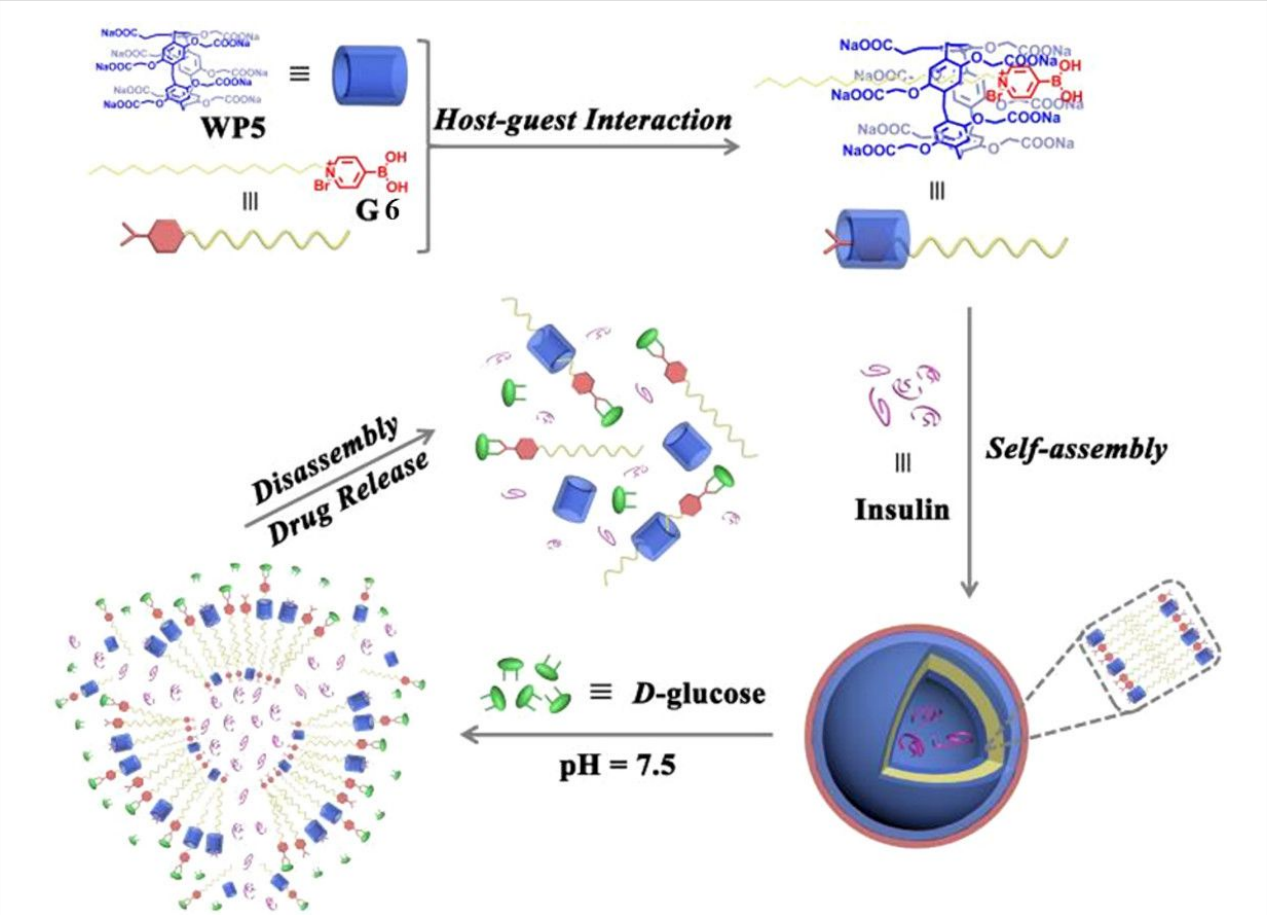

Figure 21: Schematic illustration of the formation of supramolecular vesicles based on the WP5⊃G super-amphiphile and their stimulus-responsive release [129]. Figure 21 was reproduced from [129], L. Gao et al., "Glucose-Responsive Supramolecular Vesicles Based on Water-Soluble Pillar[5]arene and Pyridylboronic Acid Derivatives for Controlled Insulin Delivery", *Chem. Eur. J.*, with permission from John Wiley and Sons. Copyright © 2017 Wiley-VCH Verlag GmbH & Co. KGaA, Weinheim. This content is not subject to CC BY 4.0.

boronic acid motif to the cis-diol of D-glucose and the pH-sensitive solubility changes. Under physiological pH conditions (7.4), the vesicle structure rapidly dissociates upon the addition of D-glucose or when the pH is lowered to 6.0, as evidenced by the disappearance of the Tyndall effect and the absence of vesicular structures in TEM images. This response mechanism is attributed to: 1) competitive binding of glucose leading to the dissociation of the host–guest complex; and 2) protonation of the WP5 carboxyl groups under acidic conditions, forming insoluble precipitates. The system can efficiently encapsulate insulin and precisely release it in response to high glucose levels or acidic environments demonstrating excellent potential for diabetes therapy. This intelligent delivery system achieves on-demand drug release and provides new insights for the development of glucose-responsive insulin formulations.

In 2022, Pei and collaborators unveiled a dual-stimuli-responsive supramolecular drug delivery system that relies on host–guest interactions, with sodium xanthate derivatives (SXD) serving as guest molecules and quaternary ammonium pillar[5]arene (QAP5) acting as host molecules (Figure 22) [130]. The hydrophobic SXD and the hydrophilic QAP5 interact through host–guest interactions driven by electrostatic forces to form the QAP5–SXD complex. The amphiphilic nature of QAP5–SXD enables its self-assembly into stable QAP5–SXD nanoparticles in aqueous solution, which are identified as vesicles by TEM. In this study, the xanthate group, which responds to both pH and hydrogen peroxide, shows great potential for the development of dual-responsive drug delivery systems. Using DOX as a model anticancer drug, they synthesized DOX@QAP5⊃SXD nanoparticles. Under conditions of low pH and high hydrogen peroxide concentration, SXD can rapidly decompose, triggering the disassembly of DOX@QAP5⊃SXD nanoparticles and the release of the encapsulated drug DOX.

Du and his team engineered MSN functionalized with dimethyl benzimidazolium (DMBI) and bipyridinium (BP) groups [131],

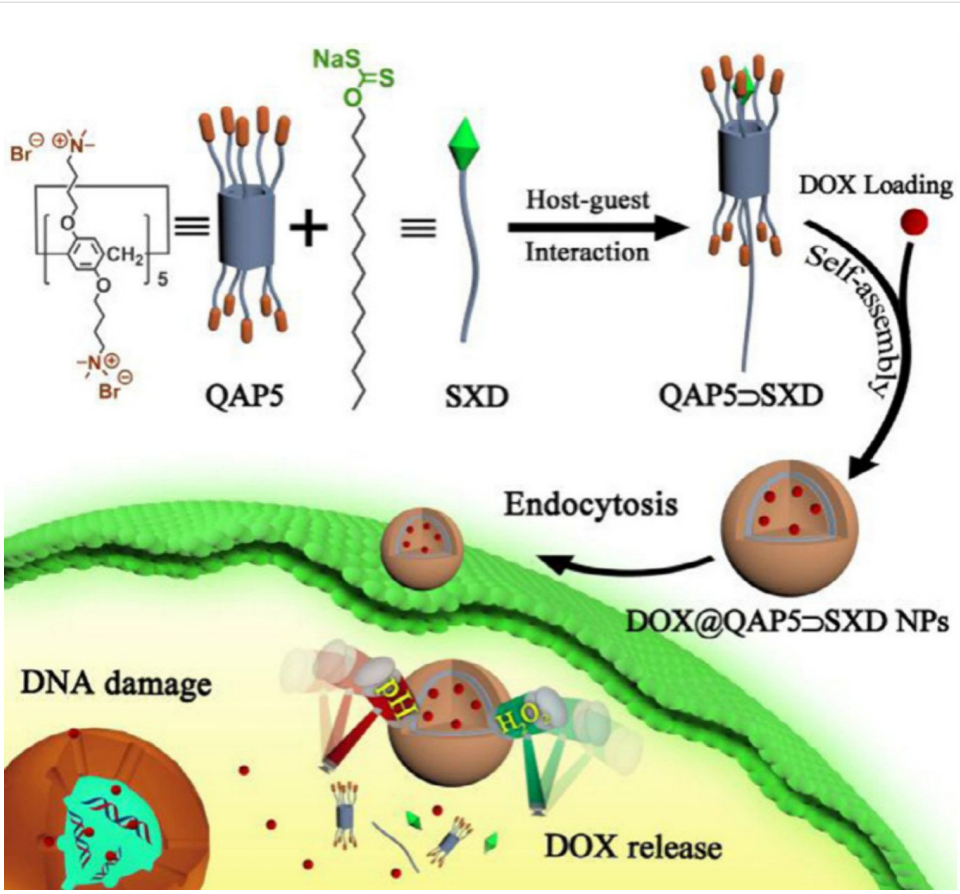

Figure 22: Schematic illustrations of the host–guest recognition of QAP5⊃SXD, the formation of the nanoparticles DOX@QAP5⊃SXD, and the stimulus-responsive release of DOX under pH and H_2O_2 conditions [130]. Figure 22 was reprinted from [130], *Chinese Chemical Letters*, vol. 33, by Shen, Z.; Ma, N.; Wang, F.; Ren, J.; Hou, C.; Chao, S.; Pei, Y.; Pei, Z., "pH-and H_2O_2-sensitive drug delivery system based on sodium xanthate: dual-responsive supramolecular vesicles from one functional group", pages 4563-4566, Copyright (2022), with permission from Elsevier on behalf of Chinese Chemical Society and Institute of Materia Medica, Chinese Academy of Medical Sciences. This content is not subject to CC BY 4.0.

as well as carboxylic acid-modified PA6 hydrocarbons (CPA6) to create multi-responsive controlled-release systems. CPA6 can rotate around DMBI or BP to form supramolecular nanovalves that encapsulate drugs within the MSN pores. The release of drugs is triggered by competitive binding at acidic pH or CPA6 de-threading, which then opens the nanovalves. In 2016, Fu and colleagues [132] designed and constructed an acid/base/Zn^{2+} stimulus-responsive controlled release system on the outer surface of a WP5-based bistable[2]pseudorotaxane (Figure 23). WP5 bonds with 1,6-hexane diamine (HDA) under neutral conditions, acting as a plug to block the retained cargo, and the two dissociate in acidic, basic, or Zn^{2+} environments, leading to controlled drug release.

Intelligent cargo delivery systems have been utilized to develop pesticide delivery nanoplatforms, thanks to their controlled release characteristics. In 2021, Yang et al. engineered a supramolecular fungicide nanoplatform using quaternary ammonium salt (Q)-modified MSN (MSN-Q NPs) as nanocarriers to encapsulate berberine hydrochloride (BH) and carboxyl pillar[5]arene (CP5A) (Figure 24) [133]. CP5A acts as a nanogate and is anchored on the surface of MSN-P through host–guest interactions between the positively charged P groups and the electron-rich cavity of CP5A, forming CP5A@MSN-P NPs loaded with BH to combat Botrytis cinerea. CP5A imparted the nanoplatform with pH or elevating temperatures-stimuli-responsive release capabilities. The encapsulated BH, a natural plant-derived fungicide, served as an eco-friendly substitute for synthetic fungicides. They employed oxalic acid (OA) secreted by B. cinerea as a trigger to release BH on demand within the pathogen microenvironment. This study capitalized on the acidic microenvironment created by B. cinerea to construct a fungicide nanoplatform that releases fungicides on demand, distinguishing it from previous nanoplatforms that relied on exogenous stimuli. Results demonstrated that the nanoplatform effectively curbed mycelial growth and spore germination, offering a novel strategy for gray mold management.

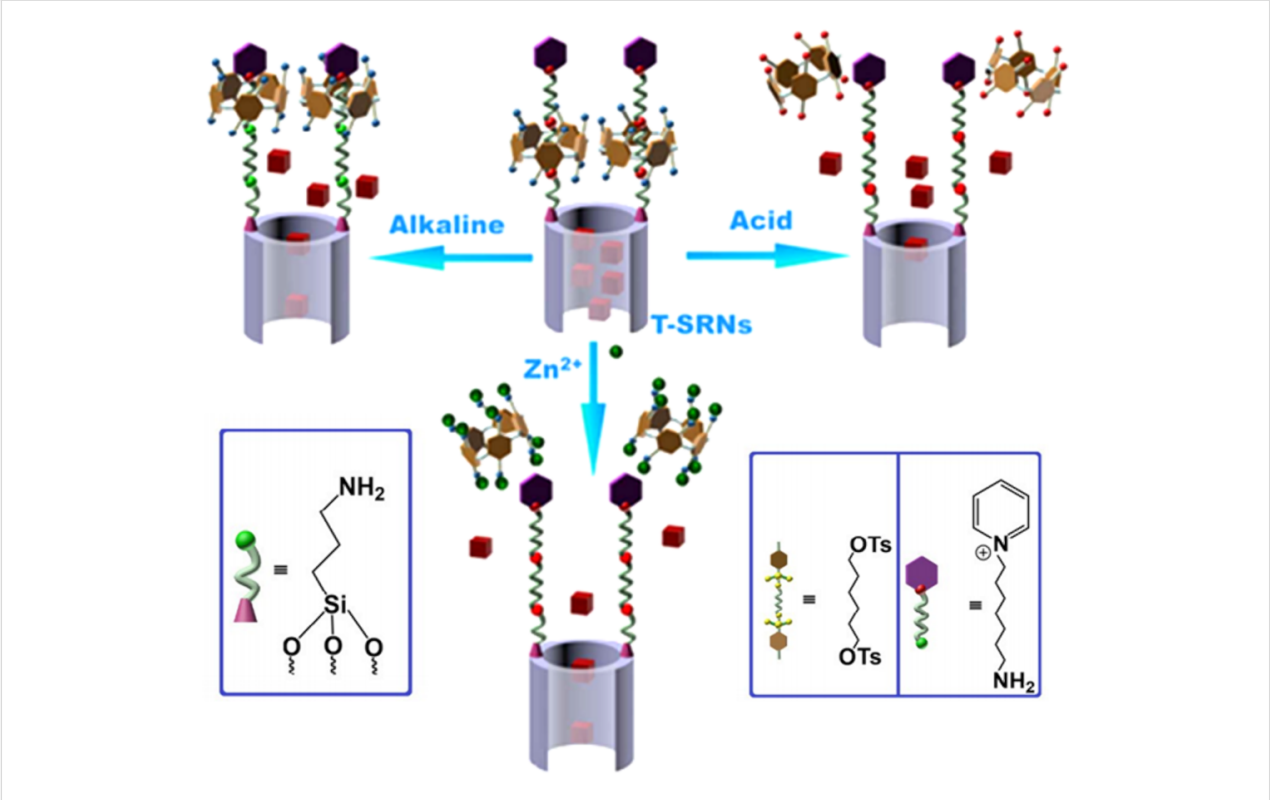

Figure 23: Schematic illustration of the activation of T-SRNs by acid, alkali, or Zn^{2+} stimuli to regulate the release of the model drug Rhodamine B (RhB) [132]. Figure 23 was used with permission of The Royal Society of Chemistry, from [132] ("Triple-stimuli-responsive nanocontainers assembled by water-soluble pillar [5] arene-based pseudorotaxanes for controlled release" by C. Ding et al., *J. Mater. Chem. B*, vol. 4, issue 16, © 2016); permission conveyed through Copyright Clearance Center, Inc. This content is not subject to CC BY 4.0.

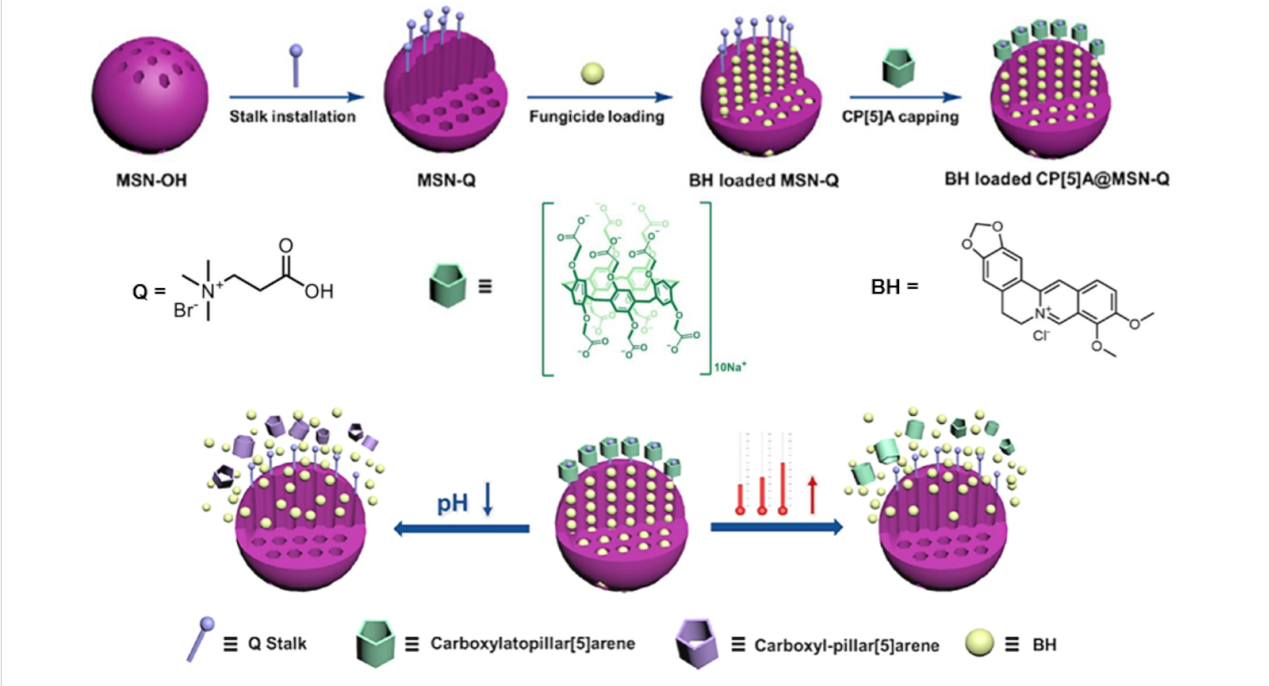

Figure 24: Illustration of the triggered release of BH from CP[5]A@MSNs-Q NPs in response to a drop in pH or a rise in temperature [133]. Figure 24 was adapted with permission from [133], Copyright 2021 American Chemical Society. This content is not subject to CC BY 4.0.

In 2022, Liu Yu and colleagues developed a pH and glutathione (GSH) dual-responsive supramolecular assembly by combining disulfide bond-containing pillar[4]arene (PA4) with tetraphenylethylene (TPE)-derived quaternary ammonium salts ($TPENC_n$, n = 6, 12) (Figure 25) [134]. The system leverages the acidic pH and reductive microenvironment of cancer cells to trigger targeted drug release. PA4, featuring acid-labile carboxylate groups and reduction-sensitive disulfide bonds, forms amphiphilic nanoparticles with $TPENC_n$ through electrostatic interactions, where the negatively charged PA4 pairs with the positively charged $TPENC_n$. The hydrophilic segments consist of PA4's carboxylate anions and $TPENC_n$'s quaternary ammonium sites, while their aromatic backbones constitute the hydrophobic core. This assembly lowers the CAC of $TPENC_n$, facilitating nanoparticle formation. Morphological studies confirmed well-structured nanoparticles optimized for cellular uptake. The dynamic non-covalent interactions enable stimulus-responsive behavior, allowing rapid drug release in acidic, high-GSH environments. Specifically, the TPENC6@PA4 nanoparticles demonstrated efficient DOX delivery, highlighting their potential as adaptive nanotherapeutics for cancer treatment.

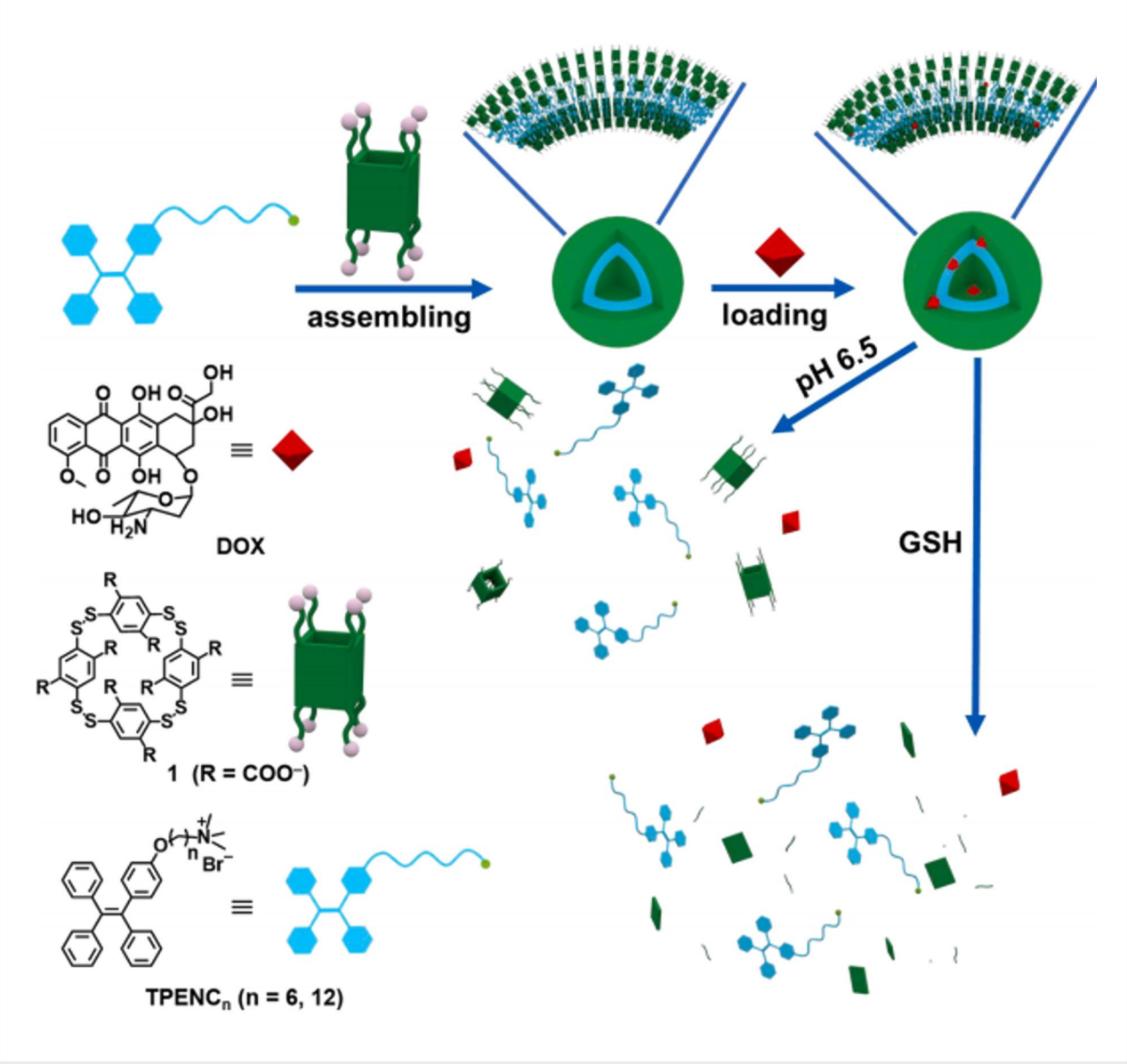

Figure 25: Illustration of the supramolecular amphiphiles $TPENC_n$@1 (n = 6 and 12) self-assembling with disulfide bond-PA4 to form vesicles, which then load DOX and respond to acidic environments and overexpressed GSH for degradation [134]. Figure 25 was reprinted from [134], *Bioorganic & Medicinal Chemistry*, vol. 57, by Tang, M.; Liu, Y. H.; Xu, X. M.; Zhang, Y. M.; Liu, Y. "Dual-responsive drug release and fluorescence imaging based on disulfide-pillar [4] arene aggregate in cancer cells", article no. 116649, Copyright (2022), with permission from Elsevier. This content is not subject to CC BY 4.0.

Conclusion

In summary, in recent years, supramolecular chemists have designed a series of easily synthesized aromatic macrocycles with electron-rich hydrophobic cavities. PAs and CAs, as intelligent hosts for drug-loading channels/holes, exhibit superior characteristics in supramolecular drug delivery systems. Most calix/pillar[*n*]arene hosts become water-soluble after modification with sulfonic acid, carboxyl, and phosphate groups. These calix/pillar[*n*]arene have good biocompatibility, ideal targeting ability, efficient operational capability, and precise response to various internal and external stimuli, and can be widely used as biomedicinal carriers. Researchers have connected functional groups that respond to specific stimuli to the aromatic macrocycle hosts. These specific functional groups endow supramolecular systems with rich responsiveness to light, pH, enzymes, and hypoxia-triggered, constructing different categories of supramolecular systems such as host–guest interactions, supramolecular self-assembly systems, and supramolecular nanovalves to achieve recognition, loading, and controlled entry and exit of drugs. It is worth mentioning that some of the constructed pH and enzyme-based controlled release systems can spontaneously generate stimulus responses in the tumor microenvironment without external human intervention to provide stimuli, thereby precisely releasing drugs, and have broad application prospects in cancer therapy.

Although there have been many reports on controlled release systems based on calix/pillar[*n*]arene in recent years, research in this field is still in its infancy, and it is challenging to conduct clinical trials for these systems. First, most stimulus-responsive nanosystems reported so far are based on SCA4 and CPA5−6. Compared to the extensive diversity of calix/pillar[*n*]arene, the currently developed types are just a tiny portion of the possible structures, greatly restricting the development of stimulus-responsive systems. Second, the known controlled release systems are usually limited to small molecules or ions, such as the anticancer drug DOX, the antibacterial MTZ, and ciprofloxacin. Due to the complexity and fragility of biomolecules, there are almost no reports on the encapsulation and release of larger biomolecules. Therefore, it is urgent to establish new stimulus-responsive controlled release systems that can contain large molecular drugs.

In view of the above, we hope that further improvement and overcoming can be achieved in future research. Different categories of aromatic macrocycles, such as tetralactam macrocycles and naphthotubes, can be tried to be modified with functional groups that respond to specific stimuli and used as hosts in release systems. Additionally, diverse stimulus-responsive systems derived from various group-modified aromatic macrocycles can be designed to align with the in vivo microenvironment, thereby facilitating the development of stimulus-responsive drug delivery systems. The photo-responsive systems based on CAs/PAs can be further optimized to improve their photo-responsive efficiency and stability. The applications of this system in more biomedical fields, such as targeted drug delivery and bioimaging, can be explored. The diversity of hypoxia-responsive systems can also be expanded by investigating CAs modified with different azobenzene structures for the treatment of tumor-related diseases. The drug release process is highly correlated with the disassembly of supramolecular nanoparticles. It can be anticipated that advanced drug loading and delivery efficiency combined with in situ monitoring of drug release will ultimately lead to effective chemotherapy and significantly inhibit tumor growth. In the future, the structure and properties of supramolecular amphiphiles can be further optimized to improve drug delivery efficiency and targeting ability. The applications of supramolecular amphiphiles in the treatment of other diseases can be explored, and the long-term safety and stability of supramolecular amphiphiles can be investigated. In the future, more biologically relevant molecules that have affinity for water-soluble CAs/PAs should be identified to achieve precise control over the size, shape, and stability of the assemblies. Other stimulus-responsive modes can be explored to expand the applications of these functional materials in other fields. Nevertheless, the clinical application of drug-controlled release systems based on aromatic macrocycles is still in its infancy. Extensive fundamental research and clinical trials are required to evaluate their safety, effectiveness, and practicality. Only through such rigorous assessment can these systems be more broadly implemented in clinical drug delivery, ultimately improving the precision and efficiency of drug administration and enhancing drug bioavailability. The development of supramolecular release systems new hope for improving drug targeting and bioavailability. Although there is still a need for innovation and progress in many aspects, we believe that with the in-depth research on stimulus-responsive host–guest chemistry, there is great potential in designing new therapies using release systems.

Acknowledgements

We are grateful to all of our co-workers for their contributions.

Funding

This research was financially supported by National Natural Science Foundation of China (No. 22174059 and 22201128). We thank USC for the technical support.

Author Contributions

Liu-Huan Yi: conceptualization; writing – original draft; writing – review & editing. Jian Qin: resources; writing – original draft. Si-Ran Lu: writing – original draft. Liu-Pan Yang:

funding acquisition; supervision; writing – review & editing. Li-Li Wang: conceptualization; funding acquisition; supervision; writing – review & editing. Huan Yao: funding acquisition; project administration; visualization; writing – review & editing.

ORCID® iDs

Li-Li Wang - https://orcid.org/0000-0001-9424-2972
Huan Yao - https://orcid.org/0000-0002-7114-1340

Data Availability Statement

Data sharing is not applicable as no new data was generated or analyzed in this study.

References

1. U.S. Food and Drug Administration. Federal Food, Drug, and Cosmetic Act, Section 201(g)(1), 21 USC §321(g)(1). 2025; https://www.accessdata.fda.gov/scripts/cdrh/cfdocs/cfcfr/CFRSearch.cfm?fr=201.128 (accessed June 28, 2025).
2. Vasan, N.; Baselga, J.; Hyman, D. M. *Nature* **2019,** *575,* 299–309. doi:10.1038/s41586-019-1730-1
3. Wu, S.; Yan, M.; Liang, M.; Yang, W.; Chen, J.; Zhou, J. *Cancer Drug Resist.* **2023,** *6,* 805–827. doi:10.20517/cdr.2023.77
4. Ward, R. A.; Fawell, S.; Floc'h, N.; Flemington, V.; McKerrecher, D.; Smith, P. D. *Chem. Rev.* **2021,** *121,* 3297–3351. doi:10.1021/acs.chemrev.0c00383
5. Tibbitt, M. W.; Dahlman, J. E.; Langer, R. *J. Am. Chem. Soc.* **2016,** *138,* 704–717. doi:10.1021/jacs.5b09974
6. Jing, Y.; Zhu, Y.; Yang, X.; Shen, J.; Li, C. *Langmuir* **2011,** *27,* 1175–1180. doi:10.1021/la1042734
7. Borgquist, P.; Körner, A.; Piculell, L.; Larsson, A.; Axelsson, A. *J. Controlled Release* **2006,** *113,* 216–225. doi:10.1016/j.jconrel.2006.05.004
8. Spang-Brunner, B. H.; Speiser, P. P. *J. Pharm. Pharmacol.* **1976,** *28,* 23–28. doi:10.1111/j.2042-7158.1976.tb04017.x
9. Mura, S.; Nicolas, J.; Couvreur, P. *Nat. Mater.* **2013,** *12,* 991–1003. doi:10.1038/nmat3776
10. Liu, M.; Du, H.; Zhang, W.; Zhai, G. *Mater. Sci. Eng., C* **2017,** *71,* 1267–1280. doi:10.1016/j.msec.2016.11.030
11. Park, K. *J. Controlled Release* **2014,** *190,* 3–8. doi:10.1016/j.jconrel.2014.03.054
12. Davoodi, P.; Lee, L. Y.; Xu, Q.; Sunil, V.; Sun, Y.; Soh, S.; Wang, C.-H. *Adv. Drug Delivery Rev.* **2018,** *132,* 104–138. doi:10.1016/j.addr.2018.07.002
13. Kamaly, N.; Yameen, B.; Wu, J.; Farokhzad, O. C. *Chem. Rev.* **2016,** *116,* 2602–2663. doi:10.1021/acs.chemrev.5b00346
14. Bernhard, S.; Tibbitt, M. W. *Adv. Drug Delivery Rev.* **2021,** *171,* 240–256. doi:10.1016/j.addr.2021.02.002
15. Yang, Y.; Li, P.; Feng, H.; Zeng, R.; Li, S.; Zhang, Q. *Molecules* **2024,** *29,* 3828. doi:10.3390/molecules29163828
16. Skorjanc, T.; Benyettou, F.; Olsen, J.-C.; Trabolsi, A. *Chem. – Eur. J.* **2017,** *23,* 8333–8347. doi:10.1002/chem.201605246
17. Liu, Y.-Y.; Yu, X.-Y.; Pan, Y.-C.; Yin, H.; Chao, S.; Li, Y.; Ma, H.; Zuo, M.; Teng, K.-X.; Hou, J.-L.; Chen, Y.; Guo, D.-S.; Wang, R.; Pei, Y.; Pei, Z.; Xu, J.-F.; Hu, X.-Y.; Li, C.; Yang, Q.-Z.; Wang, L.; Liu, Y.; Li, Z.-T. *Sci. China: Chem.* **2024,** *67,* 1397–1441. doi:10.1007/s11426-024-1971-4
18. Webber, M. J.; Langer, R. *Chem. Soc. Rev.* **2017,** *46,* 6600–6620. doi:10.1039/c7cs00391a
19. Liu, Z.; Nalluri, S. K. M.; Stoddart, J. F. *Chem. Soc. Rev.* **2017,** *46,* 2459–2478. doi:10.1039/c7cs00185a
20. Dong, R.; Zhou, Y.; Huang, X.; Zhu, X.; Lu, Y.; Shen, J. *Adv. Mater. (Weinheim, Ger.)* **2015,** *27,* 498–526. doi:10.1002/adma.201402975
21. Webber, M. J.; Appel, E. A.; Meijer, E. W.; Langer, R. *Nat. Mater.* **2016,** *15,* 13–26. doi:10.1038/nmat4474
22. Zhou, J.; Yu, G.; Huang, F. *Chem. Soc. Rev.* **2017,** *46,* 7021–7053. doi:10.1039/c6cs00898d
23. Fang, L.; Olson, M. A.; Benítez, D.; Tkatchouk, E.; Goddard III, W. A.; Stoddart, J. F. *Chem. Soc. Rev.* **2010,** *39,* 17–29. doi:10.1039/b917901a
24. Li, Y.; Li, Y.; Zhang, X.; Xu, X.; Zhang, Z.; Hu, C.; He, Y.; Gu, Z. *Theranostics* **2016,** *6,* 1293–1305. doi:10.7150/thno.15081
25. Terao, J.; Tang, A.; Michels, J. J.; Krivokapic, A.; Anderson, H. L. *Chem. Commun.* **2004,** 56–57. doi:10.1039/b311762f
26. Wang, S.; Yu, G.; Wang, Z.; Jacobson, O.; Tian, R.; Lin, L.-S.; Zhang, F.; Wang, J.; Chen, X. *Adv. Mater. (Weinheim, Ger.)* **2018,** *30,* 1803926. doi:10.1002/adma.201803926
27. Yu, G.; Ma, Y.; Han, C.; Yao, Y.; Tang, G.; Mao, Z.; Gao, C.; Huang, F. *J. Am. Chem. Soc.* **2013,** *135,* 10310–10313. doi:10.1021/ja405237q
28. Zhang, D.-W.; Zhao, X.; Li, Z.-T. *Acc. Chem. Res.* **2014,** *47,* 1961–1970. doi:10.1021/ar5000242
29. Yoon, H.-J.; Jang, W.-D. *J. Mater. Chem.* **2010,** *20,* 211–222. doi:10.1039/b910948j
30. Pitt, M. A.; Johnson, D. W. *Chem. Soc. Rev.* **2007,** *36,* 1441–1453. doi:10.1039/b610405n
31. Pluth, M. D.; Raymond, K. N. *Chem. Soc. Rev.* **2007,** *36,* 161–171. doi:10.1039/b603168b
32. Tashiro, K.; Aida, T. *Chem. Soc. Rev.* **2007,** *36,* 189–197. doi:10.1039/b614883m
33. Yang, Q.; Xu, W.; Cheng, M.; Zhang, S.; Kovaleva, E. G.; Liang, F.; Tian, D.; Liu, J.-a.; Abdelhameed, R. M.; Cheng, J.; Li, H. *Chem. Commun.* **2022,** *58,* 3255–3269. doi:10.1039/d1cc05584d
34. Lou, X. Y.; Li, Y. P.; Yang, Y. W. *Biotechnol. J.* **2018,** 14. doi:10.1002/biot.201800354
35. Peng, S.; Barba-Bon, A.; Pan, Y.-C.; Nau, W. M.; Guo, D.-S.; Hennig, A. *Angew. Chem., Int. Ed.* **2017,** *56,* 15742–15745. doi:10.1002/anie.201707979
36. Pan, Y.-C.; Barba-Bon, A.; Tian, H.-W.; Ding, F.; Hennig, A.; Nau, W. M.; Guo, D.-S. *Angew. Chem., Int. Ed.* **2021,** *60,* 1875–1882. doi:10.1002/anie.202011185
37. Martins, J. N.; Raimundo, B.; Rioboo, A.; Folgar-Cameán, Y.; Montenegro, J.; Basílio, N. *J. Am. Chem. Soc.* **2023,** *145,* 13126–13133. doi:10.1021/jacs.3c01829
38. Yu, N.; Li, G.; Gao, Y.; Liu, X.; Ma, S. *Int. J. Biol. Macromol.* **2016,** *93,* 971–977. doi:10.1016/j.ijbiomac.2016.09.068
39. Alabrahim, O. A. A.; Fahmy, S. A.; Azzazy, H. M. E.-S. *ACS Appl. Nano Mater.* **2023,** *6,* 3139–3158. doi:10.1021/acsanm.2c05391
40. Lai, G.-S.; Zhang, H.-L.; Jin, C.-M. *Electroanalysis* **2007,** *19,* 496–501. doi:10.1002/elan.200603751
41. Zhang, H.; Liu, Z.; Xin, F.; Hao, A. *Chin. J. Org. Chem.* **2012,** *32,* 219. doi:10.6023/cjoc1107141
42. Yang, L.; Zhong, L.; Yamato, K.; Zhang, X.; Feng, W.; Deng, P.; Yuan, L.; Zeng, X. C.; Gong, B. *New J. Chem.* **2009,** *33,* 729–733. doi:10.1039/b902495f

43. Liu, H.; Huang, Z.; Wen, K.; Jiang, B. *Chin. J. Org. Chem.* **2014,** *34,* 316–324. doi:10.6023/cjoc201307029
44. Jose, P.; Menon, S. *Bioinorg. Chem. Appl.* **2007,** No. 65815. doi:10.1155/2007/65815
45. Chen, L.; Cai, Y.; Feng, W.; Yuan, L. *Chem. Commun.* **2019,** *55,* 7883–7898. doi:10.1039/c9cc03292d
46. Li, P.; Chen, Y.; Liu, Y. *Chin. Chem. Lett.* **2019,** *30,* 1190–1197. doi:10.1016/j.cclet.2019.03.035
47. Basilio, N.; Francisco, V.; Garcia-Rio, L. *Int. J. Mol. Sci.* **2013,** *14,* 3140–3157. doi:10.3390/ijms14023140
48. Guo, D.-S.; Liu, Y. *Chem. Soc. Rev.* **2012,** *41,* 5907–5921. doi:10.1039/c2cs35075k
49. Ovsyannikov, A.; Solovieva, S.; Antipin, I.; Ferlay, S. *Coord. Chem. Rev.* **2017,** *352,* 151–186. doi:10.1016/j.ccr.2017.09.004
50. Chen, M.; Wang, C.; Fang, W.; Wang, J.; Zhang, W.; Jin, G.; Diao, G. *Langmuir* **2013,** *29,* 11858–11867. doi:10.1021/la4017799
51. Español, E. S.; Villamil, M. M. *Biomolecules* **2019,** *9,* 90. doi:10.3390/biom9030090
52. Guo, D.-S.; Liu, Y. *Acc. Chem. Res.* **2014,** *47,* 1925–1934. doi:10.1021/ar500009g
53. Ludwig, R. *Microchim. Acta* **2005,** *152,* 1–19. doi:10.1007/s00604-005-0422-8
54. Abd El-Rahman, M. K.; Mazzone, G.; Mahmoud, A. M.; Sicilia, E.; Shoeib, T. *Microchem. J.* **2019,** *146,* 735–741. doi:10.1016/j.microc.2019.01.046
55. Arduini, A.; Demuru, D.; Pochini, A.; Secchi, A. *Chem. Commun.* **2005,** 645–647. doi:10.1039/b411883a
56. Ostos, F. J.; Lebrón, J. A.; Moyá, M. L.; López-López, M.; Sánchez, A.; Clavero, A.; García-Calderón, C. B.; Rosado, I. V.; López-Cornejo, P. *Chem. – Asian J.* **2017,** *12,* 679–689. doi:10.1002/asia.201601713
57. Wang, J.; Ding, X.; Guo, X. *Adv. Colloid Interface Sci.* **2019,** *269,* 187–202. doi:10.1016/j.cis.2019.04.004
58. Li, R.; Liu, N.; Liu, R.; Jin, X.; Li, Z. *Curr. Drug Delivery* **2024,** *21,* 184–192. doi:10.2174/1567201820666230417084210
59. Ma, X.; Tian, H. *Acc. Chem. Res.* **2014,** *47,* 1971–1981. doi:10.1021/ar500033n
60. Ukhatskaya, E. V.; Kurkov, S. V.; Matthews, S. E.; El Fagui, A.; Amiel, C.; Dalmas, F.; Loftsson, T. *Int. J. Pharm.* **2010,** *402,* 10–19. doi:10.1016/j.ijpharm.2010.09.011
61. Xu, Z. Y.; Zhang, Y. C.; Lin, J. L.; Wang, H.; Zhang, D. W.; Li, Z. T. *Prog. Chem.* **2019,** *31,* 1540–1549. doi:10.7536/pc190817
62. Feng, W. W.; Jin, M.; Yang, K.; Pei, Y. X.; Pei, Z. C. *Chem. Commun.* **2018,** *54,* 13626–13640. doi:10.1039/c8cc08252a
63. Antimisiaris, S. G.; Mourtas, S.; Marazioti, A. *Pharmaceutics* **2018,** *10,* 218. doi:10.3390/pharmaceutics10040218
64. Xing, P.; Zhao, Y. *Small Methods* **2018,** *2,* 1700364. doi:10.1002/smtd.201700364
65. Gao, H.; Gao, L.; Lin, J.; Lu, Y.; Wang, L.; Cai, C.; Tian, X. *Macromolecules* **2020,** *53,* 3571–3579. doi:10.1021/acs.macromol.0c00146
66. Liu, J.-H.; Wu, X.; Zhang, Y.-M.; Liu, Y. *Asian J. Org. Chem.* **2018,** *7,* 2444–2447. doi:10.1002/ajoc.201800552
67. Estapé Senti, M.; de Jongh, C. A.; Dijkxhoorn, K.; Verhoef, J. J. F.; Szebeni, J.; Storm, G.; Hack, C. E.; Schiffelers, R. M.; Fens, M. H.; Boross, P. *J. Controlled Release* **2022,** *341,* 475–486. doi:10.1016/j.jconrel.2021.11.042
68. Lu, B.; Lv, X.; Le, Y. *Polymers (Basel, Switz.)* **2019,** *11,* 304. doi:10.3390/polym11020304
69. Tian, H.-W.; Xu, Z.; Li, H.-B.; Hu, X.-Y.; Guo, D.-S. *Supramol. Chem.* **2021,** *33,* 527–533. doi:10.1080/10610278.2022.2087523
70. Wang, Y.-X.; Guo, D.-S.; Duan, Y.-C.; Wang, Y.-J.; Liu, Y. *Sci. Rep.* **2015,** *5,* 9019. doi:10.1038/srep09019
71. Basílio, N.; Garcia-Rio, L.; Martín-Pastor, M. *Langmuir* **2012,** *28,* 2404–2414. doi:10.1021/la204004h
72. Suwinska, K.; Lesniewska, B.; Jebors, S.; Coleman, A. W. *Acta Crystallogr., Sect. A: Found. Crystallogr.* **2009,** *65,* s90. doi:10.1107/s0108767309098237
73. Lee, M.; Lee, S.-J.; Jiang, L.-H. *J. Am. Chem. Soc.* **2004,** *126,* 12724–12725. doi:10.1021/ja045918v
74. Ogoshi, T.; Kanai, S.; Fujinami, S.; Yamagishi, T.-a.; Nakamoto, Y. *J. Am. Chem. Soc.* **2008,** *130,* 5022–5023. doi:10.1021/ja711260m
75. Ogoshi, T.; Yamagishi, T.-a.; Nakamoto, Y. *Chem. Rev.* **2016,** *116,* 7937–8002. doi:10.1021/acs.chemrev.5b00765
76. Cao, M.; Hao, Y.; Xu, Z.; Hua Liu, S.; Yin, J. *Curr. Org. Chem.* **2016,** *20,* 1299–1313. doi:10.2174/1385272819666151022221121
77. Shu, X.; Chen, W.; Hou, D.; Meng, Q.; Zheng, R.; Li, C. *Chem. Commun.* **2014,** *50,* 4820–4823. doi:10.1039/c4cc00800f
78. Yu, G.; Zhou, X.; Zhang, Z.; Han, C.; Mao, Z.; Gao, C.; Huang, F. *J. Am. Chem. Soc.* **2012,** *134,* 19489–19497. doi:10.1021/ja3099905
79. Chen, W.; Zhang, Y.; Li, J.; Lou, X.; Yu, Y.; Jia, X.; Li, C. *Chem. Commun.* **2013,** *49,* 7956–7958. doi:10.1039/c3cc44328k
80. Yu, G.; Yang, J.; Xia, D.; Yao, Y. *RSC Adv.* **2014,** *4,* 18763–18771. doi:10.1039/c4ra01820f
81. Lin, Q.; Liu, L.; Zheng, F.; Mao, P.-P.; Liu, J.; Zhang, Y.-M.; Yao, H.; Wei, T.-B. *RSC Adv.* **2017,** *7,* 34411–34414. doi:10.1039/c7ra05750d
82. Wei, P.; Gangapurwala, G.; Pretzel, D.; Wang, L.; Schubert, S.; Brendel, J. C.; Schubert, U. S. *Nanoscale* **2020,** *12,* 13595–13605. doi:10.1039/d0nr01881c
83. Peng, H.; Xie, B.; Cen, X.; Dai, J.; Dai, Y.; Yang, X.; He, Y. *Mater. Chem. Front.* **2022,** *6,* 360–367. doi:10.1039/d1qm01459e
84. Sun, Y.-L.; Yang, Y.-W.; Chen, D.-X.; Wang, G.; Zhou, Y.; Wang, C.-Y.; Stoddart, J. F. *Small* **2013,** *9,* 3224–3229. doi:10.1002/smll.201300445
85. Song, N.; Yang, Y.-W. *Sci. China: Chem.* **2014,** *57,* 1185–1198. doi:10.1007/s11426-014-5190-z
86. Wang, C.; Li, H.; Dong, J.; Chen, Y.; Luan, X.; Li, X.; Du, X. *Chem. – Eur. J.* **2022,** *28,* e202202050. doi:10.1002/chem.202202050
87. Song, N.; Lou, X.-Y.; Ma, L.; Gao, H.; Yang, Y.-W. *Theranostics* **2019,** *9,* 3075–3093. doi:10.7150/thno.31858
88. Tan, L. L.; Li, H. W.; Qiu, Y. C.; Chen, D. X.; Wang, X.; Pan, R. Y.; Wang, Y.; Zhang, S. X. A.; Wang, B.; Yang, Y. W. *Chem. Sci.* **2015,** *6,* 1640–1644. doi:10.1039/c4sc03749a
89. Colilla, M.; González, B.; Vallet-Regí, M. *Biomater. Sci.* **2013,** *1,* 114–134. doi:10.1039/c2bm00085g
90. Huang, X.; Wu, S.; Ke, X.; Li, X.; Du, X. *ACS Appl. Mater. Interfaces* **2017,** *9,* 19638–19645. doi:10.1021/acsami.7b04015
91. Hu, X.; Yang, H. *RSC Adv.* **2021,** *11,* 7450–7453. doi:10.1039/d0ra10871e
92. Braegelman, A. S.; Webber, M. J. *Theranostics* **2019,** *9,* 3017–3040. doi:10.7150/thno.31913
93. Duan, Q. P.; Cao, Y.; Li, Y.; Hu, X. Y.; Xiao, T. X.; Lin, C.; Pan, Y.; Wang, L. Y. *J. Am. Chem. Soc.* **2013,** *135,* 10542–10549. doi:10.1021/ja405014r
94. Xia, W.; Ni, M.; Yao, C.; Wang, X.; Chen, D.; Lin, C.; Hu, X.-Y.; Wang, L. *Macromolecules* **2015,** *48,* 4403–4409. doi:10.1021/acs.macromol.5b00889
95. Guo, D.-S.; Zhang, T.-X.; Wang, Y.-X.; Liu, Y. *Chem. Commun.* **2013,** *49,* 6779–6781. doi:10.1039/c3cc41918e

96. Tao, Y.; Chan, H. F.; Shi, B.; Li, M.; Leong, K. W. *Adv. Funct. Mater.* **2020,** *30,* 2005029. doi:10.1002/adfm.202005029
97. Cafeo, G.; Carbotti, G.; Cuzzola, A.; Fabbi, M.; Ferrini, S.; Kohnke, F. H.; Papanikolaou, G.; Plutino, M. R.; Rosano, C.; White, A. J. P. *J. Am. Chem. Soc.* **2013,** *135,* 2544–2551. doi:10.1021/ja307791j
98. Zhu, H.; Li, Q.; Khalil-Cruz, L. E.; Khashab, N. M.; Yu, G.; Huang, F. *Sci. China: Chem.* **2021,** *64,* 688–700. doi:10.1007/s11426-020-9932-9
99. Xu, W.; Cheng, M.; Zhang, S.; Wu, Q.; Liu, Z.; Dhinakaran, M. K.; Liang, F.; Kovaleva, E. G.; Li, H. *Chem. Commun.* **2021,** *57,* 7480–7492. doi:10.1039/d1cc01501j
100. Li, Z. T.; Yang, J.; Huang, F. H. *Chin. J. Chem.* **2018,** *36,* 59–62. doi:10.1002/cjoc.201700601
101. Xue, Y.; Guan, Y.; Zheng, A.; Xiao, H. *Colloids Surf., B* **2013,** *101,* 55–60. doi:10.1016/j.colsurfb.2012.06.022
102. Li, Z.; Yang, J.; Yu, G.; He, J.; Abliz, Z.; Huang, F. *Org. Lett.* **2014,** *16,* 2066–2069. doi:10.1021/ol500686r
103. Sreedevi, P.; Nair, J. B.; Joseph, M. M.; Murali, V. P.; Suresh, C. H.; Varma, R. L.; Maiti, K. K. *J. Controlled Release* **2021,** *339,* 284–296. doi:10.1016/j.jconrel.2021.09.038
104. Cao, Y.; Li, Y.; Hu, X.-Y.; Zou, X.; Xiong, S.; Lin, C.; Wang, L. *Chem. Mater.* **2015,** *27,* 1110–1119. doi:10.1021/cm504445r
105. Yang, J.; Yu, G.; Xia, D.; Huang, F. *Chem. Commun.* **2014,** *50,* 3993–3995. doi:10.1039/c4cc00590b
106. Yu, G.; Xue, M.; Zhang, Z.; Li, J.; Han, C.; Huang, F. *J. Am. Chem. Soc.* **2012,** *134,* 13248–13251. doi:10.1021/ja306399f
107. Cao, Y.; Hu, X.-Y.; Li, Y.; Zou, X.; Xiong, S.; Lin, C.; Shen, Y.-Z.; Wang, L. *J. Am. Chem. Soc.* **2014,** *136,* 10762–10769. doi:10.1021/ja505344t
108. Chen, Y.; Rui, L.; Liu, L.; Zhang, W. *Polym. Chem.* **2016,** *7,* 3268–3276. doi:10.1039/c6py00505e
109. Zhou, W.; Chen, S.; Ouyang, Y.; Huang, B.; Zhang, H.; Zhang, W.; Tian, J. *Chem. Sci.* **2023,** *14,* 11481–11489. doi:10.1039/d3sc03797e
110. Zhu, H.; Shangguan, L.; Xia, D.; Mondal, J. H.; Shi, B. *Nanoscale* **2017,** *9,* 8913–8917. doi:10.1039/c7nr03160b
111. Qu, D.-H.; Wang, Q.-C.; Zhang, Q.-W.; Ma, X.; Tian, H. *Chem. Rev.* **2015,** *115,* 7543–7588. doi:10.1021/cr5006342
112. Shao, L.; Hua, B.; Yang, J.; Yu, G. *Chem. Commun.* **2016,** *52,* 6573–6576. doi:10.1039/c6cc02434c
113. Shao, L.; Hua, B.; Sun, J.; Li, Q.; Yang, J.; Yu, G. *Tetrahedron Lett.* **2017,** *58,* 1863–1867. doi:10.1016/j.tetlet.2017.03.091
114. Wang, Y.-X.; Zhang, Y.-M.; Liu, Y. *J. Am. Chem. Soc.* **2015,** *137,* 4543–4549. doi:10.1021/jacs.5b01566
115. Jiang, B.-P.; Guo, D.-S.; Liu, Y.-C.; Wang, K.-P.; Liu, Y. *ACS Nano* **2014,** *8,* 1609–1618. doi:10.1021/nn405923b
116. Liu, K.; Liu, Y.; Yao, Y.; Yuan, H.; Wang, S.; Wang, Z.; Zhang, X. *Angew. Chem., Int. Ed.* **2013,** *52,* 8285–8289. doi:10.1002/anie.201303387
117. Pang, H.; Xu, P.; Li, C.; Zhan, Y.; Zhang, Z.; Zhang, W.; Yang, G.; Sun, Y.; Li, H. *Chem. Commun.* **2018,** *54,* 2978–2981. doi:10.1039/c8cc01196f
118. Prigyai, N.; Bunchuay, T.; Ruengsuk, A.; Yoshinari, N.; Manissorn, J.; Pumirat, P.; Sapudom, J.; Kosiyachinda, P.; Thongnuek, P. *ACS Appl. Mater. Interfaces* **2024,** *16,* 8250–8265. doi:10.1021/acsami.3c14760
119. Guo, D.-S.; Wang, K.; Wang, Y.-X.; Liu, Y. *J. Am. Chem. Soc.* **2012,** *134,* 10244–10250. doi:10.1021/ja303280r
120. Li, Y.; Bai, H.; Li, C.; Shi, G. *ACS Appl. Mater. Interfaces* **2011,** *3,* 1306–1310. doi:10.1021/am200101n
121. Sun, Y.-L.; Zhou, Y.; Li, Q.-L.; Yang, Y.-W. *Chem. Commun.* **2013,** *49,* 9033–9035. doi:10.1039/c3cc45216f
122. Zhang, T.-X.; Zhang, Z.-Z.; Yue, Y.-X.; Hu, X.-Y.; Huang, F.; Shi, L.; Liu, Y.; Guo, D.-S. *Adv. Mater. (Weinheim, Ger.)* **2020,** *32,* 1908435. doi:10.1002/adma.201908435
123. Guo, J.-S.; Li, J.-J.; Wang, Z.-H.; Liu, Y.; Yue, Y.-X.; Li, H.-B.; Zhao, X.-H.; Sun, Y.-J.; Ding, Y.-H.; Ding, F.; Guo, D.-S.; Wang, L.; Chen, Y. *Nat. Commun.* **2023,** *14,* 5634. doi:10.1038/s41467-023-41388-2
124. Chen, M.-M.; Tang, X.; Li, J.-J.; Chen, F.-Y.; Jiang, Z.-T.; Fu, R.; Li, H.-B.; Hu, X.-Y.; Geng, W.-C.; Guo, D.-S. *J. Controlled Release* **2024,** *368,* 691–702. doi:10.1016/j.jconrel.2024.03.017
125. Zheng, W.; Yao, S.-Y.; Hu, H.; Chen, X.; Qian, Z.; Liu, W.; Zhu, Y.; Mao, Z.; Guo, D.-S.; Gao, C. *Nano Today* **2024,** *54,* 102064. doi:10.1016/j.nantod.2023.102064
126. Geng, Y.-Q.; Qiu, L.-N.; Cheng, Y.-Q.; Li, J.-J.; Ma, Y.-L.; Zhao, C.-C.; Cai, Y.; Zhang, X.-B.; Chen, J.; Pan, Y.-C.; Wang, K.-R.; Yao, X.-H.; Guo, D.-S.; Wu, J.-L. *Adv. Sci.* **2024,** *11,* 2309517. doi:10.1002/advs.202309517
127. Wang, K.; Guo, D.-S.; Wang, X.; Liu, Y. *ACS Nano* **2011,** *5,* 2880–2894. doi:10.1021/nn1034873
128. Chen, X.; Wang, Z.; Sun, X.; Han, Y.; Huang, Y.; Xi, J.; Bian, X.; Han, J.; Guo, R. *Chem. Eng. J.* **2021,** *403,* 126423. doi:10.1016/j.cej.2020.126423
129. Gao, L.; Wang, T.; Jia, K.; Wu, X.; Yao, C.; Shao, W.; Zhang, D.; Hu, X.-Y.; Wang, L. *Chem. – Eur. J.* **2017,** *23,* 6605–6614. doi:10.1002/chem.201700345
130. Shen, Z.; Ma, N.; Wang, F.; Ren, J.; Hou, C.; Chao, S.; Pei, Y.; Pei, Z. *Chin. Chem. Lett.* **2022,** *33,* 4563–4566. doi:10.1016/j.cclet.2022.01.069
131. Huang, X.; Du, X. *ACS Appl. Mater. Interfaces* **2014,** *6,* 20430–20436. doi:10.1021/am506004q
132. Ding, C.; Liu, Y.; Wang, T.; Fu, J. *J. Mater. Chem. B* **2016,** *4,* 2819–2827. doi:10.1039/c6tb00459h
133. Wang, C.-Y.; Lou, X.-Y.; Cai, Z.; Zhang, M.-Z.; Jia, C.; Qin, J.-C.; Yang, Y.-W. *ACS Appl. Mater. Interfaces* **2021,** *13,* 32295–32306. doi:10.1021/acsami.1c08582
134. Tang, M.; Liu, Y. H.; Xu, X. M.; Zhang, Y. M.; Liu, Y. *Bioorg. Med. Chem.* **2022,** *57,* 116649. doi:10.1016/j.bmc.2022.116649

License and Terms

BEILSTEIN JOURNAL OF ORGANIC CHEMISTRY

Synthesis and characterization of a isothiouronium-calix[4]arene derivative: self-assembly and anticancer activity

Giuseppe Granata[‡1], Loredana Ferreri[‡1], Claudia Giovanna Leotta[2,3], Giovanni Mario Pitari[2,3] and Grazia Maria Letizia Consoli[*1]

Full Research Paper

Open Access

Address:
[1]CNR-Institute of Biomolecular Chemistry, Via Paolo Gaifami 18, 95126 Catania, Italy, [2]Dream Factory Lab, Vera Salus Ricerca S.r.L., Via Sigmund Freud 62/B, 96100, Siracusa, Italy and [3]J4Med Lab, Via Paolo Gaifami 9, 95126 Catania, Italy

Email:
Grazia Maria Letizia Consoli[*] - graziamarialetizia.consoli@cnr.it

* Corresponding author ‡ Equal contributors

Keywords:
anticancer agent; calixarene; nanostructure; self-assembly

Beilstein J. Org. Chem. **2025,** *21,* 2535–2541.
https://doi.org/10.3762/bjoc.21.195

Received: 07 August 2025
Accepted: 10 October 2025
Published: 14 November 2025

This article is part of the thematic issue "Novel macrocycles: from synthesis to supramolecular function".

Guest Editor: C. Gaeta

Abstract

Calix[*n*]arenes are polyphenolic macrocycles known for their remarkable synthetic versatility, which supports their broad application in various areas, including drug discovery. Their unique conformational features, functionality, and low toxicity make calixarene derivatives valuable drug candidates against cancer. The aim of the present study was the synthesis and characterization of a calix[4]arene derivative in which known anticancer isothiouronium groups were clustered on a calix[4]arene scaffold bearing long C12 alkyl chains at the lower rim. The resulting amphiphilic calix[4]arene derivative **3** spontaneously self-assembled into nanoscale aggregates in aqueous medium, as demonstrated by dynamic light scattering analysis. The cytotoxicity of compound **3** towards cancer cells was assessed using human renal carcinoma cells (786-O cells) and compared with that in non-malignant fibroblast cells (SW1 cells). Compound **3** showed a significantly greater antiproliferative effect on cancer cells (IC_{50} 37.4 μM) than on normal fibroblasts (517 μM). The importance of the isothiouronium moieties in the observed cytoxic effect was confirmed by comparison with the calix[4]arene precursor (**1**) lacking these functional units. The selective antiproliferative profile of compound **3** highlights its potential as a lead anticancer agent. Moreover, compound **3** holds promise for further development in combination multidrug therapy due to the potential to load drug molecules in the bioactive nanoassembled structure.

Introduction

Cancer remains one of the leading causes of morbidity and mortality worldwide. Despite significant advancements in chemotherapy, more effective and less toxic, targeted treatments are still urgently needed [1]. Among the most promising avenues in cancer therapy research, multivalent compounds have emerged as a powerful class of agents for tumor diagnosis, analysis, and therapy [2]. By exposing multiple functional groups within a single molecular framework, these compounds

offer the potential for enhanced therapeutic efficacy through a multivalency effect. Multivalency is a strategy employed by nature to improve selectivity, specificity, and avidity in molecular recognition events responsible for both physiological and pathological processes. Multiple ligand–receptor interactions can significantly enhance receptor binding affinity and cellular uptake, as well as more effectively modulate signal transduction pathways, for instance when receptor clustering is necessary on the cell membrane [3]. Designing multivalent bioactive compounds thus represents a promising approach to overcoming several limitations associated with traditional monovalent therapeutics, including drug resistance, off-target effects, high dosage requirements, and insufficient specificity. This strategy may pave the way for next-generation anticancer therapies more effective and precise than current treatments. Numerous multivalent constructs have been reported in literature, both as compounds with intrinsic anticancer activity [4] and nanocarriers for anticancer drug delivery [5,6].

In the development of multivalent compounds, macrocyclic scaffolds such as cyclodextrins [7], cyclic peptides [8], cucurbiturils [9], resorcinarenes [10], pillarenes [11], prismarenes [12], and calix[*n*]arenes have proven to be particularly valuable.

Calix[*n*]arenes, a family of polyphenolic macrocyclic oligomers, are widely utilized in applications ranging from materials science to life sciences [13-17]. Their synthetic versatility, ease of functionalization, conformational rigidity or flexibility, steric bulk, and low cost make them highly attractive in the development of novel, non-conventional anticancer agents with a great potential for overcoming the toxicity of cancer chemotherapy and achieving targeted treatments [18-20].

In the era of nanotechnology, a promising strategy for developing more effective treatments against cancer [21,22], calixarene derivatives are also emerging as valid building blocks for the development of nanoscale multivalent constructs [23]. Due to the nanosize, the calixarene-based nanoconstructs could preferentially accumulate in cancer tissues by exploiting the enhanced tumor permeability and retention (EPR) effect [24] or selectively penetrate cancer cells through specific ligand–receptor interactions on the surface of target cells [25,26]. A variety of calixarene-based nanoconstructs have been reported, including nanosystems with light-triggered anticancer activity [27], potential anticancer vaccine candidates [28], and nanocarriers for anticancer drug delivery [29-33].

Numerous bioactive groups have been introduced into the calixarene skeleton to develop anticancer derivatives, including proline [34], carbonyl amide [35], glycoureido [36], ureido [37], picolylamine [38], 5-bromopentyltrimethylammonium bromide and 3-bromopropyltriphenylphosphonium bromide [39], among others.

Isothiouronium salts represent another class of interest in the search for new chemotherapeutic agents. They are known inhibitors of protein kinase C [40] and agonists of the GABA-type [41] and histamine-H3 receptors [42]. *S*-Allylic isothiouronium salts substituted with aliphatic groups have shown to combine high antitumor activity against leukemia cells and low toxicity toward non-cancerous cells [43].

Therefore, the aim of this study was to evaluate whether introducing isothiouronium moieties at the upper rim of a calix[4]arene scaffold, bearing long C12 alkyl chains at the lower rim, could yield a novel derivative (compound **3**) with anticancer activity. The synthesis and structural characterization of compound **3** were carried out, and its self-assembly behavior in aqueous medium was investigated using dynamic light scattering (DLS) and electrophoretic light scattering (ELS). The anticancer potential of compound **3** was assessed in human renal carcinoma cells (786O) and normal human fibroblasts (SW1), and the tumor cells selectivity was evaluated. To elucidate the role of the isothiouronium groups, antiproliferative effects were also estimated on calix[4]arene precursor **1** lacking these functional groups.

Results and Discussion

Synthesis and characterization of compound 3

For the synthesis of isothiouronium-calix[4]arene derivative **3** (Scheme 1), the chloromethylcalix[4]arene derivative **2** was prepared by adopting a procedure reported in the literature [44].

In brief, starting from the commercial *p*-H-calix[4]arene **1**, four C-12 alkyl chains were tethered to the calixarene hydroxy groups (lower rim) by reaction with dodecyl iodide in the presence of NaH. At the upper rim of this derivative, four formyl groups were introduced by reaction with hexamethylenetetramine in trifluoroacetic acid. The formyl groups were reduced to alcohol groups by sodium borohydride and then converted to chloromethyl groups by treatment with thionyl chloride, to give compound **2**.

The reaction of compound **2** with thiourea in THF gave compound **3** as a white solid in 96% yield. Compound **3** was characterized by ^{1}H and ^{13}C NMR in DMSO-d_6 as a solvent (Figure 1). The proton signals of the NH_2 and CH_2S groups of the isothiouronium substituents were clearly observed at 9.04 ppm and 4.23 ppm, respectively. Additionally, the carbon signal of the CH_2S group appeared at 169.3 ppm. The NMR

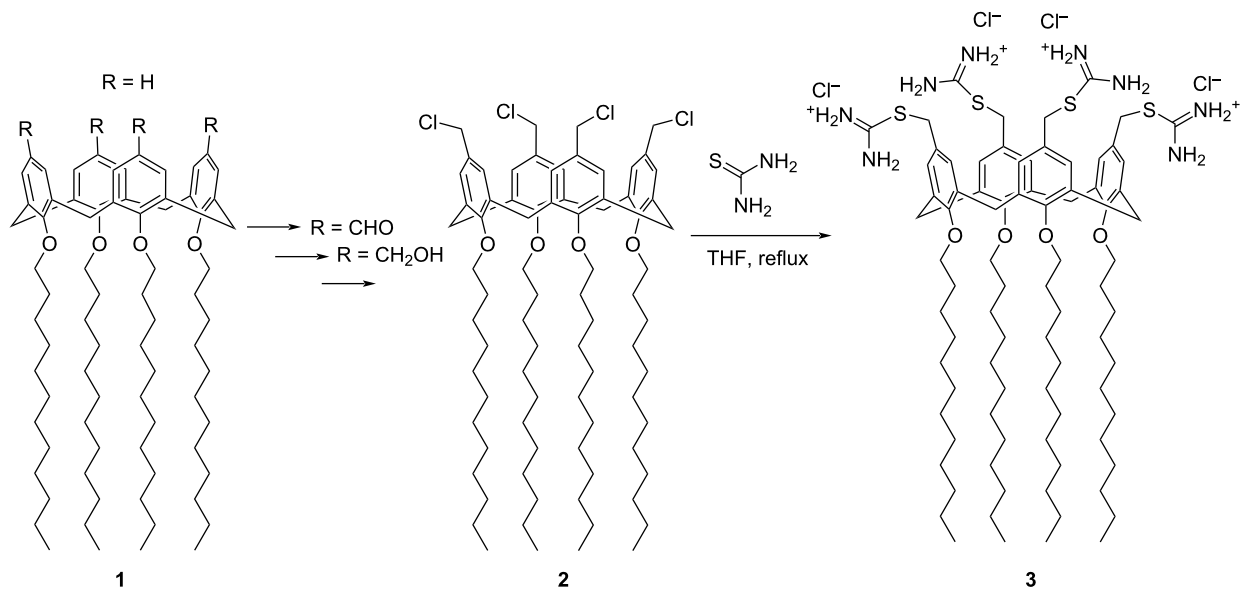

Scheme 1: Procedure for the synthesis of compound **3**.

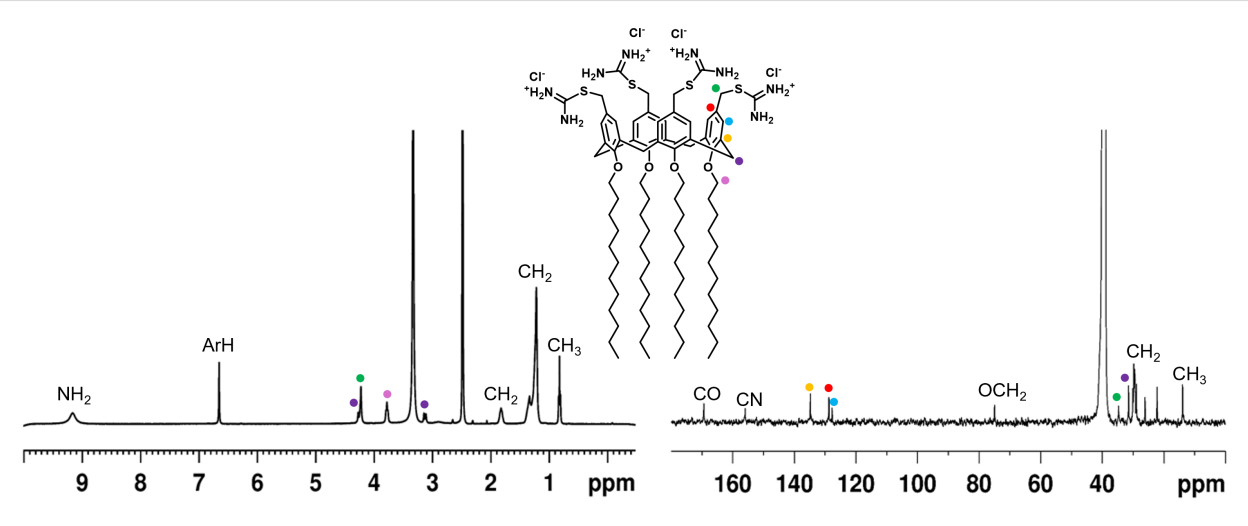

Figure 1: ^{1}H NMR (left) and ^{13}C NMR (right) spectra of compound **3** in DMSO-d_6 (400.13 MHz, 297 K).

signals, consistent with a fully symmetric structure, evidenced the exhaustive functionalization of the calix[4]arene skeleton blocked in cone conformation, as evidenced by the AX system (3.13 and 4.26 ppm) for the bridged CH_2 protons.

Spontaneous self-assembly

Due to the amphiphilic nature, compound **3** could spontaneously self-assemble in aqueous medium. This was confirmed by dynamic light scattering measurements, which showed the presence of nanoaggregates with mean hydrodynamic diameters of 125 ± 1 nm in the aqueous colloidal solution of compound **3** (Figure 2).

A polydispersity index of 0.18 ± 0.01 was indicative of a good dimensional homogeneity of the nanoaggregates in the suspension.

The zeta potential is a measure of the electrical potential between the surface of nanoaggregates and the surrounding fluid. Electrophoretic light scattering (ELS) provided for the nanoaggregates of compound **3** a zeta potential (ζ) value of +64 ± 1 mV (Figure 3), indicative of stable nanoassemblies. Indeed, it is generally accepted that values higher than ±40 mV are associated with strong stability by repulsion, preventing further aggregation phenomena.

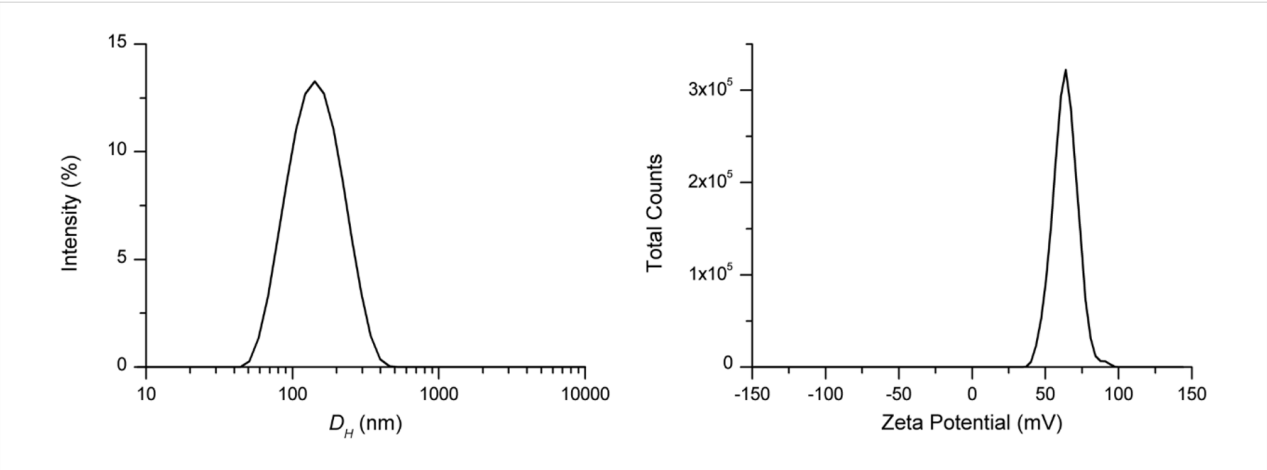

Figure 2: Intensity-weighted mean hydrodynamic diameter (left), and zeta potential distribution (right) of compound **3** (1 mg/mL water), after vortex and sonication.

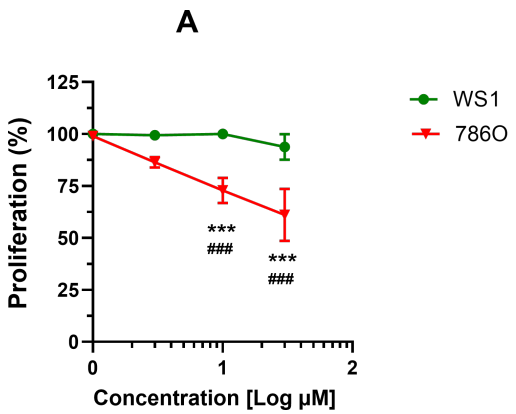

B

IC_{50} (µM)	786O	WS1
Compound **3**	37.40 ± 25.86	517.1 ± 292.74
Compound **1**	662.8 ± 342.24	1014 ± 545.48
Doxorubicin	0.34 ± 0.07	0.16 ± 0.02

Figure 3: Antiproliferative effects by compound **3** and its chemical precursor **1**. A) Results on proliferative kinetics in renal cancer 786O and skin fibroblast WS1 cells. Data represent the percentage of proliferation with respect to the correspondent vehicle DMSO controls. ***, $p < 0.001$ vs the respective vehicle control by 2-way ANOVA; ###, $p < 0.001$ vs correspondent WS1 conditions by 2-way ANOVA. B) Calculated IC_{50} for compounds **3** and **1** in renal cancer 786O and skin fibroblast WS1 cells. Doxorubicin, the positive control. Data are expressed as means ± SD.

Cytotoxicity and cancer cell selectivity

Thiouronium-containing molecules can inhibit cancer cells, inducing apoptosis or necrosis, by different mechanisms including elevation of reactive oxygen species (ROS) or interference with redox homeostasis, and inhibition of kinase or topoisomerase activities essential for cancer cell proliferation. The selective activity of thiouronium salts against cancer cells compared to non-malignant cells can be related to a specific sensitivity of cancer cells [43]. In fact, cancer cells operate under higher oxidative stress than normal cells and often overexpress kinases or topoisomerases, which make them more vulnerable than normal cells.

The anticancer effect of compound **3** was assessed on human renal carcinoma 786O cells, through evaluation of proliferative kinetics with the acridine orange staining assay [45]. The 786O cell line is a widely used in vitro model for studying clear cell renal cell carcinoma (ccRCC) [46], which accounts for over 90% of all renal malignancies and is characterized by poor responsiveness to conventional chemotherapy.

To the best of our knowledge, calixarene derivatives have not been previously tested as anticancer agents against human renal carcinoma cells.

Compound **3** suppressed the proliferation of the renal cancer cells (Figure 3) with a calculated 50% inhibitory concentration (IC_{50}) of 37.40 µM. In contrast, compound **3** was poorly effective against normal WS1 fibroblasts (Figure 3), exhibiting an IC_{50} value of 517 µM. These values yielded a selectivity index (SI) of approximately 14, indicating that tumor cells are significantly more sensitive to the cytotoxic effects of compound **3**

than healthy, non-malignant cells. In general, SI values above 12 are associated to remarkable selectivity, 6–12 to moderate selectivity and 1–5 to weak selectivity [43,47]. In contrast, the potent antineoplastic agent doxorubicin, used as the positive control for anticancer effects, did not discriminate between normal and cancer cells, as demonstrated by the calculated SI of 0.47. The high SI value by compound **3** evidenced the isothiouronium moieties retain the selective cytotoxicity towards cancer cells also when tethered to the calixarene scaffold.

Since the long alkyl chains in compound **3** could be responsible for molecular disruptive events at the cell membrane through intercalation in the lipidic bilayer, the effects of *p*-H-calix[4]arene-*O*-dodecyl derivative **1**, a precursor lacking isothiouronium moieties, on cell proliferation were also investigated. The absence of the isothiouronium groups substantially blunted the antiproliferative activity in both cancer and normal cells, as demonstrated by the higher IC_{50} values exhibited by compound **1** (Figure 3). These data clearly demonstrated that isothiouronium moieties are crucial for the anticancer activity of compound **3**.

Conclusion

The introduction of four isothiouronium functional groups at the upper rim of a calix[4]arene macrocycle, bearing four dodecyl aliphatic chains at the lower rim, yields an amphiphilic derivative that spontaneously self-assembles into nanoscale structures with a mean hydrodynamic diameter of approximately 100 nm and a positively charged surface (zeta potential + 64 mV). These values are suitable for potential applications in the field of nanomedicine. Remarkably, the isothiouronium-calix[4]arene derivative, unlike its precursor lacking isothiouronium functionalities, inhibited the proliferation of human renal carcinoma cells with notable selectivity over normal human fibroblasts. To the best of our knowledge, this is the first study evaluating the antiproliferative activity of both a thiouronium salt and a calix[4]arene derivative in renal carcinoma cells. The isothiouronium-calix[4]arene nanoassemblies may be promising candidates for further investigations as a drug delivery system. The entrapment of different drugs combined with the intrinsic anticancer activity of the nanoassemblies could provide new agents for a combination multidrug anticancer treatment.

Experimental

Materials and methods: All chemicals were purchased from Sigma-Aldrich (Milan, Italy) and used without further purification. Human renal adenocarcinoma 786-O cells were obtained from the American Type Culture Collection (ATCC; Manassas, VA, USA). Cells (passages 2-10) were maintained at 37 °C (5% CO_2) in RPMI 1640 medium, containing 10% FBS, 2 mM L-glutamine, 100 units/mL penicillin and 100 µg/mL streptomycin. All cell media and reagents were from Euroclone S.p.A. (Pero, Milan, Italy).

Procedure for the synthesis of compound 3: Compound **3** was synthesized from the chloro-methyl-calix[4]arene precursor **2** [44] adopting a procedure described for the synthesis of an analogous tetrakis(thiuroniumethyl)tetramethoxycalix[4]arene tetrachloride [48]. Compound **2** (100 mg, 0.077 mmol) and thiourea (1.5 equiv per chloromethyl unit) were dissolved in THF (4 mL) and the solution was refluxed for 15 h to give a white precipitate. After cooling, the solid precipitate was recovered by filtration and washed several times with ethyl ether, to give pure compound **3** (118 mg, 96% yield).

Characterization of compound 3: NMR spectra were acquired on a Bruker Avance 400TM spectrometer. Chemical shifts (δ, ppm) are reported referring to the residual peak of the solvent (DMSO-d_6). ^{1}H NMR (400.13 MHz, DMSO-d_6, 297 K) δ 0.83 (t, J = 6.6 Hz, 12H, 4 × dodecyl CH_3), 1.22 (br s, 72H, 36 × dodecyl CH_2), 1.34 (br s, 8H, 4 × dodecyl CH_2), 1.82 (t, 8H, 4 × dodecyl CH_2), 3.13 (d, J = 14.3 Hz, 4H, 2 × $ArCH_2Ar$), 3.78 (t, 8H, 4 × dodecyl OCH_2), 4.23 (s, 8H, 4 × $ArCH_2S$), 4.26 (d, J = 14.3 Hz, 4H, 2 × 4 $ArCH_2Ar$), 6.66 (s, 8H, 8 × ArH); ^{13}C NMR (100.6 MHz, DMSO-d_6, 297 K) δ 13.9 (q, dodecyl CH_3), 22.2, 26.2, 29.0, 29.5, 29.8, 30.1 (t, dodecyl $_{CH2}$), 31.5 (t, $ArCH_2Ar$), 34.7 (t, CH_2S), 75.0 (t, OCH_2), 127.8 (d, ArH), 128.8 (s, ArC-$_{CH2S}$), 135.0 (s, ArC-CH_2S), 156.0 (s, ArCO), 169.4 (s, C-NH_2).

Size and zeta potential measurements: DLS and ELS measurements were performed on a sample of compound **3** (1 mg) dissolved in 1 mL pure water. The colloidal solution was centrifuged at 10,000 rpm for 10 min and the supernatant was collected and analyzed by a Zetasizer NanoZS90 analyzer (Malvern Instrument, Malvern, UK) equipped with a 633 nm laser, at a scattering angle of 90° and 25 °C temperature. The size of the particles was calculated from the diffusion coefficient using the Stokes–Einstein equation:

$$D = \frac{kT}{6\eta R\pi}$$

where D is the diffusion coefficient, k is the Boltzmann constant, T is the absolute temperature, η is the solvent viscosity, and R is the solute radius.

The zeta potential (Z) was calculated by using Henry's equation

$$UE = \frac{2\varepsilon\zeta}{3\eta} f(Ka)$$

where *UE* is the electrophoretic mobility, ζ is the dielectric constant, *f*(*Ka*) is the Henry's function, and η is the viscosity.

Biological assays: Cell viability was measured by the acridine orange staining assay. Briefly, cancer cells were seeded in 96-well plates and grown at optimum culture conditions for 72 h (at a confluence of ≈60–80%). Then, cells were treated with the indicated concentrations of compounds for additional 48 h. Control cells received an equal volume of vehicle (DMSO). At the end of incubations, cells were fixed (in 4% paraformaldehyde) and stained with acridine orange solution (50 µg/mL), as previously described [45]. Acridine orange staining was then quantified as the resulting fluorescence intensity (excitation 485/20 nm, emission 528/20 nm) with a microplate reader (Synergy HT, BioTek).

Statistical analyses: Results are shown as mean ± SEM of three independent experiments, performed at least in triplicate. Statistical comparisons were performed by 2-way ANOVA. *P* values were considered significant at $p \leq 0.05$. All analyses were done with GraphPad Prism 10.4.1 (GraphPad Software, Inc., San Diego, CA).

Selectivity index determination: The selectivity index of compound **3** was calculated as the ratio of the IC_{50} in the cancer cell line to the IC_{50} in the non-malignant cell line, according to the following formula

$$SI = \frac{IC_{50}\ normal\ cells}{IC_{50}\ cancer\ cells}$$

Funding

This study was in part funded by European Union (Next-Generation EU), through the MUR-PNRR project SAMOTHRACE (ECS00000022).

Author Contributions

Giuseppe Granata: investigation; methodology. Loredana Ferreri: investigation; methodology. Claudia Giovanna Leotta: data curation; formal analysis; investigation; methodology. Giovanni Mario Pitari: conceptualization; resources; writing – review & editing. Grazia Maria Letizia Consoli: conceptualization; funding acquisition; methodology; project administration; resources; supervision; writing – original draft; writing – review & editing.

ORCID® iDs

Giuseppe Granata - https://orcid.org/0000-0001-9428-3985
Loredana Ferreri - https://orcid.org/0000-0002-3134-0409
Claudia Giovanna Leotta - https://orcid.org/0000-0002-9950-1205
Giovanni Mario Pitari - https://orcid.org/0000-0003-0698-8112
Grazia Maria Letizia Consoli - https://orcid.org/0000-0002-9608-5138

Data Availability Statement

All data that supports the findings of this study is available in the published article and/or the supporting information of this article.

References

1. Siegel, R. L.; Kratzer, T. B.; Giaquinto, A. N.; Sung, H.; Jemal, A. *Ca-Cancer J. Clin.* **2025,** *75,* 10–45. doi:10.3322/caac.21871
2. Zeng, H.; Zeng, W.; Liang, Y. *Oncol. Lett.* **2025,** *30,* 325. doi:10.3892/ol.2025.15071
3. Kiessling, L. L.; Lamanna, A. C. Multivalency in Biological Systems. In *Chemical Probes in Biology;* Schneider, M. P., Ed.; NATO Science Series, Vol. 129; Springer: Dordrecht, Netherlands, 2003; pp 345–357. doi:10.1007/978-94-007-0958-4_26
4. Carlson, C. B.; Mowery, P.; Owen, R. M.; Dykhuizen, E. C.; Kiessling, L. L. *ACS Chem. Biol.* **2007,** *2,* 119–127. doi:10.1021/cb6003788
5. Bakshi, A. K.; Haider, T.; Tiwari, R.; Soni, V. *Drug Delivery Transl. Res.* **2022,** *12,* 2335–2358. doi:10.1007/s13346-021-01103-4
6. Porębska, N.; Ciura, K.; Chorążewska, A.; Zakrzewska, M.; Otlewski, J.; Opaliński, Ł. *Biotechnol. Adv.* **2023,** *67,* 108213. doi:10.1016/j.biotechadv.2023.108213
7. Ou, C.; Li, C.; Feng, C.; Tong, X.; Vasta, G. R.; Wang, L.-X. *Bioorg. Med. Chem.* **2022,** *72,* 116974. doi:10.1016/j.bmc.2022.116974
8. Martian, P. C.; Tertis, M.; Leonte, D.; Hadade, N.; Cristea, C.; Crisan, O. *J. Pharm. Biomed. Anal.* **2025,** *252,* 116488. doi:10.1016/j.jpba.2024.116488
9. Yin, H.; Cheng, Q.; Bardelang, D.; Wang, R. *JACS Au* **2023,** *3,* 2356–2377. doi:10.1021/jacsau.3c00273
10. Della Sala, P.; Vanni, C.; Talotta, C.; Di Marino, L.; Matassini, C.; Goti, A.; Neri, P.; Šesták, S.; Cardona, F.; Gaeta, C. *Org. Chem. Front.* **2021,** *8,* 6648–6656. doi:10.1039/d1qo01048d
11. Buffet, K.; Nierengarten, I.; Galanos, N.; Gillon, E.; Holler, M.; Imberty, A.; Matthews, S. E.; Vidal, S.; Vincent, S. P.; Nierengarten, J.-F. *Chem. – Eur. J.* **2016,** *22,* 2955–2963. doi:10.1002/chem.201504921
12. Del Regno, R.; Santonoceta, G. D. G.; Della Sala, P.; De Rosa, M.; Soriente, A.; Talotta, C.; Spinella, A.; Neri, P.; Sgarlata, C.; Gaeta, C. *Org. Lett.* **2022,** *24,* 2711–2715. doi:10.1021/acs.orglett.2c00819
13. Neri, P.; Sessler, J. L.; Wang, M.-X., Eds. *Calixarenes and Beyond;* Springer International Publishing: Cham, Switzerland, 2016. doi:10.1007/978-3-319-31867-7
14. Asfari, Z.; Böhmer, V.; Harrowfield, J.; Vicens, J.; Saadioui, M., Eds. *Calixarenes 2001;* Kluwer Academic Publishers: Dordrecht, Netherlands, 2001. doi:10.1007/0-306-47522-7
15. Rodik, R.; Cherenok, S.; Kalchenko, O.; Yesypenko, O.; Lipkowski, J.; Kalchenko, V. *Curr. Org. Chem.* **2018,** *22,* 2200–2222. doi:10.2174/1385272822666181015141327
16. Mecca, T.; Consoli, G. M. L.; Geraci, C.; Cunsolo, F. *Bioorg. Med. Chem.* **2004,** *12,* 5057–5062. doi:10.1016/j.bmc.2004.07.037
17. Mecca, T.; Consoli, G. M. L.; Geraci, C.; La Spina, R.; Cunsolo, F. *Org. Biomol. Chem.* **2006,** *4,* 3763–3768. doi:10.1039/b608887b
18. Paul, S.; Jeyaprakash, R. S.; Pai, A.; Venkatachalam, H.; Jayashree, B. S. *Med. Chem.* **2023,** *19,* 939–945. doi:10.2174/1573406419666230703114605

19. Yousaf, A.; Hamid, S. A.; Bunnori, N. M.; Ishola, A. A. *Drug Des., Dev. Ther.* **2015,** *9,* 2831–2838. doi:10.2147/dddt.s83213
20. Wojaczyńska, E.; Ostrowska, M.; Lower, M.; Czyżyk, N.; Jakieła, A.; Marra, A. *Molecules* **2024,** *29,* 4240. doi:10.3390/molecules29174240
21. Sabir, S.; Thani, A. S. B.; Abbas, Q. *Front. Bioeng. Biotechnol.* **2025,** *13,* 1548588. doi:10.3389/fbioe.2025.1548588
22. Chehelgerdi, M.; Chehelgerdi, M.; Allela, O. Q. B.; Pecho, R. D. C.; Jayasankar, N.; Rao, D. P.; Thamaraikani, T.; Vasanthan, M.; Viktor, P.; Lakshmaiya, N.; Saadh, M. J.; Amajd, A.; Abo-Zaid, M. A.; Castillo-Acobo, R. Y.; Ismail, A. H.; Amin, A. H.; Akhavan-Sigari, R. *Mol. Cancer* **2023,** *22,* 169. doi:10.1186/s12943-023-01865-0
23. Baldini, L.; Casnati, A.; Sansone, F. *Eur. J. Org. Chem.* **2020,** 5056–5069. doi:10.1002/ejoc.202000255
24. Sun, R.; Xiang, J.; Zhou, Q.; Piao, Y.; Tang, J.; Shao, S.; Zhou, Z.; Bae, Y. H.; Shen, Y. *Adv. Drug Delivery Rev.* **2022,** *191,* 114614. doi:10.1016/j.addr.2022.114614
25. Consoli, G. M. L.; Granata, G.; Fragassi, G.; Grossi, M.; Sallese, M.; Geraci, C. *Org. Biomol. Chem.* **2015,** *13,* 3298–3307. doi:10.1039/c4ob02333a
26. Zhang, Y.; Xiao, J.; Cao, J.; Pan, J.; Li, C.; Zheng, Y. *J. Fluoresc.* **2025,** in press. doi:10.1007/s10895-025-04294-y
27. Consoli, G. M. L.; Forte, G.; Maugeri, L.; Consoli, V.; Sorrenti, V.; Vanella, L.; Buscarino, G.; Agnello, S.; Camarda, M.; Granata, G.; Ferreri, L.; Petralia, S. *ACS Appl. Nano Mater.* **2023,** *6,* 358–369. doi:10.1021/acsanm.2c04501
28. Geraci, C.; Consoli, G. M. L.; Granata, G.; Galante, E.; Palmigiano, A.; Pappalardo, M.; Di Puma, S. D.; Spadaro, A. *Bioconjugate Chem.* **2013,** *24,* 1710–1720. doi:10.1021/bc400242y
29. Gidwani, B.; Gupta, S. K.; Sahu, J. *Int. J. Pharm. Sci. Nanotechnol.* **2023,** *16,* 6546–6555. doi:10.37285/ijpsn.2023.16.3.8
30. Isik, A.; Oguz, M.; Kocak, A.; Yilmaz, M. *J. Inclusion Phenom. Macrocyclic Chem.* **2022,** *102,* 439–449. doi:10.1007/s10847-022-01134-5
31. Al-Ahmary, K. M.; Shafie, A.; Adnan Ashour, A.; S. Alrashdi, K.; Babalghith, A. O.; Alharthi, S. S.; Sabei, F. Y. *Crit. Rev. Anal. Chem.* **2024,** 1–26. doi:10.1080/10408347.2024.2402820
32. Li, R.; Liu, N.; Liu, R.; Jin, X.; Li, Z. *Curr. Drug Delivery* **2024,** *21,* 184–192. doi:10.2174/1567201820666230417084210
33. Basilotta, R.; Mannino, D.; Filippone, A.; Casili, G.; Prestifilippo, A.; Colarossi, L.; Raciti, G.; Esposito, E.; Campolo, M. *Molecules* **2021,** *26,* 3963. doi:10.3390/molecules26133963
34. Oguz, M.; Gul, A.; Karakurt, S.; Yilmaz, M. *Bioorg. Chem.* **2020,** *94,* 103207. doi:10.1016/j.bioorg.2019.103207
35. An, L.; Wang, C.; Zheng, Y.-G.; Liu, J.-d.; Huang, T.-h. *Eur. J. Med. Chem.* **2021,** *210,* 112984. doi:10.1016/j.ejmech.2020.112984
36. Viola, S.; Consoli, G. M. L.; Merlo, S.; Drago, F.; Sortino, M. A.; Geraci, C. *J. Neurochem.* **2008,** *107,* 1047–1055. doi:10.1111/j.1471-4159.2008.05656.x
37. Viola, S.; Merlo, S.; Consoli, G. M. L.; Drago, F.; Geraci, C.; Sortino, M. A. *Pharmacology* **2010,** *86,* 182–188. doi:10.1159/000317518
38. Oguz, M.; Gul, A.; Karakurt, S.; Yilmaz, M. *ChemistrySelect* **2020,** *5,* 12250–12254. doi:10.1002/slct.202002881
39. Oğuz, M. *Konya J. Eng. Sci.* **2022,** *10,* 189–199. doi:10.36306/konjes.1039091
40. Hendricks, R. T.; Sherman, D.; Strulovici, B.; Broka, C. A. *Bioorg. Med. Chem. Lett.* **1995,** *5,* 67–72. doi:10.1016/0960-894x(94)00460-w
41. Allan, R. D.; Dickenson, H. W.; Hiern, B. P.; Johnston, G. A. R.; Kazlauskas, R. *Br. J. Pharmacol.* **1986,** *88,* 379–387. doi:10.1111/j.1476-5381.1986.tb10214.x
42. Ganellin, C. R.; Bang-Andersen, B.; Khalaf, Y. S.; Tertiuk, W.; Arrang, J. M.; Garbarg, M.; Ligneau, X.; Rouleau, A.; Schwartz, J. C. *Bioorg. Med. Chem. Lett.* **1992,** *2,* 1231–1234. doi:10.1016/s0960-894x(00)80219-x
43. Ferreira, M.; Assunção, L. S.; Silva, A. H.; Filippin-Monteiro, F. B.; Creczynski-Pasa, T. B.; Sá, M. M. *Eur. J. Med. Chem.* **2017,** *129,* 151–158. doi:10.1016/j.ejmech.2017.02.013
44. Eggers, P. K.; Becker, T.; Melvin, M. K.; Boulos, R. A.; James, E.; Morellini, N.; Harvey, A. R.; Dunlop, S. A.; Fitzgerald, M.; Stubbs, K. A.; Raston, C. L. *RSC Adv.* **2012,** *2,* 6250–6257. doi:10.1039/c2ra20491f
45. Hathaway, W. E.; Newby, L. A.; Githens, J. H. *Cryobiology* **1965,** *2,* 143–146. doi:10.1016/s0011-2240(65)80101-8
46. Shapiro, D. D.; Virumbrales-Muñoz, M.; Beebe, D. J.; Abel, E. J. *Front. Oncol.* **2022,** *12,* 871252. doi:10.3389/fonc.2022.871252
47. Callacondo-Riva, D.; Quispe-Mauricio, A.; Lindo-Gamarra, S.; Vaisberg, A. *J. Rev. Peru. Med. Exp. Salud Publica* **2008,** *25,* 380–385.
48. Nagasaki, T.; Tajiri, Y.; Shinkai, S. *Recl. Trav. Chim. Pays-Bas* **1993,** *112,* 407–411. doi:10.1002/recl.19931120617

License and Terms

BEILSTEIN JOURNAL OF ORGANIC CHEMISTRY

Silica gel with covalently attached bambusuril macrocycle for dicyanoaurate sorption from water

Michaela Šusterová[1,2] and Vladimír Šindelář*[1,2]

Full Research Paper

Open Access

Address:
[1]Department of Chemistry, Faculty of Science, Masaryk University, Kamenice 5, 625 00 Brno, Czech Republic and [2]RECETOX, Faculty of Science, Masaryk University, Kamenice 5, 625 00 Brno, Czech Republic

Email:
Vladimír Šindelář* - sindelar@chemi.muni.cz

* Corresponding author

Keywords:
anion binding; anion extraction; anion receptor; gold mining; macrocycles

Beilstein J. Org. Chem. **2025,** *21,* 2604–2611.
https://doi.org/10.3762/bjoc.21.201

Received: 21 August 2025
Accepted: 13 November 2025
Published: 24 November 2025

This article is part of the thematic issue "Novel macrocycles: from synthesis to supramolecular function".

Guest Editor: C. Gaeta

Abstract

Anion removal from aqueous solutions remains a major challenge due to the strong hydration of anions. Here, we report the preparation of silica gel functionalized with covalently anchored bambusuril macrocycles. In aqueous solution, this material efficiently sorbs dicyanoaurate(I), the key anion in gold mining, even in the presence of competing dicyanoargentate(I) anions. We also examine the recyclability of the material and assess its stability in organic solvents, comparing its performance with that of a previously developed material containing noncovalently bound bambusuril.

Introduction

Inorganic anions play essential roles in a variety of biological and biochemical mechanisms and are also involved in many industrial and manufacturing processes. Due to their significant environmental impact, it is important to monitor their presence and control their concentrations, particularly in water. To maintain anion levels within acceptable ranges, their removal from the environment is often necessary [1,2].

Current technologies for removing anions from aqueous solutions include chemical coprecipitation [3], ion-exchange [4], or membrane filtration [5]. In the field of anion extraction, there is growing interest in solid-phase substrates functionalized with synthetic macrocyclic receptors. These materials employ a supramolecular approach based on specific host–guest interactions between the immobilized macrocycle and the guest in solution, often leading not only to improved extraction effectivity but also to enhanced selectivity [2]. Anion extractants based on functionalized polystyrene or silica gel typically incorporate calixarenes [6] and their analogues, calixpyrroles [7,8], azacalixarene derivatives [9], or expanded porphyrin-like sapphyrin [10].

Although synthetic anion receptors have attracted increasing attention in the field of supramolecular chemistry, there are still

relatively few reports of materials that employ macrocyclic receptors to recognize and selectively bind anionic species specifically in aqueous environments. For example, an amphiphilic poly(methyl methacrylate)-based polymer modified with calix[4]pyrrole was found to form micelles in water that capture anions from caesium salts and can be precipitated from solution upon heating [11]. Similarly, a hydrogel composed of poly(vinyl alcohol) cross-linked by a "Texas-sized" molecular box has been used to extract various anions from water [12].

Another family of macrocyclic compounds suitable for anion recognition and binding are bambusurils (BUs). BUs act as very potent anion receptors in both organic solvents and water. Furthermore, their portals can be variously functionalized, for instance by carboxylic moieties [13], making them available for further reactions with different substrates. We have recently presented a material (SG-BnBU) based on silica gel containing dodecabenzylbambus[6]uril (BnBU) non-covalently bound on its surface [14]. We showed that this material is able to remove dicyanoaurate(I) anion from water, the principal cyanide-based species generated during gold mining processes. However, the use of the SG-BnBU material is problematic as BnBU can leach from the material into the solution. To address this limitation, we have developed and herein report a new material, SG-NHCO-BU1, in which the BU1 macrocycle is covalently grafted onto the surface of silica gel. We demonstrate that this hybrid material can be used for the selective dicyanoaurate(I) sorption from water. Moreover, it is shown that unlike SG-BnBU, SG-NHCO-BU1 exhibits good stability in organic solvents.

Results and Discussion

Decoration of silica gel with bambusuril

For the modification of silica gel (SG), we selected previously reported bambus[6]uril BU1 (Scheme 1) containing 12 carboxyalkyl substituents [13]. This macrocycle was chosen for several reasons: BU1 can be attached to SG not only by electrostatic interactions but also covalently, the BU1 synthesis is straightforward lacking difficult and time-consuming purification, and it is obtained in relatively high yield over 60%. Once BU1 was prepared, its covalent attachment on the surface of SG was achieved in two steps. First, SG, chosen as the solid substrate, was reacted with an excess of 3-aminopropyltriethoxysilane (APTES) in toluene under reflux to obtain a-SG material with

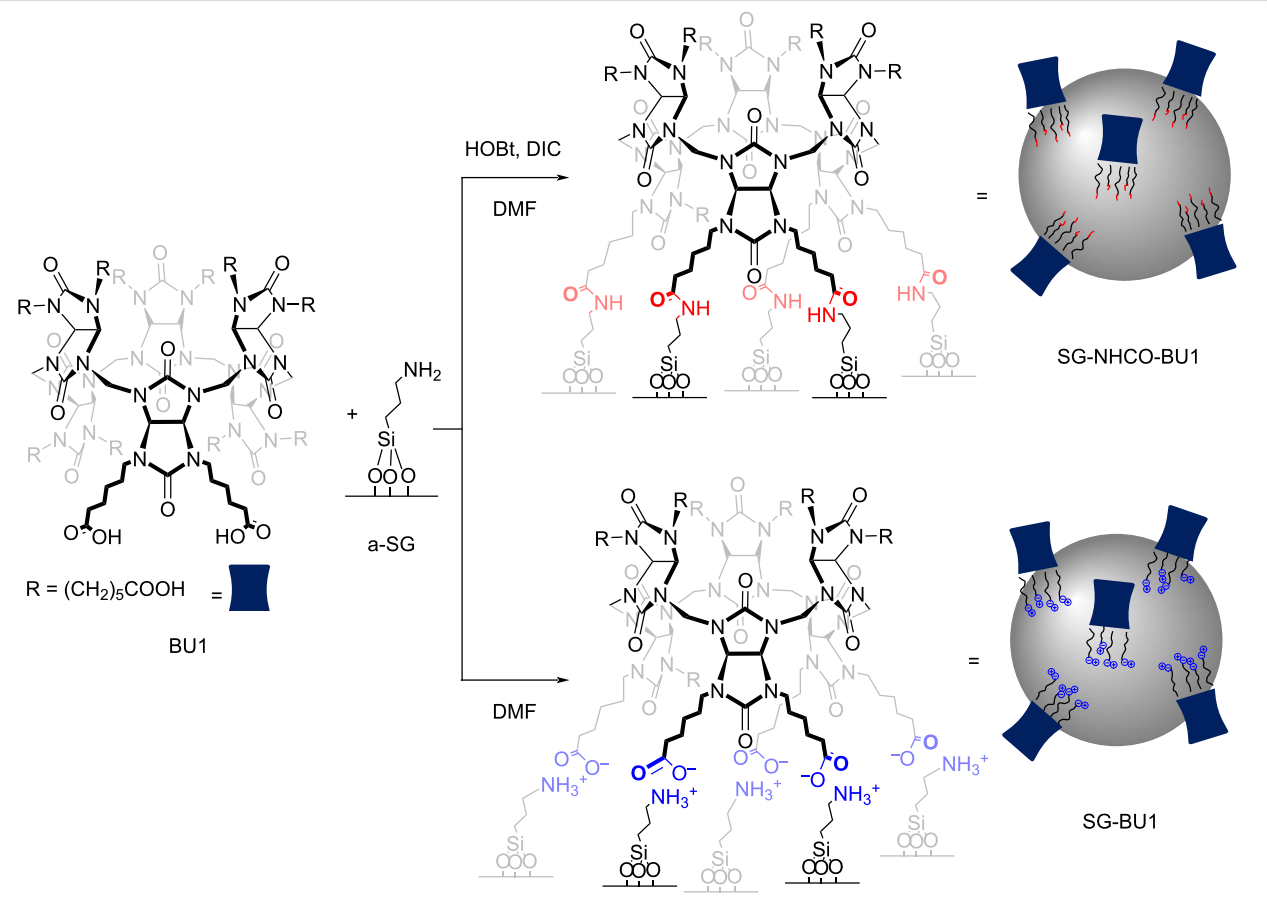

Scheme 1: Synthesis of SG-NHCO-BU1 and SG-BU1 materials based on covalently and non-covalently attached BU1 on the SG surface.

amino groups introduced on the SG surface [15,16]. In the second step, a-SG was treated with BU1, in the presence of 1-hydroxybenzotriazole (HOBt) and 1,3-diisopropylcarbodiimide (DIC) in DMF, resulting in SG-NHCO-BU1 with BU1 covalently attached through amide bonds (Scheme 1). The material was thoroughly washed with DMF, water, and methanol to remove byproducts and unreacted BU1. The grafting reaction was conducted using a 9:1 (w/w) ratio of a-SG to BU1. This ratio was selected based on our previously published results for the noncovalent SG-BnBU system [14]. Besides the covalent SG-NHCO-BU1 material, we also prepared the noncovalent SG-BU1 material, in which BU1 is attached on the SG surface through electrostatic interactions (Scheme 1). The latter reaction was also done using a 9:1 (w/w) ratio of a-SG to BU1, by treatment of a-SG with the macrocycle in DMF at ambient temperature (Scheme 1). The material was then isolated by filtration and washed with DMF and methanol.

The prepared a-SG, SG-NHCO-BU1, and SG-BU1 materials were characterized by FTIR spectroscopy (Supporting Information File 1, Figure S1). In comparison to crude silica gel, the diminished band corresponding to the –OH group (around 980 cm^{-1}) and the appearance of new bands characteristic of amino groups (around 3000 cm^{-1}) indicate the successful introduction of amino groups onto the silica gel surface, confirming the formation of a-SG. Upon modification of a-SG with BU1, additional bands characteristic of BU1 appeared. When comparing BU1 with the SG-NHCO-BU1 material, the C=O vibration band shifted from 1703 cm^{-1} to 1696 cm^{-1} indicating the formation of an amide bond. Additionally, a new absorption band at 1558 cm^{-1} was observed in the spectra of SG-NHCO-BU1 further confirming covalent attachment of BU1 through an amide bond. In the case of SG-BU1, a C=O vibrational band is observed at 1705 cm^{-1}, which corresponds to the vibration of the C=O of BU1 carboxylic acid groups. Other bands corresponding to BU1 were also visible in the spectrum, confirming the presence of the macrocycle in both materials.

The attachment of APTES and subsequently BU1 on SG was further confirmed by thermogravimetric analysis (TGA) (Figure 1A). Pure SG is highly thermally stable, undergoing only minimal decomposition at temperatures below 800 °C as

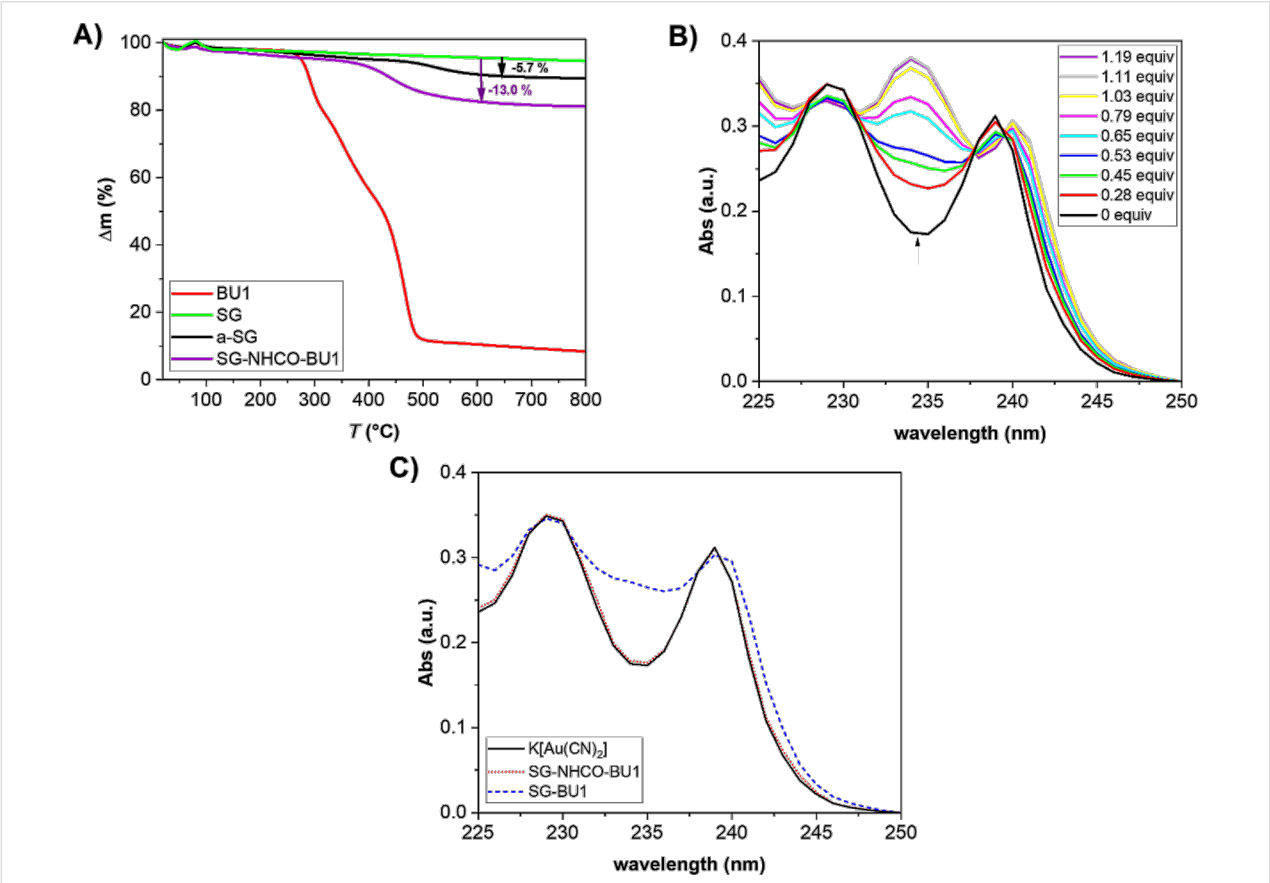

Figure 1: A) Thermogravimetric analyses of BU1, SG, a-SG, and SG-NHCO-BU1. B) UV–vis titration of $K[Au(CN)_2]$ (0.5 mM) with increasing amount of BU1. C) UV–vis spectra of $K[Au(CN)_2]$ (0.5 mM) before and after additions of supernatants obtained by treatment of SG-NHCO-BU1 and SG-BU1 with aqueous 1 M KOH.

confirmed by the analysis. In contrast, a-SG, SG-NHCO-BU1, and SG-BU1 exhibited reduced thermal stability due to the presence of organic substituents (Figure 1A and Supporting Information File 1, Figure S1C). A weight loss of 10% for BU1, SG-NHCO-BU1, and SG-BU1 was observed at 289 °C, 427 °C, and 438 °C.

Additionally, TGA allowed determination of the content of BU1 grafted on the surface in SG-NHCO-BU1 and SG-BU1. As stated above, the material was prepared by mixing of a-SG to BU1 in a 9:1 (w/w) ratio. The analysis revealed that there is approximately 7.3 wt % of BU1 in SG-NHCO-BU1, which corresponds to 74% of the used BU1 attached during its reaction with a-SG (Figure 1A). SG-BU1 contained 7.7 wt % of BU1 which is comparable with the material of covalently attached BU1 (Supporting Information File 1, Figure S1). Thus, according to the TGA, SG-NHCO-BU1 contains 73 mg of BU1 per 1 g of material, which corresponds to 0.032 mmol of BU1 per gram and SG-BU1 comprises 0.034 mol of BU1 per gram.

In order to prove that BU1 is bound through amide bonds on the substrate and it does not leach into solution, we have treated the SG-NHCO-BU1 material with 1 M KOH, followed by addition of dicyanoaurate ($[Au(CN)_2]^-$) to the supernatant. It was shown previously that the absorption spectrum of dicyanoaurate in aqueous solution changes upon formation of an inclusion complex between the anion and a bambusuril macrocycle [17]. A solution of dicyanoaurate in 1 M KOH was titrated by BU1 and the changes in the absorption spectra of the anion were in agreement with those previously reported in pure water (Figure 1B). Dicyanoaurate absorption bands with maxima at 239 and 229 nm decreased in their intensity in the presence of BU1, while a new band appeared at 234 nm. As the complex formation is almost quantitative at millimolar concentrations (association constant is 1.3×10^6 M^{-1} in water) [17], dicyanoaurate can be utilized for the determination of the BU1 content in solution in case BU1 leaches from the substrate. For comparison, SG-BU1 was treated in the same way. After the treatment of the SG-NHCO-BU1 material with 1 M KOH, the supernatant was analyzed in the presence of 1 mM dicyanoaurate by UV–vis spectroscopy (Figure 1C). The measured spectra were identical with the spectrum of pure dicyanoaurate solution revealing that SG-NHCO-BU1 did not release any BU1 and therefore, the macrocycle is indeed covalently bound in the SG-NHCO-BU1 material. This is in contrast with the SG-BU1 material, which released BU1 to the KOH solution as evidenced by marked changes of dicyanoaurate in its absorption spectra (Figure 1C).

A potential application of these materials depends on their stability in different solvents. In terms of practical implementation, BU must stay attached to the solid substrate and should not leach into solution upon usage; for example, as shown above, SG-BU1 has limitations to be used in basic environments. To investigate further the stability of the prepared materials, we compared the behavior of SG-NHCO-BU1, SG-BU1, and SG-BnBU in different solvent systems (Supporting Information File 1, Figure S3). Chloroform, dichloromethane, and methanol were investigated due to their frequent use as mobile phases in liquid chromatography; aqueous phosphate buffer (pH 7.1) was chosen to test the materials' stability in an aqueous environment. ^{1}H NMR measurements showed that neither material released BU into organic solvents in the absence of anions. This was unexpected for SG-BnBU, since BnBU is readily soluble in chloroform and dichloromethane and is only physically adsorbed on SG. However, upon addition of chloride anions, either as tetrabutylammonium (TBA) or sodium salt, BnBU formed a complex with the anion and dissolved in chloroform and dichloromethane and even in methanol. Thus, SG-BnBU remained stable only in water in the absence and presence of salt showing it is suitable for applications in an aqueous environment. SG-BU1 proved to be stable in chloroform, dichloromethane, and methanol even after addition of TBACl or NaCl, respectively. We did not detect any release of BU1 from SG-BU1 in aqueous phosphate buffer by NMR, but we observed leaching of BU1 into solution upon addition of NaCl (Supporting Information File 1, Figure S4) to this solvent system. As expected, SG-NHCO-BU1 with covalently bound BU1 remained stable in all tested solvents in the absence as well as in the presence of salts.

Anion sorption by SG-NHCO-BU1

Silica gel modified either with covalently or noncovalently immobilized BU1 was further investigated for its ability to sorb anions from water and in terms of recyclability. For this purpose, dicyanoaurate ($[Au(CN)_2]^-$) was selected as this anion can be monitored by UV–vis spectroscopy (Figure 2) and plays a central role in gold mining industry [18]. In addition, it allows comparison with the previously prepared SG-BnBU material with noncovalently bound BnBU, which was also tested using the same anion. When either SG-NHCO-BU1 or SG-BU1 was treated with a 1 mM solution of $K[Au(CN)_2]$ in water, the anion concentration in solution reached equilibrium after 15 minutes, consistent with the equilibration time previously established for the non-covalent system SG-BnBU (Supporting Information File 1, Figure S5). Therefore, all subsequent sorption experiments were performed with an equilibration time of 15 minutes.

Next, we evaluated the efficiency of the SG-NHCO-BU1 material in sorbing dicyanoaurate. First, we showed that SG-BU1 is stable under the experimental conditions (Supporting Information File 1, Figure S5C) and next, we investigated both materi-

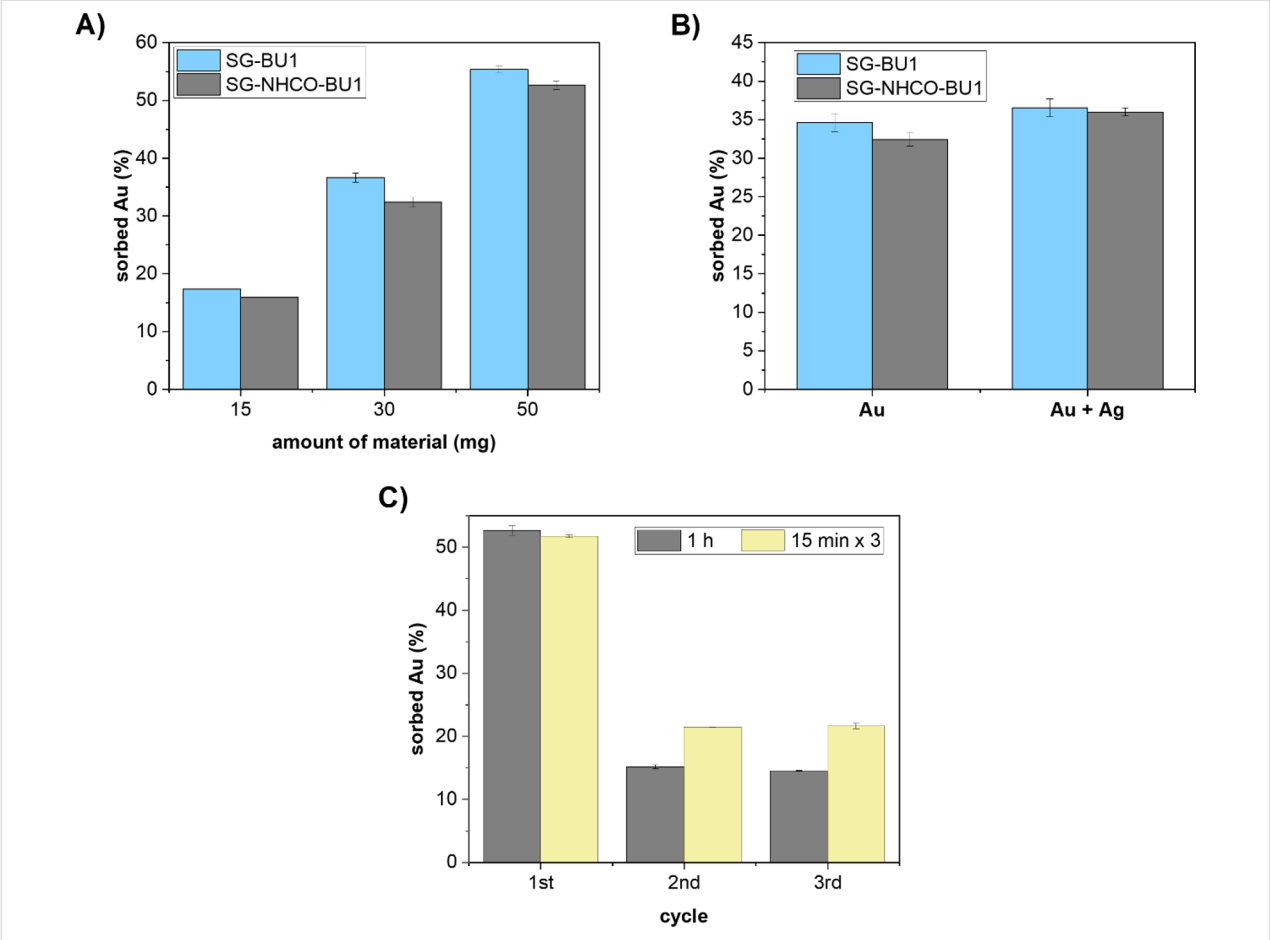

Figure 2: The efficiency of materials (blue SG-BU1, grey SG-NHCO-BU1) in sorbing dicyanoaurate from its water solution (1 mM, 3 mL). A) Depending on the amount of the used material. B) Measured in the absence (Au) and in the presence of $K[Ag(CN)_2]$ (Au + Ag); experiments were done using 30 mg of the materials. C) Dicyanoaurate sorption efficiency before (1st cycle) and after (following cycles) washing with NaBr solution (10 mM) for 1 h or 3 × 15 min; experiments were done using 50 mg of SG-NHCO-BU1.

als for dicyanoaurate sorption. Thus, we gradually increased the amount of SG-NHCO-BU1/SG-BU1 in the 1 mM water solution of $K[Au(CN)_2]$ and observed an uptake of dicyanoaurate based on the changes in the absorption spectra of $K[Au(CN)_2]$. Assuming the molar content of BU1 in the SG-NHCO-BU1/SG-BU1 materials is 0.032/0.034 mmol g^{-1} (based on TGA), we calculated that 1.3/1.4 equivalents of BU1 on the material are required to bind a single dicyanoaurate anion. A similar macrocycle-to-anion ratio was previously determined for the SG-BnBU material. In contrast, water-soluble BU and dicyanoaurate have been reported to form complexes of 1:1 stoichiometry, exhibiting near-quantitative binding at millimolar concentrations [17]. The lower binding efficiency of BUs attached to the material compared to the free macrocycle in solution can likely be attributed to the heterogeneous nature of the solid-phase system. Moreover, the anion binding ability of BU1 may be affected by its long aliphatic arms terminated with carboxylic groups, whose flexibility can enable intramolecular complexation competing for an anion binding [13].

Bambusurils are known to bind a wide range of anions with varying selectivity. Dicyanoaurate is particularly relevant to the gold mining industry, whereas dicyanoargentate is considered a contaminant in this context. To assess selectivity, we measured the sorption of dicyanoaurate from a 1 mM aqueous solution both in the absence and in the presence of an equimolar amount of dicyanoargentate. The measurements revealed that dicyanoaurate uptake was similarly high in both experiments – in the absence and in the presence of the silver salt (Figure 2B) for both materials. The minimal effect of dicyanoargentate on dicyanoaurate sorption aligns with previous findings that BU binds the former anion over 100-fold more weakly in aqueous solution [17]. The finding is also in agreement with our reported results on the noncovalent SG-BnBU system, which showed significantly higher sorption efficiency towards dicyanoaurate over dicyanoargentate [14].

We next examined the recyclability of the materials. Only SG-NHCO-BU1 was used in these experiments as SG-BU1 is

not stable under the experimental conditions as the complex of BU1@$[Au(CN)_2]^-$ was leached into the solution (Figure S6, Supporting Information File 1). After the first sorption, SG-NHCO-BU1 was washed with an excess of aqueous NaBr solution (10 mM, 3 mL, 1 h) to replace $[Au(CN)_2]^-$ in the BU1 cavity with Br^- (Figure 2C). This washing procedure was repeated three times, and the sorption efficiency after each cycle was determined. A decrease in the uptake efficiency was observed after the first washing, but the efficiency remained preserved in following cycles. Prior to the first sorption cycle, the macrocycle is anion-free, whereas in later cycles, it remains occupied by bromide ions due to NaBr treatment, which explains differences during the first and following cycles. We further optimized the regeneration procedure by replacing a single long wash (1 hour) with multiple shorter washes (3 × 15 minutes). The uptake efficiency of SG-NHCO-BU1 improved from 15% to 21% (Figure 2C). Furthermore, the ability of SG-NHCO-BU1 to capture anions was very well in accordance to how much of dicyanoaurate was released – the amount of captured dicyanoaurate corresponded to its released amount during previous washing step (Figure S6B, Supporting Information File 1).

Conclusion

In summary, we have developed organic–inorganic hybrid materials for anion extraction. Through a two-step modification of silica gel, two materials were obtained: SG-NHCO-BU1, in which the BU1 macrocycle is covalently attached to the silica surface via amide bonds, and SG-BU1, where the macrocycle is bound by electrostatic interactions. Both materials proved to be an efficient extractant of dicyanoaurate anions from water, achieving maximum sorption within 15 minutes. The covalent attachment of BU1 enables the material to be recycled using NaBr solution, while the SG-BU1 material disintegrates under similar conditions. We also showed that both SG-NHCO-BU1 and SG-BU1 are stable in organic solvents including chloroform, dichloromethane, and methanol even after addition of halide salts. This stability stands in contrast to previously published SG-BnBU, which contains noncovalently immobilized BnBU and undergoes macrocycle loss in all of three tested organic solvents after addition of halide salts. These results illustrate that the choice of material for anion sorption depends on the specific experimental conditions. While SG-BnBU and SG-NHCO-BU1 are suitable for dicyanoaurate sorption from aqueous solutions, SG-NHCO-BU1 and SG-BU1 could be used for anion extraction in organic media.

Experimental

Materials and instruments

Silica gel (Silikagel 60 (0.015–0.040 mm) for column chromatography, product number 1.15111) was dried in vacuo at 50 °C overnight before use. 3-Aminopropyltriethoxysilane (APTES), 1-hydroxybenzotriazole (HOBt), 1,3-diisopropylcarbodiimide (DIC), potassium dicyanoaurate, potassium dicyanoargentate, sodium chloride, tetrabutylammonium chloride and sodium bromide were purchased from Merck and used without further purification. Dodecakis(5-carboxypentyl)bambus[6]uril (BU1) was synthesized according to a previously published procedure [13].

Infrared spectra were recorded with an Alpha spectrophotometer (Bruker). Thermogravimetric analyses were done with a Netzsch STA 449C Jupiter and carried out in nitrogen atmosphere. The dicyanoaurate concentration in solution was determined according to UV–vis spectra recorded with a CARY 60 spectrophotometer (Agilent Technologies). NMR spectra were recorded on a Bruker Avance III 300 spectrometer (300.15 Hz, 298.15 K).

Preparation of SG-NHCO-BU1

Silica gel (8.01 g) was dispersed in toluene (24 mL) and stirred under argon atmosphere, while heated up to 115 °C. Then, APTES (6 mL) was added, and the dispersion was stirred under inert atmosphere at elevated temperature for 5 h. After cooling, the dispersion was filtered, washed thoroughly with toluene, ethanol and acetone to remove unreacted APTES and dried in vacuo (50 °C) overnight in order to get a-SG [15,16]. Further, to prepare covalent SG-NHCO-BU1, a-SG (0.9 g) was suspended in DMF (15 mL) and shaken at ambient temperature for 30 min. BU1 (0.1 g, 1 equiv) was dissolved in a minimum amount of DMF and a solution of HOBt (12 equiv) in DMF was added, followed by addition of DIC (12 equiv). Then, the activated BU1 was added to the suspension of a-SG. The reaction was performed under Ar atmosphere for 5.5 h at ambient temperature under constant shaking (180 rpm). The resulting material was filtered and thoroughly washed with DMF, water and methanol in order to remove byproducts and unreacted BU1. After air-drying, SG-NHCO-BU1 was obtained.

Preparation of SG-BU1

For the preparation of SG-BU1 with electrostatically bound BU1 on the surface of silica gel, a-SG (0.9 g) was suspended in DMF (15 mL) and BU1 (0.1 g), dissolved in a minimum amount of DMF, was added. The dispersion was mechanically shaken (180 rpm) at ambient temperature for 5.5 h. Afterwards, the dispersion was filtered, washed with DMF (5×) and methanol (5×) to remove unattached BU1. After air-drying in a hood overnight at ambient temperature, SG-BU1 was obtained.

Sorption experiments with SG-NHCO-BU1

The potential of SG-NHCO-BU1 to bind anions from solution was investigated by UV–vis spectroscopy. SG-NHCO-BU1 or

SG-BU1 was placed in a vial and anion solution (1 mM, 3 mL) was added. The system was shaken for 15 min at 250 rpm. Afterwards, SG-NHCO-BU1 or SG-BU1 was left to settle and the supernatant was analyzed. The actual concentration of the anion left in the solution was calculated from a calibration curve.

Supporting Information

Supporting Information File 1

Characterization of materials and additional experiments regarding anion uptake.
[https://www.beilstein-journals.org/bjoc/content/supplementary/1860-5397-21-201-S1.pdf]

Acknowledgements

We thank Dr. Zdeněk Moravec for the TGA measurements and Dr. Arico Del Mauro for assistance with the BU1 synthesis.

Funding

The authors thank the RECETOX Research Infrastructure (LM2023069) financed by the Ministry of Education, Youth, and Sports, and the Operational Programme Research, Development, and Education. This project was supported by the European Union's Horizon 2020 Research and Innovation Programme under grant agreement No. 857560. This publication reflects only the author's view and the European Commission is not responsible for any use that may be made of the information it contains. The authors acknowledge the support from National Infrastructure for Chemical Biology (CZ-OPENSCREEN, LM2023052).

Author Contributions

Michaela Šusterová: investigation; visualization; writing – original draft. Vladimír Šindelář: conceptualization; funding acquisition; supervision; writing – review & editing.

ORCID® iDs

Vladimír Šindelář - https://orcid.org/0000-0003-0090-5961

Data Availability Statement

All data that supports the findings of this study is available in the published article and/or the supporting information of this article.

References

1. Mohammed, F. A.; Xiao, T.; Wang, L.; Elmes, R. B. P. *Chem. Commun.* **2024,** *60,* 11812–11836. doi:10.1039/d4cc04521a
2. Zhang, Q.; Zhou, Y.; Ahmed, M.; Khashab, N. M.; Han, W.; Wang, H.; Page, Z. A.; Sessler, J. L. *J. Mater. Chem. A* **2022,** *10,* 15297–15308. doi:10.1039/d2ta03791b
3. Reyes-Serrano, A.; López-Alejo, J. E.; Hernández-Cortázar, M. A.; Elizalde, I. *Chin. J. Chem. Eng.* **2020,** *28,* 1107–1111. doi:10.1016/j.cjche.2019.12.023
4. Li, D.; Ning, X.-a.; Yuan, Y.; Hong, Y.; Zhang, J. *J. Environ. Sci.* **2020,** *91,* 62–72. doi:10.1016/j.jes.2020.01.002
5. Jiang, M.; Ye, K.; Deng, J.; Lin, J.; Ye, W.; Zhao, S.; Van der Bruggen, B. *Environ. Sci. Technol.* **2018,** *52,* 10698–10708. doi:10.1021/acs.est.8b02984
6. Memon, S.; Tabakci, M.; Roundhill, D. M.; Yilmaz, M. *React. Funct. Polym.* **2006,** *66,* 1342–1349. doi:10.1016/j.reactfunctpolym.2006.03.017
7. Sessler, J. L.; Gale, P. A.; Genge, J. W. *Chem. – Eur. J.* **1998,** *4,* 1095–1099. doi:10.1002/(sici)1521-3765(19980615)4:6<1095::aid-chem1095>3.0.co;2-1
8. Aydogan, A. *Supramol. Chem.* **2016,** *28,* 117–124. doi:10.1080/10610278.2015.1092538
9. Zhao, W.; Lou, X.; Guo, J.; Sun, P.; Jia, Y.; Zheng, L.; He, L.; Zhang, S. *J. Sep. Sci.* **2018,** *41,* 2110–2118. doi:10.1002/jssc.201701185
10. Iverson, B. L.; Thomas, R. E.; Kral, V.; Sessler, J. L. *J. Am. Chem. Soc.* **1994,** *116,* 2663–2664. doi:10.1021/ja00085a074
11. Ji, X.; Guo, C.; Chen, W.; Long, L.; Zhang, G.; Khashab, N. M.; Sessler, J. L. *Chem. – Eur. J.* **2018,** *24,* 15791–15795. doi:10.1002/chem.201804335
12. Ji, X.; Wu, R.-T.; Long, L.; Guo, C.; Khashab, N. M.; Huang, F.; Sessler, J. L. *J. Am. Chem. Soc.* **2018,** *140,* 2777–2780. doi:10.1021/jacs.7b13656
13. Havel, V.; Babiak, M.; Sindelar, V. *Chem. – Eur. J.* **2017,** *23,* 8963–8968. doi:10.1002/chem.201701316
14. Šusterová, M.; Šindelář, V. *RSC Adv.* **2025,** *15,* 12982–12986. doi:10.1039/d5ra02404h
15. Gambero, A.; Kubota, L. T.; Gushikem, Y.; Airoldi, C.; Granjeiro, J. M.; Taga, E. M.; Alcântara, E. F. C. *J. Colloid Interface Sci.* **1997,** *185,* 313–316. doi:10.1006/jcis.1996.4566
16. Lee, Y. K.; Ryu, Y. K.; Ryu, J. W.; Kim, B. E.; Park, J. H. *Chromatographia* **1997,** *46,* 507–510. doi:10.1007/bf02496369
17. Rando, C.; Vázquez, J.; Sokolov, J.; Kokan, Z.; Nečas, M.; Šindelář, V. *Angew. Chem., Int. Ed.* **2022,** *61,* e202210184. doi:10.1002/anie.202210184
18. Liu, W.; Jones, L. O.; Wu, H.; Stern, C. L.; Sponenburg, R. A.; Schatz, G. C.; Stoddart, J. F. *J. Am. Chem. Soc.* **2021,** *143,* 1984–1992. doi:10.1021/jacs.0c11769

BEILSTEIN JOURNAL OF ORGANIC CHEMISTRY

Cone *p*-aminocalix[4]arenes enriched with ‘clickable’ alkyne or azide functionalities

Ilia Korniltsev[1], Vasily Bazhenov[1], Alexander Gorbunov[1], Dmitry Cheshkov[2], Stanislav Bezzubov[3], Vladimir Kovalev[1] and Ivan Vatsouro[*1]

Full Research Paper

Open Access

Address:
[1]Department of Chemistry, M. V. Lomonosov Moscow State University, Lenin’s Hills 1, 119991 Moscow, Russia, [2]State Research Institute for Chemistry and Technology of Organoelement Compounds, Sh. Entuziastov 38, 105118 Moscow, Russia and [3]Kurnakov Institute of General and Inorganic Chemistry, Russian Academy of Sciences, Leninskii pr. 31, 119991 Moscow, Russia

Email:
Ivan Vatsouro[*] - vatsouro@petrol.chem.msu.ru

* Corresponding author

Keywords:
calixarene amines; dimeric capsules; functionalization; tetraureacalixarenes; triazoles

Beilstein J. Org. Chem. **2026,** *22,* 399–415.
https://doi.org/10.3762/bjoc.22.28

Received: 02 December 2025
Accepted: 12 February 2026
Published: 09 March 2026

This article is part of the thematic issue "Novel macrocycles: from synthesis to supramolecular function".

Guest Editor: C. Gaeta

Abstract

Efficient approaches have been developed for the synthesis of heteromultifunctional cone calix[4]arenes containing four amino groups at the wide rim and one, two or four propargyl or 2-azidoethyl groups at the narrow rim of the macrocycle, which can be used for expanding functionalization of the calixarene core in the well-known amine acylation (or similar reactions) and CuAAC ‘click’ reactions. Two different strategies were implemented to obtain propargylated and 2-azidoethylated *p*-aminocalixarenes. In the case of propargylated calixarenes, sterically crowding silyl protection was introduced into the alkyne groups of *p-tert*-butylcalix[4]arene (multiple) propargyl ethers, and the resulting compounds were *ipso*-nitrated followed by reduction of the nitro groups. To prepare 2-azidoethylated macrocycles, the *ipso*-nitration/reduction sequence was applied to *p-tert*-butylcalix[4]arenes containing 2-tosyloxyethyl groups at the narrow rims followed by replacement of the tosyloxy groups with azide ones. In all cases, *p*-aminocalix[4]arenes were obtained as the readily cleavable *tert*-butoxycarbonyl (Boc) derivatives, which was crucial for certain transformation and purification steps. To confirm the functionalization capabilities of the five obtained multifunctional calixarenes, they were reacted with excess benzyl azide or phenylacetylene, taken as representatives, under copper(I) catalysis, resulting in the narrow-rim triazolated macrocycles. By removing the Boc protecting groups and involving the free amino groups in reactions with *p*-tolyl isocyanate, a series of narrow-rim triazolated tetraureacalix[4]arenes was obtained. Examination of the ^{1}H NMR spectra of the tetraureas in $CDCl_3$ showed that in most cases triazole heterocycles do not intervene the formation of homo- and heterodimeric capsules by these compounds. Thus, considering the synthetic value of CuAAC and amine transformations, *p*-aminocalix[4]arenes enriched with alkyne or azide functionalities can be readily used as multifunctional platforms to obtain even higher functionalized macrocycles. As an example, they can be used for the preparation of sophisticated supramolecular assemblies with homo- or heterodimeric calixarene cores and virtually any functional units attached to them via triazole groups.

Introduction

Considered generally as multifunctional molecular cores, calixarenes in their native forms as cyclic oligophenols actually possess just limited functionalization capabilities unless synthetically more valuable groups are introduced into their structures. Due to the synthetic approaches well-developed in the first decades of calixarene chemistry, these groups can be arranged in a certain number and order at the phenolic oxygen atoms and/or in the aromatic *p*-positions to them, which form respectively the narrow (lower) and wide (upper) rims of the calixarene macrocycle when it possesses a cone shape. Both the core functionalization and shape control strategies are most developed for calix[4]arene cores, and that is exactly why these cyclic tetramers may be regarded as virtually universal molecular platforms for the construction of unique multifunctional structures capable of diverse supramolecular interactions [1-4].

Amino groups attached directly to all four positions of the wide rim of the cores are among the most important functionalities which can be introduced into calix[4]arene structures either through a wide-rim exhaustive nitration followed by reduction of the nitro groups [5-13], or through azo coupling followed by cleavage of the calixarene azo compounds thus formed [14-17]. (Multi)calix[4]arenes having (dialkyl)amino groups at the wide rims are soluble in aqueous media at physiological pHs and may be used in protein sensing [18], DNA binding/recognition [19-23], and cell transfection [24-26]. Their water-soluble guanidinium derivatives are also biocompatible compounds capable of interacting with proteins, nucleic acids, and polysaccharides [27-31], and may also mimic phosphodiesterase functions [32-35]. Beyond biorelevant structures, *p*-aminocalix[4]arenes serve as preorganizing platforms that may graft together four functional/receptor units, thus drastically improving their supramolecular interaction capabilities. This property of *p*-aminocalix[4]arenes has been widely utilized in constructing *f*-element-targeted extractants for nuclear waste treatment, having four carbamoylmethylphosphine oxide groups introduced to the macrocyclic core through simple acylation of *p*-aminocalix[4]arenes with the respective phosphorous-containing activated esters. Such grafting of well-known receptor units onto a common platform has led to substantial amplification of the efficiency of lanthanide and actinide extraction from acidic media by carbamoylmethylphosphine oxides along with enrichment of the extraction selectivity [36-45]. Even more impressive is the effect from grafting of four urea groups at the wide rims of calix[4]arene macrocycles achieved by reacting *p*-aminocalix[4]arenes with aryl- or arylsulfonyl isocyanates. In aprotic media, these compounds, referred to as 'tetraureacalix[4]arenes', assemble into well-defined homo- or heterodimeric capsules, which are held together by cyclic belts of hydrogen bonds between interpenetrated urea groups from two molecules and are able to include a single neutral molecule or a trialkylammonium cation inside the joint cavity formed by two cone calix[4]arene macrocycles [46-54]. This phenomenon has been thoroughly investigated, including the effects from substituents in the urea groups and/or at the calixarene narrow rim upon the thermodynamic and kinetic stability of the capsules and the guest exchange processes [55-60]. This has made dimerization of tetraureacalix[4]arenes one of the most explored self-organization processes in calixarene supramolecular chemistry, which has been used in the template synthesis of calixarene-based multi(macrocycles) and multi(catenanes) having impressive topology [61-69].

Over the past two decades, azide and alkyne groups have also appeared among the most synthetically valuable functionalities introduced into calixarene cores due to the ease of their conversion into diverse 1,4-disubstituted 1,2,3-triazole units under CuAAC (copper(I)-catalyzed azide–alkyne cycloaddition) 'click' conditions [70-73]. The first implementation of the CuAAC approach for calixarene modification was published shortly after its introduction into chemistry in general, and used cone calix[4]arenes having four propargyl or 2-azidoethyl groups at their narrow rims as CuAAC substrates [74]. Since then, hundreds of publications have reported the application of the CuAAC reaction for the introduction of diverse biorelevant, receptor or sensory functionalities into the structures of calixarenes and related macrocycles [75-78]. Many of them relied on the introduction of propargyl or azidoalkyl groups to the phenolic oxygen atoms for synthesizing the CuAAC-ready calixarene cores. Within this area of research, our studies on the CuAAC reactions applied to cone propargylated and 2-azidoethylated calix[4]arenes revealed their enhanced efficiency, resulting in the preferential formation of exhaustively triazolated macrocycles over mixed triazolated/propargylated or triazolated/2-azidoethylated ones [79,80]. Furthermore, it has been proved that triazolated calixarenes derived from propargylated and 2-azidoethylated precursors possess drastically different complexation abilities towards transition-metal cations [81-84] including the formation of unique inherently dinuclear iridium(III) complexes with cone calix[4]arenes having pairs of 2-(4-aryltriazol-1-yl)ethyl groups at their narrow rims [85]. Regarding the synthetic capabilities of propargyl and 2-azidoethyl groups residing the calixarene core, we have established a series of triazolated calix[4]semitubes in which two or three calix[4]arene macrocycles are connected to each other by pairs of triazole units formed via two-fold CuAAC macrocyclizations [86,87]. We have also developed a straightforward approach to the functionalization of water-soluble *p*-sulfonatocalix[4]arenes by their enrichment with propargyl groups at the

narrow rims followed by CuAAC reactions with various azides [88].

Inspired by the above benefits brought to the calixarene structures by amino groups, the power of CuAAC reactions in building multifunctional architectures, and following the pioneering work on bifunctional "Janus" calix[4]arenes joining propargyl groups and nitro/amino/azide groups in the structures [9], we herein report on the synthesis approaches to a series of cone *p*-aminocalix[4]arenes having propargyl or 2-azidoethyl groups at the narrow rims (Figure 1). The newly synthesized compounds may be thus treated as novel building blocks in calixarene chemistry capable of step-wise orthogonal transformations into various multifunctional structures and sophisticated supramolecular systems.

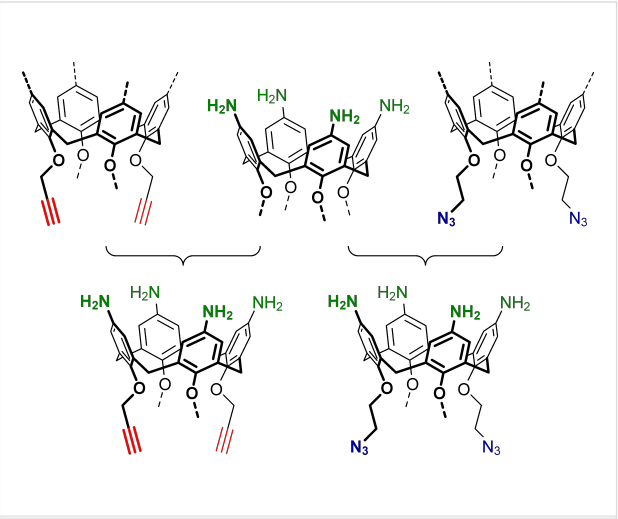

Figure 1: General concept of building multifunctional calix[4]arenes by joining propargyl/2-azidoethyl and *p*-amino groups on a common platform.

Results and Discussion

In the majority of cases, the introduction of four amino groups into the calix[4]arene wide rim requires exhaustive (*ipso*-)nitration of the core followed by reduction of the resulting *p*-nitrocalix[4]arene. Notably, the alternative strategy of utilizing an azo coupling/cleavage sequence has only been applied thus far for the wide-rim modification of narrow-rim unsubstituted calixarenes. Since the exhaustive nitration and reduction steps proceed under relatively drastic conditions, which are poorly compatible with propargyl or 2-azidoethyl functionalities residing at the calixarene narrow rims, these 'simple' transformations are not applicable to the available propargylated/2-azidoethylated *p*-*tert*-butyl- or *p*-H-calix[4]arenes. Therefore, the multistep reaction sequences presented below have been developed for the preparation of the targeted multifunctionalized calixarenes.

Propargylated *p*-aminocalix[4]arenes

Following the published example [9], for the preparation of propargylated *p*-aminocalix[4]arenes a three-step synthesis strategy was selected, which involved protection of the calixarene propargyl ethers by *tert*-butyldimethyl-silylation followed by the calixarene wide-rim exhaustive nitration and reduction of the nitro groups. The readily available cone calix[4]arenes **1**–**5** [89-92] bearing up to four propargyl groups at their narrow rims and *n*-propyl groups completing the substitution patterns were selected as the starting materials to enable further preparation of the respective mono-, di- and tetrapropargylated calix[4]arene tetraamines and their derivatives.

The silylation of propargyl ethers **1**–**5** was first attempted using *tert*-butyldimethylsilyl chloride (TBSCl) and the commercially available lithium bis(trimethylsilyl)amide (LiHMDS), but the latter was found inconvenient for routine syntheses due to high moisture sensitivity which prevented reproducibility of the reaction conditions. To overcome this difficulty, the LiHMDS solution was instead prepared in situ by reacting bis(trimethylsilyl)amine (HMDS) with *n*-butyllithium in THF immediately before the addition of a propargylated calixarene followed by TBSCl. This allowed us to improve the yield of the known calix[4]arene **6** [9] having four silylated propargyl groups at the narrow rim, and to obtain the respective persilylated propargyl ethers **7**–**10** from precursors **2**–**5** (Scheme 1).

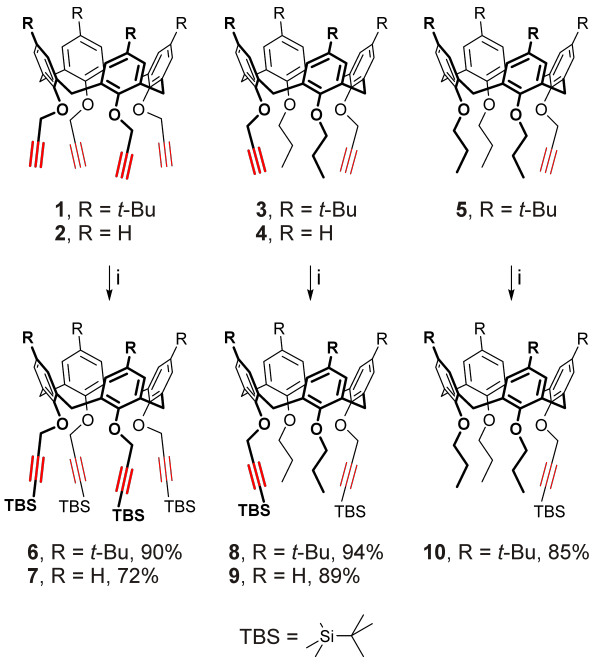

Scheme 1: Silylation of the calixarene propargyl ethers. Conditions: i) LiHMDS (HMDS + *n*-BuLi), TBSCl, THF, –95 °C → rt.

Expectedly, (*ipso*-)nitration of calixarenes **6**–**10** by mixtures of fuming nitric acid and glacial acetic acid in dichloromethane solutions could potentially be complicated by both the incomplete conversion of the starting materials and also by formation of side products, due to acid-promoted cleavage and undesired transformations of the TBS-protected propargyl groups and/or due to unwanted oxidation/nitration of the calixarene core [93]. Indeed, nitration of calixarene **6** has been reported to furnish the desired wide-rim exhaustively nitrated calix[4]arene **11** having four TBS-protected propargyl groups at the narrow rim in only moderate yield of 37% [9]. In our hands, according to the NMR spectra of the reaction mixture, under the reported conditions (>30 equiv of fuming HNO_3 per calixarene aromatic unit in a 1:1 dichloromethane/acetic acid mixture, from 0 °C → rt, overnight) the nitration of calixarene **6** resulted in a mixture of exhaustively nitrated product **11**, partially nitrated calixarenes having nitro and *tert*-butyl groups at the wide rims, and a large amount of other calixarene side product(s) having broadened and non-interpretable NMR spectra. Upon tuning the reaction conditions, it was found that a more complete nitration of calixarene **6** along with some suppression of the undesired side reactions could be achieved by decreasing the nitric acid excess (to ≈10 equiv per calixarene aromatic unit) and its concentration in dichloromethane (to ≈1 M), reducing the content of acetic acid in the mixture (to 1 mol per mol of HNO_3) and extending the room-temperature reaction time to 72 h. Yet, under these conditions, the desired calix[4]arene **11** was obtained in only 31% yield (Scheme 2), and further variations in reagent excess/concentration and reaction time did not significantly improve the yield. Also an attempt to obtain calixarene **11** by nitration of the silylated *p*-H-calix[4]arene tetrapropargyl ether **7** failed, as no complete conversion of the starting calixarene could be achieved likely due to a slower nitration of unsubstituted calixarene aromatic units in comparison with the *ipso*-nitration of the corresponding *tert*-butylated ones. Even larger amounts of side products were formed, thus confirming the involvement of the tightly arranged narrow-rim substituents in calixarene **6** and **7** in undesired side processes under nitration conditions.

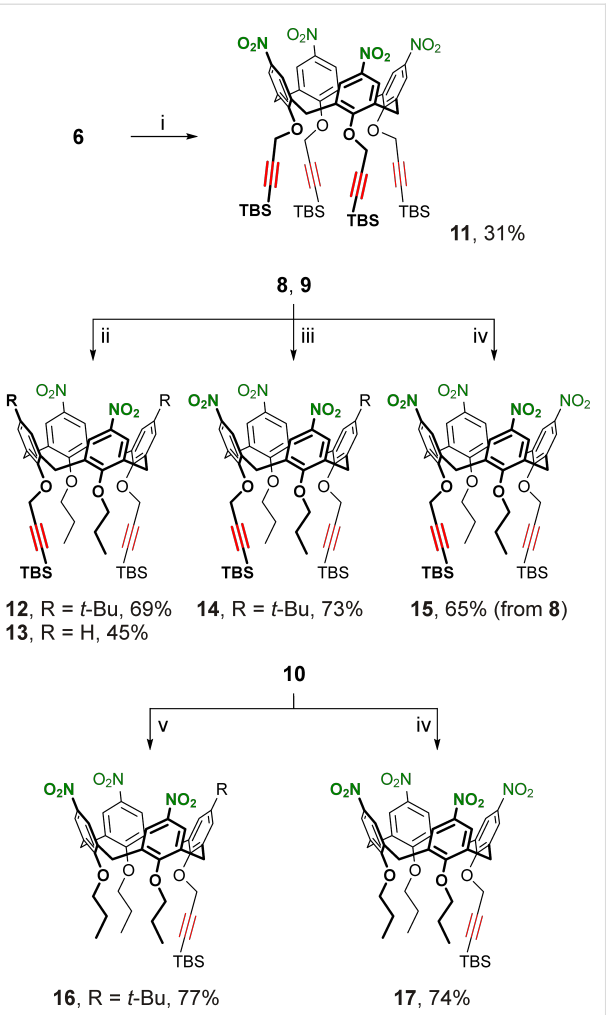

Scheme 2: Nitration of calixarenes **6**, **8**–**10**. Conditions: i) HNO_3 (fuming, 10 equiv per calixarene aromatic unit, $c \approx 1$ M), AcOH, dichloromethane, rt, 72 h; ii) HNO_3 (fuming, 2.5 equiv per calixarene aromatic unit, $c \approx 0.2$ M), AcOH, dichloromethane, rt, 12 h; iii) HNO_3 (fuming, 2.5 equiv per calixarene aromatic unit, $c \approx 1$ M), AcOH, dichloromethane, rt, 12 h; iv) HNO_3 (fuming, 10 equiv per calixarene aromatic unit, $c \approx 2.5$ M), AcOH, dichloromethane, rt, 48 h; v) HNO_3 (fuming, 2.5 equiv per calixarene aromatic unit, $c \approx 1$ M), AcOH, dichloromethane, rt, 48 h.

In line with this, compounds **8**–**10** having less sterically hindered narrow-rim substitution patterns were found to be more resistant to side reactions during wide-rim nitration as well as to the target exhaustive nitration itself. These reactions required a higher nitric acid concentration of ≈2.5 M to complete the process and to obtain the *p*-nitrocalix[4]arenes **15** and **17** in good yield (Scheme 2). Upon further fine-tuning the reaction conditions it was found that some of the partially nitrated products could also be successfully prepared by using smaller amounts of the nitrating agent. Thus, the room-temperature nitration of the silylated *p*-*tert*-butylcalix[4]arene ether **8** using 2.5 equiv of HNO_3 per calixarene aromatic unit resulted in di- or trinitrated macrocycles **12** and **14** as the major products, when ≈0.2 and ≈1 M nitric acid concentrations were used. Similarly, the wide-rim unsubstituted calixarene **9** was successfully converted into the dinitro-derivative **13** using the dichloromethane-diluted nitric acid/acetic acid mixture. Also, it was found that calixarene **10** could be converted to the trinitrated product **16** under the same conditions as for the synthesis of calixarene **14**, with only the reaction time increased (Scheme 2).

The 1D NMR spectra for the dinitrocalix[4]arenes **12** and **13** provided no definitive data on the substitution patterns at their wide-rims except for the presence of two nitro groups in the

distal aromatic units. To localize the nitro groups in the structures of calixarenes **12** and **13**, $^{1}H,^{13}C$ HMBC spectra were acquired (Figure 2), which clearly showed that the nitro groups are attached to the propylated aromatic units of the macrocycle in both cases. Notably, the correlations showed that the signals from the nitrated calixarene aromatic units appeared upfield-shifted in the ^{1}H NMR spectra with respect to those from the aromatic units bearing no electron-withdrawing groups. This uncommon signal position may indicate a specific time-averaged conformation of the calixarene core in compounds **12** and **13** due to the presence of the bulky TBS-protected propargyl groups in their structures, in which the nitrated aromatic units experience an additional shielding. This may be also responsible for the selectivity of the two-fold nitration of compounds **8** and **9** leading to calixarenes **12** and **13** rather than to their isomers containing nitro groups in the propargylated aromatic units of the macrocycles.

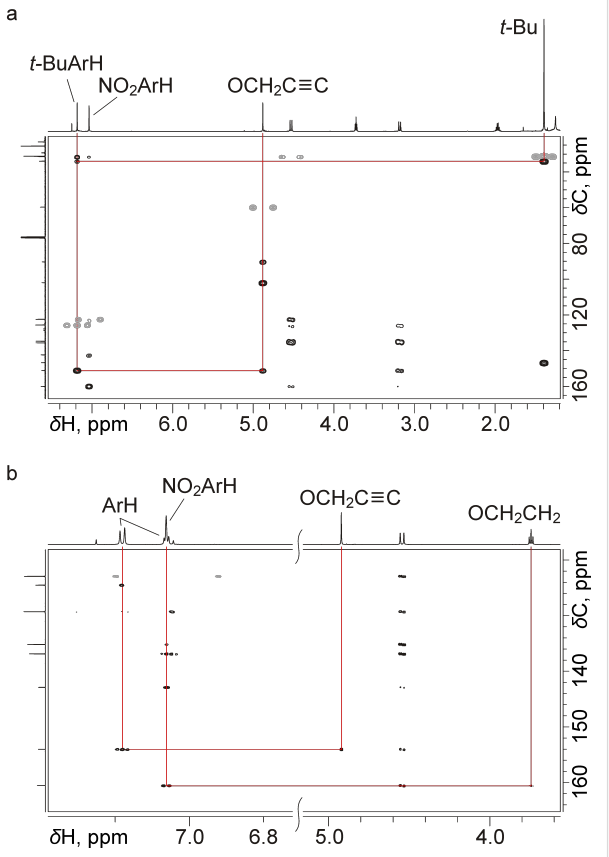

Figure 2: Parts of $^{1}H,^{13}C$ HMBC spectra of calixarenes **12** (a) and **13** (b) recorded in $CDCl_3$ solutions at 600 MHz. Red lines show the key correlations between signals from the calixarene narrow-rim substituents and aromatic units.

There was no doubt in establishing the structure of the trinitrated calix[4]arene **14**, as its NMR spectra contained a single set of resonances from propyl groups and two sets of those from the TBS-protected propargyl groups, which indicated clearly the symmetry plane passing through the propargylated aromatic units of the calixarene. Assuming a step-wise nitration of calixarene **8**, the dinitrated calixarene **12** must be the immediate precursor of compound **14**. The presence of the nitro groups in both of the propylated aromatic units of this calixarene can only be derived from calixarene **12**, which is additional evidence for its structure.

The structure of trinitrated calix[4]arene **16** having a single TBS-protected propargyl group at the narrow rim was unambiguously established from X-ray diffraction data. Suitable crystals were collected upon slow evaporation of a dichloromethane/methanol solution of compound **16**. Similarly, single crystals of the exhaustively nitrated calix[4]arene **15** having two TBS-protected propargyl groups at the narrow rim were collected, and the molecular structure of this compound was also established (Figure 3) [94]. The results showed clearly, that in calixarene **16** all three propylated aromatic units were nitrated, and the propargylated one still contained a *tert*-butyl group. Thus, within a step-wise nitration paradigm, the narrow-rim propargylated aromatic units are more stable against nitration when compared to the propylated aromatic units of the calixarene core. This correlates well with the above selectivity of nitration observed for calixarenes **8** and **9** and may be tentatively explained by an electron-withdrawing effect of the propargyl groups.

However, in the molecular structures of calixarenes **15** and **16**, another feature was observed: in both cases the calixarene aromatic units containing the TBS-protected propargyl groups (and the opposed one in the case of compound **16**) are extremely flattened, while the other aromatic units are pinched and bring the two nitro groups into very close contact. Similar effects from the TBS-protected propargyl groups may be also expected in calixarenes **6**–**10** and their partially nitrated products. Thus complex conformational transitions in the calixarene cores may also interfere with the reaction, and, in particular, may hamper the exhaustive nitration of calixarenes **6** and **7** each bearing four TBS-protected propargyl groups at their narrow rims.

The formation of the partially nitrated calix[4]arenes **12**–**14** and **16** as major reaction products described above was quite unexpected, and these compounds were not used further in this study which was more concerned with calix[4]arenes having four equal substituents at the wide rims. But surely, the partially nitrated calix[4]arenes bearing protected propargyl groups in their structures may be further explored as multifunctional cores capable of other potential applications in calixarene chemistry.

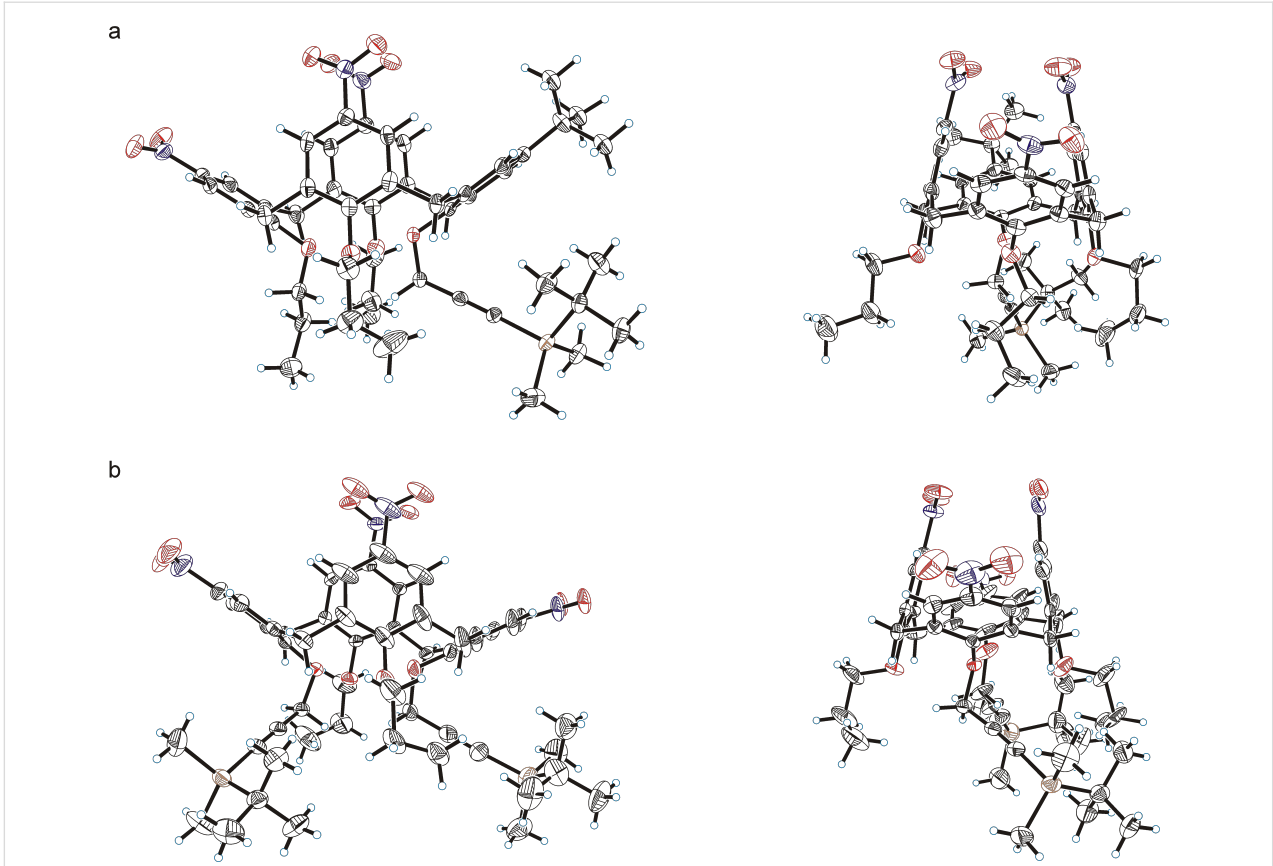

Figure 3: Molecular structures of partially nitrated calixarene **16** (a) and exhaustively nitrated calixarene **15** (b). Two projections shown in each case and thermal ellipsoids are drawn at a 50% probability level.

TBS units attached to the propargyl groups of calixarenes appeared to be not bulky enough to protect the alkyne from a Raney-Ni-catalyzed reduction by gaseous hydrogen, as a trial hydrogenation of the nitrated/propargylated calix[4]arene **11** resulted in only trace amounts of the desired *p*-aminocalix[4]arene **18** among numerous other reaction products. Due to this, a homogeneous reduction using tin(II) chloride in ethanol was used after fine-tuning of the published reaction conditions [9]: the reduction was conducted by gentle heating of a mixture of calixarene **11**, $SnCl_2{\cdot}2H_2O$, aqueous HCl and ethanol at 70 °C (instead of prolonged boiling of the reaction mixture) in a closed vessel to prevent the product oxidation. At the work-up step sodium hydroxide was replaced with potassium hydroxide which provided better water solubility of inorganic salts for their extractive removal. As a result, tetraamine **18** having four TBS-protected propargyl groups at the narrow rim was obtained in substantially improved yield and the nitrated calixarenes **15** and **17** were similarly reduced to the corresponding tetraamines **19** and **20** (Scheme 3).

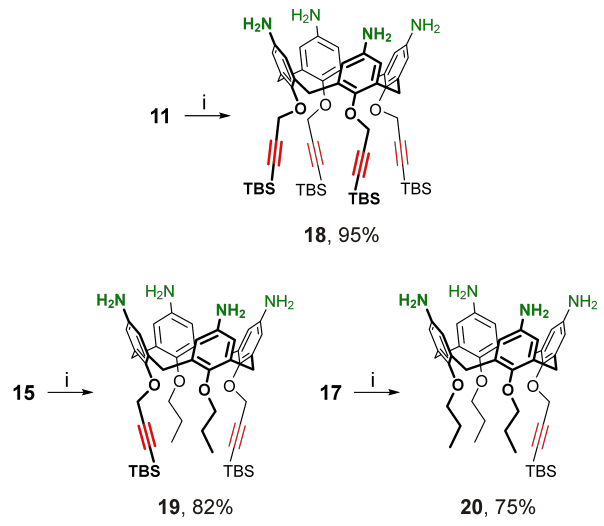

Scheme 3: Reduction of calixarenes **11**, **15** and **17**. Conditions: i) $SnCl_2{\cdot}2H_2O$, HCl, EtOH, H_2O, 70 °C, then KOH, H_2O.

Chemical modifications of propargylated *p*-aminocalix[4]arenes may be performed by the amine acylation followed by the CuAAC involving the propargyl groups, or vice versa. Of these two possibilities, the triazole synthesis conducted prior to the target acylation of amines seems to be more convenient, as the

acylation may proceed under milder conditions than the CuAAC reaction. Even more important, the amine-derived functional units may interfere or affect the cycloaddition by, for instance, binding copper cations or counter anions, and thus their presence in the structures of calixarenes at the CuAAC step must be avoided. On the other hand, the unmodified amines may also contribute to undesired Cu(I) stabilization and complicate the CuAAC work up in acidic conditions, so the amino groups in calixarenes **18**–**20** must be deactivated prior to the cycloaddition. Following the above reasons, a two-step replacement of protecting groups in calixarenes **18**–**20** was performed. First, the amino groups were acylated with di-*tert*-butyl dicarbonate (Boc_2O) and next the TBS-protecting groups were removed from the acetylene units in the Boc-protected tetraamines **21**–**23** (Scheme 4).

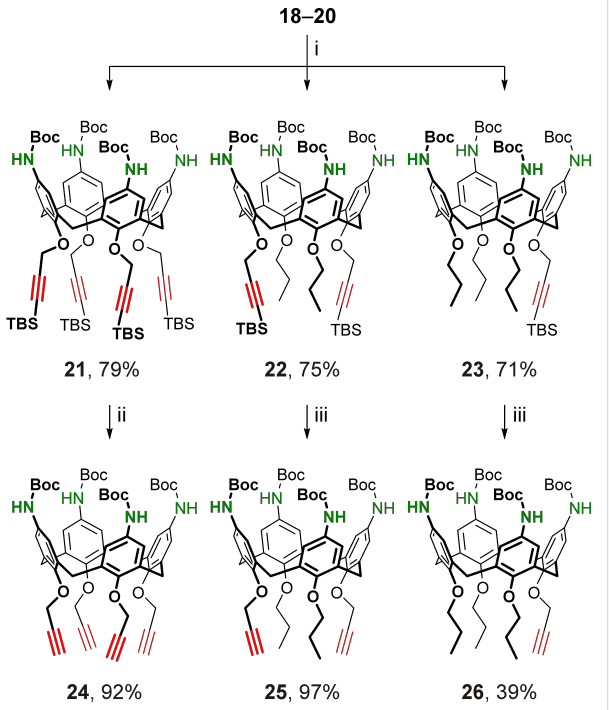

Scheme 4: Protecting group replacement in propargylated *p*-aminocalix[4]arenes. Conditions: i) Boc_2O, Et_3N, dichloromethane, rt; ii) H_2O, *n*-$Bu_4NF{\cdot}3H_2O$, THF, rt; iii) H_2O, *n*-$Bu_4NF{\cdot}3H_2O$, THF, 50 °C.

For the removal of the TBS groups, instead of using an equivalent amount of *n*-Bu_4NF, it was used as a catalyst in a water/THF mixture, which showed excellent efficiency for the room-temperature preparation of the tetrapropargyl ether **24** from its silylated precursor **21**. Surprisingly, attempts to apply these conditions to a complete removal of TBS groups in the less sterically hindered propargyl ethers **22** and **23** failed, and large amounts of the starting materials (as well as the partially desilylated product in the case of calixarene **22**) remained in the reaction mixtures even after their stirring at room temperature for 72 h. In the case of calixarene **22**, heating of the mixture at 50 °C for 48 h was enough to complete the process and *p*-amino-calix[4]arene **25** having two propargyl groups at the narrow rim was obtained in 97% yield. Still, the deprotection of calixarene **23** to the desired propargyl ether **26** was far from complete even under heating, which significantly reduced the yield of this compound (Scheme 4).

The difference in the efficiency of catalytic removal of the TBS groups observed for calixarenes **21**–**23** may be due to a reaction rate enhancement upon increasing the number of TBS-protected propargyl groups attached to the same calixarene core. Tentatively, this rate enhancement may be due to entrapment of the catalytic F^- and/or water molecule(s) inside a pocket formed by the four TBS-protected propargyl groups in calixarene **21**, which thus may be responsible for an autocatalytic process. Of course, this phenomenon needs to be studied in further detail.

2-Azidoethylated *p*-aminocalix[4]arenes

Due to the instability of azide groups in the presence of reducing agents, a synthesis strategy similar to that described above for the preparation of calixarenes **24**–**26** involving nitration of calix[4]arenes followed by selective reduction of the nitro groups could not be implemented for the preparation of *p*-aminocalix[4]arenes bearing 2-azidoethyl groups at their narrow rims. To overcome this, calixarenes **27** [95,96] and **28** [97] decorated with four or two 2-tosyloxyethyl groups which are precursors to the desired 2-azidoethyl groups, were subjected to a nitration/reduction sequence as shown in Scheme 5.

The *ipso*-nitration step proceeded smoothly in both cases under the optimized conditions, and the wide-rim pernitrated tetra- and ditosylates **29** and **30** were obtained in good yield. However, the subsequent reduction step was expectedly complicated. On the one hand, even partial reduction of the tosyl groups in calixarenes **29** and **30** might result in poisoning of a metal catalyst, thus hampering or preventing a catalytic hydrogenation of these compounds. On the other hand, in calixarenes **31** and **32**, which are immediate products of the selective reduction of the nitro groups in compounds **29** and **30** under neutral or basic conditions, the free amino groups may be alkylated by a neighboring tosylate-containing molecule, resulting in undesired polymeric/oligomeric substances. To avoid this, the reduction must be conducted in acidic medium, and no strong base must be applied during the work-up step. Thus, reduction of calixarenes **29** and **30** with tin(II) chloride, similar to the preparation of propargylated calix[4]arene tetraamines **18**–**20**, proceeds under acidic conditions, but it has limited applicability as a complete removal of a large amount of inorganic by-products could only be achieved using alkaline solutions. This causes the

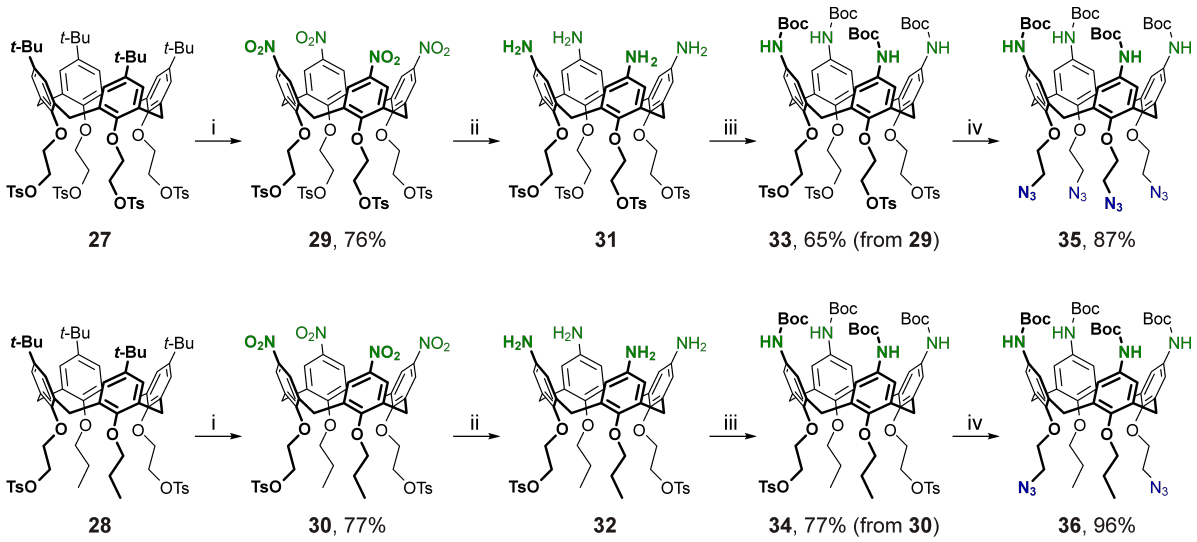

Scheme 5: Synthesis of 2-azidoethylated *p*-aminocalix[4]arenes. Conditions: i) HNO_3 (fuming, 10 equiv per calixarene aromatic unit, $c \approx 2.5$ M), AcOH, dichloromethane, rt, 48 h; ii) $FeSO_4{\cdot}7H_2O$, NH_4Cl, Zn, EtOH, THF, H_2O, 50 °C; iii) Boc_2O, Et_3N, dichloromethane, rt; iv) NaN_3, DMF, 60 °C.

unwanted self-conversions of free tetraamines **31** and **32**. Reduction of nitro compounds with activated iron generated from Zn and $FeSO_4$ in the presence of NH_4Cl [98] was found to be a good alternative to the above tin(II) chloride reduction. Under these conditions, *p*-aminocalixarenes **31** and **32** were successfully prepared from the nitrated precursors **29** and **30** using simple filtration to remove the inorganic by-product components from the reaction mixtures. Although the free amines **31** and **32** were pure enough according to their ^{1}H NMR data, these compounds were not fully characterized in order to avoid the risk of self-alkylation of the amines during their storage. Thus, the freshly prepared amines **31** and **32** were immediately treated with Boc_2O and the resultant Boc-protected calix[4]arene tetraamines **33** and **34** bearing four or two 2-tosyloxyethyl groups at the narrow rims were obtained in good yields. By replacement of the tosyloxy groups with the azide ones, the desired tetraazidoethyl and diazidoethyl products **35** and **36** were prepared, thus completing the series of bifunctionalized cone calix[4]arenes having four protected amino groups at the wide rims and a CuAAC-ready propargyl (compounds **24**–**26**) or 2-azidoethyl (compounds **35**, **36**) groups at the narrow rims of the macrocycles.

Some transformations of propargylated/2-azidoethylated *p*-aminocalix[4]arenes

To evaluate the synthetic potential of the obtained heterobifunctionalized calix[4]arenes, they were subjected to three-step chemical transformations, including the synthesis of triazoles under CuAAC conditions, followed by deprotection of the amino groups, and their conversion to urea moieties (Schemes 6–9).

The propargylated calix[4]arenes **24**–**26** were reacted with benzyl azide in the presence of CuI activated with triethylamine (20 equiv per Cu, Scheme 6). Under these conditions all three reactions were completed in 72 h at room temperature, and the desired Boc-protected *p*-aminocalix[4]arenes **37**, **38**, and **39** having four, two distal or one 1-benzyltriazol-4-ylmethyl moiety at their narrow rims were obtained. The lowered isolated yield of tetratriazole **37** was most likely due to incomplete destruction of its copper complex (although an extraction procedure for complex destruction using $Na_2S_2O_3$ was applied), which was difficult to separate from the relatively polar free calixarene **37** using column chromatography. In line with this, when toluene-soluble CuI·$P(OEt)_3$ was used as a catalyst (in this case heating was required to complete the cycload-

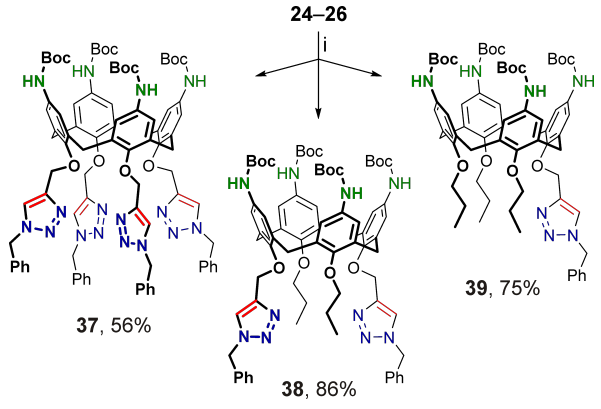

Scheme 6: Synthesis of triazolated *p*-aminocalix[4]arenes **37**–**39** from the propargylated calixarene precursors **24**–**26**. Conditions: i) benzyl azide, CuI, Et_3N, toluene, rt.

dition), an even lower isolated yield of calixarene **37** (≈35%) was observed, indicating that a large portion of Cu^+ was complexed with the calixarene product when no excess competing ligand such as triethylamine was present in the reaction mixture.

Following our previous findings on the reactivity of 2-azidoethylated calix[4]arenes with arylacetylenes under CuAAC conditions [81], calixarene **35** bearing four 2-azidoethyl groups at the narrow rim was reacted with phenylacetylene under heating using CuI·P(OEt)$_3$ as a catalyst (Scheme 7). In contrast to the synthesis of calixarene **37**, there were no problems encountered with the copper complex destruction and the yield of the isomeric calixarene **40** having four 2-(4-phenyltriazol-1-yl)ethyl moieties at the narrow rim was much higher, indicating a weaker binding in the **40**/Cu^+ system than in the **37**/Cu^+ one, due to the outer arrangement of the triazole N(3)-atoms relative to the calixarene core in compound **40**.

It was established previously, that *p*-*tert*-butylcalix[4]arene having two distal 2-azidoethyl groups at the narrow rim could not efficiently react with phenylacetylene under copper(I) catalysis unless a huge excess of Cu^+-competing triethylamine is added to the system. This is most likely due to specific interactions of the diazide with polymeric/oligomeric copper(I) phenylacetylide hindering the cycloaddition [81]. To avoid similar issues, the Boc-protected *p*-aminocalix[4]arene **36** was reacted with phenylacetylene in the presence of CuI using a mixture of toluene and triethylamine (4:1) as solvent. Under these conditions, the reaction proceeded smoothly at room temperature and the desired ditriazole **41** was obtained in high yield (Scheme 7).

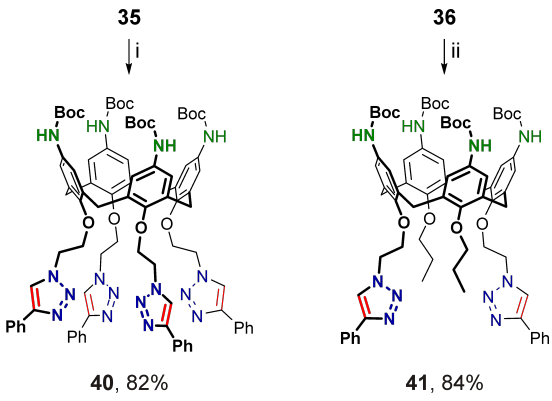

Scheme 7: Synthesis of triazolated *p*-aminocalix[4]arenes **40** and **41** from the 2-azidoethylated calixarene precursors **35** and **36**. Conditions: i) phenylacetylene, CuI·P(OEt)$_3$, toluene, 100 °C; ii) phenylacetylene, CuI, toluene/Et_3N, rt.

The *tert*-butoxycarbonyl groups in calix[4]arenes **37**–**41** were cleaved under standard conditions using trifluoroacetic acid, and after basification, free *p*-aminocalix[4]arenes **42**–**46** substituted at the narrow rims with either 1-benzyltriazol-4-ylmethyl or 2-(4-phenyltriazol-1-yl)ethyl groups were obtained (Scheme 8). Then, amines **42**–**46** were reacted with excess *p*-tolyl isocyanate to afford the corresponding tetraurea-calix[4]arenes **47**–**51** (Scheme 9), the structures of which were unambiguously confirmed by their ^{1}H NMR and ^{13}C NMR spectra obtained from solutions in polar DMSO-d_6.

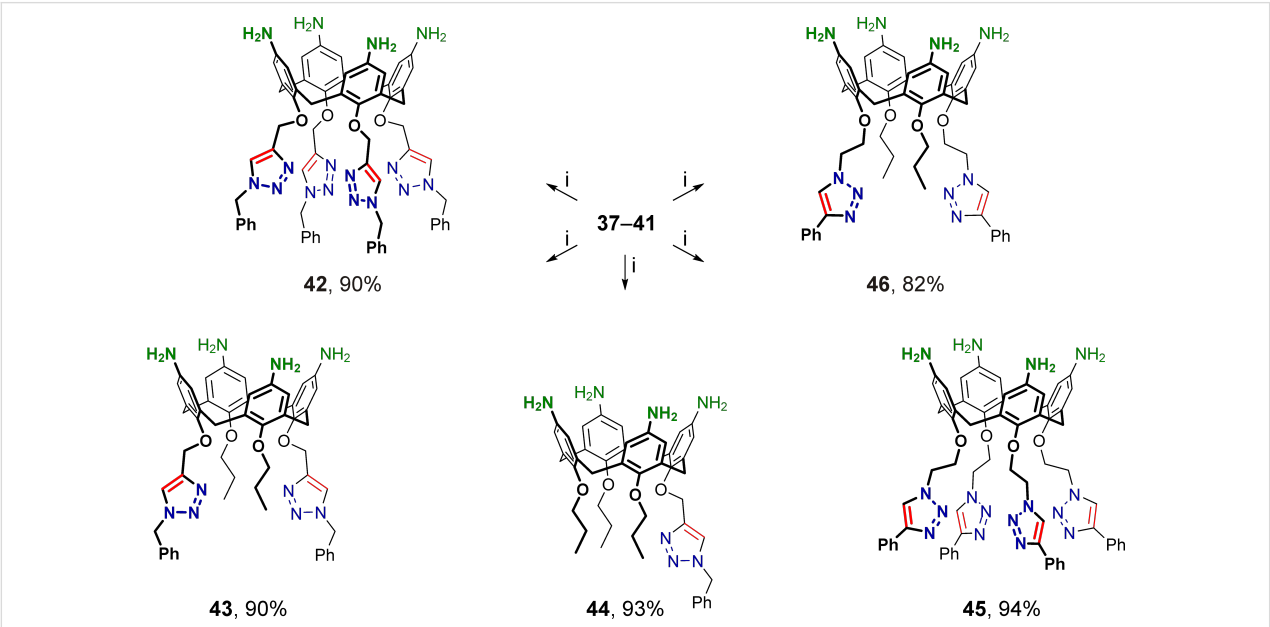

Scheme 8: Removal of Boc protection in calixarenes **37**–**41**; (i) CF_3CO_2H, dichloromethane, rt, then $NaHCO_3/H_2O$.

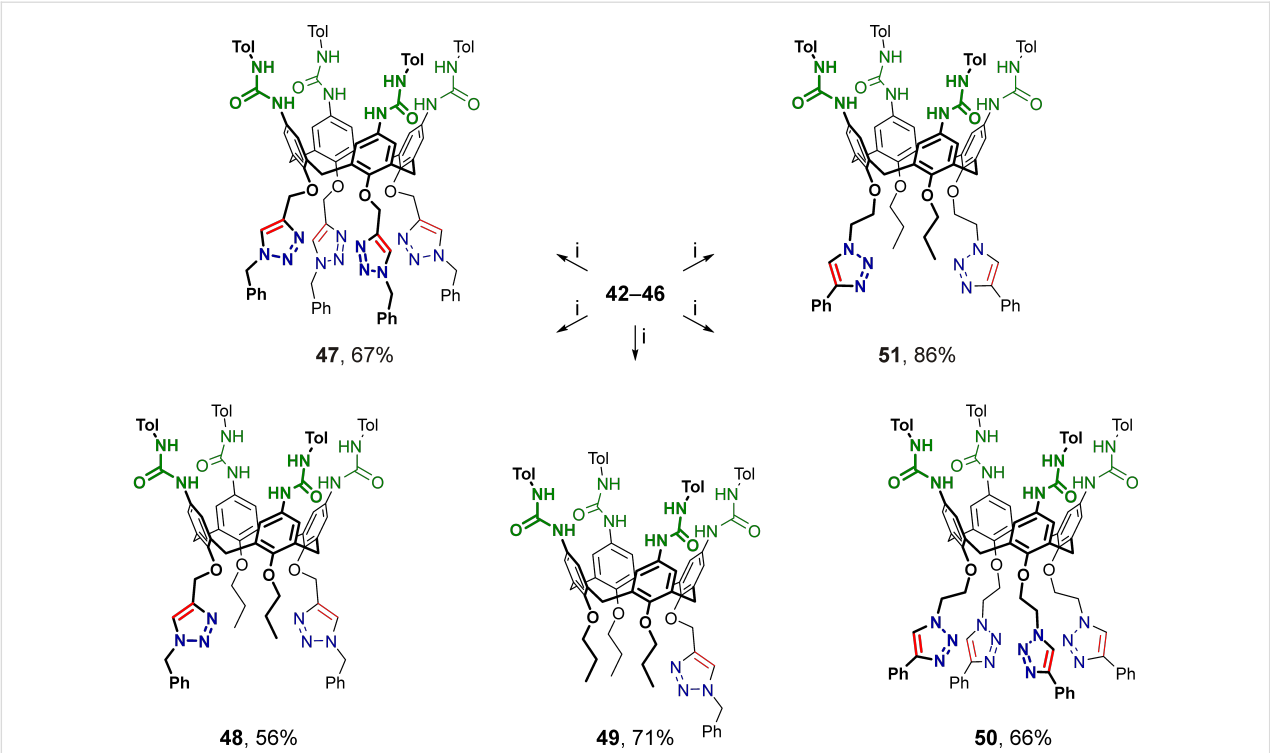

Scheme 9: Synthesis of triazolated tetraureacalix[4]arenes **47**–**51**. Conditions: (i) *p*-tolyl isocyanate, toluene, 60 °C.

Being calix[4]arene tetraureas, compounds **47**–**51** should form homodimeric capsules in H-bond non-competing solvents (e.g., chloroform) with the inclusion of one of the solvent molecules into the capsules. However, triazole heterocycles attached to the calixarene core can serve as weak hydrogen-bond acceptors [99] and thus may interfere with capsule formation, including the exclusive formation of heterodimeric capsules from the calixarene tetraaryl- and tetraarylsulfonylureas if co-dissolved in a 1:1 molar ratio [51-53]. Furthermore, tetraureas **47**–**51** contain relatively bulky substituents at the phenolic oxygen atoms, which may influence the conformational behavior of the macrocycle (e.g., pinched cone-to-pinched cone conformational interconversions), thereby favoring or disfavoring the C_{4v}-symmetric 'ideal' cone conformation of the calixarene core required for capsule formation [59]. To check this, ^{1}H NMR spectra from the $CDCl_3$ solutions of multifunctionalized calixarenes **47**–**51** and their 1:1 mixtures with the known *O*-pentylated tetratosylureacalix[4]arene **52** [51] were acquired and analyzed.

In terms of time-averaged molecular symmetry, tetraureacalix[4]arenes of three types were prepared in this work: C_s-symmetric calixarene **49** with one triazole heterocycle at the narrow rim, C_{2v}-symmetric calixarenes **48** and **51** with pairs of distal triazole groups, and C_{4v}-symmetric tetraureas **47** and **50**. Due to the phenomenon of supramolecular chirality caused by the direction of hydrogen bonds in the capsules [100], tetraureacalixarenes of the first type should form two regioisomeric homodimers possessing C_1-symmetry or a single heterodimer with a C_{4v}-symmetric tetratosylureacalix[4]arene **52** (each as a pair of enantiomers). Similarly, the C_{2v}-symmetric tetraureacalixarenes of the second type should furnish C_2-symmetric homo- or heterodimers as single regioisomers (each as a pair of enantiomers), whereas homo- and heterodimers formed by C_{4v}-symmetric tetraureas of the third type are expected to have S_8 (achiral meso) and C_4 (as two enantiomers) symmetry, respectively. These features must immediately affect the signal patterns in the ^{1}H NMR spectra of triazolated tetraureacalix[4]arenes and may also complicate their interpretation. Indeed, the ^{1}H NMR spectrum of the triazolated tetraurea **49** obtained from its solution in $CDCl_3$ turned out to be overcomplicated (see Figure 4). The spectral pattern apparently arises from the superposition of signals from two asymmetric homodimers, $\mathbf{49}_2$ isomer 1 and $\mathbf{49}_2$ isomer 2 (Figure 4a), which are present in a ratio of ≈1:1. The ratio of the isomers cannot be easily obtained from the spectrum except by analyzing the group of the most downfield-shifted signals corresponding to the half of the urea NHs involved in hydrogen bonds. According to the symmetry features discussed above, this group of signals should consist of eight singlets from each of the isomeric homodimers, thus giving sixteen partially overlapping signals (see insert in Figure 4d). Integration of the resolved

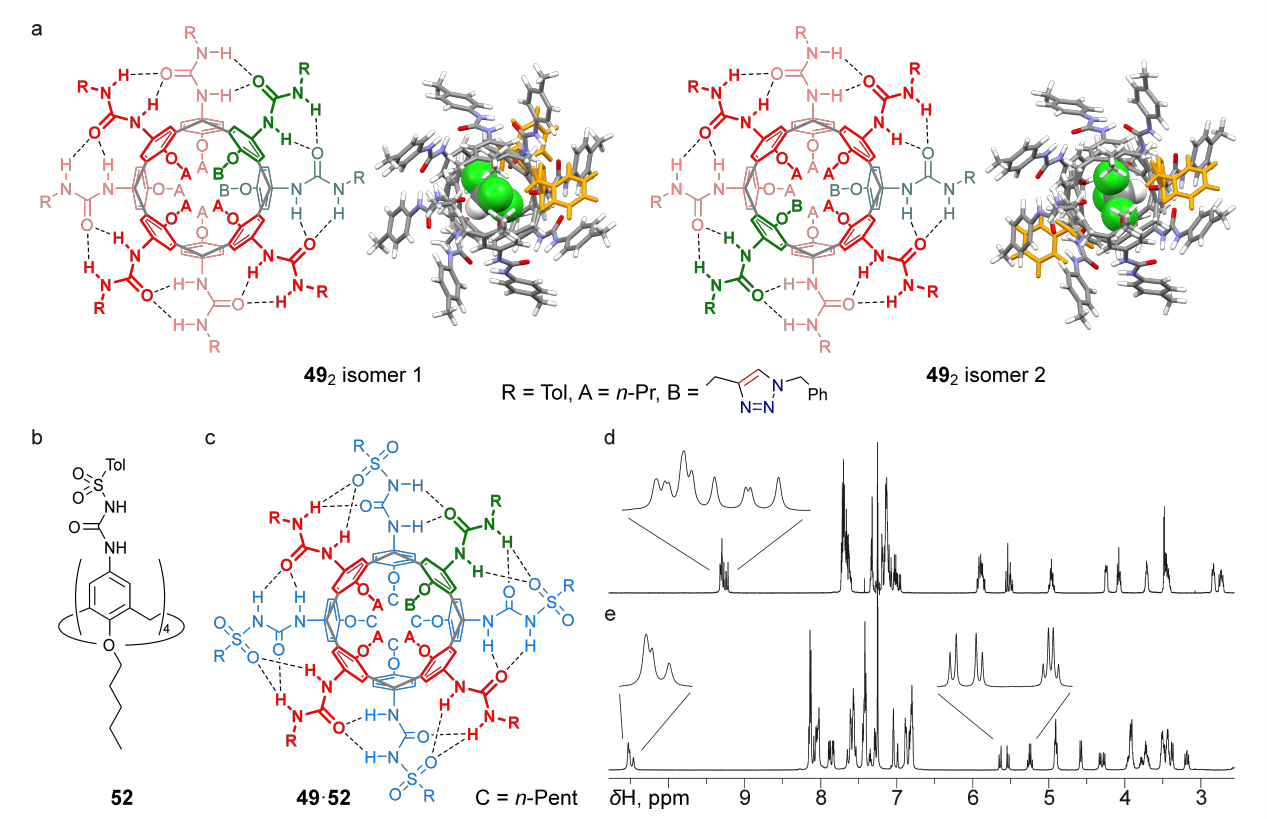

Figure 4: Planar and energy-minimized structures (with $CHCl_3$ molecule included and triazole groups highlighted) of isomeric homodimers of tetraurea **49** (a); structure of tetratosylureacalix[4]arene **52** (b); planar structure of heterodimer **49**·**52** (c); fragment of the ^{1}H NMR spectrum of calixarene **49** in $CDCl_3$ (d); fragment of the ^{1}H NMR spectrum of an equimolar mixture of calixarenes **49** and **52** in $CDCl_3$ (e). All spectra were acquired using a 600 MHz NMR spectrometer.

signals of this group showed that their relative intensities are almost exactly multiples of 1, which is most likely in the case where the entire group is formed by sixteen signals of the same intensity.

In support of this, the energy-minimized structures of two regioisomeric capsules, **49**$_2$ isomer 1 and **49**$_2$ isomer 2, each containing a chloroform molecule (Figure 4a, PBE0/def2-SVP, gCP, D4, SMD (chloroform), ORCA 6.0.1 package [101-109]), were obtained and the calculated difference in their full-electron energies was found to be less than 0.1 kcal mol^{-1}, which is well below the error threshold. Thus, in contrast to tetraureas containing several different substituents in the urea groups [100], the presence of one bulky moiety at the narrow rim of the tetraureacalix[4]arene does not lead to a significant difference in the stability of the homodimers formed by compound **49**, at least in a chloroform solution. To further confirm the ability of calixarene **49** to form capsules, the ^{1}H NMR spectrum of its equimolar mixture with tetratosylureacalix[4]arene **52** in $CDCl_3$ was also analyzed (Figure 4e). Despite the presence of a second calixarene molecule, the ^{1}H NMR spectrum turned out to be simplified compared to the spectrum of homodimers **49**$_2$, which is due to the formation of only one heterodimer **49**·**52**. The spectrum clearly shows even more downfield-shifted resonances from the four NH groups involved in hydrogen bonding with the sulfonyl groups, as well as clear signals from the two AB spin systems of the methylene groups attached to the single triazole moiety, in which the protons have become diastereotopic due to the supramolecular chirality of the heterodimeric capsule (see inserts in Figure 4e).

Due to the higher symmetry of both homo- and heterodimeric capsules formed by ditriazolated tetraureas **48** and **51** (Figure 5), the ^{1}H NMR spectra acquired from solutions of these compounds or their mixtures with tetrasulfonylurea **52** in $CDCl_3$ turned out to be much more interpretable. In particular, the spectra of the homodimers (Figure 5b,c) contained four clearly recognizable downfield-shifted singlets from hydrogen-bonded NH groups, and all other signals appearing in the spectra corresponded to chiral C_2-symmetric homodimeric capsules in both cases. The ^{1}H NMR spectrum of the equimolar mixture **48**/**52** (taken as an example) contained one set of signals from the C_2-symmetric heterodimer **48**·$CDCl_3$·**52**, but not from the homodimers **48**·$CDCl_3$·**48** and **52**·$CDCl_3$·**52**, and thus reflected

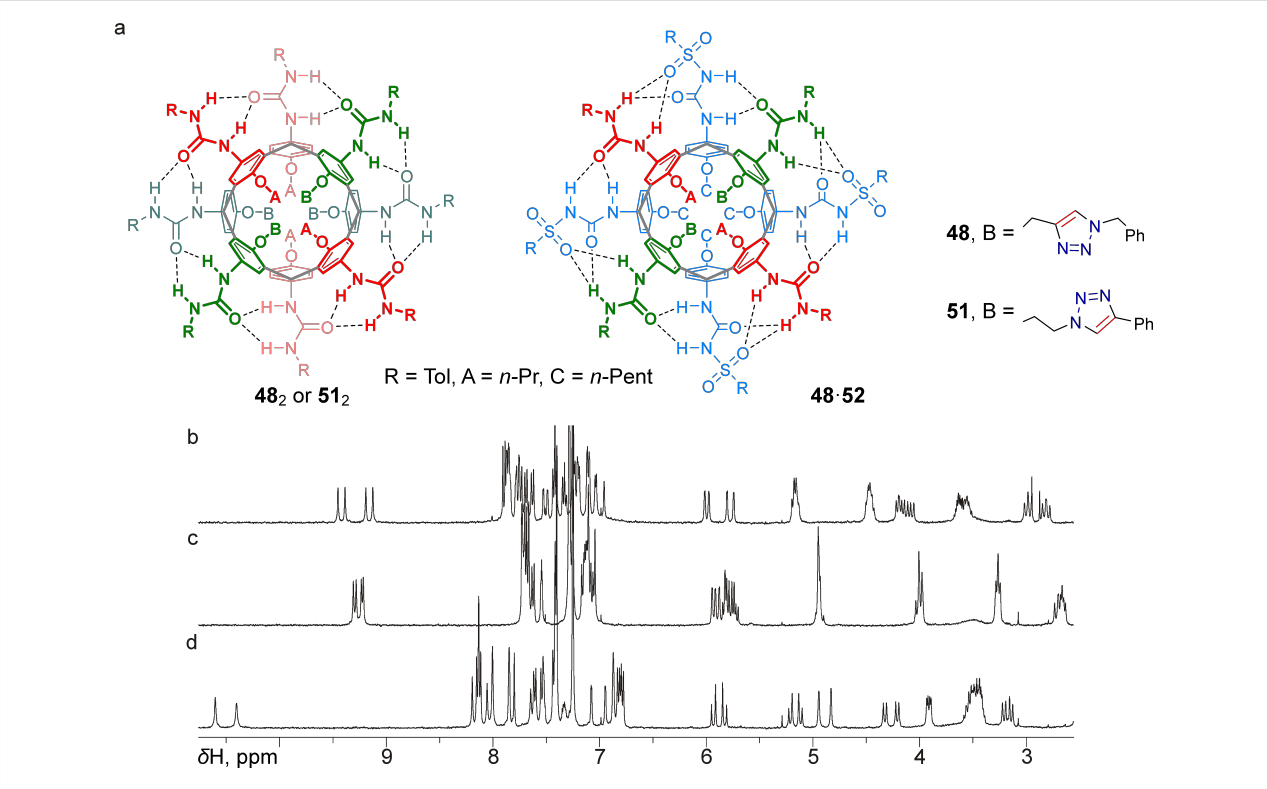

Figure 5: Planar structures of homodimers **48**$_2$, **51**$_2$, and heterodimer **48·52** (a); fragment of the ^{1}H NMR spectrum of calixarene **51** in $CDCl_3$ (b); fragment of the ^{1}H NMR spectrum of calixarene **48** in $CDCl_3$ (c); fragment of the ^{1}H NMR spectrum of an equimolar mixture of calixarenes **48** and **52** in $CDCl_3$ (d). All spectra were acquired using a 400 MHz NMR spectrometer.

the expected exclusive formation of heterocapsular assemblies, which was thus not hindered by the two triazole heterocycles arranged at the narrow rim of the calixarene core.

Except for a slight broadening of the signals caused by the limited solubility of the compound, the ^{1}H NMR spectrum obtained for a $CDCl_3$ solution of tetraureacalixarene **50** having four 2-(4-phenyltriazol-1-yl)ethyl groups at the narrow rim was in good agreement with the expected spectrum of homodimer **50**$_2$ possessing S_8 symmetry (Figure 6a). Indeed, the spectrum contained two ^4J-coupled doublets from the diastereotopic aromatic protons of the calixarene core and just one pair of ^2J-coupled doublets from its methylene bridges, two well-distant singlets from the urea NHs participating in the hydrogen-bond belt, one resonance from the triazole protons, as well as only one set of signals from the tolyl and phenyl groups, which confirms the formation of homodimer **50**$_2$ (Figure 6b).

Quite surprisingly, such a clear pattern was not observed in the ^{1}H NMR spectrum of a $CDCl_3$ solution of tetraurea **47**, which is an isomer of calixarene **50**, having 1-benzyltriazol-4-ylmethyl groups replacing 2-(4-phenyltriazol-1-yl)ethyl groups, and thus possessing less flexible linkers between the calixarene core and the differently arranged triazole heterocycles. In addition to what could be interpreted as a set of signals from homodimer **47**$_2$, a set of broadened resonances was observed in the spectrum (Figure 6c). Neither prolonged heating of the sample at 50 °C before the spectrum acquisition, nor measuring the spectrum at elevated temperature resulted in a simplification of the spectral pattern, indicating no significant contribution of any slow rotational/conformational motions to the complexity of the spectrum. Similar additional signals were observed in the ^{1}H NMR spectrum of an equimolar mixture of calixarenes **47** and **52** in $CDCl_3$ (Figure 6e). Reasonably, additional non-covalent interactions possibly occurred between two or more calixarene molecules, partially destroying the dimeric capsules and promoting the formation of more complex assemblies, which was characteristic exclusively of calixarene **47** (of the five calixarene tetraureas studied). Since nothing other than hydrogen bonds involving triazole heterocycles could be proposed for such non-covalent interactions, a drop of methanol-d_4 was added to a solution of tetraurea **47** in $CDCl_3$ to break these additional bonds. However, the effect of adding this polar solvent turned out to be too strong, and the resulting spectrum only contained signals from the tetraurea monomer **47**, indicating the disruption of intermolecular hydrogen bonds between the urea moieties as well.

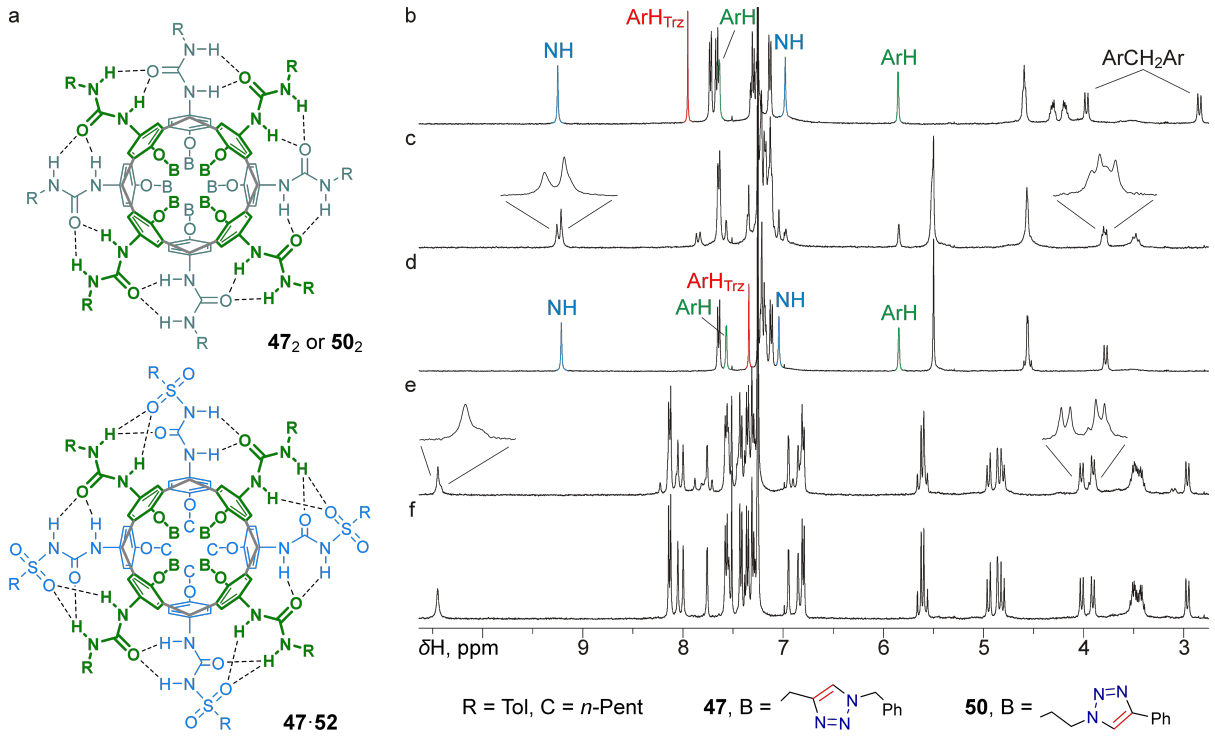

Figure 6: Planar structures of homodimers 47_2, 50_2, and heterodimer **47·52** (a); fragment of the ^{1}H NMR spectrum of calixarene **50** in $CDCl_3$ (b); fragment of the ^{1}H NMR spectrum of calixarene **47** in $CDCl_3$ (c); fragment of the ^{1}H NMR spectrum of the same sample washed with water (d); fragment of the ^{1}H NMR spectrum of an equimolar mixture of calixarenes **47** and **52** in $CDCl_3$ (e); fragment of the ^{1}H NMR spectrum of the same sample washed with water (f). All spectra were acquired using a 400 MHz NMR spectrometer.

Still, it was discovered by chance that simply washing of a solution of calixarene **47** in $CDCl_3$ with water solved the issue. Indeed, the ^{1}H NMR spectrum of the sample obtained after separation of the aqueous phase turned out to be easily interpretable (Figure 6d) and contained a set of signals from homodimer 47_2 similar to those in the spectrum of homodimer 50_2. A drastic simplification of the spectrum was also observed for a water-washed solution of a mixture of calixarenes **47** and **52** in $CDCl_3$, and only clear resonances from the heterodimer **47·52** were detected there (Figure 6f). In a separate series of experiments, the ^{1}H NMR spectra of unstable emulsions obtained by shaking solutions of calixarenes **47**–**51** in $CDCl_3$ with water were rapidly collected. Although lowered-resolution NMR spectra were obtained, in all cases only resonances of the respective homodimers were detected, despite the presence in the spectra of a large signal from the aqueous phase (at ≈4.8 ppm) along with a signal from dissolved water (1.56 ppm). Considering the low solubility of water in chloroform, the stability of the capsules in water-saturated $CDCl_3$ seems reasonable, because the dimers are held together by at least 16 hydrogen bonds between the urea groups. On the other hand, this water content is apparently sufficient to disrupt weaker intermolecular contacts involving triazole heterocycles as hydrogen-bond acceptors. Since the structures of the above mentioned non-capsular aggregate(s) formed by calixarene **47** cannot be drawn based on the available data, it is unclear why only four 1-benzyltriazol-4-ylmethyl groups attached to the narrow rim of the tetraurea calixarene are responsible for the unwanted aggregation, whereas one or two 1-benzyltriazol-4-ylmethyl groups (calixarenes **48**, **49**) or two or four 2-(4-phenyltriazol-1-yl)ethyl groups (calixarenes **50**, **51**) do not interfere with the capsule formation.

Due to the mentioned limited solubility of calixarene **50** in $CDCl_3$, it was not possible to conduct an accurate experiment to study any preferential heterodimerization between isomeric tetraureas **47** and **50**, which possess a set of narrow rim substituents of different flexibility. However, preliminary NMR data showed that a turbid $CDCl_3$ solution of both calixarenes, taken in a more or less equimolar ratio, contained signals from both homodimers 47_2 and 50_2, a set of broadened signals from non-capsular aggregates (readily removed from the spectrum by washing the solution with water) and a set of signals that could be interpreted as those from heterodimer **47·50**. Thus, the difference in the spatial preorganization of the four urea groups in calixarenes **47** and **50**, caused by the different constraints

related to their narrow-rim substituents, is apparently not sufficient to provide any significant selectivity for the formation of homo/heterocapsules.

Finally, since the triazole groups arranged at the narrow rim of the calix[4]arene macrocycle are capable of complexation with transition-metal cations, showing different complexation preferences depending on the triazole attachment mode [81], the attractive idea of combining complexation and capsule formation using triazolated tetraureas was explored. For preliminary NMR complexation experiments, zinc and silver cations were chosen to target 1-benzyltriazol-4-ylmethyl- and 2-(4-phenyltriazol-1-yl)ethyl-decorated calix[4]arenes, respectively, but unfortunately this study was unsuccessful due to solubility issues. Indeed, CD_3CN or its mixtures with $CDCl_3$, in which $Zn(ClO_4)_2{\cdot}6H_2O$ is soluble, turned out to be solvents which were too polar and destroyed dimers $\mathbf{47}_2$ or $\mathbf{48}_2$, although some changes in the ^{1}H NMR spectra of monomers **47** and **48** could be detected upon addition of the salt. Attempts to conduct the experiment using solid–liquid extraction in neat $CDCl_3$ were also unsuccessful, since no changes in the ^{1}H NMR spectrum of capsule $\mathbf{47}_2$ were detected upon the addition of excess solid $Zn(ClO_4)_2{\cdot}6H_2O$, even after prolonged storing of the mixture at room temperature or under moderate (55 °C) heating. Although anhydrous $AgPF_6$, which is soluble in non-polar solvents, was used for trial binding experiments with 2-(4-phenyltriazol-1-yl)ethyl-containing capsules $\mathbf{50}_2$ and $\mathbf{51}_2$, no data on the complexation processes were obtained in these cases either; adding excess salt to solutions of these calixarenes in $CDCl_3$ or in $CDCl_3$/benzene-d_6 mixtures resulted in the formation of insoluble precipitates containing the entire portions of the hosts, thus indicating a complexation process but the concentrations of dissolved compounds was too low for NMR analysis. Thus, additional experiments need to be designed to reveal whether the triazolated tetraureacalix[4]arenes can be used to include pairs of triazole-bound cations into supramolecules via intermolecular hydrogen bonding between the urea groups.

Conclusion

We have expanded the functionalization capabilities of cone calix[4]arenes by combining orthogonally transformable functional groups of two types within a single macrocyclic core. Both wide and narrow rims of the calixarene macrocycles were used to introduce four amino groups along with propargyl or 2-azidoethyl groups into the molecules. This allowed for further step-wise functionalization of the core using CuAAC 'click' reactions involving alkyne or azide moieties and amine acylation or similar reactions. Five heteromultifunctional *N*-protected *p*-aminocalix[4]arenes comprising one/two/four propargyl groups or two/four 2-azidoethyl groups at the narrow rims of the macrocycles were prepared using synthetic strategies that involved wide rim *ipso*-nitration of prefunctionalized macrocycles (containing either silyl-protected propargyl groups or the synthetic precursors of 2-azidoethyl groups) followed by reduction of the exhaustively nitrated products. During thorough fine-tuning of the nitration conditions, several partially nitrated calix[4]arene propargyl ethers bearing *tert*-butyldimethylsilyl protecting groups in the alkyne moieties were also obtained and their exact structures were determined using 2D NMR and X-ray diffraction data, contributing to a general understanding of the selectivity of nitration when applied to calixarenes containing bulky narrow-rim substituents.

The functionalization capabilities of the propargylated/2-azidoethylated *p*-aminocalix[4]arenes were demonstrated by their facile conversion into the narrow-rim triazolated macrocycles of two types (differing in the mutual arrangement of the calixarene core and the triazole heterocycles) and then into the wide-rim tetraurea derivatives. A preliminary study of the aggregation of triazolated calix[4]arene tetraureas showed that the triazole groups, despite their relatively large size and hydrogen-bond accepting ability, have only a minor effect on the formation of homo/heterodimeric capsules by these compounds in chloroform. Thus, a variety of functional units can be introduced into the narrow rims of the developed propargylated/2-azidoethylated calixarenes using CuAAC reactions, and the resulting triazolated calixarenes can be further functionalized at their amino groups, including the preparation of self-assembled capsular aggregates of virtually unlimited complexity.

Supporting Information

Supporting Information File 1

Synthesis details, copies of ^{1}H and ^{13}C NMR spectra of novel compounds, details of X-ray diffraction measurements and crystal structure data.
[https://www.beilstein-journals.org/bjoc/content/supplementary/1860-5397-22-28-S1.pdf]

Supporting Information File 2

Crystallographic information file for compound **16**.
[https://www.beilstein-journals.org/bjoc/content/supplementary/1860-5397-22-28-S2.cif]

Supporting Information File 3

Crystallographic information file for compound **15**.
[https://www.beilstein-journals.org/bjoc/content/supplementary/1860-5397-22-28-S3.cif]

Acknowledgements

X-ray diffraction studies were performed at the Centre of Shared Equipment of IGIC RAS. 2D NMR studies were performed at the Center of Shared Equipment of GNIIChTEOS.

Funding

The study was conducted under the state assignment of Lomonosov Moscow State University, project no. 121031300092-6

ORCID® iDs

Ilia Korniltsev - https://orcid.org/0000-0003-4774-1466
Alexander Gorbunov - https://orcid.org/0000-0003-0146-765X
Dmitry Cheshkov - https://orcid.org/0000-0002-9024-4353
Stanislav Bezzubov - https://orcid.org/0000-0002-2017-517X
Vladimir Kovalev - https://orcid.org/0000-0003-4473-1107
Ivan Vatsouro - https://orcid.org/0000-0001-8629-1897

Data Availability Statement

All data that supports the findings of this study is available in the published article and/or the supporting information of this article.

References

1. Asfari, Z.; Böhmer, V.; Harrowfield, J.; Vicens, J., Eds. *Calixarenes 2001;* Kluwer Academic Publishers: Dordrecht, Netherlands, 2001. doi:10.1007/0-306-47522-7
2. Böhmer, V. Calixarenes. In *The Chemistry of Phenols;* Rappoport, Z., Ed.; PATAI'S Chemistry of Functional Groups; John Wiley & Sons: Chichester, UK, 2003; pp 1369–1454. doi:10.1002/0470857277.ch19
3. Vicens, J.; Harrowfield, J.; Baklouti, L., Eds. *Calixarenes in the Nanoworld;* Springer: Dordrecht, Netherlands, 2007. doi:10.1007/978-1-4020-5022-4
4. Neri, P.; Sessler, J. L.; Wang, M.-X., Eds. *Calixarenes and Beyond;* Springer International Publishing: Cham, Switzerland, 2016. doi:10.1007/978-3-319-31867-7
5. Arduini, A.; Mirone, L.; Paganuzzi, D.; Pinalli, A.; Pochini, A.; Secchi, A.; Ungaro, R. *Tetrahedron* **1996,** *52,* 6011–6018. doi:10.1016/0040-4020(96)00238-4
6. Jakobi, R. A.; Böhmer, V.; Grüttner, C.; Kraft, D.; Vogt, W. *New J. Chem.* **1996,** *20,* 493–501.
7. Mulder, A.; Auletta, T.; Sartori, A.; Del Ciotto, S.; Casnati, A.; Ungaro, R.; Huskens, J.; Reinhoudt, D. N. *J. Am. Chem. Soc.* **2004,** *126,* 6627–6636. doi:10.1021/ja0317168
8. Gattuso, G.; Grasso, G.; Marino, N.; Notti, A.; Pappalardo, A.; Pappalardo, S.; Parisi, M. F. *Eur. J. Org. Chem.* **2011,** 5696–5703. doi:10.1002/ejoc.201100812
9. Buttress, J. P.; Day, D. P.; Courtney, J. M.; Lawrence, E. J.; Hughes, D. L.; Blagg, R. J.; Crossley, A.; Matthews, S. E.; Redshaw, C.; Bulman Page, P. C.; Wildgoose, G. G. *Langmuir* **2016,** *32,* 7806–7813. doi:10.1021/acs.langmuir.6b02222
10. Hosseinzadeh, R.; Maliji, F.; Golchoubian, H.; Bekhradnia, A. *ChemistrySelect* **2019,** *4,* 3914–3920. doi:10.1002/slct.201900241
11. Mattiuzzi, A.; Troian-Gautier, L.; Mertens, J.; Reniers, F.; Bergamini, J.-F.; Lenne, Q.; Lagrost, C.; Jabin, I. *RSC Adv.* **2020,** *10,* 13553–13561. doi:10.1039/d0ra01011a
12. Gaeta, M.; Rodolico, E.; Fragalà, M. E.; Pappalardo, A.; Pisagatti, I.; Gattuso, G.; Notti, A.; Parisi, M. F.; Purrello, R.; D'Urso, A. *Molecules* **2021,** *26,* 704. doi:10.3390/molecules26030704
13. Weeden, C.; Hartlieb, K. J.; Lim, L. Y. *J. Pharm. Pharmacol.* **2012,** *64,* 1403–1411. doi:10.1111/j.2042-7158.2012.01518.x
14. Morita, Y.; Agawa, T.; Kai, Y.; Kanehisa, N.; Kasai, N.; Nomura, E.; Taniguchi, H. *Chem. Lett.* **1989,** *18,* 1349–1352. doi:10.1246/cl.1989.1349
15. Morita, Y.; Agawa, T.; Nomura, E.; Taniguchi, H. *J. Org. Chem.* **1992,** *57,* 3658–3662. doi:10.1021/jo00039a027
16. Ak, M. S.; Deligöz, H. *J. Inclusion Phenom. Macrocyclic Chem.* **2007,** *59,* 115–123. doi:10.1007/s10847-007-9300-9
17. Burilov, V.; Makarov, E.; Mironova, D.; Sultanova, E.; Bilyukova, I.; Akyol, K.; Evtugyn, V.; Islamov, D.; Usachev, K.; Mukhametzyanov, T.; Solovieva, S.; Antipin, I. *Int. J. Mol. Sci.* **2022,** *23,* 14889. doi:10.3390/ijms232314889
18. Kolusheva, S.; Zadmard, R.; Schrader, T.; Jelinek, R. *J. Am. Chem. Soc.* **2006,** *128,* 13592–13598. doi:10.1021/ja064957z
19. Zadmard, R.; Schrader, T. *Angew. Chem., Int. Ed.* **2006,** *45,* 2703–2706. doi:10.1002/anie.200502946
20. Breitkreuz, C. J.; Zadmard, R.; Schrader, T. *Supramol. Chem.* **2008,** *20,* 109–115. doi:10.1080/10610270701747040
21. Shahgaldian, P.; Sciotti, M. A.; Pieles, U. *Langmuir* **2008,** *24,* 8522–8526. doi:10.1021/la801083h
22. Blecking, C. J.; Hu, W.; Zadmard, R.; Dasgupta, A.; Schrader, T. *Synthesis* **2011,** 1193–1204. doi:10.1055/s-0030-1259980
23. Hu, W.; Blecking, C.; Kralj, M.; Šuman, L.; Piantanida, I.; Schrader, T. *Chem. – Eur. J.* **2012,** *18,* 3589–3597. doi:10.1002/chem.201100634
24. Lalor, R.; DiGesso, J. L.; Mueller, A.; Matthews, S. E. *Chem. Commun.* **2007,** 4907–4909. doi:10.1039/b712100h
25. Lalor, R.; Baillie-Johnson, H.; Redshaw, C.; Matthews, S. E.; Mueller, A. *J. Am. Chem. Soc.* **2008,** *130,* 2892–2893. doi:10.1021/ja0782596
26. Nault, L.; Cumbo, A.; Pretôt, R. F.; Sciotti, M. A.; Shahgaldian, P. *Chem. Commun.* **2010,** *46,* 5581–5583. doi:10.1039/b926025k
27. Dudic, M.; Colombo, A.; Sansone, F.; Casnati, A.; Donofrio, G.; Ungaro, R. *Tetrahedron* **2004,** *60,* 11613–11618. doi:10.1016/j.tet.2004.09.047
28. Sansone, F.; Dudič, M.; Donofrio, G.; Rivetti, C.; Baldini, L.; Casnati, A.; Cellai, S.; Ungaro, R. *J. Am. Chem. Soc.* **2006,** *128,* 14528–14536. doi:10.1021/ja0634425
29. Huang, Q.; Zhao, H.; Shui, M.; Guo, D.-S.; Wang, R. *Chem. Sci.* **2020,** *11,* 9623–9629. doi:10.1039/d0sc03922e
30. Hu, X.-Y.; Hu, Z.-Y.; Tian, J.-H.; Shi, L.; Ding, F.; Li, H.-B.; Guo, D.-S. *Chem. Commun.* **2022,** *58,* 13198–13201. doi:10.1039/d2cc04963e
31. Gasparello, J.; Papi, C.; Zurlo, M.; Volpi, S.; Gambari, R.; Corradini, R.; Casnati, A.; Sansone, F.; Finotti, A. *Pharmaceutics* **2023,** *15,* 2121. doi:10.3390/pharmaceutics15082121
32. Baldini, L.; Cacciapaglia, R.; Casnati, A.; Mandolini, L.; Salvio, R.; Sansone, F.; Ungaro, R. *J. Org. Chem.* **2012,** *77,* 3381–3389. doi:10.1021/jo300193y
33. Salvio, R.; Casnati, A.; Mandolini, L.; Sansone, F.; Ungaro, R. *Org. Biomol. Chem.* **2012,** *10,* 8941–8943. doi:10.1039/c2ob26688a
34. Lisi, D.; Vezzoni, C. A.; Casnati, A.; Sansone, F.; Salvio, R. *Chem. – Eur. J.* **2023,** *29,* e202203213. doi:10.1002/chem.202203213
35. Vezzoni, C. A.; Casnati, A.; Orlanducci, S.; Sansone, F.; Salvio, R. *ChemCatChem* **2024,** *16,* e202301477. doi:10.1002/cctc.202301477

36. Arnaud-Neu, F.; Böhmer, V.; Dozol, J.-F.; Grüttner, C.; Jakobi, R. A.; Kraft, D.; Mauprivez, O.; Rouquette, H.; Schwing-Weill, M.-J.; Simon, N.; Vogt, W. *J. Chem. Soc., Perkin Trans. 2* **1996,** 1175–1182. doi:10.1039/p29960001175
37. Delmau, L. H.; Simon, N.; Dozol, J.-F.; Eymard, S.; Tournois, B.; Schwing-Weill, M.-J.; Arnaud-Neu, F.; Böhmer, V.; Grüttner, C.; Musigmann, C.; Tunayar, A. *Chem. Commun.* **1998,** 1627–1628. doi:10.1039/a802555j
38. Matthews, S. E.; Saadioui, M.; Böhmer, V.; Barboso, S.; Arnaud-Neu, F.; Schwing-Weill, M.-J.; Garcia Carrera, A.; Dozol, J.-F. *J. Prakt. Chem.* **1999,** *341,* 264–273. doi:10.1002/(sici)1521-3897(199904)341:3<264::aid-prac264>3.0.co;2-f
39. Arduini, A.; Böhmer, V.; Delmau, L.; Desreux, J.-F.; Dozol, J.-F.; Carrera, M. A. G.; Lambert, B.; Musigmann, C.; Pochini, A.; Shivanyuk, A.; Ugozzoli, F. *Chem. – Eur. J.* **2000,** *6,* 2135–2144. doi:10.1002/1521-3765(20000616)6:12<2135::aid-chem2135>3.0.co;2-a
40. Matthews, S. E.; Parzuchowski, P.; Garcia-Carrera, A.; Grüttner, C.; Dozol, J.-F.; Böhmer, V. *Chem. Commun.* **2001,** 417–418. doi:10.1039/b009679m
41. Schmidt, C.; Saadioui, M.; Böhmer, V.; Host, V.; Spirlet, M.-R.; Desreux, J. F.; Brisach, F.; Arnaud-Neu, F.; Dozol, J.-F. *Org. Biomol. Chem.* **2003,** *1,* 4089–4096. doi:10.1039/b307929e
42. Böhmer, V.; Dozol, J.-F.; Grüttner, C.; Liger, K.; Matthews, S. E.; Rudershausen, S.; Saadioui, M.; Wang, P. *Org. Biomol. Chem.* **2004,** *2,* 2327–2334. doi:10.1039/b405602g
43. Peters, C.; Braekers, D.; Kroupa, J.; Kasyan, O.; Miroshnichenko, S.; Rudzevich, V.; Böhmer, V.; Desreux, J.-F. *Radiochim. Acta* **2008,** *96,* 203–210. doi:10.1524/ract.2008.1480
44. May, E. M.; Solovyov, A.; Guo, Y.; Drapailo, A.; Matveev, Y.; Kalchenko, V.; Nitsche, H.; Katz, A. *Eur. J. Inorg. Chem.* **2016,** 4542–4545. doi:10.1002/ejic.201600946
45. Putkov, A. E.; Vasiliev, A. N.; Zubavichus, Y. V.; Teterin, Y. A.; Ivanov, K. E.; Trigub, A. L.; Kovalev, V. V.; Vatsouro, I. M. *Mendeleev Commun.* **2021,** *31,* 188–190. doi:10.1016/j.mencom.2021.03.014
46. Shimizu, K. D.; Rebek, J., Jr. *Proc. Natl. Acad. Sci. U. S. A.* **1995,** *92,* 12403–12407. doi:10.1073/pnas.92.26.12403
47. Mogck, O.; Böhmer, V.; Vogt, W. *Tetrahedron* **1996,** *52,* 8489–8496. doi:10.1016/0040-4020(96)00404-8
48. Hamann, B. C.; Shimizu, K. D.; Rebek, J., Jr. *Angew. Chem., Int. Ed. Engl.* **1996,** *35,* 1326–1329. doi:10.1002/anie.199613261
49. Cho, Y. L.; Rudkevich, D. M.; Shivanyuk, A.; Rissanen, K.; Rebek, J., Jr. *Chem. – Eur. J.* **2000,** *6,* 3788–3796. doi:10.1002/1521-3765(20001016)6:20<3788::aid-chem3788>3.0.co;2-y
50. Vysotsky, M. O.; Pop, A.; Broda, F.; Thondorf, I.; Böhmer, V. *Chem. – Eur. J.* **2001,** *7,* 4403–4410. doi:10.1002/1521-3765(20011015)7:20<4403::aid-chem4403>3.0.co;2-j
51. Rudzevich, Y.; Vysotsky, M. O.; Böhmer, V.; Brody, M. S.; Rebek, J., Jr.; Broda, F.; Thondorf, I. *Org. Biomol. Chem.* **2004,** *2,* 3080–3084. doi:10.1039/b410462e
52. Thondorf, I.; Rudzevich, Y.; Rudzevich, V.; Böhmer, V. *Org. Biomol. Chem.* **2007,** *5,* 2775–2782. doi:10.1039/b708679b
53. Bolte, M.; Thondorf, I.; Böhmer, V.; Rudzevich, V.; Rudzevich, Y. *CrystEngComm* **2008,** *10,* 270–272. doi:10.1039/b716368a
54. Rudzevich, V.; Rudzevich, Y.; Böhmer, V. *Synlett* **2009,** 1887–1904. doi:10.1055/s-0029-1217513
55. Mogck, O.; Pons, M.; Böhmer, V.; Vogt, W. *J. Am. Chem. Soc.* **1997,** *119,* 5706–5712. doi:10.1021/ja970078o
56. Vysotsky, M. O.; Böhmer, V. *Org. Lett.* **2000,** *2,* 3571–3574. doi:10.1021/ol0064967
57. Vysotsky, M. O.; Thondorf, I.; Böhmer, V. *Chem. Commun.* **2001,** 1890–1891. doi:10.1039/b105613c
58. Vysotsky, M. O.; Mogck, O.; Rudzevich, Y.; Shivanyuk, A.; Böhmer, V.; Brody, M. S.; Cho, Y. L.; Rudkevich, D. M.; Rebek, J., Jr. *J. Org. Chem.* **2004,** *69,* 6115–6120. doi:10.1021/jo049128f
59. Vatsouro, I.; Rudzevich, V.; Böhmer, V. *Org. Lett.* **2007,** *9,* 1375–1377. doi:10.1021/ol0702775
60. Vatsouro, I.; Alt, E.; Vysotsky, M.; Böhmer, V. *Org. Biomol. Chem.* **2008,** *6,* 998–1003. doi:10.1039/b719053k
61. Vysotsky, M. O.; Bolte, M.; Thondorf, I.; Böhmer, V. *Chem. – Eur. J.* **2003,** *9,* 3375–3382. doi:10.1002/chem.200304912
62. Wang, L.; Vysotsky, M. O.; Bogdan, A.; Bolte, M.; Böhmer, V. *Science* **2004,** *304,* 1312–1314. doi:10.1126/science.1096688
63. Vysotsky, M. O.; Bogdan, A.; Wang, L.; Böhmer, V. *Chem. Commun.* **2004,** 1268–1269. doi:10.1039/b402719a
64. Bogdan, A.; Vysotsky, M. O.; Ikai, T.; Okamoto, Y.; Böhmer, V. *Chem. – Eur. J.* **2004,** *10,* 3324–3330. doi:10.1002/chem.200400195
65. Gaeta, C.; Vysotsky, M. O.; Bogdan, A.; Böhmer, V. *J. Am. Chem. Soc.* **2005,** *127,* 13136–13137. doi:10.1021/ja054184z
66. Molokanova, O.; Vysotsky, M. O.; Cao, Y.; Thondorf, I.; Böhmer, V. *Angew. Chem., Int. Ed.* **2006,** *45,* 8051–8055. doi:10.1002/anie.200602166
67. Rudzevich, Y.; Cao, Y.; Rudzevich, V.; Böhmer, V. *Chem. – Eur. J.* **2008,** *14,* 3346–3354. doi:10.1002/chem.200701694
68. Janke, M.; Rudzevich, Y.; Molokanova, O.; Metzroth, T.; Mey, I.; Diezemann, G.; Marszalek, P. E.; Gauss, J.; Böhmer, V.; Janshoff, A. *Nat. Nanotechnol.* **2009,** *4,* 225–229. doi:10.1038/nnano.2008.416
69. Jaschonek, S.; Schäfer, K.; Diezemann, G. *J. Phys. Chem. B* **2019,** *123,* 4688–4694. doi:10.1021/acs.jpcb.9b02676
70. Tornøe, C. W.; Christensen, C.; Meldal, M. *J. Org. Chem.* **2002,** *67,* 3057–3064. doi:10.1021/jo011148j
71. Rostovtsev, V. V.; Green, L. G.; Fokin, V. V.; Sharpless, K. B. *Angew. Chem., Int. Ed.* **2002,** *41,* 2596–2599. doi:10.1002/1521-3773(20020715)41:14<2596::aid-anie2596>3.0.co;2-4
72. Meldal, M.; Tornøe, C. W. *Chem. Rev.* **2008,** *108,* 2952–3015. doi:10.1021/cr0783479
73. Singh, M. S.; Chowdhury, S.; Koley, S. *Tetrahedron* **2016,** *72,* 5257–5283. doi:10.1016/j.tet.2016.07.044
74. Ryu, E.-H.; Zhao, Y. *Org. Lett.* **2005,** *7,* 1035–1037. doi:10.1021/ol047468h
75. Pineda-Castañeda, H. M.; Rivera-Monroy, Z. J.; Maldonado, M. *ACS Omega* **2023,** *8,* 3650–3666. doi:10.1021/acsomega.2c06269
76. Sreenivasu Mummidivarapu, V. V.; Joseph, R.; Pulla Rao, C.; Kumar Pathak, R. *Coord. Chem. Rev.* **2023,** *493,* 215256. doi:10.1016/j.ccr.2023.215256
77. Makarov, E.; Iskhakova, Z.; Burilov, V.; Solovieva, S.; Antipin, I. *J. Inclusion Phenom. Macrocyclic Chem.* **2023,** *103,* 319–353. doi:10.1007/s10847-023-01200-6
78. Song, M.; Sun, Z.; Han, C.; Tian, D.; Li, H.; Kim, J. S. *Chem. – Asian J.* **2014,** *9,* 2344–2357. doi:10.1002/asia.201400024
79. Gorbunov, A.; Cheshkov, D.; Kovalev, V.; Vatsouro, I. *Chem. – Eur. J.* **2015,** *21,* 9528–9534. doi:10.1002/chem.201500946

80. Gorbunov, A.; Kuznetsova, J.; Deltsov, I.; Molokanova, A.; Cheshkov, D.; Bezzubov, S.; Kovalev, V.; Vatsouro, I. *Org. Chem. Front.* **2020,** *7,* 2432–2441. doi:10.1039/d0qo00650e
81. Gorbunov, A.; Kuznetsova, J.; Puchnin, K.; Kovalev, V.; Vatsouro, I. *New J. Chem.* **2019,** *43,* 4562–4580. doi:10.1039/c8nj06464d
82. Gorbunov, A.; Sokolova, N.; Kudryashova, E.; Nenajdenko, V.; Kovalev, V.; Vatsouro, I. *Chem. – Eur. J.* **2016,** *22,* 12415–12423. doi:10.1002/chem.201601818
83. Malakhova, M.; Gorbunov, A.; Lentin, I.; Kovalev, V.; Vatsouro, I. *Org. Biomol. Chem.* **2022,** *20,* 8092–8103. doi:10.1039/d2ob01588a
84. Syakaev, V. V.; Masliy, A. N.; Podyachev, S. N.; Sudakova, S. N.; Shvedova, A. E.; Lentin, I. I.; Gorbunov, A. N.; Vatsouro, I. M.; Lapaev, D. V.; Mambetova, G. S.; Kovalev, V. V.; Kuznetsov, A. M.; Mustafina, A. R. *Inorg. Chim. Acta* **2024,** *561,* 121848. doi:10.1016/j.ica.2023.121848
85. Bezzubov, S.; Ermolov, K.; Gorbunov, A.; Kalle, P.; Lentin, I.; Latyshev, G.; Kovalev, V.; Vatsouro, I. *Dalton Trans.* **2021,** *50,* 16765–16769. doi:10.1039/d1dt03579g
86. Gorbunov, A.; Ozerov, N.; Malakhova, M.; Eshtukov, A.; Cheshkov, D.; Bezzubov, S.; Kovalev, V.; Vatsouro, I. *Org. Chem. Front.* **2021,** *8,* 3853–3866. doi:10.1039/d1qo00636c
87. Malakhova, M.; Gorbunov, A.; Ozerov, N.; Korniltsev, I.; Ermolov, K.; Bezzubov, S.; Kovalev, V.; Vatsouro, I. *Org. Chem. Front.* **2022,** *9,* 3084–3092. doi:10.1039/d2qo00432a
88. Gorbunov, A.; Iskandarova, A.; Puchnin, K.; Nenajdenko, V.; Kovalev, V.; Vatsouro, I. *Chem. Commun.* **2020,** *56,* 4122–4125. doi:10.1039/d0cc01196g
89. Chetcuti, M. J.; Devoille, A. M. J.; Othman, A. B.; Souane, R.; Thuéry, P.; Vicens, J. *Dalton Trans.* **2009,** 2999–3008. doi:10.1039/b821144b
90. Gullo, M. C.; Baldini, L.; Casnati, A.; Marchiò, L. *Cryst. Growth Des.* **2020,** *20,* 3611–3616. doi:10.1021/acs.cgd.0c00442
91. Cecioni, S.; Lalor, R.; Blanchard, B.; Praly, J.-P.; Imberty, A.; Matthews, S. E.; Vidal, S. *Chem. – Eur. J.* **2009,** *15,* 13232–13240. doi:10.1002/chem.200901799
92. Chang, K.-C.; Chen, C.-Y.; Hsu, C.-Y.; Lee, L.-W.; Chung, W.-S. *Analyst* **2022,** *147,* 5105–5112. doi:10.1039/d2an01201d
93. Mogck, O.; Böhmer, V.; Ferguson, G.; Vogt, W. *J. Chem. Soc., Perkin Trans. 1* **1996,** 1711–1715. doi:10.1039/p19960001711
94. The CIF files have been deposited at the Cambridge Crystallographic Data Centre: CCDC 2431889 (compound **16**), 2431890 (compound **15**).
95. Arnaud-Neu, F.; Browne, J. K.; Byrne, D.; Marrs, D. J.; McKervey, M. A.; O'Hagan, P.; Schwing-Weill, M. J.; Walker, A. *Chem. – Eur. J.* **1999,** *5,* 175–186. doi:10.1002/(sici)1521-3765(19990104)5:1<175::aid-chem175>3.0.co;2-p
96. Knoblauch, S.; Falana, O. M.; Nam, J.; Roundhill, D. M.; Hennig, H.; Zeckert, K. *Inorg. Chim. Acta* **2000,** *300–302,* 328–332. doi:10.1016/s0020-1693(99)00577-0
97. Webber, P. R. A.; Cowley, A.; Drew, M. G. B.; Beer, P. D. *Chem. – Eur. J.* **2003,** *9,* 2439–2446. doi:10.1002/chem.200204518
98. Liu, Y.; Lu, Y.; Prashad, M.; Repič, O.; Blacklock, T. J. *Adv. Synth. Catal.* **2005,** *347,* 217–219. doi:10.1002/adsc.200404236
99. Bolshchikov, B.; Volkov, S.; Sokolova, D.; Gorbunov, A.; Serebryannikova, A.; Gloriozov, I.; Cheshkov, D.; Bezzubov, S.; Chung, W.-S.; Kovalev, V.; Vatsouro, I. *Org. Chem. Front.* **2019,** *6,* 3327–3341. doi:10.1039/c9qo00859d
100. Pop, A.; Vysotsky, M. O.; Saadioui, M.; Böhmer, V. *Chem. Commun.* **2003,** 1124–1125. doi:10.1039/b301418e
101. Neese, F. *Wiley Interdiscip. Rev.: Comput. Mol. Sci.* **2022,** *12,* e1606. doi:10.1002/wcms.1606
102. Neese, F.; Wennmohs, F.; Hansen, A.; Becker, U. *Chem. Phys.* **2009,** *356,* 98–109. doi:10.1016/j.chemphys.2008.10.036
103. Garcia-Ratés, M.; Neese, F. *J. Comput. Chem.* **2020,** *41,* 922–939. doi:10.1002/jcc.26139
104. Helmich-Paris, B.; de Souza, B.; Neese, F.; Izsák, R. *J. Chem. Phys.* **2021,** *155,* 104109. doi:10.1063/5.0058766
105. Neese, F. *J. Comput. Chem.* **2023,** *44,* 381–396. doi:10.1002/jcc.26942
106. Caldeweyher, E.; Bannwarth, C.; Grimme, S. *J. Chem. Phys.* **2017,** *147,* 034112. doi:10.1063/1.4993215
107. Caldeweyher, E.; Ehlert, S.; Hansen, A.; Neugebauer, H.; Spicher, S.; Bannwarth, C.; Grimme, S. *J. Chem. Phys.* **2019,** *150,* 154122. doi:10.1063/1.5090222
108. Caldeweyher, E.; Mewes, J.-M.; Ehlert, S.; Grimme, S. *Phys. Chem. Chem. Phys.* **2020,** *22,* 8499–8512. doi:10.1039/d0cp00502a
109. Wittmann, L.; Gordiy, I.; Friede, M.; Helmich-Paris, B.; Grimme, S.; Hansen, A.; Bursch, M. *Phys. Chem. Chem. Phys.* **2024,** *26,* 21379–21394. doi:10.1039/d4cp01514b

License and Terms

BEILSTEIN JOURNAL OF ORGANIC CHEMISTRY

Synthesis and uranyl(VI) extraction performance of a calix[4]pyrrole–tetrahydroxamic acid receptor

Sara Karnib[1,2], Rana Baydoun[2], Wissam Zaidan[2], Nancy AlHaddad[1], Omar El Samad[2], Bilal Nsouli[2], Francine Cazier-Dennin[1] and Pierre-Edouard Danjou[*1]

Full Research Paper

Open Access

Address:
[1]Unité de Chimie Environnementale et Interactions sur le Vivant, UR 4492, Université du Littoral Côte d'Opale, 145 Avenue Maurice Schumann, MREI 1, Dunkerque, France and [2]Lebanese Atomic Energy Commission, National Council for Scientific Research CNRS –L, P.O. Box: 11-8281, Riad el soleh, 1107 2260, Beirut, Lebanon

Email:
Pierre-Edouard Danjou[*] - danjou@univ-littoral.fr

* Corresponding author

Keywords:
gamma spectroscopy; hydroxamic acid; phenoxycalix[4]pyrrole; solid–liquid extraction; uranyl(VI) extraction

Beilstein J. Org. Chem. **2026,** *22,* 486–494.
https://doi.org/10.3762/bjoc.22.36

Received: 08 December 2025
Accepted: 06 March 2026
Published: 18 March 2026

This article is part of the thematic issue "Novel macrocycles: from synthesis to supramolecular function".

Guest Editor: C. Gaeta

Abstract

The contamination of water by uranium poses a serious threat to ecosystems and human health, creating a need for efficient and selective remediation strategies. Supramolecular materials, with their pre-organized structures, offer a promising route for uranium removal. Phenoxycalix[4]pyrroles (PCP) are well-known supramolecular scaffolds capable of selective metal binding, making them attractive candidates for designing uranium extractants. Here, we report the design and synthesis of PCP HA, a phenoxycalix[4]pyrrole scaffold functionalized with four hydroxamic acid (HA) groups, and evaluate its uranium(VI) extraction potential. PCP HA was synthesized from its ester precursor (PCP E) via hydroxyaminolysis using KOH, achieving a 95% yield. Its structure was confirmed by ^{1}H NMR, ^{13}C NMR, and HRMS. The uranium(VI) extraction efficiency of PCP HA was evaluated by solid–liquid extraction experiments, using uranyl acetate as the uranium source, with measurements performed by gamma spectroscopy. PCP HA demonstrated good performance, removing up to 95% of uranyl(VI) from aqueous solutions (1 mM) at acidic pH, likely due to the strong coordination provided by its hydroxamic acid groups. Further studies revealed that the extraction efficiency also depends on the ligand-to-metal molar ratio. These findings establish PCP HA as a promising supramolecular material for the removal of uranyl from aqueous media.

Introduction

Over the past few decades, supramolecular chemistry has advanced intensively establishing itself as a central discipline in modern chemistry [1-3]. This tremendous growth allowed the field to transcend the traditional chemistry boundaries and move toward real-life applications [4]. In this context, supramolecular materials with pre-organized structures have been designed

and exploited for diverse environmental, industrial and biological applications [5-8].

Among these macrocycles, calix[4]pyrroles (CPs) represent a modern generation of supramolecular materials with interesting chelation properties [9]. These nonplanar, non-aromatic, tetrapyrrolic macrocycles consist of four pyrrolic units linked together at their 2,5-positions through sp^3-hybridized *meso*-carbon atoms [10]. The ability of CPs to selectively bind anions [11], cations, ion pairs and neutral guest species, combined with the versatility to introduce diverse functional groups, has enabled the fabrication of calix[4]pyrrole-based supramolecular matrices for a broad range of applications [9]. Notable examples include catalysis, chromogenic sensors and fluorescent sensors, as well as heavy metals extraction [12-16].

One CP molecule that has attracted the attention of several research groups is the *meso*-tetra-methyltetrakis(4-hydroxyphenyl)calix[4]pyrrole, commonly referred to as phenoxycalix[4]pyrrole (PCP). It was first reported in 1999 by two independent research groups, Floriani et al. and Sessler et al., via the acid-catalyzed condensation of pyrrole with *p*-hydroxyacetophenone [17,18]. PCP and its derivatives were first known for their anion chelation capability achieved through the formation of hydrogen bonds with the pyrrolic units [19-22]. Subsequent studies have demonstrated that the introduction of additional chelation sites via extension of the phenolic groups of PCP can yield anionic receptors, ditopic receptors bearing both anion- and cation-binding sites, as well as systems capable of promoting ion-pair formation [23,24].

As effective chelating agents for a broad range of transition metals, hydroxamic acids constitute an important class of organic compounds that have attracted considerable attention and have found diverse applications across both biomedical and industrial fields [25,26]. Hydroxamic acids are also well known for their strong chelating ability toward uranyl, forming stable complexes through the synergistic coordination of the carbonyl and hydroxylamine groups [27]. Uranium is a naturally occurring radionuclide and is thus an integral constituent of the environment [28]. However, beyond its extensive use as fuel for nuclear power generation, uranium is released into the environment through various industrial processes, such as phosphate fertilizer production and metal refining, contributing to the increased accumulation of uranium in ecosystems [29-31]. Owing to its radioactivity, chemical toxicity, and long half-life, environmental uranium contamination poses serious ecological and public health risks [32]. In this context, hydroxamic acid functionalities have been successfully incorporated on supramolecular architectures to explore their potential for the removal of uranium from aqueous media. For instance, it has been long known that hydroxamic acid derivatives of calix[4]arenes and calix[6]arenes act as excellent uranophiles as demonstrated in early studies from 1991 [33]. A calix[4]resorcinarene hydroxamic acid has also shown a pronounced binding tendency and selectivity for uranyl and proved to be applicable for the determination of uranium in standard and environmental samples [34]. Importantly, more recent studies have demonstrated that pre-organized or cyclic hydroxamate ligands can display significantly enhanced binding toward uranyl relative to their linear hydroxamic acid counterparts, emphasizing the beneficial role of structural organization in uranyl chelation [35]. This beneficial role of pre-organization of chelating groups within one molecule was also highlighted for supramolecular platforms like calixarenes for actinides and lanthanides extraction [36,37].

In light of this background, we report here the incorporation of hydroxamic acid into phenoxycalix[4]pyrrole and examine its effectiveness in extracting uranyl from aqueous solution using gamma spectroscopy. The extraction performance was systematically evaluated as a function of pH and ligand-to-metal molar ratio to study the effect of these two key parameters on the extraction process. In doing so, this work aligns with current research dedicated to the design of functional supramolecular materials capable of remediating uranium from aqueous environments [38,39].

Results and Discussion

PCP HA synthesis and characterization

Various strategies have been developed for the synthesis of hydroxamic acid derivatives over the years [40]. Classical and most popular routes involve the direct reaction of carboxylic acid derivatives such as esters, acyl chlorides and anhydrides with hydroxylamine salts [41]. A variety of coupling or activating agents were also employed in case of simple addition of hydroxylamine to carboxylic acid compounds [42-44]. In addition, alternative methods starting from aldehydes [45], alcohols [46], and amides [47] have also been reported. However, the literature states that there is no particular reagent or reaction condition that can serve as a general rule for the synthesis of hydroxamic acids [48].

In this study, the direct reaction of hydroxylamine with the PCP ester was first examined, since the ester functions as the synthetic precursor to the corresponding acid used in the preparation of PCP derivatives from PCP [21]. For that, PCP was initially synthesized through the molecular cyclisation of pyrrole with 4-hydroxyacetophenone in methanol in the presence of methanesulfonic acid as first reported by Floriani et al. [17] and Sessler et al. [18]. This condensation reaction produces several PCP isomers, including the targeted pre-organized α,α,α,α-isomer, which is isolated by crystallization from glacial acetic

acid, followed by removal of the acetic acid using a mixture of acetonitrile and acetone. Using this protocol, the PCP α,α,α,α-isomer was recovered in 47% yield, as previously reported by Namor and Shehab [49]. Subsequently, the synthesis of the PCP ester derivative (PCP E) was carried out via O-alkylation of PCP with ethyl bromoacetate in dry acetone/K_2CO_3, following the method reported by Camiolo and Gale [21], affording a yield of 85%.

Among several procedures used for the direct hydroxyaminolysis of carboxylic ester substrates, Beillard et al. highlighted the superiority of a DBU (1,8-diazabicyclo[5.4.0]undec-7-ene)-mediated route over the classical methods, particularly when the starting compounds are sterically hindered [50]. In this regard, a methanolic solution of PCP ester was allowed to react with a large excess of methanolic hydroxylamine in the presence of DBU for one night. At this stage, the formation of precipitated PCP hydroxamic acids was verified using thin-layer chromatography, with the appearance of the characteristic red spot upon treatment with $FeCl_3$ confirming the presence of the hydroxamic acid functionality. Moreover, the formation of the tetrahydroxamic acid product was confirmed by ^{1}H NMR spectroscopy in deuterated DMSO, as evidenced by the disappearance of the characteristic signals of the ethyl group and an upfield shift of 0.27 ppm for the O–CH_2 protons compared to the spectrum of the PCP ester. However, signals corresponding to DBU at 1.5, 2.3, and 3.1 ppm were still observed (Supporting Information File 1, Figure S7) despite several ultrasonic washings with aqueous ammonium chloride, as previously described by Verma et al. [51]. At this stage, chromatographic techniques, crystallization, and successive washing steps all failed to yield the pure compound due to the persistent presence of DBU.

Additionally, the use of a small amount of solid KCN in aqueous hydroxylamine has been reported for the solution-phase hydroxylamination of esters previously described by Ho et al. [52]. This study demonstrated that the extent of ester conversion and the formation of carboxylic acid by-products vary markedly with the structure of the ester substrate. When this method was used, the ^{1}H NMR spectra of the products revealed residual peaks corresponding to unreacted ester (Supporting Information File 1, Figure S8). This observation is consistent with the substrate-dependent behavior reported in that study, highlighting that the reaction outcome is strongly influenced by the nature of the ester substrate. As a result, this synthetic route was discontinued.

Another straightforward method for the synthesis of hydroxamic acids from esters was reported in 1994 by Hutchinson et al., for the synthesis of calixarene tetrahydroxamates from calixarene tetraethylacetate [53]. In the original procedure, KOH was added at −5 °C, and the mixture was stirred for 5 hours at this temperature, followed by 5 days of stirring at room temperature. In our hands, both the addition of KOH and stirring were performed entirely at room temperature, and ^{1}H NMR and HRMS monitoring indicated that the reaction reached completion within one day. While some studies have reported the formation of hydroxamic acids from esters at neutral pH [54], in our study the conversion leading to PCP HA (Figure 1) was observed exclusively under alkaline conditions (pH ≥ 10). This finding agrees with earlier methodologies demonstrating that the generation of free hydroxylamine [55] and consequently hydroxamic acid formation occurs efficiently only in alkaline media [48,56]. Moreover, to prevent the formation of carboxylic acid by-products, methanol was used as the solvent both for the generation of free hydroxylamine and for the subsequent synthesis of PCP HA. The resulting tetrapotassium hydroxamate intermediate was then acidified with a 10% HCl solution, inducing precipitation of the tetrahydroxamic acid form. PCP HA was isolated as a grey solid in high yield (95%).

The structure of PCP HA was fully characterized by ^{1}H NMR and ^{13}C NMR (DMSO-d_6) as well as by HRMS (ESI$^+$) (Figures S3–S6, and S9 in Supporting Information File 1). In the

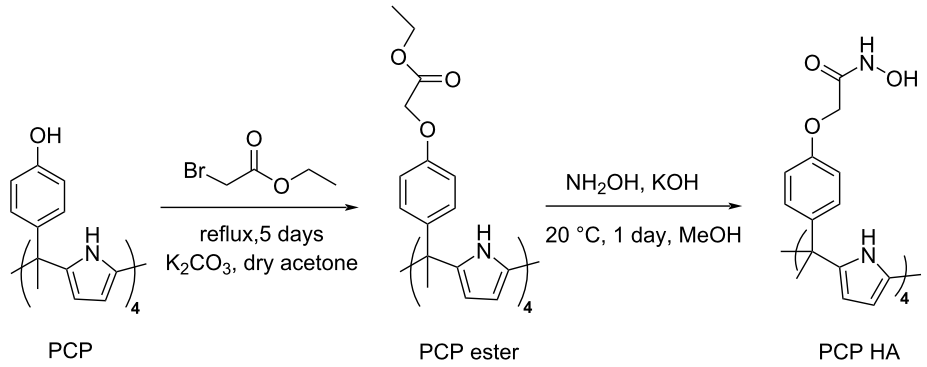

Figure 1: Synthetic route of PCP HA.

^{1}H NMR spectrum, two sets of singlets at 4.41 and 4.76 ppm (CH_2) were attributed to the –O=C–CH_2–O– groups of the *E*/*Z* isomers of the hydroxamic acid moieties, in agreement with previous reports (Supporting Information File 1, Figure S3) [57]. Additionally, two pairs of singlets at 8.97, 9.32 and 10.20, 10.93 ppm (2H total) were assigned to the hydroxy (–OH) and amide (–NH) protons of the hydroxamic acid groups (Supporting Information File 1, Figure S4). The disappearance of these resonances in the 9.0–11.0 ppm region upon D_2O exchange confirmed these assignments (Supporting Information File 1, Figure S6). Finally, characteristic resonances at 1.76, 5.95, and 8.98 ppm, together with the two doublets at 6.85 ppm, were attributed to the PCP core (Supporting Information File 1, Figure S3). The HRMS (ESI^+) spectrum exhibited a major peak at *m/z* = 1033.4081 ($[M + H]^+$) (Supporting Information File 1, Figure S9), consistent with the expected molecular formula and confirming complete conversion of the PCP ester precursor into the corresponding hydroxamic acid, with no detectable acid-derived by-products. Solubility tests revealed that PCP HA is soluble exclusively in highly polar aprotic solvents (DMSO, DMF) and remains completely insoluble in other common organic solvents (chloroform, ether, etc.) and water. The absence of ligand leaching into water was confirmed by depositing a drop of the aqueous supernatant on a TLC plate, which showed no formation of the characteristic red iron-hydroxamate complex upon treatment with $FeCl_3$. These physicochemical properties precluded standard liquid–liquid extraction but were suitable for a solid–liquid approach as previously described for calixarenes [58].

Extraction experiments

In this study, two parameters that can influence the solid-liquid extraction efficiency of PCP-HA toward uranyl, namely pH and ligand-to-metal ratio, were studied. To ensure comparison between extraction experiments, parameters like temperature, shaking time and volume of uranyl solution used were kept constant. In a typical experiment, 20 mL of a 1 mM aqueous uranyl acetate solution was adjusted to the target pH and then added to solid PCP HA. The solution was shaken at a fixed temperature of 25 °C for 4 h. This time was estimated to be sufficient to reach equilibrium. The heterogeneous solution was centrifuged and the aqueous layer was filtered prior to gamma spectroscopy analysis. Uranium activity concentrations before and after extraction were determined, and extraction efficiencies were calculated from the decrease in activity concentration. It is important to note that the extraction efficiency of PCP HA was evaluated based solely on the quantification of ^{238}U. Uranium is a naturally occurring radionuclide that exists predominantly as a mixture of three isotopes: ^{238}U, ^{235}U and ^{234}U. Among these, ^{238}U is by far the most abundant, accounting for 99.28 % by mass, followed by ^{235}U (0.72 %) and ^{234}U (0.0058 %). Although these isotopes possess identical chemical properties, they differ in their radioactive characteristics [59]. Since the extraction experiments depend on the chemical behavior of uranium rather than its radiological properties, any of these isotopes could, in principle, be used. Two main factors justify the choice of ^{238}U: its natural abundance and its reliable detectability by gamma spectroscopy, in contrast to ^{235}U, which exhibits weak gamma emission intensity [60].

The uncertainties reported have been separated into contributions from the gamma-spectrometric measurements, $\sigma(A_0)$ and $\sigma(A_1)$, and from the calculations performed to derive the extraction efficiencies' uncertainty values, $\sigma(\%\ E)$ and $\sigma(\%\ E_{mean})$. Measurement uncertainties reflect counting statistics, detector calibration, sample geometry, and matrix effects, while calculation uncertainties account for the propagation of errors during the efficiency computation [61,62]. The uncertainty of the % E was calculated using the law of propagation of uncertainty which accounts for the variability of individual replicates [63]. The reported mean extraction efficiency (% E_{mean}) represents the weighted mean of the replicate measurements, with weights inversely proportional to the variance of each replicate [64]. The weights and the equations used in the calculation are provided in Supporting Information File 1, Tables S1–S4.

Effect of pH

To gain insight into the binding behavior of PCP HA toward uranyl, the effect of pH on the extraction efficiency was evaluated, as variations in pH can significantly influence metal–ligand complexation equilibria [65]. The results of this experiment are summarized in Table 1. The pH range of 2–5 was specifically chosen based on two considerations: first to avoid PCP HA degradation observed during its synthesis at pH values below 2; and second to prevent the precipitation of uranyl hydroxide solution at pH values above 5 [66]. PCP HA exhibited consistently high extraction efficiencies, 83–95%, across the studied pH range (Table 1), indicating that it maintains strong affinity toward uranyl under moderately acidic conditions. In particular, high extraction efficiencies were observed at pH 2–3, reaching up to 95% at pH 3 (Figure 2). Although a slight increase is observed between pH 2 and pH 3, the extraction efficiencies remain overall comparable within experimental uncertainty, suggesting that uranyl uptake is already near maximal in this acidic region.

This behavior is consistent with previous studies in which ligands displayed high uranyl uptake within an optimal pH window. For instance, calix[4]arene-based 8-hydroxyquinoline ligands showed nearly quantitative extraction of uranyl between pH 4 and 9, with efficiency decreasing under more acidic conditions [67]. Likewise, phosphoramide-functionalized mag-

Table 1: Effect of pH on uranyl extraction by PCP HA.[a]

pH	Replicate	A_0 (Bq/Kg)	σ(A_0)	A_1 (Bq/Kg)	σ(A_1)	Extraction efficiency (%)	σ(% E)
5	1	2856	362	406	54	86	2.7
	2	2756	367	476	97	83	6.4
4	1	2683	354	399	52	85	2.7
	2	2601	329	287	59	89	4.4
3	1	2525	516	144	31	94	1.8
	2	2611	533	128	28	95	1.6
2	1	2561	518	244	50	90	2.8
	2	2630	532	242	52	91	2.9

[a]A_0 and A_1 represent the activity concentrations of ^{238}U in the uranyl acetate working solution before and after extraction, respectively. σ(A_0) and σ(A_1) denote the uncertainties associated with the measured activity concentrations determined by gamma spectroscopy. σ(% E) represents the uncertainties of the individual extraction efficiencies. Extractions were carried out at 25 °C using aqueous uranyl acetate solutions of 1 mM, with the pH being adjusted with 0.1 M HCl. PCP HA was added at a ligand-to-metal molar ratio of 1:1. Samples were equilibrated for 4 h under constant agitation before phase separation and activity measurements.

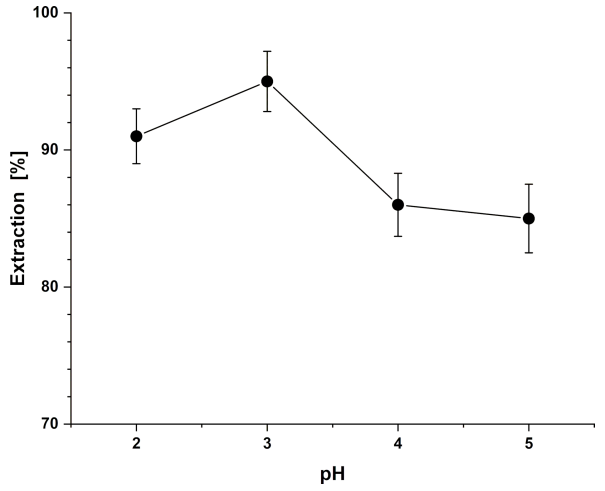

Figure 2: Effect of pH on the mean uranyl extraction efficiency (% E_{mean}) of PCP HA.

netic nanoparticles showed high uranyl adsorption (80–95%) between pH 4 and 8, with reduced uptake outside this range [68].

Although hydroxamic acids typically have pK_a values of 7–9 [69], supramolecular systems bearing these groups do not exhibit uniform uranyl extraction behavior under identical pH conditions. Consequently, some systems achieve maximum extraction under weakly acidic conditions, while others perform better at higher pH values. For instance, an octa-functionalized calix[4]resorcinarenehydroxamic acid exhibits quantitative extraction of uranyl into ethyl acetate solution at pH value of 8 [34]. On the other hand, calix[4]arenes and calix[6]arenes functionalized with hydroxamic acid groups show a marked increase in uranyl extractability from aqueous solution into chloroform at pH 3–4, reaching nearly 100% extractability at pH 5. The enhanced extraction efficiency observed in the acidic pH region has been attributed to the metal-ion-assisted deprotonation. The coordination of the hydroxamic acid groups to the uranyl cation stabilizes the deprotonated hydroxamate form, effectively lowering the apparent pK_a and enabling strong binding even at low pH [33]. It is important to mention that the formation of the stable 5-membered chelate between the uranyl ion and the Z-isomer of hydroxamic acid effectively shifts the *Z*/*E* equilibrium [70] towards the *Z*-conformation through a metal-induced fit mechanism [71,72]. Consistent with known hydroxamate coordination chemistry, coordination-induced deprotonation of the hydroxamic acid at low pH provides the conditions required for effective uranyl complexation in our system.

Effect of ligand–metal molar ratio

To further understand the complexation behavior of PCP HA toward uranyl, the effect of the ligand-to-metal molar ratio on the extraction efficiency was investigated. Although the previous experiment revealed maximum extraction at pH values of 2 and 3, the investigation of the ligand-to-metal molar ratio was conducted at pH 4. This adjustment was made to allow a clearer assessment of the molar ratio effect. At pH 3, a 1:1 ratio of PCP HA to uranyl already yielded about 95% extraction, leaving little sensitivity to detect variations at higher ligand mass. By performing the experiment at pH 4, where the extraction efficiency was approximately 86%, the system remained sufficiently responsive to changes in ligand mass.

Starting from a ligand-to-metal molar ratio of 0.9:1, the extraction efficiency increased steadily with increasing ligand mass, reaching a maximum of about 94% at a ratio of 7:1 (Table 2). Beyond this point, the ligand mass was increased to achieve a 20:1 ratio, yet no further improvement in extraction efficiency

Table 2: Effect of ligand–metal ratio on uranyl extraction by PCP HA.

Ligand–metal molar ratio	Replicate	A_0 (Bq/Kg)	σ(A_0)	A_1 (Bq/Kg)	σ(A_1)	Extraction efficiency (%)	σ(% E)
0.9:1	1	1535	166	224	28	85	
	2	1576	177	277	31	82	2.8
4:1	1	1520	308	164	21	89	1.7
	2	1524	173	147	30	90	4.2
7:1	1	1577	178	100	21	94	2.8
	2	1574	169	94	20	94	2.8
20:1	1	1476	174	95	23	94	3.7
	2	1509	163	94	21	94	3.2

was observed (Figure 3). This finding indicates that at pH 4, a ligand-to-metal molar ratio of 7:1 is sufficient to ensure nearly complete complexation of uranyl. This apparent excess reflects the heterogeneous nature of the system. Since a significant portion of the hydrophilic groups responsible complexation with uranium [58] is likely buried within the solid bulk and thus inaccessible, a high nominal ratio is necessary to provide a sufficient number of available coordination sites at the water–solid interface to quantitatively capture the uranyl ions [73].

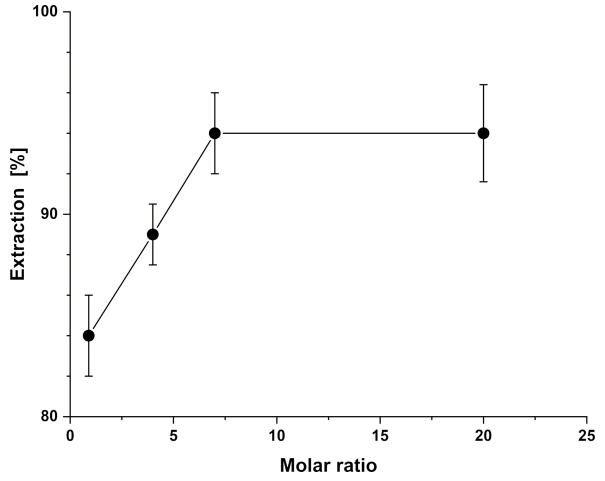

Figure 3: Effect of ligand-to-metal molar ratio on the mean uranyl extraction efficiency (% E_{mean}) of PCP HA.

The observed efficiency depends not only on ligand mass but also on the intrinsic coordination preferences with uranyl. In aqueous solution, hexavalent uranium, the most dominant oxidation state, exists predominantly as the linear uranyl ion UO_2^{2+}. In this ion, two oxo ligands occupy axial positions while the equatorial plane accommodates four to six donor atoms [74,75]. Complexes of UO_2^{2+} often adopt either a pseudoplanar pentacoordinate or hexacoordinate structure, as shown by X-ray crystallographic studies. Consequently, to bind UO_2^{2+} effectively, a ligand must present donor atoms positioned to match the uranyl equatorial coordination sites [76].

Hydroxamic acids act as bidentate ligands, with each functional unit offering two donor atoms, a carbonyl oxygen and a hydroxy oxygen, that can simultaneously coordinate to a uranyl ion [77]. In supramolecular systems, not all hydroxamic acid groups necessarily bind uranyl ions, as steric hindrance and site accessibility can limit coordination to a subset of available sites [78]. A relevant example is a calix[6]arene functionalized with three hydroxamic acid groups, where a theoretical study using density functional theory (DFT) calculations showed that the complex with the uranyl is most stabilized when only two of the three hydroxamic acid units participate in binding [78]. This concept of partial participation and cooperative interactions between hydroxamic acid units may also be relevant in the PCP HA system, where not all functional groups are necessarily involved in uranyl binding.

Conclusion

In this study, we have efficiently synthesized PCP HA, a phenoxycalix[4]pyrrole scaffold functionalized with four hydroxamic acid groups, and demonstrated its uranyl extraction potential. Solid–liquid extraction studies showed that it removes up to 95% of uranyl at pH 3. Subsequent investigation at pH 4 revealed that a 7:1 ligand-to-metal molar ratio is sufficient to achieve near-quantitative uranium removal (≈94%). The strong coordination provided by the hydroxamic acid groups within the pre-organized cavity likely underlies its high extraction efficiency. These results highlight PCP HA as a promising supramolecular platform for uranyl removal and open the door for its application in the remediation of uranium-contaminated environmental samples. Future work will focus on the covalent anchoring of this macrocycle onto solid matrixes (polymer or silica). The development of such functionalized material is intended to allow for implementation in continuous flow filtration systems for industrial effluent remediation or for the challenging task of uranium extraction from seawater [79].

Experimental

Detailed synthetic procedures, compound characterization (^{1}H and ^{13}C NMR, HRMS), and uranyl extraction protocols, including pH and ligand-to-metal ratio studies, are described in Supporting Information File 1.

Supporting Information

Supporting Information File 1

Experimental part.
[https://www.beilstein-journals.org/bjoc/content/supplementary/1860-5397-22-36-S1.pdf]

Acknowledgements

The authors express their gratitude to the Lebanese Atomic Energy Commission- LAEC and the Unité de Chimie Environnementale et Interactions sur le Vivant- UCEIV for their support of this work.

Funding

The authors would like to thank the National Council for Scientific Research Lebanon (CNRS/L) and the Université du Littoral Côte d'Opale (ULCO) for funding this work.

Conflict of Interest

The authors declare no conflicts of interest.

ORCID® iDs

Wissam Zaidan - https://orcid.org/0009-0009-9341-9989
Pierre-Edouard Danjou - https://orcid.org/0000-0001-8824-1420

Data Availability Statement

All data that supports the findings of this study is available in the published article and/or the supporting information of this article.

Preprint

A non-peer-reviewed version of this article has been previously published as a preprint: https://doi.org/10.26434/chemrxiv-2025-7m265

References

1. Lehn, J.-M. *Proc. Natl. Acad. Sci. U. S. A.* **2002,** *99,* 4763–4768. doi:10.1073/pnas.072065599
2. Steed, J. W.; Atwood, J. L. *Supramolecular Chemistry,* 3rd ed.; John Wiley & Sons: Hoboken, NJ, USA, 2022.
3. Kubik, S. *Supramolecular Chemistry: From Concepts to Applications,* 2nd ed.; De Gruyter: Berlin, Germany, 2024. doi:10.1515/9783111315171
4. Kolesnichenko, I. V.; Anslyn, E. V. *Chem. Soc. Rev.* **2017,** *46,* 2385–2390. doi:10.1039/c7cs00078b
5. Teresa Albelda, M.; Frías, J. C.; García-España, E.; Schneider, H.-J. *Chem. Soc. Rev.* **2012,** *41,* 3859. doi:10.1039/c2cs35008d
6. Williams, G. T.; Haynes, C. J. E.; Fares, M.; Caltagirone, C.; Hiscock, J. R.; Gale, P. A. *Chem. Soc. Rev.* **2021,** *50,* 2737–2763. doi:10.1039/d0cs00948b
7. Ma, X.; Zhao, Y. *Chem. Rev.* **2015,** *115,* 7794–7839. doi:10.1021/cr500392w
8. Lemire, D.; Dumas, T.; Guillaumont, D.; Solari, P. L.; Menut, D.; Giusti, F.; Arrachart, G.; Dourdain, S.; Pellet-Rostaing, S. *Inorg. Chem.* **2024,** *63,* 18809–18819. doi:10.1021/acs.inorgchem.4c02880
9. Rather, I. A.; Wagay, S. A.; Hasnain, M. S.; Ali, R. *RSC Adv.* **2019,** *9,* 38309–38344. doi:10.1039/c9ra07399j
10. Mamardashvili, G. M.; Mamardashvili, N. Z.; Koifman, O. I. *Russ. Chem. Rev.* **2015,** *84,* 275–287. doi:10.1070/rcr4439
11. Gale, P. A.; Sessler, J. L.; Král, V.; Lynch, V. *J. Am. Chem. Soc.* **1996,** *118,* 5140–5141. doi:10.1021/ja960307r
12. Buranaprasertsuk, P.; Tangsakol, Y.; Chavasiri, W. *Catal. Commun.* **2007,** *8,* 310–314. doi:10.1016/j.catcom.2006.06.022
13. Nishiyabu, R.; Anzenbacher, P. *J. Am. Chem. Soc.* **2005,** *127,* 8270–8271. doi:10.1021/ja051421p
14. Bhatt, K. D.; Shah, H. D.; Modi, K. M.; Narechania, M. B.; Patel, C. *Supramol. Chem.* **2019,** *31,* 268–282. doi:10.1080/10610278.2019.1568434
15. Abbas, I.; Shamseddine, H.; Hammud, H. H. *Complex Met.* **2014,** *1,* 57–68. doi:10.1080/2164232x.2014.884940
16. Rifai, A.; AlHaddad, N.; Noun, M.; Abbas, I.; Tabbal, M.; Shatila, R.; Cazier-Dennin, F.; Danjou, P.-E. *Org. Biomol. Chem.* **2019,** *17,* 5818–5825. doi:10.1039/c9ob01106d
17. Bonomo, L.; Solari, E.; Toraman, G.; Scopelliti, R.; Floriani, C.; Latronico, M. *Chem. Commun.* **1999,** 2413–2414. doi:10.1039/a907563a
18. Anzenbacher, P.; Jursíková, K.; Lynch, V. M.; Gale, P. A.; Sessler, J. L. *J. Am. Chem. Soc.* **1999,** *121,* 11020–11021. doi:10.1021/ja993195n
19. Sessler, J. L.; Anzenbacher, P., Jr.; Jursíková, K.; Miyaji, H.; Genge, J. W.; Tvermoes, N. A.; Allen, W. E.; Shriver, J. A.; Gale, P. A.; Král, V. *Pure Appl. Chem.* **1998,** *70,* 2401–2408. doi:10.1351/pac199870122401
20. Sessler, J. L.; Anzenbacher, P.; Miyaji, H.; Jursíková, K.; Bleasdale, E. R.; Gale, P. A. *Ind. Eng. Chem. Res.* **2000,** *39,* 3471–3478. doi:10.1021/ie000102y
21. Camiolo, S.; Gale, P. A. *Chem. Commun.* **2000,** 1129–1130. doi:10.1039/b003229h
22. Woods, C. J.; Camiolo, S.; Light, M. E.; Coles, S. J.; Hursthouse, M. B.; King, M. A.; Gale, P. A.; Essex, J. W. *J. Am. Chem. Soc.* **2002,** *124,* 8644–8652. doi:10.1021/ja025572t
23. Chi, X.; Peters, G. M.; Hammel, F.; Brockman, C.; Sessler, J. L. *J. Am. Chem. Soc.* **2017,** *139,* 9124–9127. doi:10.1021/jacs.7b04529
24. Escobar, L.; Sun, Q.; Ballester, P. *Acc. Chem. Res.* **2023,** *56,* 500–513. doi:10.1021/acs.accounts.2c00839
25. Sow, I. S. *Eur. J. Chem.* **2024,** *15,* 345–354. doi:10.5155/eurjchem.15.4.345-354.2565
26. Sunoqrot, R. M.; Abidin, M. H. Z.; Qian, C.; Jamaluddin, N. *Mater. Today Commun.* **2025,** *43,* 111751. doi:10.1016/j.mtcomm.2025.111751

27. Kumar Satpati, S.; Pal, S.; Roy, S. B.; Tewari, P. K. *J. Environ. Chem. Eng.* **2014,** *2,* 1343–1351. doi:10.1016/j.jece.2014.04.007
28. US EPA, O. Radionuclide Basics: Uranium. https://www.epa.gov/radiation/radionuclide-basics-uranium (accessed Sept 23, 2025).
29. Carvalho, F. P.; Fesenko, S.; Harbottle, A. R.; Lavrova, T.; Mitchel, N. G.; Payne, T. E.; Rigol, A.; Thorne, M. C.; Ulanowski, A.; Vidal, M.; Voitsekhovych, O.; West;, J. M.; Yankovich, T. The Environmental Behaviour of Uranium. https://www-pub.iaea.org/MTCD/Publications/PDF/PUB_DOC_488_web.pdf (accessed Oct 14, 2024).
30. Mwalongo, D. A.; Haneklaus, N. H.; Lisuma, J. B.; Kivevele, T. T.; Mtei, K. M. *Environ. Sci. Pollut. Res.* **2022,** *30,* 33898–33906. doi:10.1007/s11356-022-24574-5
31. Dzimbanhete, V. L.; Alakangas, L.; Karlsson, T.; Peinerud, E.; Paulsson, O.; Martinsson, O.; Aiglsperger, T. *J. Contam. Hydrol.* **2025,** *270,* 104530. doi:10.1016/j.jconhyd.2025.104530
32. Brugge, D.; deLemos, J. L.; Oldmixon, B. *Rev. Environ. Health* **2005,** *20,* 177–194. doi:10.1515/reveh.2005.20.3.177
33. Nagasaki, T.; Shinkai, S. *J. Chem. Soc., Perkin Trans. 2* **1991,** 1063–1066. doi:10.1039/p29910001063
34. Jain, V.; Pillai, S.; Pandya, R.; Agrawal, Y.; Shrivastav, P. *Talanta* **2005,** *65,* 466–475. doi:10.1016/j.talanta.2004.06.033
35. Sornosa-Ten, A.; Jewula, P.; Fodor, T.; Brandès, S.; Sladkov, V.; Rousselin, Y.; Stern, C.; Chambron, J.-C.; Meyer, M. *New J. Chem.* **2018,** *42,* 7765–7779. doi:10.1039/c8nj00166a
36. Arnaud-Neu, F.; Böhmer, V.; Dozol, J.-F.; Grüttner, C.; Jakobi, R. A.; Kraft, D.; Mauprivez, O.; Rouquette, H.; Schwing-Weill, M.-J.; Simon, N.; Vogt, W. *J. Chem. Soc., Perkin Trans. 2* **1996,** 1175–1182. doi:10.1039/p29960001175
37. Böhmer, V.; Dozol, J.-F.; Grüttner, C.; Liger, K.; Matthews, S. E.; Rudershausen, S.; Saadioui, M.; Wang, P. *Org. Biomol. Chem.* **2004,** *2,* 2327–2334. doi:10.1039/b405602g
38. Peng, H.; Li, F.; Zeng, Y.; Li, M.; Liao, J.; Lan, T.; Yang, Y.; Yang, J.; Liu, N. *J. Radioanal. Nucl. Chem.* **2021,** *329,* 289–300. doi:10.1007/s10967-021-07753-5
39. Chen, D.; Sun, M.; Zhao, X.; Shi, M.; Fu, X.; Hu, W.; Zhao, R. *J. Colloid Interface Sci.* **2024,** *668,* 343–351. doi:10.1016/j.jcis.2024.04.171
40. Ganeshpurkar, A.; Kumar, D.; Singh, S. K. *Curr. Org. Synth.* **2018,** *15,* 154–165. doi:10.2174/1570179414666170614123508
41. Yale, H. L. *Chem. Rev.* **1943,** *33,* 209–256. doi:10.1021/cr60106a002
42. Valeur, E.; Bradley, M. *Chem. Soc. Rev.* **2009,** *38,* 606–631. doi:10.1039/b701677h
43. Ech-Chahad, A.; Minassi, A.; Berton, L.; Appendino, G. *Tetrahedron Lett.* **2005,** *46,* 5113–5115. doi:10.1016/j.tetlet.2005.05.131
44. Usachova, N.; Leitis, G.; Jirgensons, A.; Kalvinsh, I. *Synth. Commun.* **2010,** *40,* 927–935. doi:10.1080/00397910903026723
45. Papadopoulos, G. N.; Kokotos, C. G. *Chem. – Eur. J.* **2016,** *22,* 6964–6967. doi:10.1002/chem.201600333
46. Dettori, G.; Gaspa, S.; Porcheddu, A.; De Luca, L. *Org. Biomol. Chem.* **2014,** *12,* 4582. doi:10.1039/c4ob00693c
47. Ohtsuka, N.; Seki, M.; Hoshino, Y.; Honda, K. *Chem. Lett.* **2019,** *48,* 1328–1331. doi:10.1246/cl.190592
48. Alam, M. A. *Curr. Org. Chem.* **2019,** *23,* 978–993. doi:10.2174/1385272823666190424142821
49. Danil de Namor, A. F.; Shehab, M. *J. Phys. Chem. B* **2005,** *109,* 17440–17444. doi:10.1021/jp0530707
50. Beillard, A.; Bhurruth-Alcor, Y.; Bouix-Peter, C.; Bouquet, K.; Chambon, S.; Clary, L.; Harris, C. S.; Millois, C.; Mouis, G.; Ouvry, G.; Pierre, R.; Reitz, A.; Tomas, L. *Tetrahedron Lett.* **2016,** *57,* 2165–2170. doi:10.1016/j.tetlet.2016.04.003
51. Verma, S. K.; Acharya, B. N.; Ghorpade, R.; Pratap, A.; Kaushik, M. P. *RSC Adv.* **2013,** *3,* 18783–18786. doi:10.1039/c3ra43179g
52. Ho, C. Y.; Strobel, E.; Ralbovsky, J.; Galemmo, R. A. *J. Org. Chem.* **2005,** *70,* 4873–4875. doi:10.1021/jo050036f
53. Hutchinson, S.; Kearney, G. A.; Horne, E.; Lynch, B.; Glennon, J. D.; Anthony McKervey, M.; Harris, S. J. *Anal. Chim. Acta* **1994,** *291,* 269–275. doi:10.1016/0003-2670(94)80022-7
54. Reddy, A. S.; Kumar, M. S.; Reddy, G. R. *Tetrahedron Lett.* **2000,** *41,* 6285–6288. doi:10.1016/s0040-4039(00)01058-3
55. Devlin, J. P.; Ollis, W. D.; Thorpe, J. E. *J. Chem. Soc., Perkin Trans. 1* **1975,** 846–848. doi:10.1039/p19750000846
56. Butler, K. V.; Kalin, J.; Brochier, C.; Vistoli, G.; Langley, B.; Kozikowski, A. P. *J. Am. Chem. Soc.* **2010,** *132,* 10842–10846. doi:10.1021/ja102758v
57. Adiguzel, E.; Yilmaz, F.; Emirik, M.; Ozil, M. *J. Mol. Struct.* **2017,** *1127,* 403–412. doi:10.1016/j.molstruc.2016.07.081
58. Toumi, N.; Kajo, F.; Fournier, D.; Vocanson, F.; Lamartine, R.; Dumazet-Bonnamour, I. *Mater. Sci. Eng., C* **2008,** *28,* 645–652. doi:10.1016/j.msec.2007.10.009
59. Grenthe, I.; Fuger, J.; Konings, R. J.; Lemire, R. J.; Muller, A. B.; Nguyen-Trung, C.; Wanner, H. *Chemical Thermodynamics of Uranium*; OECD Nuclear Energy Agency, 2004. https://www.oecd-nea.org/upload/docs/application/pdf/2019-12/uranium.pdf (accessed Feb 12, 2026).
60. Knoll, G. F. *Radiation Detection and Measurement,* 4th ed.; John Wiley & Sons: Hoboken, NJ, USA, 2010.
61. Kaminski, S.; Jakobi, A.; Wilhelm, C. *Appl. Radiat. Isot.* **2014,** *94,* 306–313. doi:10.1016/j.apradiso.2014.08.008
62. *Evaluation of Measurement Data — Guide to the Expression of Uncertainty in Measurement*, 1st ed.; JCGM, 2008. https://www.bipm.org/documents/20126/2071204/JCGM_100_2008_E.pdf (accessed Feb 12, 2026).
63. Arnold, D; Debertin, K; Heckel, A; Kanisch, G; Wershofen, H; Wilhelm, C. *Fundamentals of Gamma Spectrometry*; German Federal Ministry for the Environment, Nature Conservation, Nuclear Safety and Consumer Protection (BMUV), 2018. https://www.bundesumweltministerium.de/fileadmin/Daten_BMU/Download_PDF/Strahlenschutz/Messanleitungen_2022/gamma_spekt_grundl_v2018-03_en_bf.pdf (accessed Feb 12, 2026).
64. U.S. Environmental Protection Agency. *High Resolution Gamma-Ray Spectrometry Analyses for Normal Operations and Radiological Incident Response*; EPA 402-B-17-001; U.S. Environmental Protection Agency: Washington, D.C., October. https://www.epa.gov/sites/default/files/2020-07/documents/guide_for_high_resolution_gamma_spectrometry_analyses_camera_ready.pdf.
65. Ilton, E. S.; Wang, Z.; Boily, J.-F.; Qafoku, O.; Rosso, K. M.; Smith, S. C. *Environ. Sci. Technol.* **2012,** *46,* 6604–6611. doi:10.1021/es300501v
66. Karapanagioti, F.; Cissé, N.; Atamas, A.; Stetsenko, A.; Punter, C. M.; Zuidersma, E.; Stuart, M. C. A. *Microsc. Res. Tech.* **2025,** *88,* 2381–2391. doi:10.1002/jemt.24865
67. Bauer, A.; Jäschke, A.; Schöne, S.; Barthen, R.; März, J.; Schmeide, K.; Patzschke, M.; Kersting, B.; Fahmy, K.; Oertel, J.; Brendler, V.; Stumpf, T. *ChemistryOpen* **2018,** *7,* 467–474. doi:10.1002/open.201800085

68. Singhal, P.; Vats, B. G.; Yadav, A.; Pulhani, V. *J. Hazard. Mater.* **2020,** *384,* 121353. doi:10.1016/j.jhazmat.2019.121353
69. Agrawal, Y. K. *Russ. Chem. Rev.* **1979,** *48,* 948–963. doi:10.1070/rc1979v048n10abeh002422
70. Blasko, A.; Bunton, C. A.; Gillitt, N. D. *Langmuir* **1997,** *13,* 6439–6446. doi:10.1021/la9706025
71. García, B.; Ibeas, S.; Leal, J. M.; Secco, F.; Venturini, M.; Senent, M. L.; Niño, A.; Muñoz, C. *Inorg. Chem.* **2005,** *44,* 2908–2919. doi:10.1021/ic049438g
72. Brandès, S.; Sornosa-Ten, A.; Rousselin, Y.; Lagrelette, M.; Stern, C.; Moncomble, A.; Cornard, J.-P.; Meyer, M. *J. Inorg. Biochem.* **2015,** *151,* 164–175. doi:10.1016/j.jinorgbio.2015.06.002
73. Masoud, A. M.; El-Maadawy, M. M.; Taha, M. H.; Meawad, A. *J. Radioanal. Nucl. Chem.* **2023,** *332,* 2487–2497. doi:10.1007/s10967-023-08937-x
74. Smedley, P. L.; Kinniburgh, D. G. *Appl. Geochem.* **2023,** *148,* 105534. doi:10.1016/j.apgeochem.2022.105534
75. Denning, R. G. *J. Phys. Chem. A* **2007,** *111,* 4125–4143. doi:10.1021/jp071061n
76. Shinkai, S.; Koreishi, H.; Ueda, K.; Arimura, T.; Manabe, O. *J. Am. Chem. Soc.* **1987,** *109,* 6371–6376. doi:10.1021/ja00255a023
77. Kurzak, B.; Kozłowski, H.; Farkas, E. *Coord. Chem. Rev.* **1992,** *114,* 169–200. doi:10.1016/0010-8545(92)85002-8
78. Boulet, B.; Joubert, L.; Cote, G.; Bouvier-Capely, C.; Cossonnet, C.; Adamo, C. *Inorg. Chem.* **2008,** *47,* 7983–7991. doi:10.1021/ic7018633
79. Chen, D.; Li, Y.; Zhao, X.; Shi, M.; Shi, X.; Zhao, R.; Zhu, G. *ACS Cent. Sci.* **2023,** *9,* 2326–2332. doi:10.1021/acscentsci.3c01291

License and Terms

BEILSTEIN JOURNAL OF ORGANIC CHEMISTRY

Molecular tweezer–peptide conjugates disrupt the protein–protein interaction between survivin and histone H3 essential in mitosis

Catherine Gsell[1], Philipp Rebmann[1], Karina Opara[1], Christine Beuck[1], Peter Bayer[1], David Bier[2], Ingrid R. Vetter[*2] and Thomas Schrader[*1]

Full Research Paper

Open Access

Address:
[1]University of Duisburg-Essen, Faculty of Chemistry, Universitätsstr. 7, 45117 Essen, Germany and [2]Max-Planck-Institute of Molecular Physiology, Department of Mechanistic Cell Biology, Otto-Hahn-Straße 11, 44227 Dortmund, Germany

Email:
Ingrid R. Vetter[*] - ingrid.vetter@mpi-dortmund.mpg.de;
Thomas Schrader[*] - thomas.schrader@uni-due.de

* Corresponding author

Keywords:
click reaction; chromosomal passenger complex; protein–protein interaction; mitosis; X-ray crystallography

Beilstein J. Org. Chem. **2026,** *22,* 557–567.
https://doi.org/10.3762/bjoc.22.41

Received: 03 December 2025
Accepted: 04 March 2026
Published: 27 March 2026

This article is part of the thematic issue "Novel macrocycles: from synthesis to supramolecular function".

Guest Editor: C. Gaeta

Abstract

Peptide-modified supramolecular tweezers, a promising new class of chemical tools, were designed and employed to inhibit the interaction of the BIR domain of human survivin, a member of the chromosomal passenger complex (CPC), with the phosphorylated histone H3 N-terminal peptide. Fluorescence polarization measurements revealed a nanomolar affinity of the BIR domain for the peptide-tweezer, depending on the presence of lysine residue 121, as proven by the K121A mutant of survivin. Two crystal structures of C-terminally truncated human survivin with the peptide-tweezer molecules demonstrated that the peptide moiety binds the BIR domain as expected from the well-known published crystal structures of survivin with various peptides, but the tweezer itself, surprisingly, was bound to a putative Ca^{2+} ion and the side chain of Pro26, corresponding to a previously unknown binding mode. Guided by the accessibility of survivin's lysine residues in the CPC, a number of new promising peptide tweezers was synthesized, able to connect both binding sites on the protein.

Introduction

The fundamental process of mitosis is controlled by a very large protein complex called the kinetochore, formed by self-assembly from hundreds of single protein components [1]. For the intricate regulation of the various phases of cell division, this kinetochore interacts with a smaller ensemble, the chromosomal passenger complex (CPC) that constitutes an abundant component of the inner centromere [2,3]. The CPC itself is formed inside the cell nucleus and consists of the four proteins

survivin, borealin, INCENP (inner centromere protein), and the kinase Aurora B. During mitosis, Aurora B phosphorylates important components of the kinetochore and thus exerts control over key events of the whole process. The other three proteins localize the CPC during the different mitotic phases [4]. Survivin, borealin and INCENP are bound tightly to each other by aligning their extended α-helices (Figure 1) [5].

Intriguingly, CPC recruitment hinges on a few very distinct protein contacts, involving borealin and the BIR domain of survivin. A very dominant protein–protein interaction (PPI) is the embedding of the N-terminus of histone H3 on the BIR domain of survivin, which leads to attachment of the CPC to the inner centromere [6]. This PPI is facilitated by N-terminal H3 phosphorylation on Thr3, leading to recognition of the phosphorylated N-terminus by survivin and subsequent attachment of the CPC [7]. Jeyaprakash et al. demonstrated that survivin contributes most of the binding energy to this critical complex with histone H3 [8].

In 2011, a crystal structure was solved depicting structural details of the H3 N-terminus (1–21) bound by survivin's BIR domain (Figure 2). Only the first six residues (ARpTKQT) show electron density with well-defined localization on the survivin surface, all other amino acids are disordered [8]. This arrangement is stabilized by electrostatic interactions between histone H3's phosphothreonine (pT) and basic residues on the core of the BIR domain as well as various basic residues of survivin's α-helix. Likewise, histone's cationic groups are distributed on a negatively charged survivin patch, while hydrophobic contacts are established towards both threonine and alanine methyl groups. This favorable natural arrangement was characterized by titration at ≈1 micromolar affinity [8].

A specific inhibitor of the survivin–histone H3 tail interaction would be a very valuable chemical tool because it could allow to deliberately shut down the recruitment of the CPC to the nucleosomes and to study its effect on CPC function.

Results and Discussion

In 2005, our group discovered molecular tweezers with attached phosph(on)ate anions as powerful new hosts for the amino acids lysine and arginine. In the recent past, we demonstrated that the affinity and selectivity of our lysine-selective molecular tweezers could be improved by attaching natural peptide recognition elements. This could be documented in various projects with tailored peptide tweezer conjugates: For example, the self-complementary ELTLGEFL sequence of the

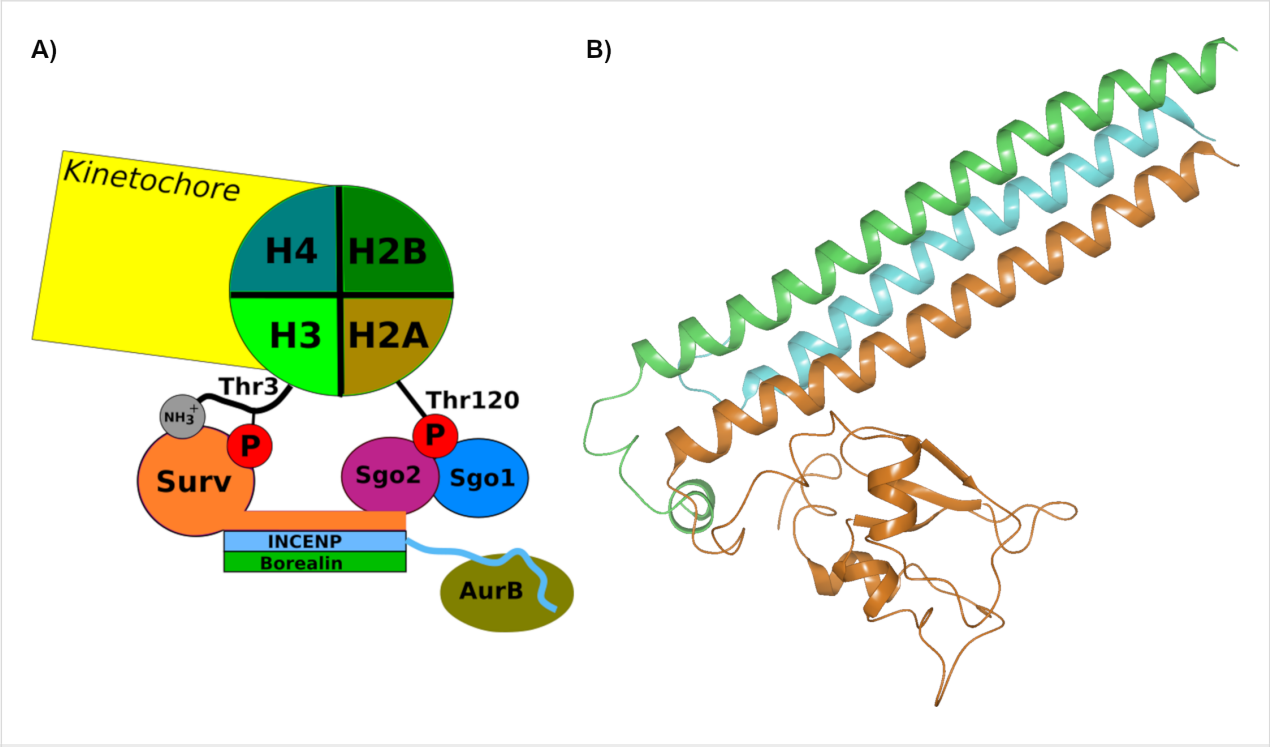

Figure 1: Mechanism of CPC recruitment to centromeres and kinetochores. A) Initially phosphomarks are placed on Thr3 of histone H3 and on Thr120 of histone H2A. In histone H3, P-Thr3 together with the free NH_3^+ of the first alanine residue contribute directly to the binding of survivin. P-T120 recruits shugoshin 1 and shugoshin 2, which in turn interact with borealin and with survivin itself, probably involving a region that is distinct from the one that interacts with P-T3-H3. B) Crystal structure of the CPC (PDB ID: 2QFA, https://doi.org/10.2210/pdb2QFA/pdb) [5] with the typical α-helix bundle from survivin (orange), borealin$_{10–109}$ (green) und INCENP$_{1–58}$ (blue).

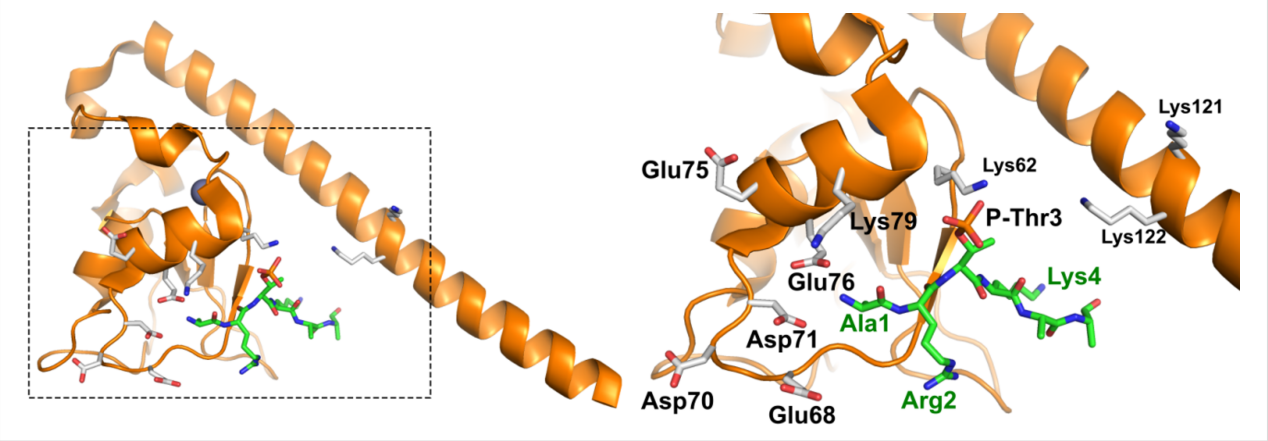

Figure 2: Ribbon model of crystal structure PDB ID 4A0J (https://doi.org/10.2210/pdb4A0J/pdb) [8] of survivin (orange) bound to the N-terminal region of histone H3 (green). The boxed region is enlarged in the right panel. Several of the residues lining the interface between survivin and histone H3 are shown.

nuclear export signal in survivin was coupled to tweezers which rendered them selective for this important interface (NMR evidence, 1:1 stoichiometry, K/A mutants) and prevented the survivin association with its export receptor CRM1 in pull-down assays with cell lysates [9]. Likewise, the ExoS interaction with its adapter protein 14-3-3 was effectively disrupted with a tweezer peptide conjugate that showed a 100-fold affinity increase and simultaneously occupied both an exposed lysine and precisely the natural binding site in the wide 14-3-3-cleft [10]. These examples for designed protein–protein interaction (PPI) inhibitors demonstrated that short but highly flexible linkers are imperative to increase selectivity and minimize entropical penalty. The design was strongly supported by computational modeling (MD and QM/MM simulations) as well as structural biology (NMR/X-ray).

Following our powerful concept of reinforcing natural peptide–protein interactions by tweezer conjugation [9,10], we envisaged to attach molecular tweezers to the histone H3 terminus at a distance which would allow a strong inclusion of a nearby R/K residue on survivin into the tweezer cavity. In fact five sterically well-accessible basic amino acids are located nearby in the survivin α-helix; their side chains point into the direction of the H3 binding site, ideally suited to accommodate the attached tweezers.

Importantly, the H3 N-terminus had to be fully conserved *(vide infra)*, so that covalent attachment of the tweezer moiety had to occur at the peptide C-terminus. A first prototype **1** could be realized with a C3-spacer and click coupling between azidopropylamide on Lys-4 at the peptide's C-terminus and a monobutynyl tweezer (Scheme 1) [11]. Simultaneous placement of the peptide on its binding site and modelling of the tweezer moiety on Lys-121 produced favorable complex structures, which remained stable over 100 ns in MD simulations.

Competitive fluorescence polarization measurements between the tweezer H3 conjugate and a FITC-labeled H3 peptide pointed to very strong binding in the nanomolar range (Figure 3). Molecular modeling revealed that the tweezer moiety could easily reach Lys-121, but could bind to Lys-129 only in an energetically unfavorable, extended conformation. Indeed, mutation of Lys-121 to alanine in the survivin protein resulted in a drastic loss of binding affinity (WT 120 nM to K121A 22 μM) for the new ligand (Figure 3). We conclude that the new tweezer conjugate specifically directs its tweezer moiety to Lys-121 and thus reinforces the H3–survivin peptide–protein interaction by roughly one order of magnitude (from 1 μM to 120 nM K_d).

For further structural proof we attempted co-crystallization of survivin with our new tweezer H3 conjugate. Unfortunately, crystallization of full length survivin 1–142 was difficult to reproduce and often resulted in low-quality crystals. Hence, we designed the truncation constructs 1–122, 1–127 and 1–134 that shorten the flexible C-terminal helix of survivin. All new constructs showed a much better expression and crystallization behavior. Fluorescence polarization measurements with the FITC-labeled H3 peptide confirmed that constructs 1–122, 1–127 as well as survivin full length (1–142) and the mutants K121A and K122A have the same affinity of approximately 1 μM to the peptide, i.e. the mutations/deletions do not influence the peptide binding site. It can therefore be expected that also with these survivin mutants there is an approximately 8-fold gain in affinity by attaching the tweezer moiety to the peptide, provided that the tweezer could reach a suitable binding partner as well.

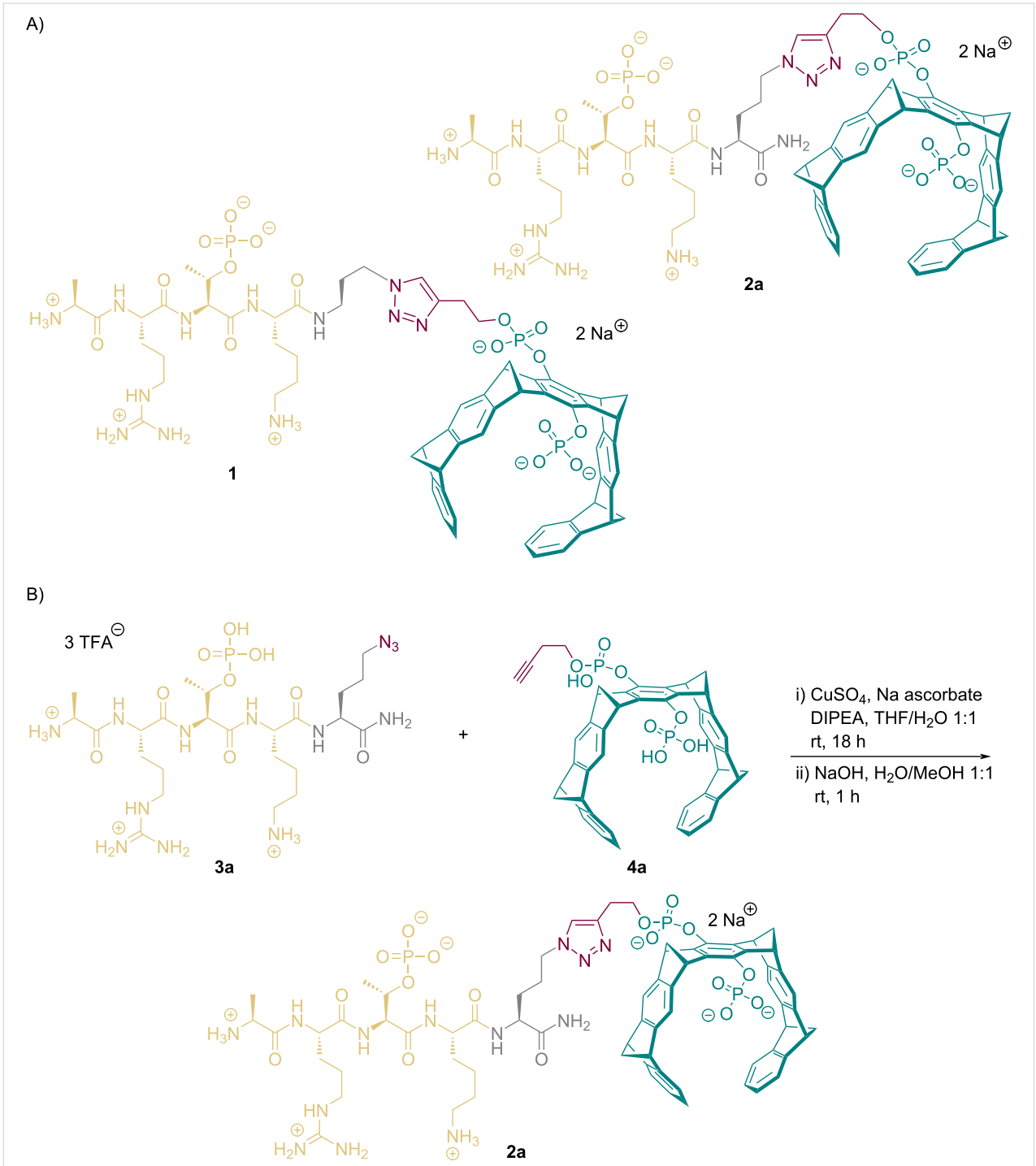

Scheme 1: A) Peptide tweezer conjugates **1** and **2a** with triazoles linking the tweezer and H3 peptide at its C-terminus. Note that both azidopropylamine as well as azidoornithine establish almost the same distance between peptide and tweezer. In addition, they place the tweezer into the vicinity of the phosphorylated threonine, complementary to the cationic surface patch on survivin. B) Click coupling (i) between the H3-T3ph peptide with C-terminal 5-azidoornithine **3** and butynyl tweezer **4a** with subsequent deprotonation (ii) to the sodium salt of peptide tweezer **2a**. Binding peptide yellow, ornithine grey, butynyl group red, tweezer green.

To allow a general commercial synthesis of the phosphorylated H3-peptide sequences for the tweezers, we used an azidoornithine extension at the C-terminus (peptide ordered from Genscript), which was subjected to click reaction with the butynyl tweezer (Scheme 1). The coupling protocol was identical to the published version [9,10]. Reaction progress was monitored by analytical HPLC and the product could be purified by preparative HPLC. After lyophilization, the product **2a**

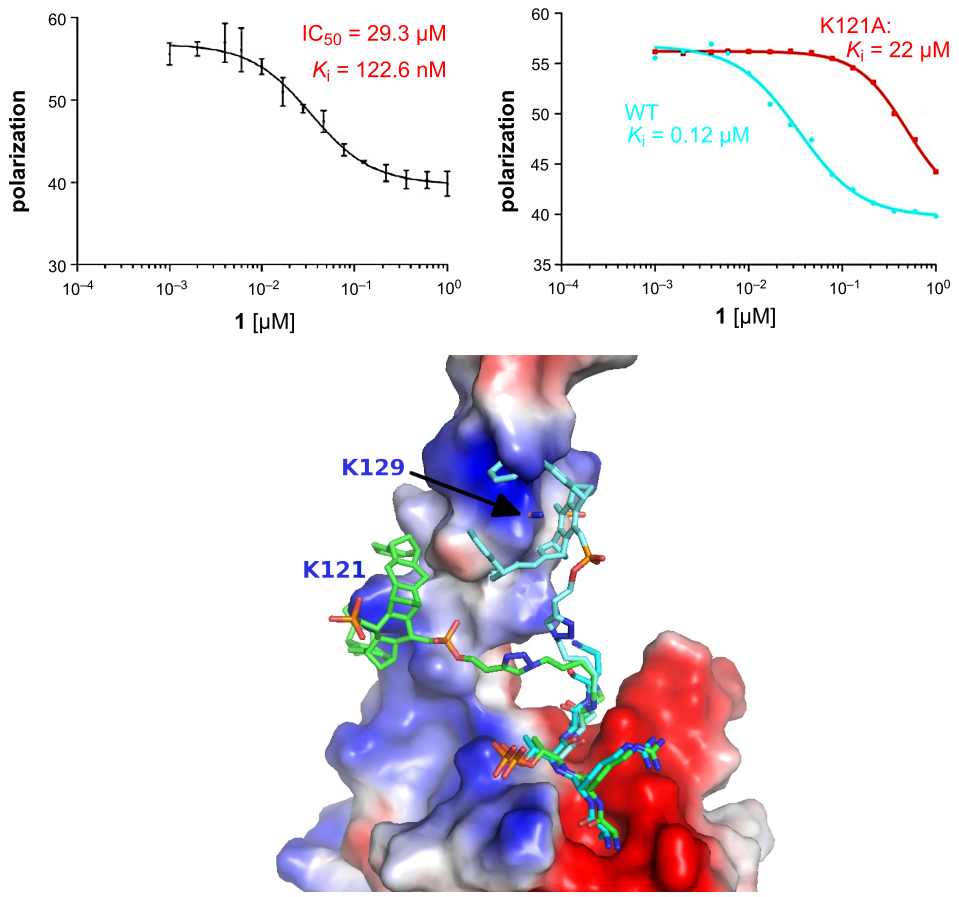

Figure 3: Survivin complexes with peptide tweezers: Fluorescence polarization measurements of wild type and mutated survivin (top) and modeling of the peptide tweezer **1** on either K-121 or K-129 (bottom). The positive residues of the H3 peptide are bound to the negatively charged area (red) whereas the phosphorylated threonine contacts a positively charged area, as known from the existing crystal structures. The tweezer moiety can associate with lysines in the C-terminal helix of survivin (positively charged blue area).

was obtained as fully protonated TFA salt (43%); deprotonation with equimolar aq. NaOH produced the sodium salt of **2a** quantitatively.

The analytical characterization of **2a** turned out to be difficult, because even in DMSO-d_6, most NMR signals remained very broad, and in part strongly shifted upfield. This may be explained by the three cationic groups in the peptide sequence, which likely interact with the negatively charged tweezer moiety by self-inclusion; it is well documented that these fast inclusion processes often lead to signal broadening and massive upfield shifts of the included side chain protons [12,13]. HPLC–HRMS analysis finally produced a single chromatographic signal with clean molecular ion peaks for $[M + 2H]^{2+}$ and $[M + 3H]^{3+}$. The high purity of **2a** was further demonstrated by successful co-crystallization of this tweezer peptide conjugate with survivin (vide infra).

Again, molecular docking of peptide and tweezer moiety **2a** on survivin led to stable arrangements on survivin, suggesting simultaneous occupation of the H3 binding site and potential complexation at Lys-121 (Figures S10 and S11 in Supporting Information File 1). The triazole linker may act as a barrier for the rearrangement of survivin's side chains and the interaction diagram reveals contacts to all nine accessible acidic amino acids on the protein surface [14].

The new tweezer H3 conjugate **2a** has a C4 spacer between the Lys-4 amide and the azide, very close to **1** with its C3 spacer. Crystallizations with this compound and the truncated survivin constructs 1–122 and 1–127 were finally successful and yielded high-resolution X-ray structures (Figure 4) [15]. The structures of both survivin truncation mutants look very similar, both have a survivin dimer in the asymmetric unit, and the H3 peptide binds in the canonical H3-peptide binding site with very well defined density. The tweezer moiety and the linker also have very well defined densities, but, contrary to our expectation, the tweezer does not bind to Lys-121, but instead packs against a proline of the second survivin monomer in the crystal (Figure 4 and Supporting Information File 1, Figure S12). Lys-121, on the

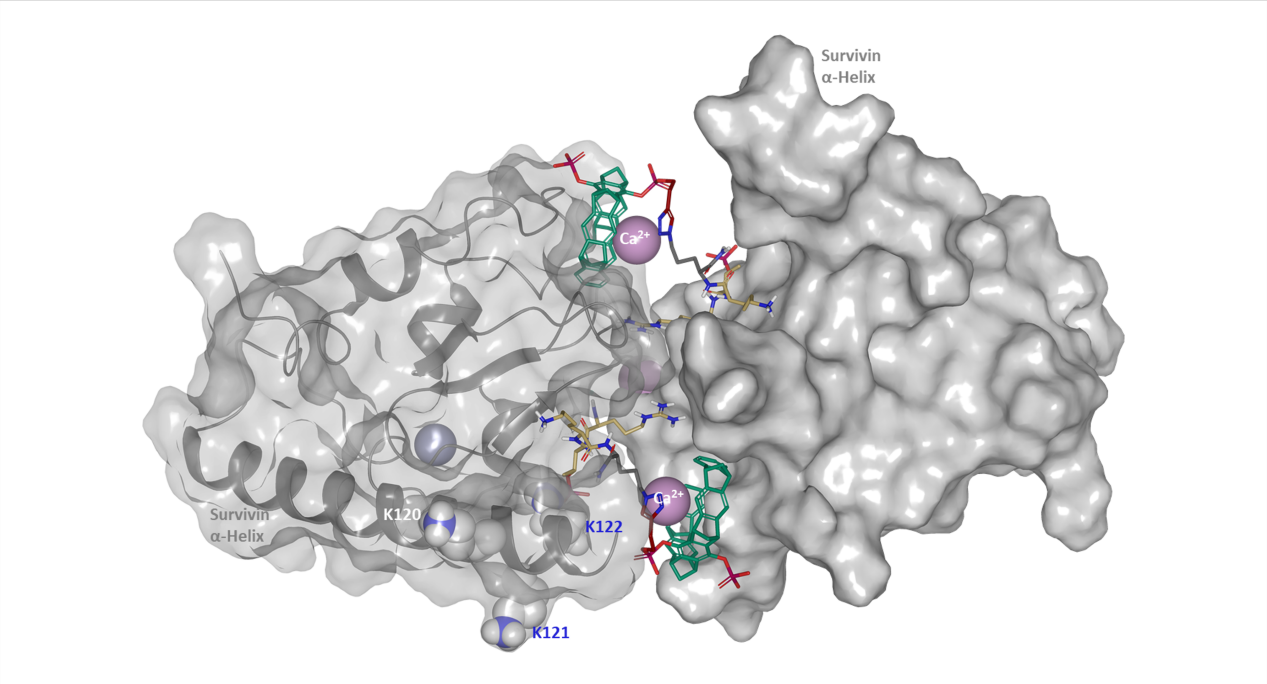

Figure 4: Crystal structure of the survivin dimer with complexed tweezer H3 conjugate **2a**. To distinguish both survivin molecules their surfaces (light grey) have been presented with a different degree of transparency. Lysines in the vicinity of the histone H3 binding as well as the Ca^{2+} ion site are labeled and shown as CPK models. The tweezer skeleton is shown in green, the H3 peptide in yellow.

other hand, is buried in a crystal contact. Thus, the crystal packing forces together with putatively competing ligands (see below) can apparently compete successfully with the tweezer that is most likely attached to Lys-121 in solution, as shown by the fluorescence polarization measurements where the K121A mutation has drastically reduced affinity.

In the new crystal structure, the apolar pyrrolidine of Pro-26 occupies half of the tweezer cavity, while from the opposite side, a density that most likely corresponds to a Ca^{2+} cation from the crystallization buffer, is visible next to the cavity (Figure S12 in Supporting Information File 1). From recent complexation experiments with lipids, it is known that even uncharged alkyl groups may occupy the tweezer cavity and gain binding energy through dispersive interactions and the hydrophobic effect [16]. Ca^{2+} may also interact with the high π-electron density inside the cavity, although in direct titrations, only small affinities in the millimolar range have been determined for this cation [17]. This observation not only indicates a competition of the (putative) calcium ion with amino acid side chains – that might also be in part be responsible for the lack of tweezer binding to Lys-121 – but also represents a new binding mode for the tweezer moiety. The (hydrated) Ca^{2+} ion is apparently too large to enter the cavity of the tweezer ring, in contrast to larger Cs^{+} ions that were surprisingly observed in the center of the aromatic ring structure, perhaps due to their weaker binding of the hydrate shell. However, this early crystal structure was obtained with the diacetoxytweezer in organic solution [18].

Interestingly, a similar unexpected inclusion of a methionine side chain was found in the crystal structure of the sulfonatocalix[4]arene (sclx4) with a trimeric RSL protein (Ralstonia solanacearum lectin, MK-RSL) that carried an engineered N-terminal Met-Lys extension [19], as well as in the protein P5CDH with a monophosphate-tweezer [20].

Close inspection of recent CPC crystal structures revealed partial burial of Lys-121 in the physiological surviving–borealin–INCENP complex (PDB ID 2QFA) [5], so that the tight alignment of three α-helices may also prevent efficient binding of our peptide tweezer to this seemingly favorable position. We therefore turned to peptide tweezers with longer linkers to address lysines which are buried neither in the crystals nor in the CPC complex. In a second approach, one of the tweezer phosphate groups was truncated to minimize steric hindrance during the tweezer approach towards survivin's α-helix within the CPC.

Importantly, the peptide moiety itself cannot be modified substantially without losing affinity as described in the literature [8,21]. In most survivin–H3 peptide crystal structures, residues 1–4 have visible electron density, and only in few cases the following glutamine/threonine could be located as well (e.g.,

PDB ID 4A0J). The remainder of the peptides is usually disordered. Comparison of different peptides revealed that the N-terminal alanine is absolutely required for survivin binding, and no modification of the N-terminus is tolerated. Position 2 is probably uncritical, but most likely sensitive to the backbone conformation since it strongly influences the conformation of the neighboring alanine. Position 3 should either be a phosphothreonine or a glutamine, and position 4 is preferred as Arg or Lys. The peptide affinity drops 3- or 4-fold when increasing the pH from 6.8 to 8.2, thus limiting the crystallization conditions [22]. Other co-crystallized peptides are AKERC from the N-terminus of shugoshin1 (6.2 μM, PDB ID 4A0I) [8] and a Smac-DIABLO 15-mer-peptide with only 121 μM affinity, that still crystallized at sufficiently high concentrations in complex with survivin (PDB ID 3UIH https://doi.org/10.2210/pdb3UIH/pdb, [23]).

A major problem of co-crystallizing tweezer compounds with proteins in general is the competition with the crystal packing, as illustrated by earlier crystal structures [20]. Since the "proof-of-concept" H3-peptide tweezer **1** targeted lysine 121 which is not only buried in the crystal, but also in the biological target, the CPC complex, two obvious design options remain: either introducing a shorter linker to address lysines closer to the peptide binding site and benefit from increased affinity due linker rigidity, or using a longer linker that could reach lysines 129 and 130 which are not buried in the known crystal forms, nor in the CPC complex (Figure 5). A 3D structure of the complex between the full CPC trimer and the hybrid H3-peptide–tweezer constructs would be very desirable to validate the binding mode in the physiological setting.

New tweezer–H3 conjugates for well-accessible lysines in the CPC. For efficient docking of a tweezer molecule onto a lysine residue on the protein surface, only one phosphate moiety is sufficient, which locks the included lysine cation into an ion pair [20]. In MD simulations between survivin and the truncated version of the tweezers conjugate **2b** (simply lacking the second phosphate) stable structures were produced which demonstrate the minimal steric demand of the remaining hydroquinone OH group, leaving much more room for tight contacts with the protein surface. In principle, a click reaction between the known unsymmetrical intermediate hydroxy-butynylphosphate tweezer and any azido histone peptide will lead to the desired truncated tweezer conjugate. This concept proved feasible and was performed with H3 peptides of different lengths to produce new peptide tweezer conjugates designed to target near and far lysines on survivin's α-helix.

As an example, Figure 6 depicts the Lewis structure of the tweezer conjugate **2b** from butynyl tweezer and the peptide. MD simulations used the new crystal structure of **2a** on survivin as starting point, and truncated one phosphate group to probe the importance of the respective phosphate ammonium ion pair. Interestingly, after 100 ns (Figure 6B) the tweezer cavity of **2b** still firmly rests on Lys-121, while the peptide remains in its binding groove. This result may reflect the comparable lysine affinities of mono- and diphosphate tweezers [24], and the

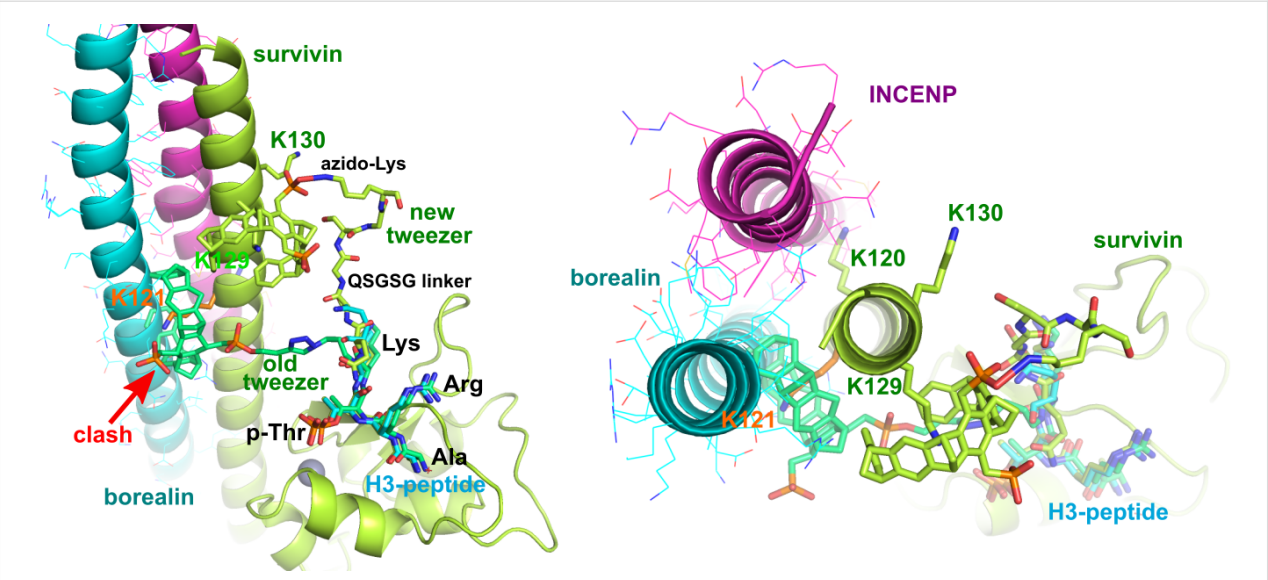

Figure 5: Survivin–borealin–INCENP complex structures (PDB ID 2QFA) [5] with tweezer model, side and top views. The original design ("old tweezer") could only reach Lys-121 which is not accessible in the CPC complex because it forms a tight trimer between survivin, borealin and INCENP. The newly designed compounds with longer linkers between the H3 peptide and the tweezer moiety could reach lysines 129 and 130 that are accessible even in the CPC complex.

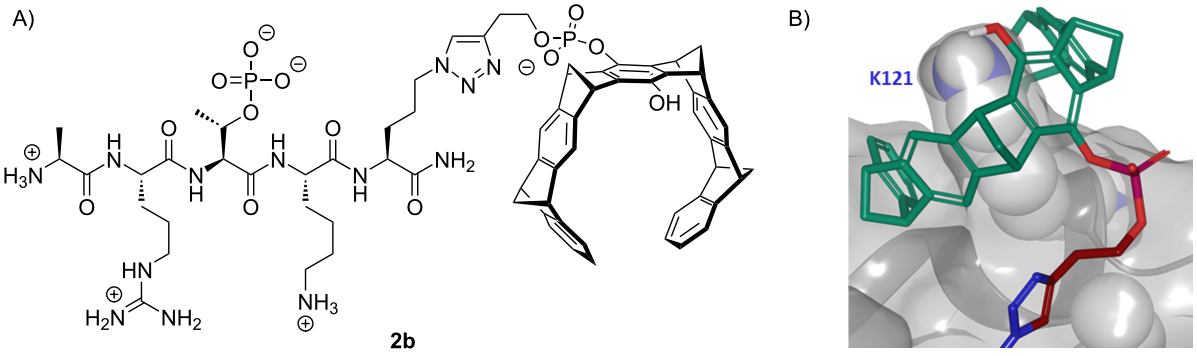

Figure 6: A) Lewis structure of the truncated tweezer peptide monophosphate **2b**. B) Close-up of the binding motif formed by **2b** (tweezer: green, butynyl ester: red) on the survivin surface encapsulating Lys-121 after MD simulation (Desmond, 100 ns, 300 K, 0.15 mM NaCl) using explicit water solvent.

compact complex structure of **2b** on K-121 leaves more room for stabilizing packing effects.

Lys-122 is also located in the vicinity of the H3-T3ph binding site; although it forms a protein contact with Asn-118, there is plenty of room around it in the crystal structure (Figure 4). However, to target this amino acid, the linker between tweezer and peptide must be considerably shortened; loss of Lys-4 would thus substantially lower the overall binding energy. Extended linkers on the other hand may allow complexation of well-accessible Lys-120, 129 or Lys-130. Just one more glycine placed between the H3 peptide and 5-azidoornithine furnishes tweezers **2c** and **2d** as mono- and diphosphate.

The small added glycine linker renders the peptide backbone more flexible, and allows the new tweezer to avoid clashes with crystal contacts. MD simulations also demonstrate that **2d** may indeed reach and rest upon Lys-120 (Figure S14 in Supporting Information File 1). Even more efficient should be the sterically compact monophosphate **2c**.

To reach Lys-139 and Lys-140, the linker must be elongated to a pentapeptide sequence. We decided to synthesize the peptide shown in Scheme 2B which features an Asn-Ser-Gly-Ser-Gly linker. The resulting tweezer peptide conjugates **2e** and **2f** are much more flexible and may reach lysines in larger distance, which did not show up in manual structure screens. Both tweezer conjugates **2e** and **2f** were synthesized, purified by preparative HPLC and analytically characterized. They are currently involved in crystallization experiments, competitive fluorescence titrations, and cell division assays.

Conclusion

This report introduces a new supramolecular attempt to interfere with the critical interaction between kinetochore and CPC during mitosis in cells. The concept builds on the discovery that a specific protein–protein interaction (PPI) recruits the CPC to the kinetochore which hinges on its histone H3 peptide binding with its N-terminal sequence to the BIR domain of survivin. The biological affinity of this interaction ($K_d \approx 1$ μM) is not sufficient as anchor point for an inhibitor; therefore a molecular tweezer selective for accessible lysine residues was covalently connected to the histone H3 peptide at various distances to add the released lysine inclusion energy ($K_d \approx 10$ μM) and reach nanomolar affinity.

Azidopeptides were conjugated to butynyl tweezers by click chemistry and subjected to competitive fluorescence titrations with wildtype and mutant survivin as well as to co-crystallization experiments. These investigations demonstrated affinities of the peptide tweezers in the 100 nM range and proved that the peptide was placed inside its known binding site in two survivin crystal structures. However, the tweezer cavity did not include Lys-121 as planned but instead was engaged in a double interaction with Ca^{2+} and Pro-126, illustrating the variability of tweezer interactions. After extensive modeling using MD simulations with explicit solvent treatment, several new tweezer peptide conjugates were identified with highly promising complex structures on survivin that were stable for 100 ns.

Our new tweezer H3 conjugates **2a**–**f** target Lys-122, Lys-129, and Lys-130 which are freely accessible even in the CPC complex. Hence we expect them to bind with much enhanced specificity and affinity to survivin and prevent its binding to histone H3, thus creating an interesting tool to specifically interfere with this interaction in the cell. If these constructs are not sufficiently cell-permeable, they may be introduced via electroporation into mammalian cells, a protocol that is well established in the Musacchio lab [25]. Affinity determination, co-crystallization attempts, and bioassays are underway in our laboratories.

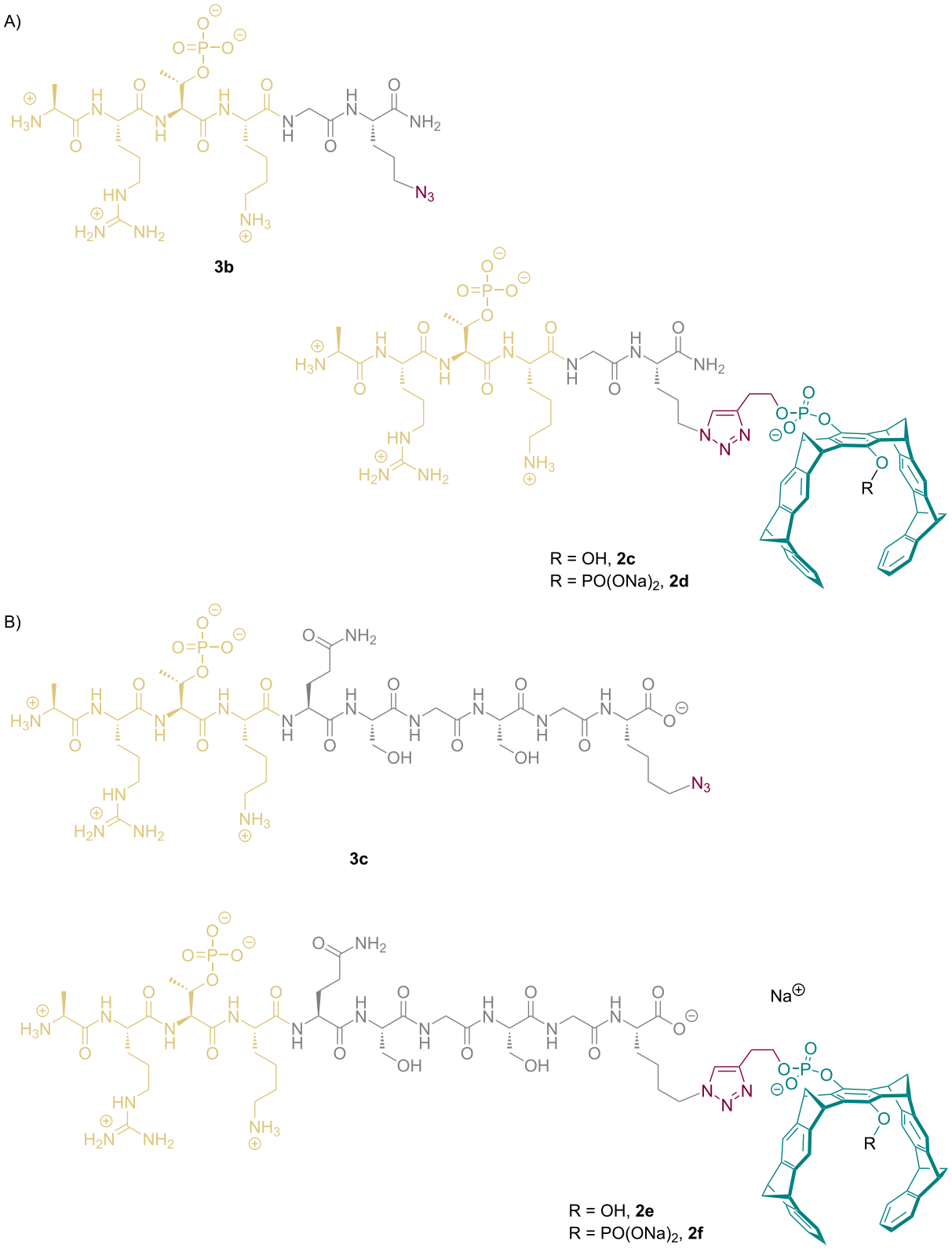

Scheme 2: A) Lewis structures of the new slightly extended binding peptide **3b** and the respective click conjugates with butynyl tweezer, mono- and diphosphate **2c** and **2d**. B) Lewis structures of the new binding peptide **3c** and the resulting mono- and diphosphate tweezer conjugates **2e** and **2f**.

Supporting Information

Supporting Information File 1

Experimental part.
[https://www.beilstein-journals.org/bjoc/content/supplementary/1860-5397-22-41-S1.pdf]

Acknowledgements

We acknowledge important conceptual help and generous support with methods and instruments from the group of Andrea Musacchio at the Max-Planck-Institute of Molecular Physiology, Dortmund.

Funding

CG, PR, CB, PB, DB, IV and TS gratefully acknowledge financial support by the Deutsche Forschungsgemeinschaft DFG to the Collaborative Research Centre CRC 1093 (Supramolecular Chemistry on Proteins).

ORCID® iDs

Christine Beuck - https://orcid.org/0000-0001-7513-7384
Ingrid R. Vetter - https://orcid.org/0000-0002-1722-425X
Thomas Schrader - https://orcid.org/0000-0002-7003-6362

Data Availability Statement

All data that supports the findings of this study is available in the published article and/or the supporting information of this article.

References

1. Santaguida, S.; Musacchio, A. *EMBO J.* **2009,** *28,* 2511–2531. doi:10.1038/emboj.2009.173
2. Musacchio, A. *Science* **2010,** *330,* 183–184. doi:10.1126/science.1197261
3. DeLuca, J. G.; Musacchio, A. *Curr. Opin. Cell Biol.* **2012,** *24,* 48–56. doi:10.1016/j.ceb.2011.11.003
4. Carmena, M.; Ruchaud, S.; Earnshaw, W. C. *Curr. Opin. Cell Biol.* **2009,** *21,* 796–805. doi:10.1016/j.ceb.2009.09.008
5. Jeyaprakash, A. A.; Klein, U. R.; Lindner, D.; Ebert, J.; Nigg, E. A.; Conti, E. *Cell* **2007,** *131,* 271–285. doi:10.1016/j.cell.2007.07.045
6. Vallet, C.; Aschmann, D.; Beuck, C.; Killa, M.; Meiners, A.; Mertel, M.; Ehlers, M.; Bayer, P.; Schmuck, C.; Giese, M.; Knauer, S. K. *Angew. Chem., Int. Ed.* **2020,** *59,* 5567–5571. doi:10.1002/anie.201915400
7. Kelly, A. E.; Ghenoiu, C.; Xue, J. Z.; Zierhut, C.; Kimura, H.; Funabiki, H. *Science* **2010,** *330,* 235–239. doi:10.1126/science.1189505
8. Jeyaprakash, A. A.; Basquin, C.; Jayachandran, U.; Conti, E. *Structure* **2011,** *19,* 1625–1634. doi:10.1016/j.str.2011.09.002
9. Meiners, A.; Bäcker, S.; Hadrović, I.; Heid, C.; Beuck, C.; Ruiz-Blanco, Y. B.; Mieres-Perez, J.; Pörschke, M.; Grad, J.-N.; Vallet, C.; Hoffmann, D.; Bayer, P.; Sánchez-García, E.; Schrader, T.; Knauer, S. K. *Nat. Commun.* **2021,** *12,* 1505. doi:10.1038/s41467-021-21753-9
10. Guillory, X.; Hadrović, I.; de Vink, P. J.; Sowislok, A.; Brunsveld, L.; Schrader, T.; Ottmann, C. *J. Am. Chem. Soc.* **2021,** *143,* 13495–13500. doi:10.1021/jacs.1c07095
11. Tang, W.; Becker, M. L. *Chem. Soc. Rev.* **2014,** *43,* 7013–7039. doi:10.1039/c4cs00139g
12. Heid, C.; Sowislok, A.; Schaller, T.; Niemeyer, F.; Klärner, F.-G.; Schrader, T. *Chem. – Eur. J.* **2018,** *24,* 11332–11343. doi:10.1002/chem.201801508
13. Gersthagen, T.; Hofmann, J.; Klärner, F.-G.; Schmuck, C.; Schrader, T. *Eur. J. Org. Chem.* **2013,** 1080–1092. doi:10.1002/ejoc.201201052
14. Interaction diagrams were visualized from the Glide module, version 2020 in Schrodinger; Schrödinger LLC: NY; available at https://www.schrodinger.com/.
15. PDB IDs: 9TPH for the complex between survivin (1-127) and H3-peptide tweezer as well as 9TPI for survivin (1-122) with H3-peptide tweezer.
16. Weil, T.; Kirupakaran, A.; Le, M.-H.; Rebmann, P.; Mieres-Perez, J.; Issmail, L.; Conzelmann, C.; Müller, J. A.; Rauch, L.; Gilg, A.; Wettstein, L.; Groß, R.; Read, C.; Bergner, T.; Axberg Pålsson, S.; Uhlig, N.; Eberlein, V.; Wöll, H.; Klärner, F.-G.; Stenger, S.; Kümmerer, B. M.; Streeck, H.; Fois, G.; Frick, M.; Braubach, P.; Spetz, A.-L.; Grunwald, T.; Shorter, J.; Sanchez-Garcia, E.; Schrader, T.; Münch, J. *JACS Au* **2022,** *2,* 2187–2202. doi:10.1021/jacsau.2c00220
17. Wilch, C.; Talbiersky, P.; Berchner-Pfannschmidt, U.; Schaller, T.; Kirsch, M.; Klärner, F.-G.; Schrader, T. *Eur. J. Org. Chem.* **2017,** 2223–2229. doi:10.1002/ejoc.201601596
18. Klärner, F.-G.; Burkert, U.; Kamieth, M.; Boese, R. *J. Phys. Org. Chem.* **2000,** *13,* 604–611. doi:10.1002/1099-1395(200010)13:10<604::aid-poc271>3.0.co;2-7
19. Mockler, N. M.; Ramberg, K. O.; Flood, R. J.; Crowley, P. B. *Biochemistry* **2025,** *64,* 1092–1098. doi:10.1021/acs.biochem.4c00729
20. Porfetye, A. T.; Stege, P.; Rebollido-Rios, R.; Hoffmann, D.; Schrader, T.; Vetter, I. R. *Molecules* **2024,** *29,* 1764. doi:10.3390/molecules29081764
21. Niedzialkowska, E.; Wang, F.; Porebski, P. J.; Minor, W.; Higgins, J. M. G.; Stukenberg, P. T. *Mol. Biol. Cell* **2012,** *23,* 1457–1466. doi:10.1091/mbc.e11-11-0904
22. Søndergaard, C. R.; Garrett, A. E.; Carstensen, T.; Pollastri, G.; Nielsen, J. E. *J. Med. Chem.* **2009,** *52,* 5673–5684. doi:10.1021/jm8016464
23. Du, J.; Kelly, A. E.; Funabiki, H.; Patel, D. J. *Structure* **2012,** *20,* 185–195. doi:10.1016/j.str.2011.12.001
24. Dutt, S.; Wilch, C.; Gersthagen, T.; Wölper, C.; Sowislok, A. A.; Klärner, F.-G.; Schrader, T. *Eur. J. Org. Chem.* **2013,** 7705–7714. doi:10.1002/ejoc.201301211
25. Alex, A.; Piano, V.; Polley, S.; Stuiver, M.; Voss, S.; Ciossani, G.; Overlack, K.; Voss, B.; Wohlgemuth, S.; Petrovic, A.; Wu, Y.; Selenko, P.; Musacchio, A.; Maffini, S. *eLife* **2019,** *8,* e48287. doi:10.7554/elife.48287

License and Terms